Insights Into Genotoxic Effects of Electromagnetic Fields

Inauguraldissertation

zur

Erlangung der Würde eines Doktors der Philosophie

vorgelegt der

Philosophisch-Naturwissenschaftlichen Fakultät

der Universität Basel

von

Frauke Focke

aus Gera, Deutschland

Basel, 2008

Genehmigt von der Philosophisch-Naturwissenschaftlichen Fakultät auf Antrag von

Prof. Dr. Martin Spiess (Fakultätsverantwortlicher)

Prof. Dr. Primo Schär (Dissertationsleiter)

Prof. Dr. Hanspeter Nägeli (Korreferent)

Basel, 11.11.08

Prof. Dr. Eberhard Parlow

“You can't solve a problem with the same mindset that created it.”

Albert Einstein

Table of contents

List of abbreviations

3ABA	3-aminobenzamide
5-FU	5-fluorouracil
AZT	3´-azido-3´-deoxythymidine
BER	base excision repair
BrdU	5-bromodeoxyuridine
DNA Pol β	DNA Polymerase β
DSB	double strand break
DTX	discontinuous transmission
ELF	extremely low frequency
EMF	electromagnetic field
γH2AX	phosphorylated histone H2AX
GFP	green fluorescent protein
GSM	Global System for Mobile Communications
H2B	histone 2B
H_2O_2	hydrogen peroxide
HR	homologous recombination
MMR	mismatch repair
MMS	methyl methanesulfonate
NER	nucleotide excision repair
NHEJ	non-homologous end-joining
OGG1	8-oxoguanine DNA glycosylase
PCNA	proliferating cell nuclear antigen
RF	radiofrequency
ROS	reactive oxygen species
RPA	replication protein A
SAR	specific absorption rate
SSB	single strand break
TDG	Thymine DNA Glycosylase

1. Summary

The increasing use of appliances, which generate electromagnetic fields (EMFs), has provoked public concern about their safety. Scientific research into possible health effects however produced conflicting results. One of the open questions is whether or not EMF exposure has genotoxic effects. Therefore, the main objective of my thesis was to investigate DNA damage formation and repair, cell cycle progression, apoptosis and DNA damage signalling in cultured human cells under EMF exposure. In particular, the nature of possible genotoxic effects and the mechanisms underlying the cellular responses were to be addressed.

As in the past, genotoxic effects of EMF exposure often could not be reproduced in independent studies, I first aimed at the validation of results of previous studies [1-3]. In these studies, different genotoxicity tests revealed increased DNA damage after exposure of human fibroblast cells to EMFs in the low frequency range, as used in power lines, as well as in the radiofrequency range, as applied by mobile phones and wireless technologies. I could show that genotoxic effects of 50Hz EMFs can be reproduced independently. Effects of radiofrequency EMF exposure, however, were detectable only in one particular cell line (HR-1d), but not in the cell line used in the original study (ES-1). Because the visual scoring method of DNA fragmentation analysis (comet assay) used in the previous studies was criticized in the scientific community, I compared this method with an automated computerized comet analysis. This established that increases of DNA fragmentation following EMF exposure are detectable in both types of analyses.

Expanding the study to other cell lines, I was able to show, that 50Hz EMF exposure in two different fibroblast cell lines but not in the cancer cell line HeLa lead to comet assay effects. Furthermore, I showed that DNA fragmentation is not found in G1 blocked cells, suggesting replicating cells to be involved in EMF directed effects. This indicated, that the DNA fragmentation detected following EMF exposure might not reflect direct induction of DNA damage but rather an EMF dependent alteration of the S-phase population. Furthermore apoptosis was suggested as confounder for comet assay effects before. Addressing this question, I found decreased replication efficiency and an increased apoptotic fraction after 50Hz EMF exposure in the fibroblast cell line showing the higher comet assay effect. Therefore, I conclude that these cells encounter problems in entering S-phase or progression

through S-phase, which could lead to apoptosis and, hence, apoptotic DNA fragmentation, in a subpopulation. These effects, however, cannot entirely explain the genotoxicity observed, as the fraction of cells with increased DNA fragmentation was higher than the proportion of apoptotic cells.

I then addressed the type of possible DNA damage generated by EMF exposure. An inhibitor of the DNA single strand break (SSB) sensor poly-ADP-ribosylation polymerase was used to examine an engagement of DNA single strand break repair following EMF exposure. The results showed that the increase of DNA fragmentation did not change further by applying both inhibitor and EMF exposure compared to inhibitor or EMF exposure alone. Therefore the effects appear to be epistatic, indicating that EMF exposure may affect DNA SSB repair rather than inducing DNA damage itself. To address the occurrence of DNA double strand breaks or stalled replication forks, I made use of phosphorylated H2AX (γH2AX) as a marker in EMF exposed cells. This revealed no difference between non-exposed and exposed cells, suggesting that the increase in DNA fragmentation is unlikely due to such lesions.

Biological effects of EMF exposure were hypothesized to reflect an influence on the free radical pool of cells and, thus oxidative stress. I examined the steady state levels of oxidative DNA damage after EMF exposure and found no indications for increased generation of indicator lesions. This result fails to support the hypothesis of EMF induced oxidative stress, although I cannot completely rule out small changes of a sub-detectable level. DNA base excision repair (BER) is the system specifically repairing small lesions including oxidative DNA base damage. To examine, if this pathway is activated during EMF exposure, I examined the formation and levels of nuclear XRCC1 foci. XRCC1 is a central component of the BER system and can be seen to localize to sites of DNA damage and repair. However, immunostaining of XRCC1 revealed no difference in numbers and distribution of foci following EMF exposure. Adding a DNA Polymerase β (the BER polymerase) inhibitor, however, the subG1 fraction of cells increased synergistically with ELF-EMF exposure. This could indicate, that either BER protects cells from entering apoptosis following EMF exposure or that the DNA damage generated by inhibiting DNA Polymerase β is less efficiently processed under EMF exposure.

Taken together, these results suggest, that the small increase in DNA fragmentation observed in human fibroblasts exposed to 50Hz EMFs can be accounted for by a combination of effects including impaired repair of endogenously arising DNA damage, disturbance of S-phase progression and apoptosis in a small fraction of cells, rather than by directly induced

DNA damage.

In a second part of my thesis, I used the highly sensitive comet assay, cell cycle analysis and immunofluorescence staining technologies established for the EMF studies to contribute to different projects addressing regulatory aspects of DNA BER. In a first study, we showed that Thymine DNA Glycosylase (TDG) levels were cell cycle regulated and TDG is absent in S-phase in biochemical assays. Regulation occurs at the protein level, as mRNA levels remain constant throughout the cell cycle. The protein is ubiquitinated and degraded by the proteasome. To provide biological evidence for such a regulation *in vivo*, I stained cells with antibodies for TDG and the S-phase marker PCNA by immunofluorescence and counted cell numbers of double and single stained cells. PCNA positive cells did not stain for TDG and vice versa. As PCNA is a marker for S-phase, this shows, that TDG is absent in S-phase cells.

In a second study we provided evidence for a regulation of DNA Polymerase β (DNA Pol β) by protein arginine methylation. This methylation has impact on its *in vitro* performance like DNA binding and processivity, but an *in vivo* relevance of this modification remained to be shown. I showed that DNA Pol β knock out cells complemented with a mutated form of DNA Pol β, not able to be methylated, showed a higher level of DNA fragmentation upon induced DNA damage than cell complemented with wild type DNA Pol β. Together with reduced survival rates and an increased subG1 fraction in cells challenged with a DNA damaging agent, this established the *in vivo* relevance of DNA Pol β methylation. Arginine methylation therefore might represent a novel regulatory protein modification in DNA BER.

In a third study, I contributed to the investigation of the toxicity mechanism of the chemotherapeutic drug 5-fluorouracil (5-FU), which is not fully understood so far. An involvement of the BER enzyme TDG was suggested by biochemical evidence, leading to the question, if TDG wild type and knock out cells respond differently to 5-FU. TDG knock out cells displayed hypersensitivity to 5-FU, which suggested a deleterious repair mechanism through TDG, probably leading to the induction of DNA SSBs. I indeed found increased DNA strand breaks in TDG wild type cells compared to knock out cells, while XRCC1, a marker for BER, was more activated in knock out cells. In cell cycle analyses 5-FU induced accumulation on S-phase of TDG deficient cells was less pronounced than in wild type cells. This suggests that TDG contributes to 5-FU mediated cytotoxicity, probably by inducing DNA SSBs due to its slow turnover rate and the resulting saturation of BER, leading then to checkpoint activation and S-phase accumulation.

2. Introduction

Damage to DNA occurs frequently in cells and has to be fixed with high accuracy in order to avoid cell death or transformation. There are different sources of DNA damage and different possibilities of repair (Figure 1).

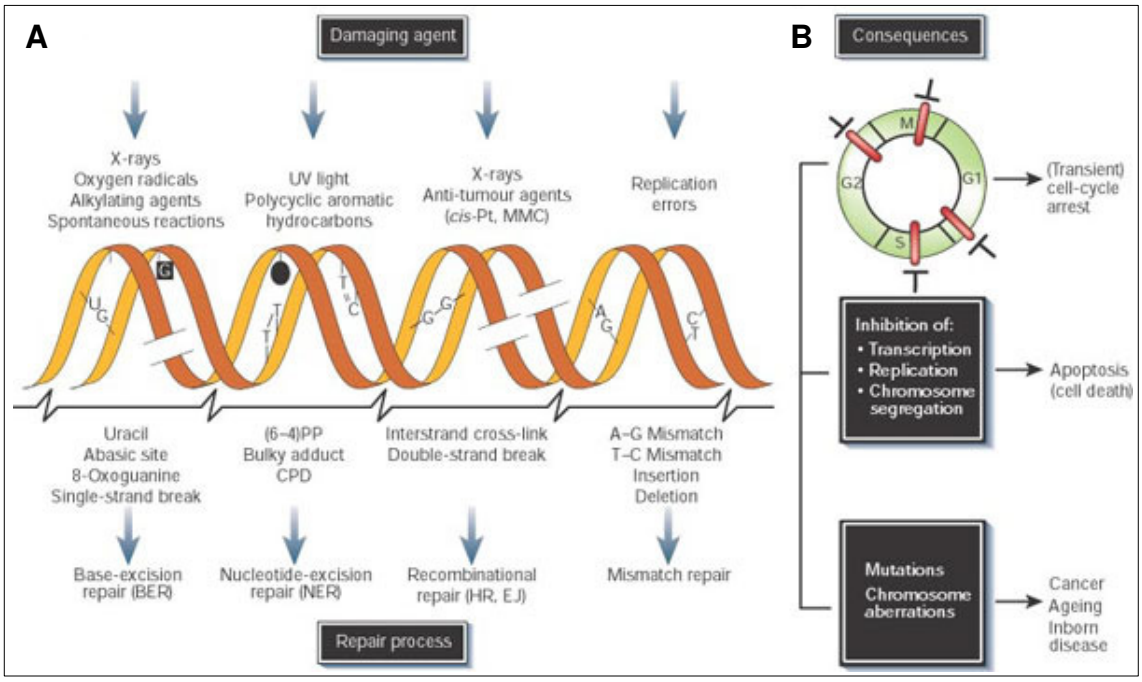

Figure 1. DNA damage and consequences.

A) Common DNA damaging agents (top), examples of DNA lesions (middle) and relevant repair mechanisms for removal of the lesion (bottom). **B)** Consequences of DNA damage: cell cycle arrest in G1, S, G2 or M phase (top), effects on DNA metabolism (middle) and long-term effects of DNA injury (bottom). Adapted from Hoeijmakers *et al.*, 2001 [4].

Sources for DNA damage can be exogenous (e.g. chemicals, UV light, X-rays) or endogenous (reaction products of normal cellular metabolism). Of the latter, oxidation, alkylation and hydrolytic deamination are responsible for the majority of lesions which, if not repaired, may lead to mispairing during DNA replication. Mispairing, deletions or insertions can also occur because DNA polymerases make errors. DNA strand breaks can be the consequence of many of these DNA damaging agents and either affect only one or both DNA strands. Electromagnetic fields are discussed as a possible source of DNA damage, but conclusive evidence has not been presented so far.

DNA damage may give rise to genomic instability and/or trigger cellular responses such as cell cycle checkpoint activation, cell cycle arrest, apoptosis, gene activation and DNA repair. Depending on the type of lesion and the cellular context of its occurrence cells make use of different and specific repair pathways for the restoration of intact DNA (for review see[4]). Failure of one of these mechanisms can lead to mutations and eventually to transformation of the cell and to cancer of the organism.

2.1. Biologic effects of electromagnetic fields

There is an ongoing debate about the biological effects of electromagnetic fields. Effects on human health and well being including sleep disturbance, headaches and interference with cognitive abilities are discussed. Alteration of immune responses or calcium homeostasis of cells have been reported. Even DNA damage induction and increased risk of cancer are being considered as possible outcomes of daily EMF exposure. The same way the exposure to electromagnetic fields increases within the recent years, public safety concerns have become a political and scientific issue. Many of the open questions have been addressed scientifically, but the currently available data is not conclusive.

2.1.1. Basic physical background

An electromagnetic field (EMF) can be seen as a wave with a certain wavelength λ and a frequency in Hertz (Hz). It is composed of an electric field (Volts per meter: V/m) and a magnetic field that can be expressed as magnetic field strength in Ampere per meter (A/m) or as magnetic flux density in Tesla (T). Both fields are perpendicular to each other. A magnetic field induces an electric field and, vice versa, moving electric charges induce a magnetic field. In the low frequency range (0-300kHz) magnetic and electric field can be distinguished, but with higher frequencies the alteration between the two is so fast that the resulting field is seen as one and is referred to as an electromagnetic field.

The electromagnetic spectrum ranges from extremely low frequencies (ELF, 0Hz-300Hz) such as that emitted by traction power and power lines, through radiofrequencies (RF, 100kHz-10GHz), including for example TV and mobile phone radiation and visible light, to X- and γ-rays (Figure 2). The latter two are also known as ionizing radiation, because their energy is high enough to ionize atoms and molecules (the energy of the field is directly proportional to

its frequency), thereby affecting chemical bonds. By contrast, the lower ranges of the spectrum are termed the non-ionizing radiation.

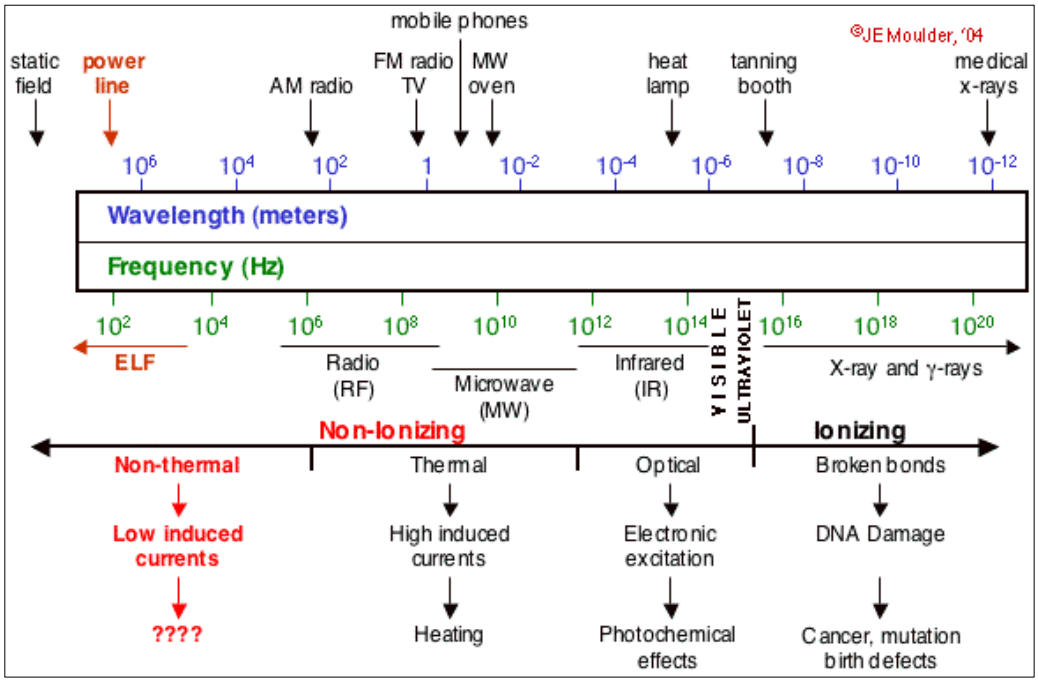

Figure 2. The electromagnetic spectrum.

Frequency-wavelength relationship of electromagnetic fields and application examples of different frequency ranges (top). Additionally shown are known consequences of the different electromagnetic fields (bottom). Adapted from Moulder, 2004.

Known consequences of non-ionizing radiation are on one hand thermal effects, which play a more important role in the RF range and on the other hand induction of electric currents in the body and therefore electric effects on nerves and muscles in the ELF range. To protect people from the consequences of such effects, an international commission (ICNIRP) has defined official EMF exposure threshold values for the population [5]. The threshold for the 50Hz magnetic field (ELF range), e.g. that produced by power lines and household appliances, is set to 100µT for the general population. For the mobile phone radiation the threshold is expressed as specific absorption rate (SAR), which is a measure for the electronic heating of the tissue through the RF field in Watt per kilogram. The whole body threshold is 0,08W/kg and the threshold for specific body parts is set to 2W/kg (e.g. a mobile phone is only affecting a part of the head). Whether or not there are non-thermal effects below these threshold values is still not definitely solved. Both power line radiation (50Hz in

Europe) and mobile phone radiation (1950MHz for GSM) is widespread and the question of adverse health effects is of great public interest.

2.1.2. Effects of extremely low frequency electromagnetic fields (ELF-EMFs)

For ELF-EMFs, epidemiologic studies have associated exposure near power lines with an increased incidence of childhood leukaemia [6-8]. An association with other types of cancer including breast cancer, acoustic neuroma or cancers of the nervous system however was not found [9, 10]. Experimental laboratory studies addressing possible genotoxic effects produced conflicting results. Genotoxicity tests like comet assay, sister chromatid exchange (SCE) analysis and micronucleus formation were applied to investigate the formation of DNA strand breaks and the occurrence of chromosomal aberrations (Review: [11]).

In the comet assay, a number of cells are embedded in agarose and, following in-gel lysis the nuclei are electrophoresed for a short time. Damaged and unwound DNA is thereby able to migrate out of the nucleus and the length of the tail and percentage of migrated DNA are therefore a measure for DNA strand breaks. Results are either expressed as tail moment (computerized measurement of tail length x % DNA in tail) or tailfactor (visual staging of events into 5 categories of damaged cells, which then are multiplied with a damage-related factor) [2, 12]. For the micronucleus test metaphase cells are stained after spindle inhibition and scored for the occurrence of micronuclei, small “nuclei” that contain acentric fragments of chromosomes or whole chromosomes. For sister chromatid exchange analysis cells are grown in BrdU containing medium to incorporate it during two rounds of replication followed by spindle inhibition and photodegradation. Metaphase cells are stained with Giemsa and scored for sister chromatid exchanges (reciprocal exchanges of DNA between two sister chromatids of a duplicating chromosome). About half of the studies applying these methods in studies about EMF effects reported genotoxicity, others did not find any effect.

Rats acutely (2 hr) exposed to a 60Hz magnetic field at intensities of 0.1-0.5mT showed dose dependent increases in DNA single- and double-strand breaks (detected by comet assay) in their brain cells from 1.1fold at 0.1mT to 1.6fold at 0.5mT [13]. In another study, mice exposed to a 0.5mT 50Hz field for 2h, 5d or 14d were found to have a significantly higher amount of tail migration in their brain cells after 14d of exposure [14]. In vitro studies with primary fibroblasts exposed to a 50Hz ELF field (100µT magnetic field) showed increased

comet assay tailfactors in a dose and time dependent manner peaking after 15h of exposure with an about 3.5fold increased tailfactor [2]. From the same group also 3fold increased micronuclei formation and 2-4fold increases of various chromosomal aberrations were reported [3]. Confirmation of a part of these results by another group, however, was not successful [15]. Elevated SCE was found to occur in human peripheral blood lymphocytes after 50Hz ELF exposure for 72h with 1µT and 1mT ELF-EMFs [16]. The changes were very small (1.04fold increase) but statistically significant. In human amniotic cells 2 fold increased numbers of chromosomal aberrations were found after exposure to a 30µT 50Hz ELF EMF [17].

A prominent cellular response to DNA strand breaks is the phosphorylation of the histone variant H2AX (γH2AX). Increased γH2AX foci formation was reported in response to a 50Hz field (0.3-0.5mT for 24 or 48h) in mouse preimplantation embryos [18].

Most robust seem to be effects caused by a combination of ELF-EMF exposure with the treatment with a known carcinogen. Reported were increases of the effects of the carcinogen after co-exposure with ELF-EMFs (for review see [19]). The carcinogens UV light and ionizing radiation and the mitogen TPA (12-tetracanoylphorbol-13-acetate) are examples of used substances.

Other experimental settings, however, (regarding magnetic field strength, exposure time, cell type or animals), failed to produce evidence for differences between exposed and non-exposed cultures. E.g. human blood cells exposed to a 1mT 50Hz field for 2h showed no increase in both comet assay tail moment, micronucleus formation and SCE [20]. Results from studies on human lymphocytes with 50 Hz exposure of varying magnetic field strengths (0.6-1.4mT) showed no increase of chromosomal aberrations in exposed cells [21]. Other cell types that did not show differences between sham and exposed cells in genotoxicity tests include the human tumor cell line K562 (50Hz, 0.2-200µT, DNA strand breaks) and Chinese hamster ovary cells (50Hz, 0.2mT, DNA double strand breaks) [22, 23].

Cell cycle and proliferation behavior were studied after exposure to ELF EMF´s. In some cases stimulation of proliferation and/or 3H-thymidine incorporation [24-26] was observed. In chicken embryonic fibroblasts exposed to a 60Hz 0.7mT ELF-EMF for instance, colorimetric and 3H-thymidine incorporation assays revealed 26-31% increase of cell proliferation [26]. Other studies showed proliferation inhibition or decrease of DNA synthesis. In growth stimulated lymphocytes 10-30% inhibition of proliferation after exposure to 3-200Hz ELF-

EMF for 6-48h was shown by 3H-thymidine incorporation rates [27]. In human amniotic cells BrdU incorporation rate was reduced after 50Hz, 1mT exposure for 24 and 30h and expression levels of cyclin D, p16INK4a and p21CIP1 decreased [28]. There are, however also studies that report an absence of any effect on cell proliferation. So did exposure of HL-60, K-562, MCF-7, A-375, and H4 cancer cells to 50 and 60Hz ELF-EMFs at 500, 100, 20 and 2µT for 3d not lead to any differences in cell number counts and 3H-thymidine incorporation [29]. Synergistic effects have been observed regarding cell cycle progression, as in γ-irradiated HeLa cells the G2 checkpoint appears to be attenuated upon co-treatment with an ELF EMF [30].

Affects on apoptosis of cells were also investigated. There have been reports about an inhibitory effect of ELF-EMF´s on UV-induced apoptosis [31, 32], while others found increased apoptosis after ELF-EMF exposure [33-35]. Thereby HL-60 cells exposed to a 45mT ELF-EMF showed increased apoptosis by microscopic analysis after 1h exposure, rat fibroblasts exhibited increased apoptosis upon exposure to 60Hz up to 0.25mT for up to 13d and human lymphoblastoid cells showed 2fold increased apoptosis after exposure to a 50Hz, 60µT ELF-EMF for 72h.

Altered expression of apoptosis-related genes like bcl-2, bax an c-myc have also been reported after exposure to a 50Hz ELF-EMF at 0.1mT, 1.0mT or 2.3mT [36, 37] [38]. Furthermore synergistic effects with apoptosis-triggering substances were shown: When using vinblastine, a known aneugen, to treat primary human lymphocytes and coexposing the cultures with 50Hz ELF-EMFs at 80 and 800µT, the vinblastine effect on micronucleus formation and apoptosis was increased by twofold [39]. All in all, the literature seems to suggest that magnetic fields alter aspects of apoptosis in cells (for review see [40]).

Possible EMF induced alterations in gene expression have also been investigated both at the mRNA and the protein level. Among the targets identified, heat shock proteins (mainly HSP25 and HSP70) seem to be predominant [41-44]. There have even been reports proposing the existence of an “electromagnetic field response element” (EMRE), represented by a CTCT-sequence in one or several copies. Such sequences can, for instance, be found in the promoter region of c-myc and HSP70 [45].

Intracellular signaling also seems to be affected by the exposure of cells to ELF-EMF´s. There are numerous reports about EMF-induced increases of intracellular calcium concentrations and altered calcium-dependent signaling [46-50]. This could be either due to calcium release

from intracellular stores or to increased influx trough calcium channels on the outer membrane. EMF induced changes on ion-channel opening times and rates have been reported [51], and these could be responsible for the altered calcium content of the cells. Modulation of intracellular calcium concentrations was reported in lymphocytes, where increased calcium influx was shown [49, 52, 53]. This goes in line with reports of stimulation of protein kinase C (PKC), an enzyme that needs calcium for activation and regulates differentiation and proliferation processes in cells. Also Lyn kinase and its downstream targets were shown to be activated by exposure to 50Hz ELF EMFs [54-56]. A possible reason for changes in calcium influx could be the change of membrane potential, which was also shown [57].

2.1.3. Effects of radiofrequency electromagnetic fields

Regarding radiofrequency (RF) EMFs in the range of mobile phones there is so far no evidence for adverse health effects from epidemiological studies, but the quantity and quality of the data available does not allow safe conclusions to be drawn (for review see[58]).

Laboratory studies again produced conflicting results. Rats exposed to a 836MHz field with SAR values between 0.0077 and 0.4 W/kg showed no altered tumorigenesis of the central nervous system [59] and there was also no effect on benzo(α)pyrene induced tumorigenesis after exposure of rats to a GSM modulated 900MHz RF field at 75 and 270mW/kg [60]. Another study reported increased DNA strand breaks in brain cells of rats exposed to 2.45GHz RF fields at SAR values of 0.6 and 1.2W/kg [61, 62], but these findings could not be reproduced independently [63]. Exposure of lymphoma-prone Pim1 mice lead to a slightly (but significant) higher tumor incidence in one study (900MHz, 0.003-0.32W/kg) but not in another (898.4MHz, 0.25-4W/kg) [64, 65].

In vitro studies on genotoxic effects of RF-EMFs also produced conflicting results. Human lymphocytes showed no significant differences of comet tail moments after exposure to a 2.45GHz RF field at 2.1W/kg [66]. In another study, comet assays, micronucleus tests, SCE and chromosomal aberrations analysis showed no difference between sham and exposed lymphocytes after exposure to a 935MHz RF field at 1 and 2 W/kg for 24h. [67]. DNA strand breaks however, could be detected after exposure of human fibroblasts and rat granulosa cells to an unmodulated and to a modulated 1.8GHz RF field (1.2 or 2W/kg) [68]. An attempt

to replicate this study with an identical cell line but unmodulated signal only however was not successful [69].

In conclusion *in vivo* and *in vitro* studies related to genotoxicity and tumor promotion led to different and sometimes conflicting outcomes. From 21 studies on exposed rats or mice reviewed in [70] only 4 reported differences between exposed and non-exposed animals. In the same review from 24 *in vitro* studies genotoxic effects were reported in only 3. In a recent review [71] 10 out of 12 studies did not find indications for tumor promotion in different rat and mouse models. From the in vitro genotoxicity studies reviewed in this report 10 out of 13 were negative. Hence the majority of the genotoxicity and cancer promotion studies in the RF range yielded negative results.

Changes of global gene expression were reported for human endothelial cells after exposure to a 900MHz RF field at 2.8W/kg [72]. A heat shock response resulting from RF exposure is discussed in [73]. In the 13 studies reviewed, HSP70 induction was shown in 4 cases and HSP27 induction in 2.

2.1.4. Quality and reproducibility aspects

A major problem of the research about biological effects of ELF- and RF-EMF exposure is the low magnitudes of effects reported and, hence, the lack of reproducibility. There is very little consistency in experimental approaches, including exposure conditions (time and field strength) and setup as well as biological systems (cell lines, animals), making direct comparisons difficult. But even when identical biologic systems and experimental conditions were applied, results were not always reproducible. Allegations of data fabrication in the case of a recent study [74] did not help clarify the situation either. So, to get conclusive answers in this field, well controlled and coordinated independent research will have to be done in the future.

2.1.5. Possible mechanism of DNA directed EMF effects

There is so far no established biophysical mechanism by which weak ELF-EMFs could impact DNA, although numerous hypotheses have been put forward.

Increased intracellular radical formation may be due to an influence of the field on the iron pool of the cell [75, 76] and via the Fenton reaction: $Fe^{2+} + H_2O_2 \rightarrow Fe^{3+} + \cdot OH + {}^{-}OH$. These radicals then could lead to increased oxidative damage.

Another hypothesis is that a temporary electric current is induced in DNA leading to a movement of electrons and therefore to the formation of temporary guanine radicals that, upon reactions with water, can be converted to oxidative damage. The possibility of an induction of electric currents in DNA was already shown *in vitro* on short double stranded DNA pieces [77, 78] and over long distances in DNA oligomers with guanine as thermodynamic sink for a positive charge [79].

Another popular hypothesis is an influence of the EMF on the structure and function of proteins that contribute to DNA metabolism. An impact of electromagnetic fields on enzymatic turnover has already been shown [80-82]. The activity of the transmembrane proteins Na,K-ATPase and cytochrome oxidase, for instance, is increased upon ELF exposure with 10µT fields between 1-2500Hz and the effect varies with the frequency applied [82]. Resonance as a mechanism of an influence on enzymes with turnover rates close to the applied frequency is therefore a possible scenario. It was also shown that chemical reactions can be influenced directly by electromagnetic fields. The Belousov-Zhabotinski (BZ) reaction (the oxidation of malonic acid in the presence of bromide, bromate, and an inorganic redox catalyst such as the Fe^{+2}/Fe^{+3} couple) was found to be accelerated upon exposure to ELF fields [83]. Moreover chromatin condensation in response to ELF and RF exposure was revealed in blood cells from healthy and EMF hypersensitive persons [84]. About half of the tested samples were positive, regardless of their hypersensitivity status.

It is so far not known, to what extent the mechanisms proposed for ELF-EMF effects on DNA also apply to possible RF-EMF effects. The frequency in the RF range is by far too high, for instance, to interfere with enzyme turnover. However in todays applications of RF-EMFs these waves are modulated to carry information (Figure 3a), e.g. in amplitude or frequency. In mobile phone communication for example different modulations are applied, which add 2, 8, and 217Hz ELF components to the GHz field. Hence, these modulations add low frequency components to the RF-EMF, which then could be responsible for biological effects. Radiofrequency fields do not penetrate tissues as deep as ELF fields do. The higher the frequency, the lower is the penetration of the field. There is, however, still penetration, which is illustrated for a phone hand set in Figure 3b. For mobile phone radiation, it is clear that 70% of the energy is absorbed by the first 1-2cm of tissue. Hence, only cells on the surface of the human body are really exposed to the field and the exposure decreases the further away a cell is from the surface. As for an *in vitro* study one would like to assess the

"worst case scenario", the highest environmental exposure value for a surface cell is taken as a reference.

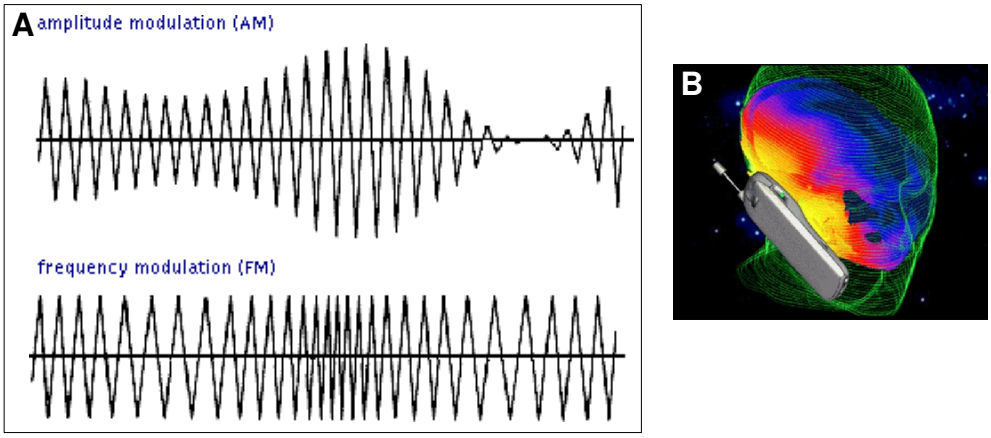

Figure 3. Radio frequency electromagnetic fields.

A) Schematic presentation of an amplitude modulated carrier wave (top) and a frequency modulated carrier wave (bottom). **B)** Computer simulation of a typical mobile phone radiation within the head of a person. Colour range from yellow (highest energy absorption) to blue (lowest energy absorption). Adapted from www.it is.ethz.ch.

2.2. DNA damage and repair

Omnipresent chemical and physical agents generate various types of damage to the DNA of living cells. To deal with this damage nature has evolved diverse and specific repair mechanisms. If repair fails or the amount of DNA lesions exceeds allover repair capacity, there are further possibilities to rescue the cell or the body like cell cycle arrest and apoptosis. Numerous signaling pathways are involved in decisions for cell cycle arrest, repair and/or apoptosis.

2.2.1. DNA damage

2.2.1.1. Endogenous sources

DNA damage of endogenous origin represents a major challenge to cells. Experimental evidence suggests that the number of lesions is about 30 000 per human cell in a day. Such lesions occur spontaneously through reactions of the DNA with oxygen, water or cellular metabolites [85]. This can involve the sugar-phosphate backbone of the DNA or DNA bases.

Hydrolytic DNA damage: A frequent form of damage is hydrolytic base loss (depurination/-pyrimidination) resulting in abasic sites (AP-sites), whereby depurination is 20x more

frequent than depyrimidination. These lesions are potentially both cytotoxic and mutagenic, especially when not repaired until DNA replication.

Deamination damage: Another frequent form of DNA damage is the spontaneous deamination of the exocyclic amino group in cytosine, adenine, guanine and 5-methylcytosine resulting in uracil, hypoxanthine, xanthine and thymine, respectively. Cytosine and 5-methylcytosine deamination are biologically important as these are relatively frequent events that can even occur enzymatically, e.g. during antibody gene hypermutation [86]. Deamination products have the potential to be mutagenic, as uracil and thymine would pair with adenine during DNA replication, hypoxanthine with cytosine. Xanthine does not pair efficiently with any of the bases and would therefore lead to a replication block.

Oxidative damage: Many metabolic processes produce potentially harmful intermediates that are able to react with DNA. Reactive oxygen species (ROS) are thereby the most abundant products and do not only react with DNA but also with lipids and proteins [87]. ROS are constantly generated as by-products of aerobic metabolism, such as in the electron transport chain and cells use multiple systems of antioxidant defense and damage removal to protect themselves against potential harmful consequences of these agents. The hydroxyl radical (·OH) is the most reactive of the primary ROS, but due to its high reactivity it never diffuses more than one or two molecules in diameter before reacting with a cellular component. So to damage DNA, it has to be produced directly next to it. However, diffusion through the cell can occur through H_2O_2, which is mainly generated as a side product of the respiratory chain in mitochondria and is able to react with a metal ion in the so called Fenton reaction ($Fe^{2+} + H_2O_2 \rightarrow Fe^{3+} + \cdot OH + {}^{-}OH$ [88]) in the vicinity of DNA. Another ROS, the superoxide radical ($\cdot O_2^-$) is not very reactive with DNA but has the potential to be converted into H_2O_2 too, or to reduce Fe^{3+} (which would be needed for Fenton reactions). It also reacts with NO· (produced by nitric oxide synthase) to produce $ONOO^-$, a diffusible anion that leads to a complex pattern of DNA damage involving mainly guanine oxidations [89]. Another mechanism for the action of ROS is through lipid peroxidation, where ROS can abstract electrons from residues of organic macromolecules and therefore initiate chain reactions that result in damage at considerable distances from the original event, which could also be DNA [90]. In general, the two main modes of DNA attack by ROS are addition to the double bonds of DNA bases (resulting e.g. in thymine glycol or 2,6-diamino-4-hydroxy-5-formamidopyrimidine (FaPy)) and hydrogen abstraction from the deoxyribose sugar units

(producing carbon-centered radicals on the sugar which can be transformed into strand breaks) [91]. The biologically most relevant oxidative lesion in DNA is guanine with a saturated imidazole ring, 7, 8,-dihydro-8-oxoguanine (8-oxoG). 8-oxoG is potentially mutagenic by pairing with adenine during replication.

Alkylation damage: A second group of metabolically derived DNA damaging agents are alkylating agents like S-adenosylmethionine (SAM) or reactive alkyl radicals as products of lipid peroxidation. The resulting lesions are described in the exogenous damage section (see 2.2.1.2.).

Polymerase errors: Another source of DNA alterations are replication errors occurring by incorporation of incorrect bases and resulting in mismatches. The rate depends on the fidelity of the polymerase involved and although replicative polymerases have a proofreading ability, there is a low amount of errors that escape proofreading.

2.2.1.2. Exogenous/environmental sources

Ionizing radiation: A constant exogenous source of DNA damage is ionizing radiation (IR). Cosmic radiation and radionuclides occur naturally in our environment and body internal decay of radionuclides (mainly potassium-40) is also occurring. Artificial sources of IR like the X-rays used in medical diagnostics and radiopharmaceuticals can increase the effective dose a person is exposed to. Ionizing radiation causes damage to all cellular components and induces a variety of DNA lesions by both direct and indirect ionization [92]. Ionization of water molecules is the most relevant reaction (as water is the most abundant molecule) and leads to the formation of hydroxyl (·OH), superoxide ($\cdot O_2^-$) and H· radicals and H_2O_2, which then lead to oxidative DNA damage as discussed in 2.2.1.1. In addition to simple radical damage, ionizing radiation can also induce ring-saturated derivatives of bases (like thymine glycol), base-dimerisation, protein-DNA cross-linking as well as DNA single- and double strand breaks resulting from direct and indirect attacks to the sugars in the DNA backbone.

Ultraviolet (UV) light: the ultraviolet component of sun light is another important source of DNA damage. The UV spectrum is subdivided into three parts according to wavelength: UV-A (320-400nm), UV-B (295-320nm) and UV-C (100-295nm). Solar UV radiation is mainly composed of UV-A and UV-B, because the ozone layer in the stratosphere prevents penetration of wavelengths below 300nm. The most frequent lesion of DNA exposed to UV is the cyclobutane pyrimidine dimer (CPD), a covalent linkage between adjacent pyrimidines,

predominantly involving thymidines [93]. CPDs are very stable and lead to bending of the DNA. They also interfere with base pairing during DNA replication, because correct hydrogen bonding cannot be established. To a lesser extent, UV radiation leads to the generation of (6-4)-photoproducts (6-4PPs), a lesion that also involves pyrimidine dimerisation (mainly TC and CC pairs). 6-4PPs are chemically less stable than CPDs, but have more helix distorting effects [94]. Other pyrimidine lesions can be 5,6,-dihydroxydihydrothymine (thymine glycol) or pyrimidine hydrates. Purine lesions (e.g. 8,8-dihydro-di-adenine or 8-(2-hydroxy-2-poropyl)guanine) have also been identified [95], but they are less well characterized and seem to play a minor role in the damage spectrum of UV light. To a minor extent UV-irradiation induces DNA-DNA interstrand and DNA-protein cross-links as well as DNA single-strand breaks. Finally, UV generates oxidative damage such as 8-oxoG via the action of cellular photosensitizers like thymine or riboflavin.

Alkylating agents: Many different chemicals damage DNA, a property frequently used in cancer therapy. An important group are the alkylating agents, such as methyl methane sulfonate (MMS), N-methyl-N´-nitro-N- nitrosoguanidine (MNNG), Mitomycin C and Cisplatin, the latter two being in use as anticancer drugs [96]. Environmentally occurring alkylating agents include methyl chloride and streptozotocin. Some substances have to undergo metabolic activation to become reactive, e.g. benzo[a]pyrene or aflatoxins, which are activated by the action of the cytochrome P-450 system [97, 98]. Alkylating agents react with nucleophilic centers in macromolecules. Numerous reaction sites were identified in all DNA bases with the N7 position of guanine and the N3 position of adenine being the most reactive [99]. Alkylated bases can be mutagenic and/or cytotoxic. Bifunctional alkylating agents like cisplatin can react with two nucleophilic centers and, if these are in opposite DNA strands, may generate inter-strand cross-links (ICLs). ICLs are a biologically important class of damage, because they result in complete block of DNA replication and transcription. Psoralens, a group of DNA intercalating substances, can react with two pyrimidines upon UV-A radiation and therefore also cross-link both DNA strands [100]. Alkylating agents can also cross-link DNA with proteins. Topoisomerase inhibitors like camptothecin and etoposide also produce DNA-protein (in this case the topoisomerase) cross-links as well as DNA strand breaks [101]. Some other chemicals also act by causing strand breaks in DNA through a free-radical based mechanism, e.g. the anticancer drug bleomycin or a group of antibiotics called enediynes [102].

2.2.1.3. 5-fluorouracil

5-fluorouracil (5-FU) is a drug widely used for treatment of cancers, including colorectal and breast cancer, but also head and neck cancers and cancers of the aerodigestive tract [103]. It was developed in the late fifties as an antimetabolite that inhibits DNA synthesis [104]. Today it is mostly used in combination with other chemotherapeutics or radiotherapy to improve tumor response rates. 5-fluorouracil is an analog of uracil with a fluorine atom at its C-5 position.

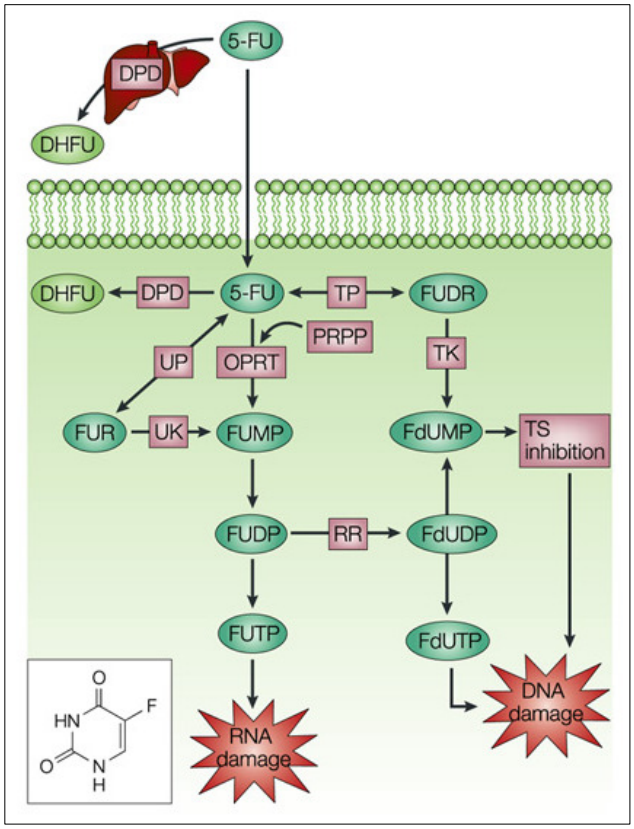

Figure 4. 5-fluorouracil (5-FU) metabolism.

80% of 5-FU are catabolized in the liver by dihydropyrimidine dehydrogenase (DPD). The remaining 20% are converted into three main active metabolites: 1. fluorodeoxyuridine monophosphate (FdUMP) by thymidine phosphorylase (TP) and thymidine kinase (TK), which leads to thymidilate synthase (TS) inhibition; 2. fluorouridine mono (-di, and –tri) phosphate (FUMP) by the action of orotate phosphoribosyltransferase (OPRT), this can become incorporated into RNA, disrupting normal RNA function and processing. 3. fluorodeoxyuridine triphosphate (FdUTP) by ribonucleotide reductase, this can (like dUTP) be incorporated into DNA, leading to DNA damage and mispairing during replication. Adapted from Longley *et al.*, 2003 [105].

Intracellularly 5-FU is converted to several different metabolites (Figure 4) [105]. Orginally, 5-FU was thought to act only as an inhibitor of thymidilate synthase (TS) after conversion to fluorodeoxyuridine monophosphate (FdUMP) by thymidine phosphorylase (TP) and thymidine kinase (TK). Since TS catalyzes the conversion of deoxyuridine monophosphate (dUMP) to deoxythymine monophosphate (dTMP), TS inhibition leads to cellular depletion of dTTP that is used in DNA replication and repair, accumulation of dUMP and through feedback mechanisms to an imbalance of the whole nucleotide pool. This imbalance is thought to severely disturb DNA synthesis resulting in cell lethality.

These DNA directed effects are not the only consequences of 5-FU anabolism. The drug is also converted to fluorouridine mono (-di, and –tri) phosphate (FUMP) by the action of orotate phosphoribosyltransferase (OPRT) and eventually becomes incorporated into RNA, affecting normal RNA function and processing [105]. But FUDP can also be converted to fluorodeoxyuridine triphosphate (FdUTP) by ribonucleotide reductase and can (like dUTP) be incorporated into DNA [105].

When used as anticancer drug, response to 5-FU varies. Increased sensitivity or resistance to 5-FU can be due to different mechanisms, involving either altered expression of targets like TS or catabolizing enzymes like DPD or altered expression of processing proteins like TP and TK. Also changes in repair pathways that process DNA aberrations induced by 5-FU can contribute.

Different repair pathways seem to be involved in the repair of 5-FU mediated DNA damage depending on the kind of lesion and the cell cycle status. Base excision repair (BER, see 2.2.2.4.) involving the uracil removing glycosylases uracil-DNA-glycosylase (UNG), thymine-DNA-glycosylase (TDG) and single-strand selective monofunctional uracil-DNA glycosylase 1 (SMUG1) as well as the mismatch repair system (MMR, see 2.2.2.2.) seem to play a role.

2.2.2. DNA repair

Depending on the type of DNA damage, cells employ different ways of repair. Single strand excision of the damage and resynthesis from the undamaged strand is used when the damage affects only one of the complementary strands, homology dependent or independent sealing is used when double strand breaks (DSB) occur, and in some cases damage tolerance pathways are engaged.

2.2.2.1. DNA Double strand break repair

A rare but dangerous lesion for the cell is a DNA double strand break (DSB). DSBs can cause from ionizing radiation, the impact of DNA reactive chemicals (including cancer drugs like Bleomycin) or can arise during DNA replication of single strand breaks. There are two different ways to repair such lesions: Homologous recombination (HR) and non-homologous end-joining (NHEJ) (Figure 5) [106].

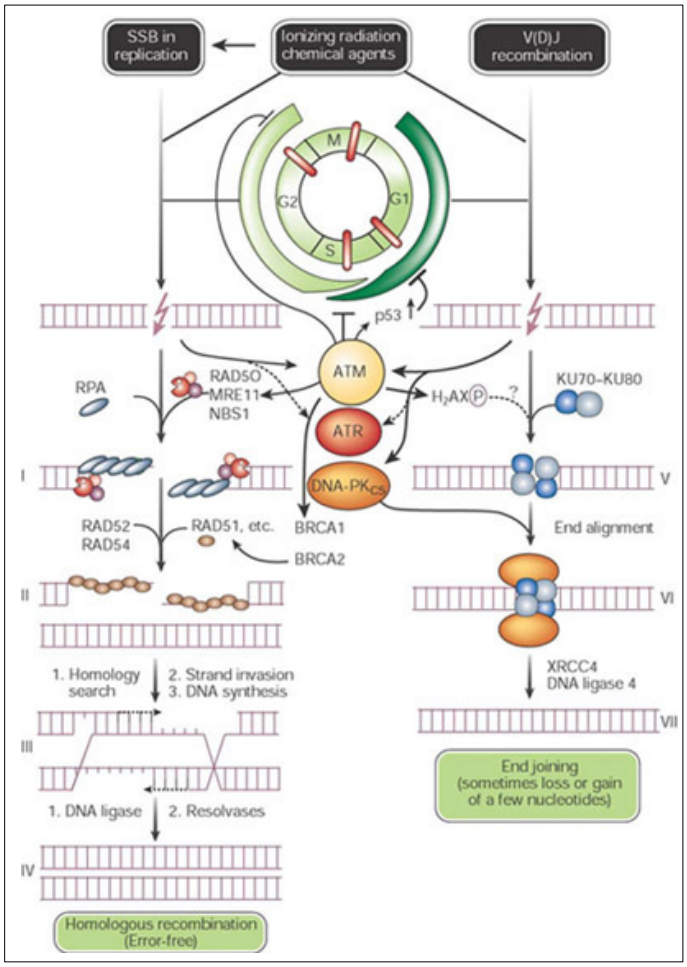

Figure 5. Double strand break repair pathways.

Double strand breaks arising from ionizing radiation, chemicals, V(D)J recombination and/or single strand break replication result in activation of the homologous recombination (left) or the non-homologous end-joining (right) pathway. In HR, DSBs are recognized by ATM and the MRN complex, which exposes the 3´ends for RPA/Rad52 facilitated Rad51 binding. Strand invasion into homologous regions and DNA synthesis follows to produce D-loops. Holliday junctions form and are then resolved by resolvases. NHEJ (mainly used in G1) starts with binding of the Ku70/Ku80 heterodimer, DNA-PK then associates to build the active kinase, one target is the XRCC4/ligase 4 complex, which ligates the break. Adapted from Hoeijmakers *et al.*, 2001 [4].

In late S and G2, when an identical copy of each DNA duplex is available, the error free HR pathway is preferred, but in G0/G1 the more error prone NHEJ pathway prevails. The two Phosphatidyl-inositol-3-OH-kinase-like kinases ATM (Ataxia teleangiectasia mutated) and ATR (ATM related) and DNA-dependent protein kinase (DNA-PK) are critical for the proper cellular response to DSBs. They transduce DNA damage signals and phosphorylate numerous substrates like histone H2AX and the MRN complex (consisting of the three proteins MRE11, RAD50 and NBS1), altogether coordinating the repair process and/or cell cycle responses.

In HR, the MRN complex first resects one strand of both ends in 5´-3´ direction and the resulting 3´ overhang is covered by several Rad51 units building a nucleoprotein filament. This step is mediated by RPA (replication protein A) and Rad52. Rad51 then promotes ATP-dependent and RPA-stimulated interaction with the undamaged homologous DNA duplex and catalyses strand invasion to form a D-loop structure. The homologous region is used as a template for DNA synthesis and the resulting Holliday-junctions are cleaved by resolvases. HR also seems to be involved in the repair of another very toxic lesion, the interstrand cross-link (see 2.2.1.2). The damage sensors of this lesion are not known so far, but seem to require factors from other DNA repair pathways like nucleotide excision repair and mismatch repair [107].

NHEJ is initiated by binding of the Ku70/Ku80 heterodimer to the end of the DNA break, followed by recruitment of the catalytic subunit of DNA-PK to form the active holoenzyme. One of the targets of the kinase is XRCC4, which together with DNA ligase IV links duplex DNA molecules with non-complementary ends. To facilitate ligation, most DSB have to be processed. This is done by either of the nucleases provided by the MRN complex (3´flaps), FEN1 (5´flaps) or Artemis (5´ and 3´ overhangs). Occasionally, a few nucleotides are gained ore lost during NHEJ, which also implies the involvement of DNA polymerases and/or nucleases.

There are several human diseases known to be caused by defects of proteins involved in DSB repair, e.g. Ataxia telangiectasia (defects of ATM), Nijmegen breakage syndrome (mutations in NBS1) or Bloom Syndrome (defects of Bloom helicase). All of them display hypersensitivity to DNA damaging agents and tumor susceptibility, but there can be also neurodegenerative and immunological diseases [108], the latter caused by defects in V(D)J recombination or immunoglobulin class switch recombination.

2.2.2.2. Repair of DNA polymerase errors and DNA damage tolerance

The postreplicative mismatch repair (MMR) system is responsible for the removal of mispairing bases resulting from DNA polymerase errors during DNA replication. It may also contribute to the removal of oxidized, methylated and deaminated bases and of chemically induced DNA lesions such as photoproducts or intrastrand cross-links [106]. Recognition of the mismatched base is thereby carried out by the MutSα complex, that consists mainly of MSH2 (MSH stands for MutS Homolog, MutS was first described in bacteria) and MSH6 or MSH3. The two complexes have different substrate spectra. Upon binding to the mismatch, this complex binds ATP and interacts with the MutLα heterodimer, consisting of MLH1 (MutL homolog) and PMS2. Excision of the mispaired base is performed by an exonuclease, such as Exonuclease I followed by DNA synthesis by a replicative DNA polymerase, e.g. Polymerase δ. Recruitment and specific binding of the complexes is facilitated by PCNA (proliferating cell nuclear antigen) [109], a homotrimer which is also involved in the other steps of MMR by interacting with Exonuclease I and Pol δ. How the discrimination between parental and newly synthesized DNA strand is achieved is not entirely clear. A generally accepted hypothesis involves recognition of unligated single strand breaks (SSB) arising during replication through interaction with nick-associated proteins [110]. As these can be separated from the mismatch, either sliding of the protein complex or DNA bending could be involved in identification of the strand to be excised. Regulation of MMR is thought to involve transcriptional as well as post-translational mechanisms, e.g. MSH2 has a p53 binding site in the promoter region and is inducible upon co-transfection with p53 and transcription factors Fos/Jun [111]. A syndrome resulting from defects in mismatch repair is the well known genetic predisposition to colorectal (and other) cancers called Hereditary Nonpolyposis Colorectal Cancer (HNPCC) syndrome, which is responsible for 2-7% of all diagnosed colorectal cancers [112].

If a bulky lesion is not repaired before S-phase, there are two possibilities for the cell to overcome the resulting replication block. In normal replication, proliferating cell nuclear antigen (PCNA) builds a homotrimeric sliding clamp around DNA and interacts with and coordinates many essential replication proteins including pol δ/ε, Ligase I, Helicase E1 and the clamp loader replication factor C (RFC). If replication is blocked, the chromatin-bound protein Rad17 gets phosphorylated by ATR and recruits the 9-1-1 heterotrimeric sliding clamp to replace PCNA. This complex then targets repair proteins to the site of the lesion

[113]. Another possibility is mono-ubiquitination of PCNA, which then can interact with the so called “error-prone” DNA polymerases (e.g. pol η, κ, μ), that are able to replicate across a lesion but with high probability of creating a mutation. This pathway is called translesion synthesis. The different polymerases have different lesion-specificities and are therefore able to replicate across different kinds of lesions [114].

2.2.2.3. Repair of bulky DNA damage

The nucleotide excision repair (NER) pathway enables cells to eliminate bulky DNA adducts like UV-light induced 6-4PPs and CPDs or chemically induced adducts such as those generated by aflatoxine or benzopyrene, as well as intrastrand cross links. There are two different NER subpathways: global genome repair (GGR), which acts independently of transcription and removes larger adducts like 6-4PPs effectively, but less DNA distorting adducts like CPDs only slowly. These lesions are removed more effectively by the other subpathway, which is called transcription coupled repair (TCR). TCR removes RNA-polymerase-blocking lesions from the transcribed strand of active genes [115].

In GGR the lesion is detected by the XPC-HR23B complex (XP from Xeroderma Pigmentosum) or by the RPA-XPA complex facilitated by DDB1/2 (DNA damage binding), but the question who comes when is still a matter of debate [116]. The transcription factor complex TFIIH, which consists of seven different proteins, including the helicases XPB and XPD, is then recruited to the site of DNA damage and mediates unwinding. This makes the DNA accessible for the two exonucleases XPF-ERCC1 (5´) and XPG (3´), which cleave ~28nt around the lesion. Resynthesis is carried out by pol δ or pol ε and ligation by ligase I. Some of the genes are inducible upon UV radiation (mediated by p53) like DDB2 and XPC. A human syndrome based on a defect in GGR is Xeroderma pigemtosum (XP). XP is characterized by severe UV sensitivity with a high incidence of skin tumors. It can occur in several of the proteins involved [117].

In TCR the two factors CSA and CSB (CS: Cockayne´s Syndrome) detect a stalled transcription elongation complex and induce ubiquitination of RNA polymerase (II) which leads to release of the complex [118] from DNA. As in the case of GGR incision is performed by the exonucleases XPG and XPF-ERCC1, synthesis by pol δ or pol ε and ligation by ligase I, after which restart of transcription can follow. CS patients suffer from growth retardation, UV sensitivity and accelerated aging but not from elevated tumor incidences, possibly because

affected cells are effectively removed by apoptosis [119]. Because of the coupling to active genes and the reduced transcription upon UV irradiation TCR deficiency is also referred to as a “transcription syndrome”. Another syndrome based on TCR deficiency is the so-called UV-sensitive syndrome, which does not belong to the CS complementation groups and does not show the developmental defects of CS, but only sensitivity to UV [120].

2.2.2.4. Repair of small DNA lesions and single-strand breaks

For smaller lesions affecting one nucleotide only there are different possibilities of repair: the simplest process is direct damage reversal. It takes place e.g. for O6-methylguanine by transfer of the methyl group from the O6-position of guanine to an active site cysteine residue in the O6-methylguanine-DNA methyltransferase (MGMT) in a one-step reaction. This transfer leads to irreversible inactivation and targeting of MGMT to ubiquitination and proteasomal degradation [121]. Other alkylation-removing proteins belong to the AlkB homologue group and have been shown to repair 1-methyladenine, 3-methylcytosine and 1-ethyladenine [122].

Small DNA base lesions, however, are generally fixed by the base excision repair (BER) pathway (Figure 6) [123]. This pathway repairs abasic sites, DNA single-strand breaks and a wide spectrum of oxidized, deaminated and alkylated DNA bases. Recognition of base damage is carried out by DNA glycosylases. These enzymes are specialized for certain kinds of damage, e.g. OGG1 for 8-oxoG, MPG for different alkylated guanines and UNG for Uracil [124]. There are two classes of glycosylases. Monofunctional DNA glycosylases (e.g. UNG, MPG) remove the modified base leaving an abasic site (AP site), while the bifunctional enzymes (e.g. OGG1) also cleave 3´ to the AP site after base removal. The resulting 3´ overhang is then trimmed by AP endonuclease (APE1) and the gap is filled by DNA Polymerase β (DNA Pol β) [125]. For the monofunctional glycosylases cleavage of the phosphodiester-bond is carried out by APE1 resulting in a 3´OH and a 5´deoxyribose-phosphate (5´dRP) end. This overhang can be removed by the lyase activity of DNA Pol β after incorporation of the missing single nucleotide [126]. The nick is then sealed by DNA Ligase III, which interacts with DNA Pol β through the XRCC1 protein. This subpathway generated short repair patches. If DNA Pol β is not able to remove the 5` overhang, because it is distorted (e.g. 5'-oxidized AP sites induced by ROS), it dissociates from the lesion and DNA synthesis of 2-10nt is accomplished by DNA Pol δ or Pol ε together with PCNA, PARP

and RFC [127]. The resulting oligonucleotide overhang is then excised by the structure specific flap endonuclease FEN1 and the nick is sealed by DNA Ligase I (long patch BER).

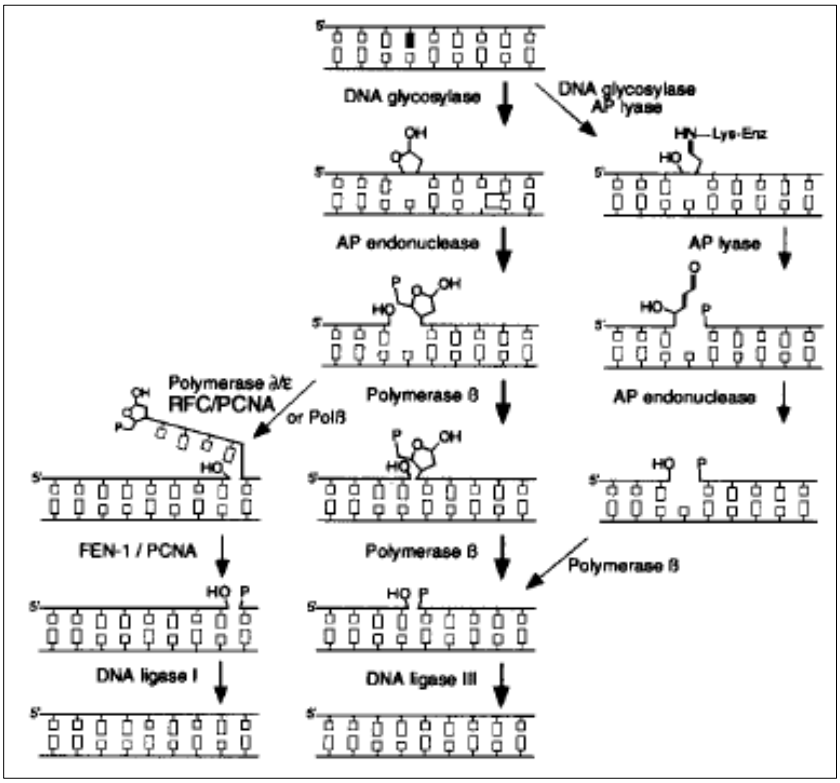

Figure 6. Base excision repair pathways.

In short patch BER (center), which is the predominant pathway, excision of the lesion by a glycosylase or spontaneous base loss generates an abasic site, which is processed to a single strand break by AP endonuclease. Polymerase β adds one nucleotide and removes the 5´ overhang by its β-lyase activity and the XRCC1/ligase III complex seals the nick. If a bifunctional glycosylase initiates BER (right), it cleaves 3´ to the AP site after base removal and the 3´ overhang is processed by AP endonuclease. Gap filling and ligation are carried out by pol β and XRCC1/lig III as before, but there is no trimming by pol β. In long patch BER (left) pol δ/ε synthesizes 2-10nt supported by RCF, PCNA and PARP, the overhang is excised by FEN1 and the nick is sealed by DNA Ligase I. Adapted from Schärer and Jiricny, 2001 [124].

Mouse knock outs of the key base excision repair proteins downstream of the DNA glycosylases are all embryonic lethal, as described for Apex1, Pol β, Xrcc1 and Lig1 [128], while glycosylase knock out animals show no or mild phenotypes in hypersensitivity to DNA damaging agents. There seems to be some redundancy among these enzymes or overlap with other pathways like TCR.

2.2.2.5. Regulation of base excision repair

Repair pathways are regulated in numerous ways at levels of gene or protein expression or activity and localization of enzymes. In base excision repair for example, p53 stimulates the pathway through its interaction with APE1 and DNA Pol β [129]. AP endonuclease activity at AP sites is furthermore enhanced by its physical interaction with heat shock protein 70 (HSP70) [130]. Other examples of proteins interacting with and modulating BER enzymes are: the MMR complex MSH2/6 interacts with and stimulates the adenine DNA glycosylase MYH [131]; the NER endonuclease XPG promotes binding of thymine glycol DNA glycosylase to its substrate [132]; the NER recognition factor XPC stimulates thymine DNA glycosylase (TDG) activity [133]. The latter are also examples for an interplay between repair pathways.

Regulation can also occur by protein modification. The SUMOs (small ubiquitin-like modifiers) seem to play an important role in this pathway, as some of its proteins are modified by them, e.g. PCNA [134], TDG [135], XRCC1 and PARP [136]. Others interact non-covalently with SUMO/SUMO-modified proteins like Uracil DNA glycosylase (UNG), TDG and XRCC1. But there are also other types of posttranslational protein modification that play a role in this pathway, namely phosphorylation, acetylation, ubiquitination, nitrosylation and methylation. For example nitrosylation of OGG1 inhibits its glycosylase activity [137] and acetylation of FEN1 reduces its substrate binding and nuclease activities [138].

2.2.2.6. Thymine DNA Glycosylase

The products of cytosine- and 5-methylcytosine- deamination, uracil and thymine, have to be repaired correctly to avoid mutation during DNA replication. While uracil can be recognized as a foreign base in DNA, thymine represents a normal DNA base and, thus, has to be recognized by virtue of its mispairing with guanine. The BER enzyme that is able to do this was isolated in the early 1990s from HeLa cells and named thymine DNA glycosylase (TDG) [139]. Later it was shown that this enzyme can also recognize uracil opposite guanine (like three other known glycosylases UNG, MBD4 and SMUG1) and process this lesion with even higher efficiency. TDG also processes modified uracils including 5-hydroxymethyluracil or 5-fluorouracil (5-FU) as well as ethenoadducts (a product of lipid peroxidation) and thymine glycol. Although TDG prefers guanine as opposite base, some of these lesions (like uracil, 5-FU and ethenoadducts) are also recognized and processed when they are opposite adenine, albeit with lower efficiency [140].

Orthologs of TDG were found in bacteria, yeast, drosophila, xenopus and mouse [140, 141]. Their common domain structure consists of a conserved core domain harboring the active site and non-conserved N- and C-terminal extensions of variable length, which are responsible for differences between the orthologs in substrate specificity, enzymatic activity and interaction partners (Figure 7) [142].

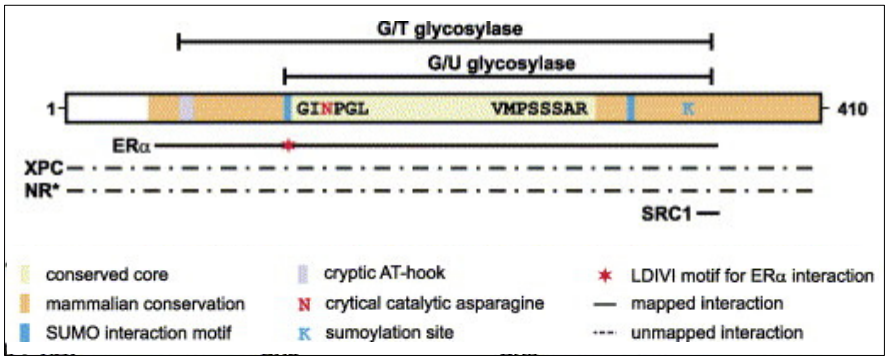

Figure 7. Domain structure protein interaction map of human thymine DNA glycosylase (TDG).
Conserved sequences, protein motifs and known interactions with other proteins are indicated. The sequence motifs G(I/L)NPG(L/I) and VMPSSSAR (hsTDG) contain critical residues of TDGs active site. Similarities in the N- and C-terminal parts of the mammalian TDGs are restricted to the SUMO-interaction motifs and the SUMOylation consensus motif VKEE. Bars on top show the minimal sequence requirement for G·U or G·T processing. The predicted AT-hook motif present in the N-terminus may provide non-specific DNA binding capacity. Bars at the bottom TDG indicate identified protein interaction domains. NR: nuclear receptors (androgen receptor, glucocorticoid receptor, progesterone receptor, peroxisome proliferator-activated receptor a, thyroid hormone receptor a, Vitamin D3 receptor). Adapted from Cortazar *et al.*, 2007 [142].

TDG is a monofunctional DNA glycosylase which, like all DNA glycosylases, acts by flipping out the substrate base from the DNA double helix for processing. Additionally, it interacts with the guanine (adenine) opposite the target base through hydrogen bonds mimicking Watson-Crick base pairing [143, 144]. Furthermore, the N-terminal domain makes unspecific DNA contacts. Together, these interactions seem to be quite strong and prevent TDG from turning over following base excision [144]. So, there is need for a factor releasing TDG from the AP-site, which could be APE1, the enzyme catalyzing the downstream step in the BER process. Indeed, APE1 was shown to be able to release TDG *in vitro*, but only when provided in a high molar excess over TDG [145], suggesting this to be passive rather than active. As already mentioned, TDG is modified by SUMO in the C-terminal domain and it was shown, that this interaction induces a conformational change, which allows the enzyme to dissociate

from the AP-site [146]. These findings lead to the concept that after base hydrolysis, SUMO modification is responsible for TDG release from the AP-site. As this modification is reversible, deSUMOylation by specific isopepdidases can recycle the enzyme for another round of repair [147].

Surprisingly for a glycosylase, TDG also seems to play a role in regulation of gene expression. Various physical and functional interactions of TDG with transcription factors and nuclear receptors were reported, e.g. retinoic acid receptors, c-Jun, estrogen receptor α or CREB binding protein [148-151]. It has also been hypothesized that TDG is involved in epigenetic changes of the genome, as the chicken homolog seems to be able to actively demethylate 5-methyl-cytosines (5-meC) in CpG islands [152, 153]. This function is not entirely clear though, as the recombinant protein has no or only poor activity on 5-meC and there seems to be no global demethylation through overexpression. Specific auxiliary factors (e.g. the transcription factors?) might be needed to target the protein to specific sites in the genome. Furthermore an interaction of TDG with de-novo-methyltransferase Dnmt3a was recently reported [154], which could implicate a role of this glycosylase in DNA methylation.

2.2.2.7. DNA Polymerase β

One of the differentially modified enzymes of the BER pathway is DNA Pol β, a small, one subunit DNA polymerase [155]. It belongs to the X-family of polymerases [156] and has two different enzymatic activities: it synthesizes short patches of DNA (up to 6 nt) and removes 5´dRP residues through its β-lyase activity. This lyase activity resides in the 8kDa aminoterminal domain of the protein (Figure 8) and is connected to the 31 kDa polymerase domain by a protease sensitive hinge region [157].

In contrast to the large replicative polymerases of the B-family, Pol β has no inherent proofreading and exonuclease activity and is therefore less accurate in DNA synthesis. Knock-out mice deficient in Pol β are not viable, they die at embryonic day 10.5, and fibroblast cell lines derived from these embryos show hypersensitivity towards DNA alkylating agents, but not towards UV, γ-radiation, H_2O_2 or Cisplatin [125]. Regulation of the polymerase activity was shown to occur through phosphorylation [158] and the β-lyase activity is modulated by acetylation of the active lysine residue by the transcriptional coactivator p300 [159].

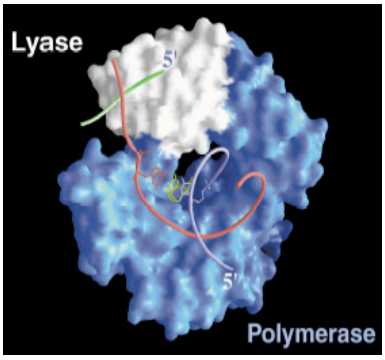

Figure 8. DNA polymerase β. Crystallographic structure for DNA polymerase β complexed with a gapped DNA substrate. Image prepared using GRASP software (Graphical Representation and Analysis of Structural Properties) [160]. Lyase domain in white and polymerase domain in blue. Adapted from Idriss *et al.*, 2002 [157].

2.3. Cell cycle

The life of a cell begins with division from a mother cell and ends with the subsequent division into daughter cells or with its death. The phases through which the cell passes from one cell division to the next is called the cell cycle. In general, the cell cycle can be divided into four main phases (Karp, 2002) (Figure 9). In G1, cells grow and carry out normal metabolism, they harbor an unreplicated copy of each chromosome. In S-phase, cells duplicate their genome (Replication). In G2, cells grow and duplicate organelles and control DNA integrity. Sister chromatids of each chromosome exist, which are distributed equally to the two daughter cells in Mitosis (M). Mitosis is again divided into four different phases: In Prophase, the chromosomes condense, the cytoskeleton, golgi and endoplasmatic reticulum (ER) disassemble, the nuclear envelope disperses and the mitotic spindle is assembled. In Metaphase, the microtubules attach to the kinetochores of the chromosomes and position them at the spindle equator. In Anaphase, centromeres split and chromatids separate and move to opposite spindle poles. In Telophase, the nuclear envelope, golgi and endoplasmatic reticulum of the daughter cells form and chromosomes become dispersed again.

At the so called restriction point in G1, cells are committed to go through another round of the cell cycle. If the conditions for another cell division are not given (e.g. lack of nutrients), the cell enters G0, a nonproliferative phase during which growth, differentiation or apoptosis may occur.

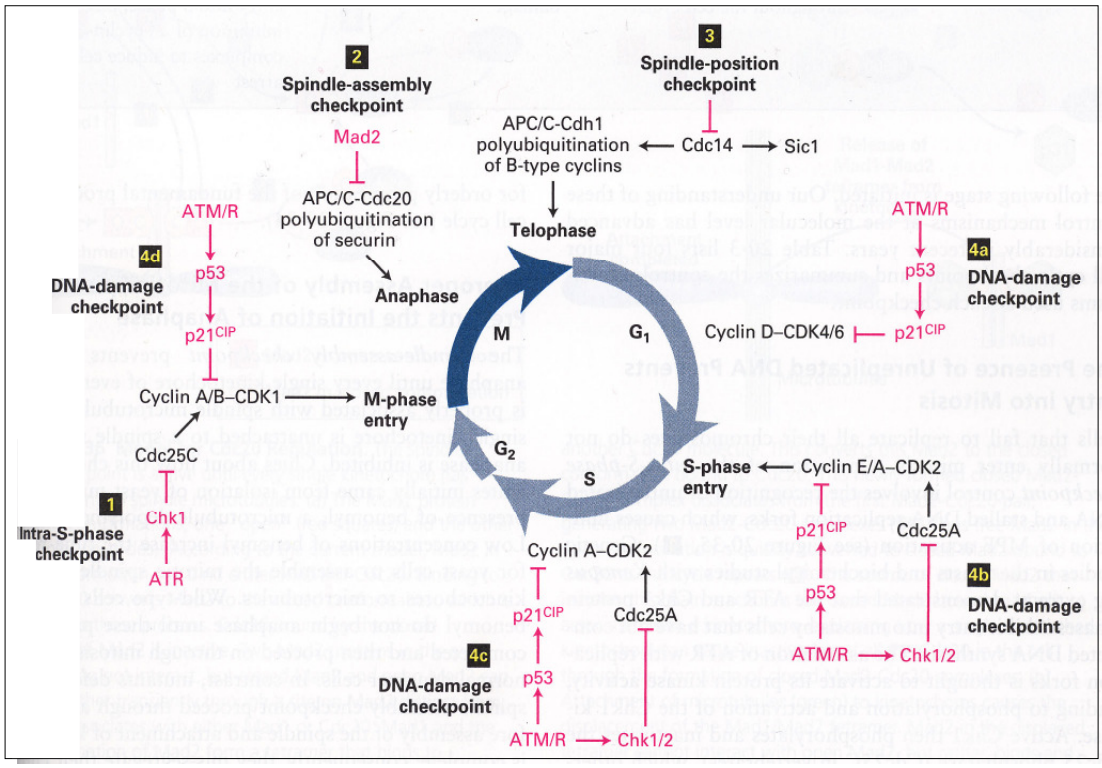

Figure 9. Cell cycle and checkpoints.

Different cell cycle phases (G1, S, G2, M) and related cyclin/cdk complexes. Additionally shown are the respective cell cycle checkpoints with the proteins involved. Adapted from Lodish, 2006.

The cell cycle is tightly regulated, as any error (e.g. unbalanced distribution of chromosomes) could lead to major problems for the organism. Regulation occurs by a family of cyclin proteins that act as regulatory subunits of the cyclin-dependent kinases (cdk). The activity of the cyclin/cdk complexes is controlled by the expression of the appropriate cyclins during a specific phase of the cell cycle (Figure 9). The cyclin/cdk complex is then activated by sequential phosphorylation/dephosphorylation steps mainly affecting the cdk subunits. The complex of early G1 is either cdk2, cdk4, or cdk6 bound to a cyclin D isoform. There are several proteins that can inhibit the cell cycle in G1. For example, if DNA damage occurs, p53 accumulates in the cell and induces a p21-mediated inhibition of cyclin D/cdk. Mdm2, by facilitating the nuclear export and inactivation of p53, becomes part of an inhibitory feedback loop that inactivates p21-mediated G1 arrest [161]. If the cyclin D/cdk complex is inhibited, the retinoblastoma protein (Rb) is in a state of low phosphorylation and is tightly bound to the transcription factor E2F, inhibiting its activity. E2F transcription factors regulate the expression of a number of genes important in cell proliferation, particularly those involved in progression through G1 and into the S-phase of the cell cycle. Passage through

the restriction point and transition to S phase is triggered by cyclin D/cdk dependent phosphorylation of Rb [162]. Phosphorylated Rb dissociates from E2F, which is then free to promote expression of DNA replication initiating proteins. Cyclin E/cdk2 accumulates during late G1 phase and triggers the passage into S phase [163]. The synthesis and accumulation of cyclin B/cdc2 begins during S-phase, but the complex is phosphorylated at Thr14 -Tyr15 and kept inactive [164]. Cyclin A/cdk2 accumulates during S phase and its activation triggers the transition to G2, a phase characterized by the accumulation of cyclin B/cdc2. When the cell reaches a critical size, the phosphatase cdc25 is activated and removes the inhibitory phosphate residues at the cdc2 subunit, while the kinase CAK transfers an activating phosphate to residue Thr 161. The resulting activation of the cdc2 kinase drives the cell into mitosis. Cyclin B/cdc2 catalyzes the phosphorylation of lamins and histone 1, and is involved in the regulation of cell division events. The metaphase to anaphase transition is triggered by its inactivation and the proteasomic degradation of cyclin B through the action of the protein ubiquitin ligase APC (anaphase promoting complex). APC is also responsible for the ubiquitination of securin, the inhibitory protein of the protease separin. Separin is then able to cleave the cohesin complex, that holds sister chromatids together from S-Phase until Metaphase. This induces the separation of chromatids and their movement to the poles of the mitotic spindle, after which the mitotic apparatus disappears, the nuclear membranes reform and the nucleoli reappear. During cytokinesis, the cytoplasm divides and the resulting daughter cells enter G1 again.

2.3.1. DNA damage checkpoints

Different DNA damage checkpoints in mammalian cells control the cell cycle at different points (Figure 9) (for review see [165]). If DNA damage is sensed, there is slow down or even arrest of the cell cycle until the damage is repaired. In general, there are damage sensor proteins, which phosphorylate their substrates upon sensing DNA damage, the signal is then transduced by these adaptor and mediator proteins to effector proteins, that can initiate cell cycle arrest, activation of repair proteins or apoptosis.

DNA damage is signaled mainly by the two Phosphatidyl-inositol-3-OH-kinase-like kinases ATM (Ataxia teleangiectasia mutated) and ATR (ATM related). ATM is thought to be engaged predominantly in signaling DNA strand breaks, while ATR is largely responsible for stalled replication forks, although it seems also to compensate partly for ATM function in cells

lacking this kinase [166]. There are other proteins recruited to sites of damage independently of ATM like MDC1, 53BP1, BRCA1 and the MRN complex, which therefore also could serve as damage sensors [167]. But their accumulation into microscopically visible foci then depends on ATM-mediated phosphorylation of the histone H2AX [168]. Also, in the case of stalled replication forks there are additional proteins and complexes recruited, namely the Rad9-Rad1-Hus1 (9-1-1) sliding clamp, ATRIP, RPA and Claspin.

There are two other DNA damage signaling proteins besides the ATM/ATR kinases, which both act throughout the cell cycle: the DNA-PK (DNA-dependent protein kinase) [169] together with the Ku70/Ku80 heterodimer, which are involved in non-homologous end-joining, and the PARPs (poly(ADP-ribose) polymerase), proteins, that catalyse poly(ADP)ribosylation (PAR) from the donor NAD+ at sites of DNA damage. They are able to detect single strand breaks (SSB) as well as double strand breaks (DSB) and contribute to multiple repair pathways [170]. Targets for poly(ADP)ribosylation by PARP are for example XRCC1, p53, XPA, MSH6, DNA-PK and Ku70 [171].

After damage recognition the signal is forwarded by the mediator proteins mentioned above (MDC1, 53BP1, BRCA1, MRN complex) and by transducers like the CHK1 and CHK2 kinases, leading to degradation or inhibition of cell cycle promoting cyclins (e.g. CDC25 phosphorylation by CHK1) to give repair systems time to act before sensitive phases of cell division like replication or mitosis are executed. In addition, DNA repair systems become activated and there is upregulation of different genes through transcription factors like p53, which is stabilized through phosphorylation by ATM and ATR.

Prominent checkpoints throughout the cycle are the G1 checkpoint, mainly mediated by ATM/CHK2 and the G1/S checkpoint, where ATR/CHK1 is more involved and which prevents cells from entering S-phase. The important intra-S checkpoint is able to slow down replication transiently, while the G2/M checkpoint prevents cells from initiating mitosis. Besides DNA damage checkpoints there are checkpoints that assess correct spindle assembly and position during mitosis.

2.3.2. Apoptosis

If the amount of DNA damage is high, repair systems may become saturated and the risk for mutations and, hence, neoplastic transformation of cells increases. Under such conditions cells can enter the so-called programmed cell death or apoptosis pathway, thereby

committing suicide and sparing the organism from the potentially devastating consequences of genetic mutations. Apoptosis is also a normal event during development, e.g. in limb development and during maturation of immune cells, where cells which react to the organism´s own proteins have to be destroyed.

Apoptosis is initiated if survival signals (trophic factors) are absent or if destruction signals are arriving from another cell or are generated within the cell. An important apoptosis activator after DNA damage is p53, whose (normally) rapid proteasomal degradation is inhibited by ATM/ATR-mediated phosphorylation. p53 activates expression of genes that control apoptosis like FAS and the Bcl-2-family members BAX, Noxa and PUMA [172-174], and it is able to repress gene expression of survival factors (e.g. survivin [175]). p53 also translocates to the mitochondria to bind to the antiapoptotic proteins Bcl-2 and Bcl-X_L [176], and mediates the release of histone 1 variant H1.2 from DNA, which then induces cytochrome c release from mitochondria [177]. p53-independent pathways of apoptosis also exist and involve proteins such as CHK2, PML (promyelocytic leukaemia), Nurr77 or the 9-1-1 complex [178-180].

Increase of permeability of the mitochondrial membrane and cytochrome c release, upregulation of proapoptotic and inhibition of antiapoptotic proteins lead to the activation of a cascade of different caspases, through which the signal is amplified. Effector caspases cleave short amino acid sequences in different target proteins, e.g. of the nuclear lamina and the cytoskeleton. Dying cells shrink and condense, DNA is fragmented and membrane vesicles are released which are eventually engulfed by phagocytotic cells. One important marker recognized by these cells is phosphatidylserine, a phospholipid that is translocated to the outer membrane in apoptotic cells [181]. Importantly, the content of the cell is never released to the surrounding medium. This distinguishes apoptosis from necrosis, whereby cells swell and burst and release their intracellular contents, which can damage surrounding cells and cause inflammation.

3. Aims of the thesis

Conflicting results have been published with regard to the genotoxic effects of extremely low frequency (ELF) and radiofrequency (RF) electromagnetic fields (EMFs) [2, 3, 13, 15-17, 20, 21, 61, 63, 66, 68, 69]. This has raised considerable public concern, which led the Swiss National Science Foundation to initiate a national research program ("Nationales Forschungsprogramm NFP 57") with the aim to provide scientific arguments for the assessment of the risk associated with electromagnetic fields. This PhD thesis was initiated as a project of the Forschungsstiftung Mobilfunk (Zürich), supporting independent research, and continued and finalized as part of the NFP57 program.

The objectives of this PhD thesis were:

- to re-examine and validate genotoxic effects of ELF- and RF- EMFs observed, but not reproduced, in previous studies [1, 2, 68],
- to address conceptual and technical shortcomings of previous studies regarding the mode of comet assay scoring and evaluation,
- to explore the molecular events underlying EMF dependent genotoxic effects (oxidative damage or other resulting DNA lesions, cell cycle effects, apoptosis)

For this purpose, I established techniques to assess genotoxicity, DNA damage signaling, cell cycle distribution and apoptosis and applied them to different ELF- and RF- exposed cell lines. Furthermore a set of fluorophore-tagged proteins was constructed as tools to facilitate live cell imaging and therefore real time assessment of ELF-EMF effects.

In addition to the EMF studies, I used the established techniques in collaboration projects to address and/or establish:

- the biological significance of cell cycle regulation of Thymine DNA Glycosylase (TDG),
- the mechanism of DNA directed cytotoxicity of the anticancer drug 5-fluorouracil,
- the role of arginine methylation in the regulation of the base excision repair associated DNA Polymerase β

4. Results

4.1. Biologic effects of electromagnetic fields

4.1.1. Molecular mechanisms that lead to DNA fragmentation under extremely low frequency electromagnetic field exposure (Appendix I)

Electromagnetic fields in the extremely low frequency range were previously found to cause genotoxicity in some studies, but not in others. Because of the considerable public concern about the safety of ELF-EMFs, this study was designed to re-examine the issue and to clarify some of the discrepancies. For this purpose, I performed comet assays analyses applying the same exposure conditions and cell line as in a previous study. I showed genotoxic effects when cells were exposed to an intermittent 50Hz, 1mT ELF-EMF for 15h. These effects were less pronounced than previously published, but nevertheless statistically significant. I then expanded the analyses to other cell lines. Human primary fibroblasts but not HeLa cells were found to have increased comet tailfactors/tail moments when exposed under the same conditions. By blocking the fibroblast cells in G1, I showed that this effect depends on cycling of the cells. Since the effect was not further increased by using an 8-oxoG glycosylase (Fpg) in the comet assay, there seems to be no increase of unrepaired oxidative purine damage after exposure. As the DNA of apoptotic and S-phase cells is also migrating into the tail of the nucleus in the comet assay, I analyzed cell cycle distribution, replication and apoptosis in the fibroblast cell lines. This revealed an about 1% decrease of replicating cells and about 1.5% more apoptotic cells in the fibroblast cell line, which showed the highest comet assay effects. These cells can account for a part but not all of the comet assay effect I measured. There, about 8% of cells were found to shift into the higher fragmentation fraction. Although the possibility of a direct damage of DNA due to ELF-EMF exposure cannot be ruled out, our data suggests that cells entering S-phase under ELF-EMF exposure may encounter replication problems, which eventually leads to the induction of apoptosis and, hence, contributes to highly fragmented nuclear DNA observed by comet assays.

4.1.2. Genotoxic Effects From Radiofrequency Electromagnetic Fields: Revisiting a Controversial Issue (Appendix II)

Two recent scientific publications regarding *in vitro* effects of RF-EMFs received considerable

public attention and concern, because they reported enhanced DNA fragmentation in different human cell lines (ES-1, IH-9 and HW-2 fibroblasts) following exposure to unmodulated and talk-modulated RF-EMF signals [68, 182]. These studies came under massive criticism on the ground of a statistical considerations, culminating in allegations of data fabrication and scientific misconduct [74]. Indeed, a first partial replication study failed to reproduce genotoxic effects in human ES-1 fibroblasts, although these analyses focused on the 1.8 GHz carrier wave only, and did not systematically address effects of modulated signals [69]. Therefore, it remains unclear whether or not RF-EMFs have a genotoxic potential. I re-examined these effects using the same exposure conditions and cell line (ES-1) as in the previously published studies.

Both studies made use of the comet assay to analyze DNA fragmentation, the first performed a visual analysis of the comet effects, the replica study a computerized analysis. In this study, I performed both types of analyses, to allow for direct comparison. Cells were exposed to a GSM modulated RF-EMF at SAR values of 1 and 2W/kg and to the carrier wave (1950MHz) without modulation at 1W/kg. Exposure was intermittent (5´field on/10´field off) for a total of 16h. In the ES-1 cell line, I did not find any significant differences by applying both the visual and the fully automated computerized analysis of the comet assay. I also used a second human primary fibroblast cell line, HR-1d, which under ELF-EMF exposure conditions proved to be more sensitive than ES-1. I found a slight but significant increase of the visually scored comet tailfactor for both SAR values in the GSM modulated field, which was a bit more pronounced at 1W/kg. When applying the automated computerized analysis, the tail moment change was only significant for the 1W/kg GSM modulated RF-EMF. Hence, these result support the visually scored data partially, i.e. for the condition that produced a slightly more robust tail factor differences (1 W/kg GSM talk modulated RF-EMFs). Applying the stringent requirement that a genotoxic effect is genuine only if both comet scoring techniques produce statistically significant differences, we conclude the RF-EMF exposure at 1W/kg slightly increases the steady-state level of DNA strand breaks in the HR1-d cell line. The results do not support the genotoxic effects reported in the first study with the ES-1 cell line, but nevertheless show, that increased DNA fragmentation is detectable under RF-EMF exposure.

4.1.3. Additional data: ELF-EMF exposure

In addition to the data summarized in 4.1.1. and 4.1.2., I performed experiments to explore the type of DNA damage generated and the biological pathways involved in electromagnetic field effects. For this purpose, I chose to use the ELF-EMF exposure conditions, as effects there are more robust and established. Materials and methods covering this part are described in Focke *et. al.* (Appendix I) and in section 4.1.4.

4.1.3.1. No detectible genotoxic effect of induced electric fields

For *in vitro* ELF-EMF exposure, induction of the magnetic field is constant throughout the whole cell culture dish. Therefore all cells are exposed to the same field strength. However, the induced electric field is different, as there is no induction in the central part of the Petri dish and increasing induction towards the peripheral areas of the dish. Thus, I examined to what extent the induced electric field contributes to the genotoxic effects found before.

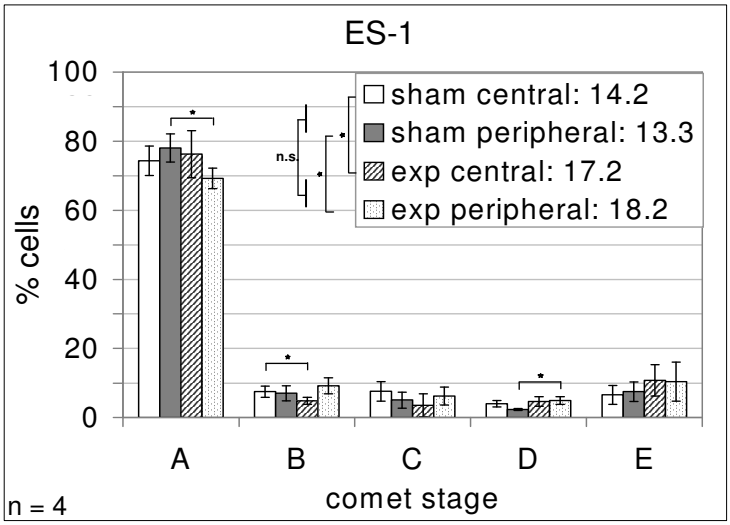

Figure 1. Contributions from the induced electric field.

ES-1 cells exposed to 50Hz, 1mT intermittent (5/10) ELF-EMF for 15h were harvested separately at the central and peripheral petri dish area, analysed with the alkaline comet assay and visually scored into five defined stages (A-E) by increasing amount of DNA in tail and tail length. Shown are mean percentages of cells in comet stages A-E for sham and exposed cells with standard errors as obtained from 4 independent experiments. Stage A represents cells without DNA migration and stages B-E cells with increasing amounts of migration (see Appendix I). The box contains mean comet tailfactor values for sham and exposed cells. Individual stages and tailfactors were compared by Student´s *t*-test.

To this end, I harvested ES-1 fibroblast cells in a 10cm Petri dish from the central and peripheral area separately after 50Hz, 1mT intermittent ELF-EMF exposure for 15h and compared them by comet analysis. The results show no significant difference between cells exposed in the central and in the peripheral area of the dish (Figure 1), but significant differences between sham and exposed cells. This indicates that the comet effects measured upon ELF-EMF exposure result from the magnetic field with negligible contributions from the induced electric field.

4.1.3.2. No adaptaion of cells under continuous ELF-EMF exposure

In Focke *et. al.* (Appendix I), I show that continuous ELF-EMF exposure, in contrast to intermittent exposure, has no effect on comet tailfactors in all cell lines. We reasoned that this might reflect a potential of cells to adapt under continuous exposure conditions, e.g. through induction, stabilization or degradation of proteins involved in DNA repair, cell cycle or apoptosis. To address this, I applied exposure protocols, where fibroblast cells were first exposed to a continuous ELF-EMF at 50Hz, 1mT for 4h followed by 24h recovery and 15h intermittent exposure (Figure 2) to see if the EMF effect is still detectable in the comet assay.

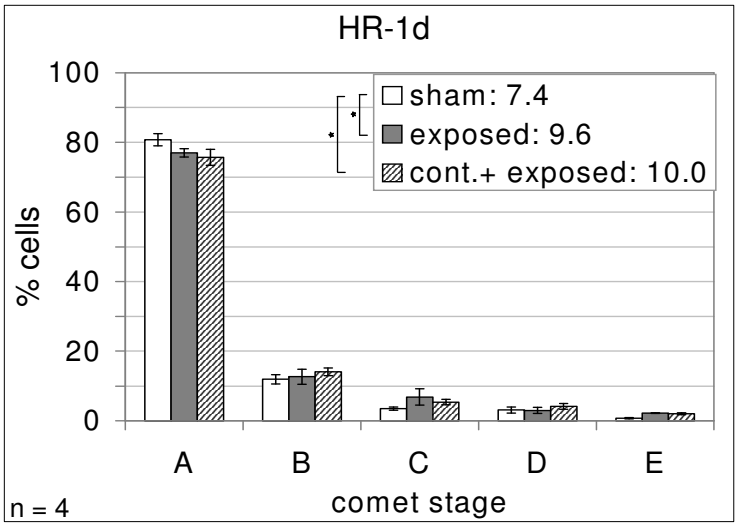

Figure 2. Potential of cells to adapt to ELF-EMF under continuous exposure.

HR-1d fibroblast cells were exposed to a continuous ELF-EMF (4h) at 50Hz, 1mT, then left to recover for 24h and then exposed to 50Hz, 1mT intermittent (5/10) ELF-EMF for 15h. They were analysed with the alkaline comet assay and visually scored as described in Appendix I. Shown are mean percentages of cells in comet stages A-E for sham and exposed cells with SEMs as obtained from 4 independent experiments. The box contains mean comet tailfactor values for sham and exposed cells. Individual stages and tailfactors were compared by Student´s *t*-test.

I found no statistically significant differences between cells that were exposed intermittently only and cells that had continuous exposure before intermittent exposure. This would argue against adaptation of cells under continuous exposure conditions. However, it could be that adaptation takes place in another time window, which was not addressed in this experiment. This question should be addressed more systematically in experiments allowing monitoring of cellular responses under “real time” exposure conditions (see 4.1.3.5.).

4.1.3.3. DNA Damage recognition after ELF-EMF exposure

Comet assay effects indicate an increase in the steady state levels of DNA strand breaks. To address whether these breaks are detected by DNA damage recognition proteins, I analysed two different factors, which are known to detect different spectra of DNA damages.

PARP recognizes DNA single strand breaks and is mainly involved in DNA BER and DNA SSB repair. Phosphorylated H2AX (γH2AX) is a prominent marker for double strand breaks and stalled replication forks.

In the case of PARP, I used the inhibitor 3-aminobenzamide (3ABA) to examine the effect of PARP (and therefore SSB repair) inhibition on the comet assay affects of ELF-EMF exposure. For this purpose, ES-1 fibroblast cells were intermittently exposed to a 50Hz, 1mT ELF-EMF for 15h in the presence of 3ABA and visual comet assay analysis was done. 3ABA increased background damage levels by 1.4 fold regarding the comet tailfactor, but there was almost no difference between cells treated with the inhibitor only and cells exposed to both ELF-EMF and inhibitor (Figure 3).

It is conceivable that the higher background damage level caused by 3ABA masked the effect of the magnetic field. However, I was not able to find an experimental condition, where no background effect of 3ABA treatment was present. Both treatments might be epistatic, indicating that PARP inhibition and ELF-EMF exposure affect the same processes. Hence, the result might suggest that ELF-EMF exposure might affect SSB repair efficiency rather than inducing DNA damage itself. Another possibility to assess the role of SSB repair in this context would be to measure poly(ADP)ribose formation directly in ELF-EMF exposed cells.

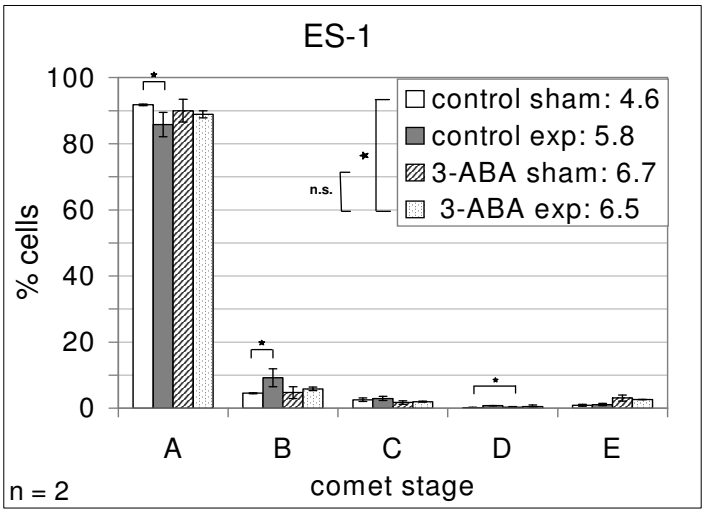

Figure 3. Inhibition of single strand break repair does not lead to increased DNA damage levels .

ES-1 cells were exposed to 50Hz, 1mT intermittent (5/10) ELF-EMF for 15h including the PARP inhibitor 3-aminobenzamide. They were analysed with the alkaline comet assay and visually scored as described in Appendix I. Shown are percentages of cells in comet stages A-E for sham and exposed cells with SEMs as obtained from 2 independent experiments. The box contains mean tailfactor values for sham and exposed cells. Individual stages and tailfactors were compared with Student´s *t*-test.

As a DNA damage marker, γH2AX can be visualised by immunofluorescence with phosphor-specific antibodies. To address the question, if DSBs and stalled replication forks are present in ELF-EMF exposed cells, I exposed ES-1, HR-1d, MCR-5 and HeLa cells to an intermittent 50Hz, 1mT ELF-EMF for 15h, fixed them and stained for γH2AX. I evaluated foci formation by counting γH2AX foci numbers and assigning cells to three classes: 0, 1-10 and >10 foci. As shown in Figure 4, there was no significant difference between sham and exposed cells in all four tested cell lines. As γH2AX does localize mainly to DSBs and stalled replication forks, the results suggest that the comet tailfactor increase is unlikely accounted for by such lesions.

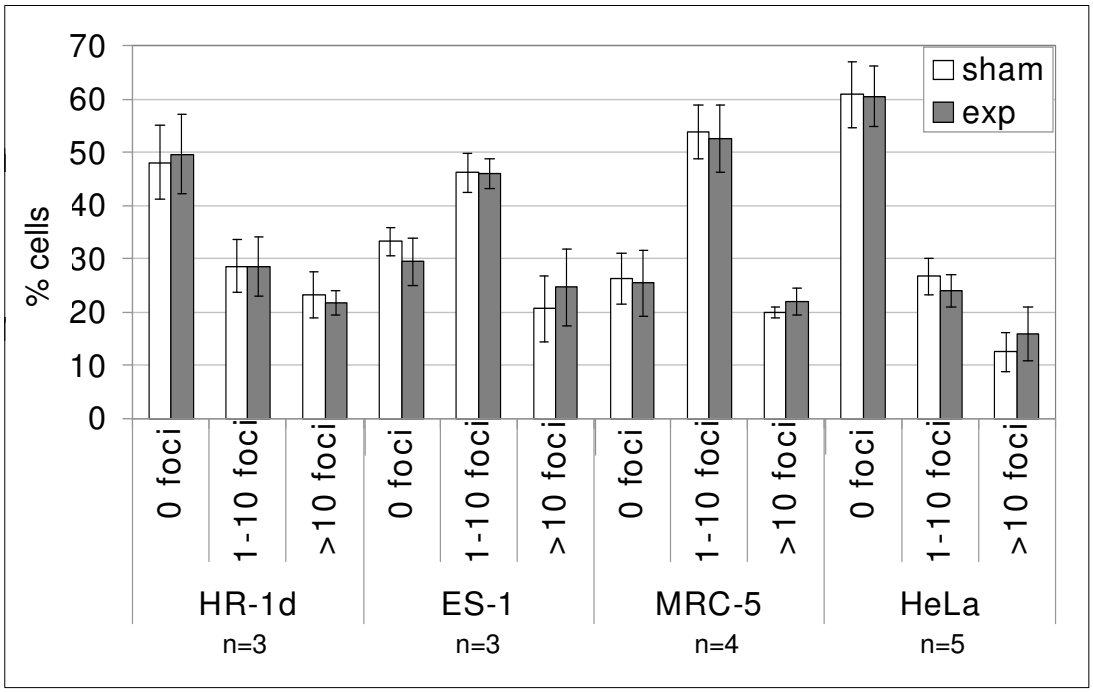

Figure 4. No detection of increased numbers of DSBs and stalled replication forks.

HR-1d, ES-1, MRC-5 and HeLa cells exposed to 50Hz, 1mT intermittent (5/10) ELF-EMF for 15h were stained with γH2AX antibody and microscopically scored for number of foci. Shown are percentages of cells in the three categories 0, 1-10 and >10 foci with SEMs as obtained from at least 3 independent experiments. Categories of sham and exposed cells were compared with Student´s *t*-test.

4.1.3.4. Addressing the role of DNA BER in ELF-EMF induced comet effects

ELF-EMF exposure has been associated with increased ROS formation, which, through fenton reactions, could generate oxidative DNA lesions. Oxidized bases and other small DNA lesions are recognized and repaired by the DNA BER system, key components of which are XRCC1 and DNA Pol β. Therefore, I addressed the role of BER in ELF-EMF induced genotoxicity by examining XRCC1 and Pol β function. First, I measured XRCC1 foci formation in two primary fibroblast cell lines and HeLa after 50Hz, 1mT intermittent ELF-EMF exposure for 15h by immunofluorescence. (Figure 5).

I found no significant difference between sham and exposed cells in all cell lines tested. Thus, ELF-EMF exposure does not affect steady state levels of XRCC1 foci in cells, although it does increase comet tailfactors, which appears to be inconsistent. The effect on foci formation, however, may be transient and dynamic, which could only be addressed in real time analyses.

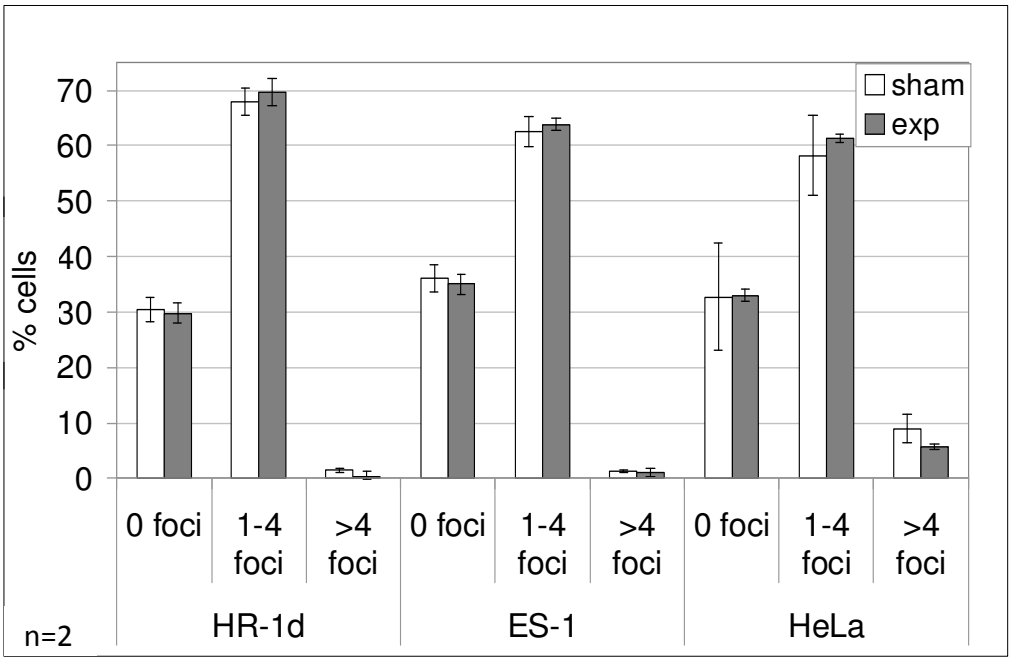

Figure 5. XRCC1 foci formation after ELF exposure.

HR-1d, ES-1 and HeLa cells exposed to 50Hz, 1mT intermittent (5/10) ELF-EMF for 15h were stained with XRCC1 antibody and microscopically scored for numbers of foci. Shown are percentages of cells in the three categories 0, 1-4 and >4 with standard errors, as obtained from 2 independent experiments. Categories of sham and exposed cells were compared with Student´s *t*-test.

To address the role of DNA Pol β, I made use of the nucleoside analogue AZT (3´-azido-3´-deoxythymidine), which is preferentially incorporated by DNA Pol β (and reverse transcriptase), but not by replicative DNA polymerases. It then blocks further processing of the lesion and, therefore, inhibits BER. To examine, if inhibition of BER affects the comet assay effect, I exposed the cells in the presence and in the absence of AZT to 50Hz, 1mT intermittent ELF-EMF for 15h and performed comet and cell cycle analysis afterwards. To find the appropriate AZT concentration, I first performed MTT survival assays for all cell lines and choose a concentration, which showed (almost) no impact on 48h survival (Figure 6A).
This was 100µM in the case of HR-1d, 200µM for ES-1 and 10µM for the HeLa cell line. Addition of AZT increased background of DNA damage levels in comet analyses in all cell lines tested (Figure 6B-D): 2.4fold in HR-1d, 2.1fold in ES-1 and 1.2fold in HeLa. Despite the increased background, however, the ELF-EMF exposure effects are still discernible in the presence of the inhibitor (difference between AZT sham and AZT exposed), but the relative tailfactor increase is not enhanced compared to AZT free conditions.

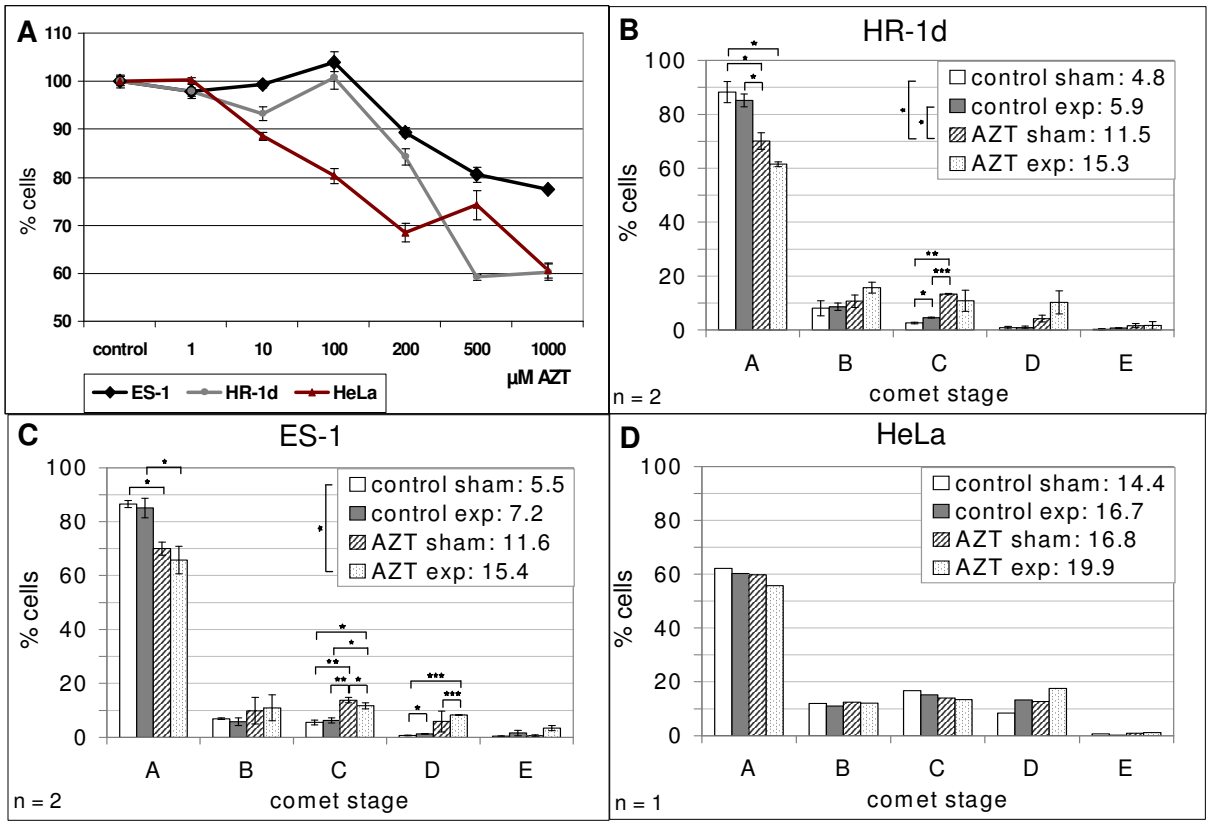

Figure 6. ELF-EMF induced comet effects under Pol β inhibition.

A) HR-1d, ES-1 and HeLa cells were treated with increasing amounts of AZT and survival was tested after 48h of incubation. **B, C, D)** HR-1d, ES-1 and HeLa cells treated with 200, 100 and 10µM AZT, respectively were exposed to 50Hz, 1mT intermittent (5/10) ELF-EMF for 15h, analysed with the alkaline comet assay and visually scored into five different stages as described in Appendix I. Shown are mean percentages of cells in comet stages A-E for sham and exposed conditions with standard errors, as obtained from 2 independent experiments (1 experiment for HeLa). The box contains mean tailfactor values for sham and exposed cells without and with inhibitor. Individual stages and tailfactors were compared with student´s *t*-test.

Cell cycle analysis by FACS then revealed a significant 2-fold increase of S-phase cells after AZT treatment in the fibroblast cultures (Figure 7), indicating S-phase accumulation and therefore problems with replication due to unrepaired DNA damage.

Besides incompletely repaired DNA damage, an accumulation of cells in S-phase could account for the increased comet tail factors observed following AZT treatment. S-phase cells naturally contain DNA fragments and therefore are scored as comet stage B-E events.

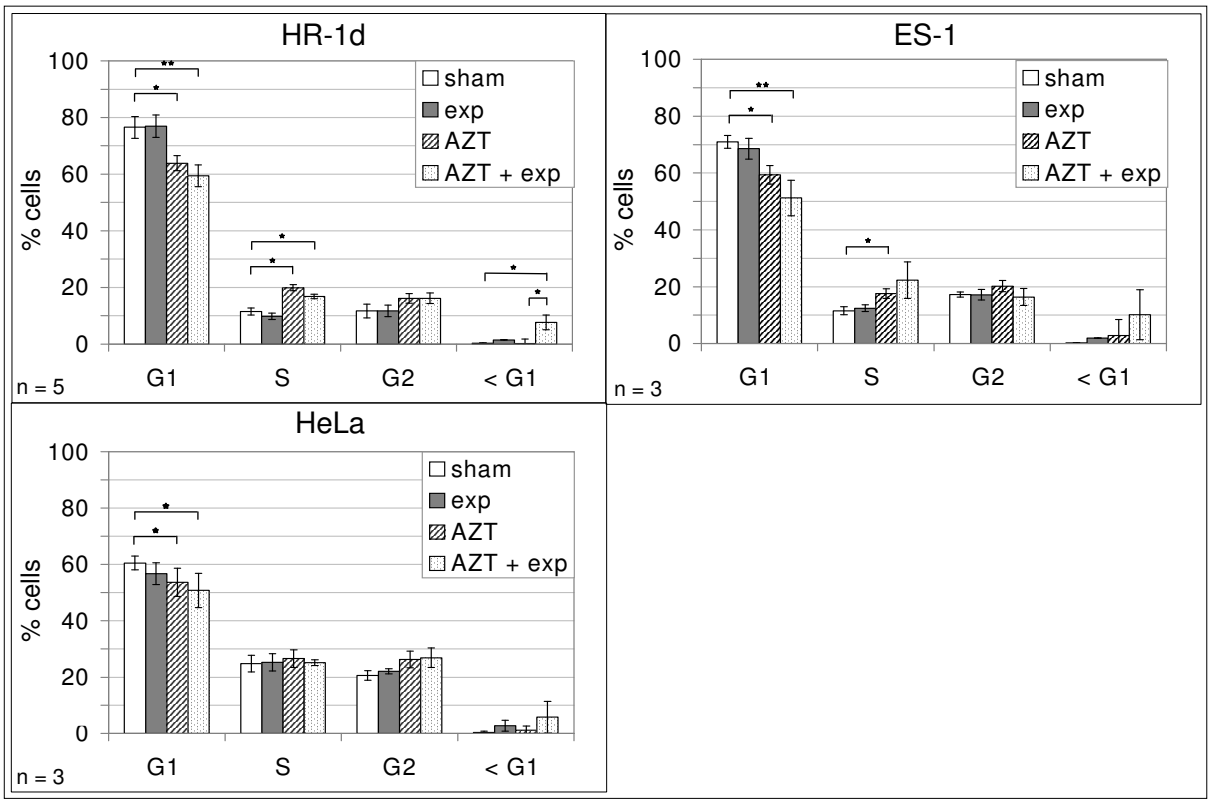

Figure 7. Cell cycle analysis after ELF-EMF exposure under Pol β inhibition.

HR-1d, ES-1 and HeLa cells treated with 200, 100 and 10µM AZT respectively were exposed to 50Hz, 1mT intermittent (5/10) ELF-EMF for 15h, stained with propidium iodid (PI) and analyzed by FACS for cell cycle distribution. Shown are percentages of cells in the different cell cycle stages according to their PI content with standard errors. Differences between single stages in sham, ELF-EMF exposed and AZT treated cells were compared with Student´s *t*-test: * $p<0.05$; ** $p<0.01$; *** $p<0.005$.

Also, the G2 population increased slightly in all three cell lines tested. Both S- and G2-effects, however, were not further increased by ELF-EMF exposure. On the other hand, the subG1 population, which might include apoptotic cells, was increased in all cell lines, but only after combining AZT with ELF-EMF treatment. This is statistically significant for HR-1d with about 7% more cells in subG1 compared to AZT alone. This could indicate, that DNA BER protects cells from entering apoptosis following ELF-EMF exposure.

This leaves us with two possible interpretations. (I) The putative DNA damage generated by ELF-EMF exposure is substrate for the BER pathway, or (II) the damage generated by AZT, i.e. unligatable DNA single strand breaks are less efficiently processed and recovered under ELF-EMF exposure.

4.1.3.5. Establishment of fluorophore-tagged proteins for live cell imaging under ELF-EMF exposure

To be able to address transient effects during ELF-EMF exposure, we started to establish tools for real time examination of cells during exposure. For this purpose, a small ELF-EMF exposure chamber is in development in collaboration with IT´IS foundation (ETH Zurich), which can be used for live cell microscopy. For real time analysis of cellular EMF responses, we started to establish constructs for expression of fluorophore tagged proteins of interest. These included: XRCC1, a BER protein known to be recruited immediately after DNA damage induction; OGG1, a DNA glycosylase recognizing the major oxidative DNA lesion 8-oxoG; TDG, a DNA glycosylase with a wide substrate spectrum including oxidative lesions; XPC, a component of NER also interacting with BER enzymes; PARP, a sensor of DNA strand breaks; APE1, a component of BER; RPA2, a ssDNA binding protein; PCNA, a replication and repair protein usable as cell cycle marker; H2B, a nucleosome component and MBD1, a methyl-CpG binding protein.

Constructs for XRCC1, PARP, APE1, TDG, XPC and MBD were already available, so I established fluorophore tagged RPA2, PCNA, H2B and OGG1. For this purpose, I reverse transcribed cDNA from total RNA of HeLa cells and PCR-amplified the four genes from this cDNA. I cloned these fragments into a pEGFP-C1 vector (Clontech, Palo Alto, CA, USA). Construction details are shown in Figure 8. Selected clones were then validated by sequencing. In the case of H2B all clones represented an in-frame H2Bj variant, which seems to be prominent in HeLa. I then subcloned H2B and OGG1 into a pEYFP-N1 vector (Clontech) to provide an alternative for combined analyses of two different proteins.

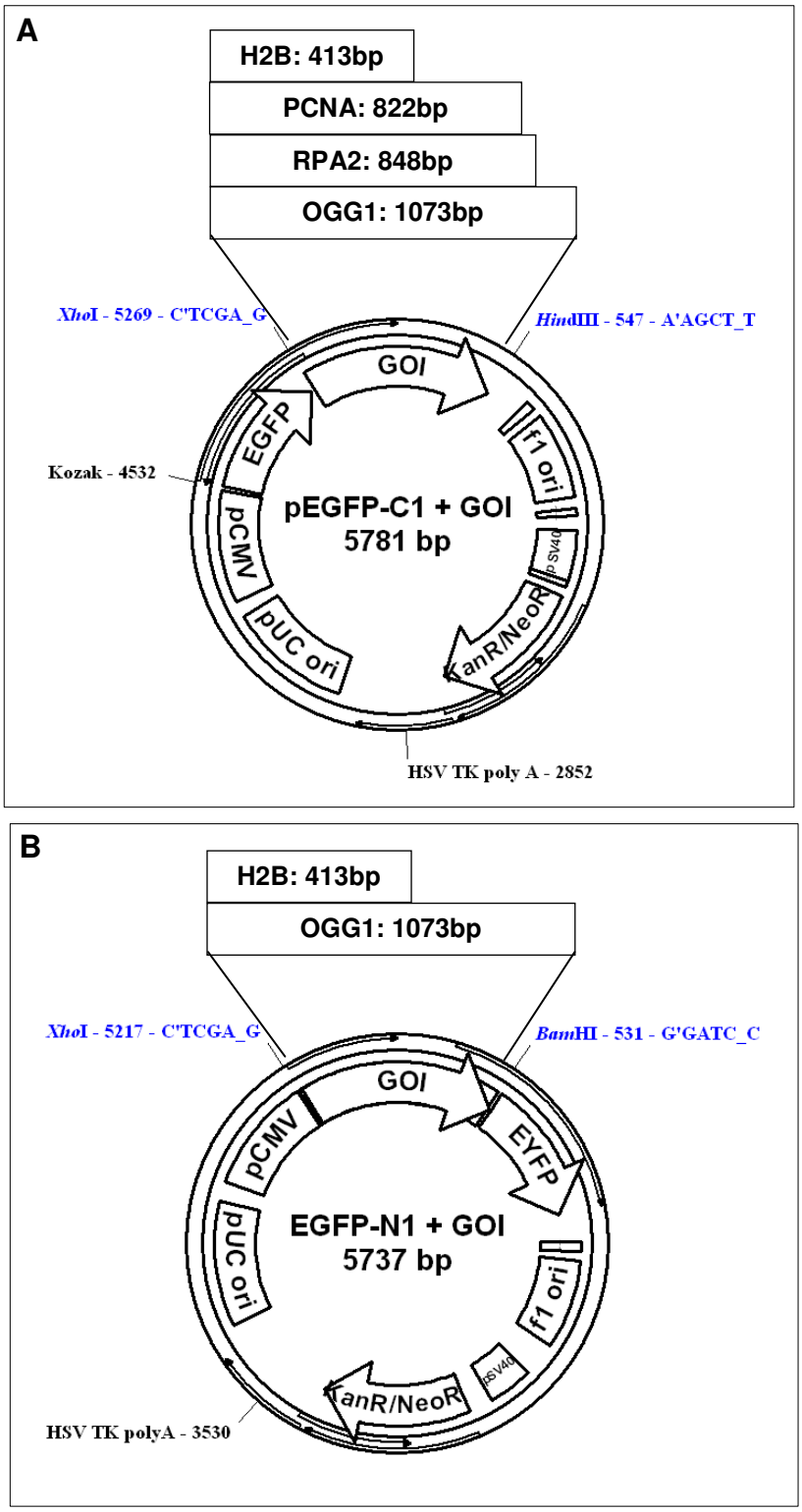

Figure 8. Vector constructs for EGFP-RPA2, EGFP-PCNA, H2B-YFP and OGG1-YFP.

A) pEGFP-C1 vector (Clontech) includes an optimized GFP variant gene with a CMV promoter, an SV40 origin of replication in mammalian cells, a pUC origin of replication for E.coli, a neomycin/ kanamycin resistance cassette and a multiple cloning site after the EGFP. The gene of interest (GOI) was cloned by using Xho I and Hind III restriction sites in the MCS to insert the gene in frame directly behind the EGFP ORF. Arrows represent ORFs, in blue are the used restriction sites. **B)** pEYFP-N1 vector (Clontech) is based on the same features as pEGFP-C1. The GOI was cloned in front of the EYFP ORF by using Xho I and BamH I restriction sites in the MCS.

Thereafter, I transiently transfected Cos7 cells (African Green Monkey SV40-transformed kidney fibroblast cell line) with the EGFP-RPA2, EGFP-PCNA, H2B-YFP or OGG1-YFP constructs. Following incubation for 48h, I harvested cells, prepared SDS extracts and examined expression of fusion proteins by Western blotting with anti-GFP antibody. I was able to identify all of the tagged proteins (Figure 9). In all cases, a small amount of degradation products (probably truncated versions or GFP only) was apparent. Expression levels of PCNA and RPA2 were low, but still detectable.

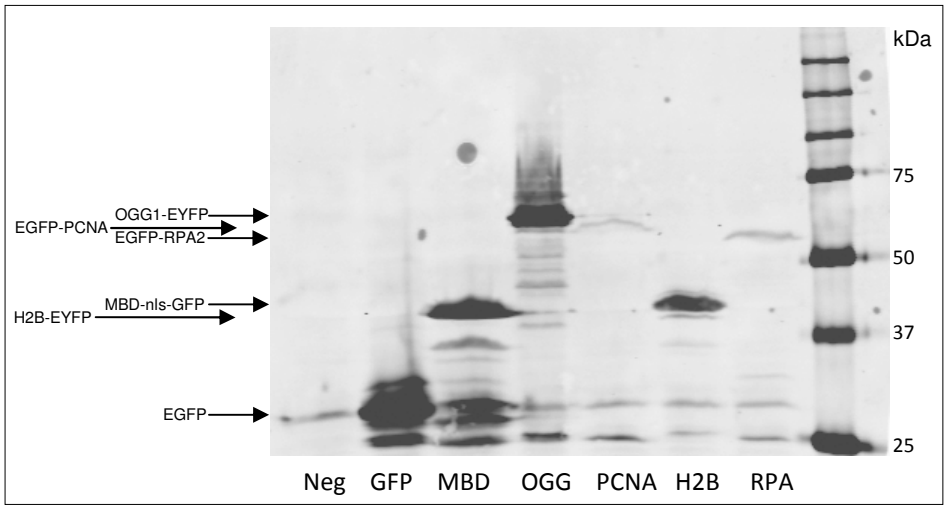

Figure 9. GFP western blot of transiently transfected Cos7 cells.

Transiently transfected Cos7 cells from a 80% confluent 3cm petri dish were harvested 48h after transfection with 100µl 2xSDS buffer and incubated at 95°C for 5min. 20µl were loaded onto a 10% SDS-polyacrylamide gel, transferred to a microcellulose membrane and stained with anti-GFP antibody. Fluorescence detection was done with the Li-COR Odyssey Infrared Imaging System. Predicted sizes: EGFP: 27kDa, MBD-nls-GFP: 50kDa, OGG1-EYFP: 65kDa, EGFP-PCNA: 56kDa, H2B-EYFP: 47kDa, EGFP-RPA2: 59kDa

Examination under live cell microscopy showed the expected localization patterns for all of the proteins (Figure 10). GFP protein alone was distributed throughout the whole cell (Figure 10A), OGG1 shows mainly nuclear staining with some spots outside (Figure 10B), probably representing mitochondria as observed before [183]. The nuclear staining pattern for OGG1 is not homogenous, there appear to be more and less condensed regions. RPA2 shows a diffuse nuclear staining (Figure 10C). MBD shows nuclear localization with condensed regions as published before [184] (Figure 10D), probably representing heterochromatin areas. APE1 has a diffuse nuclear staining pattern (Figure 10E).

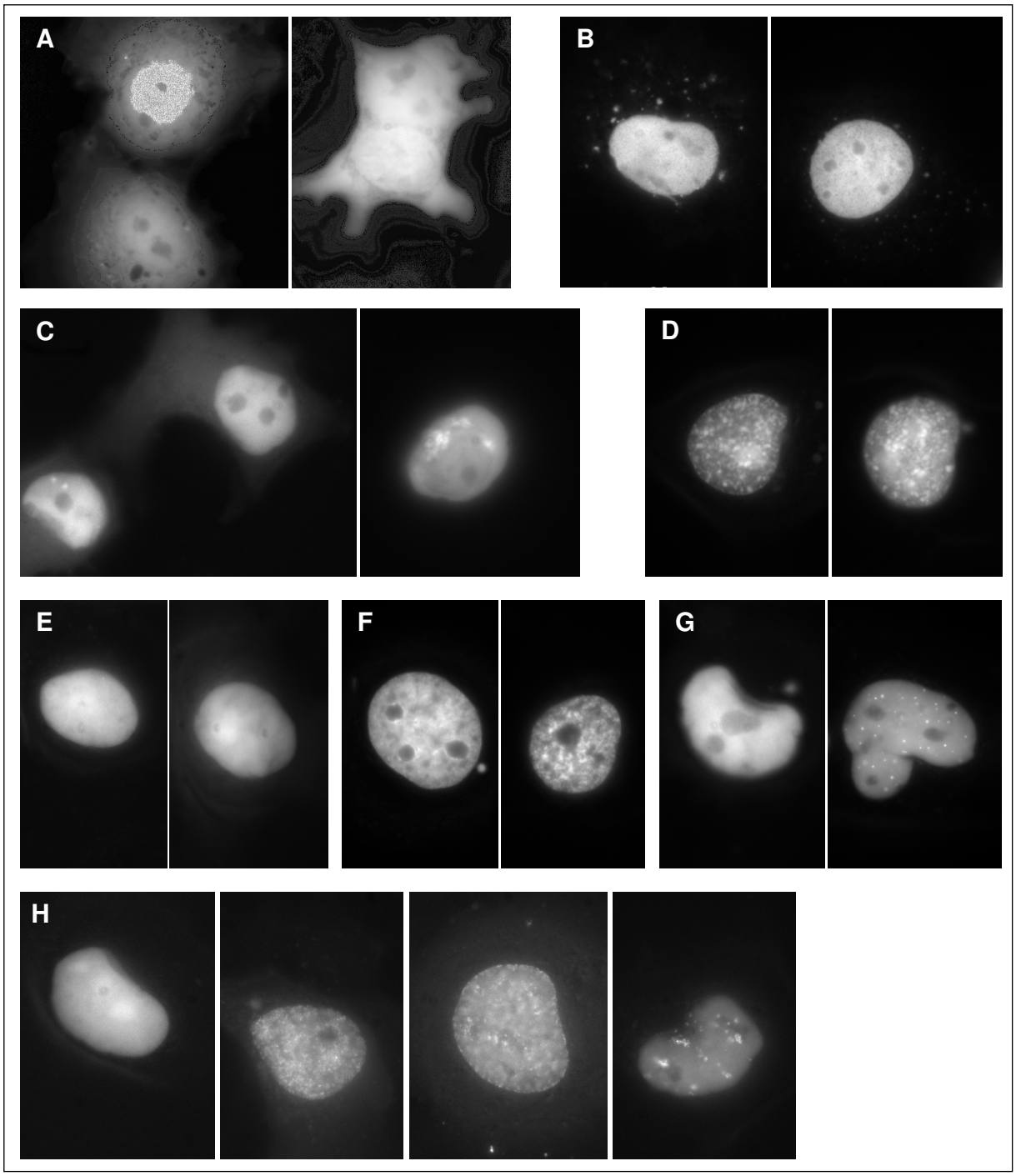

Figure 10. Localization of target genes in Cos7 cells.

Cells were analysed 24h after transfection with a Leica DMI6000B live cell imaging microscope using a Ludin chamber (Life Imaging Services) and GFP or YFP filters with a 100x magnification. **A)** EGFP alone localized throughout the whole cells **B)** OGG1-EYFP, localization mainly within the nucleus, but also mitochondrial **C)** EGFP-RPA2, nuclear localization **D)** EGFP-MBD, nuclear localization with a foci-like pattern **E)** EGFP-APE1, nuclear localization **F)** H2B-EYFP, nuclear localization with a foci-like pattern **G)** XRCC1, nuclear localization, foci in a subset of cells. **H)** EGFP-PCNA, nuclear localization, different patterns throughout the cell cycle: the first cell is outside S-phase, the others in different stages of S-phase: early, mid and late S

H2B has a nuclear staining pattern with condensed regions [185] (Figure 10F). XRCC1 has a diffuse nuclear staining pattern with foci in a subset of cells, probably representing DNA repair foci (Figure 10G). PCNA shows nuclear staining, which is diffuse from G2 to G1 and becomes condensed during S-phase [186] (Figure 10H).

To analyse, if recruitment of DNA repair proteins takes place after laser-induced DNA damage, I tested XRCC1 transfected cells by inducing DNA damage with micro-laser irradiation (355nm, 100ms per point). XRCC1 is immediately recruited to the site of irradiation and accumulates over time.

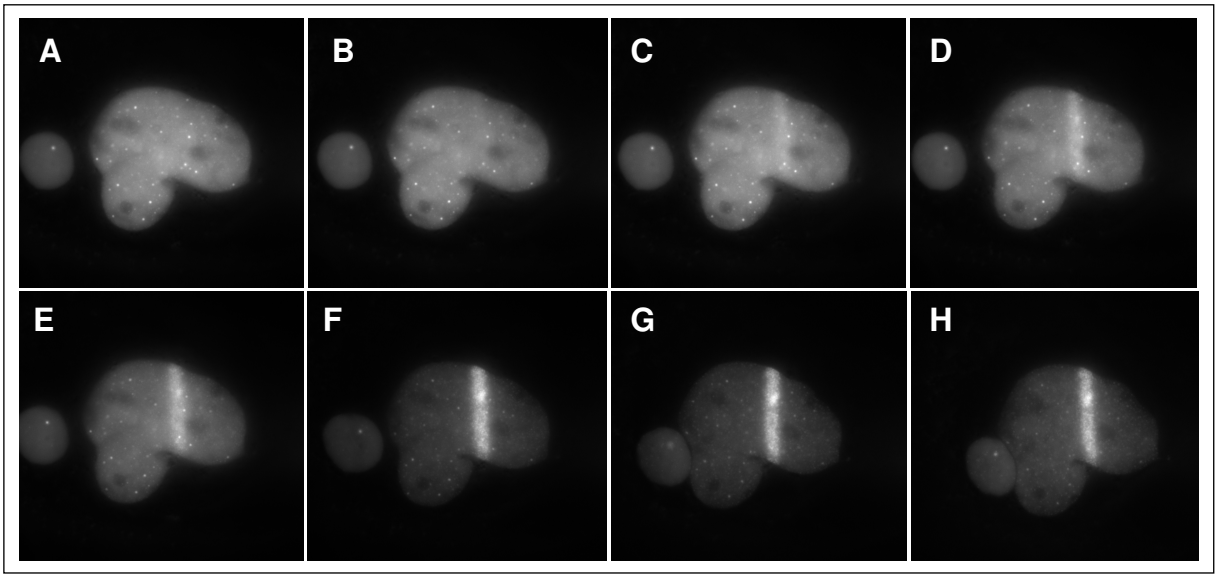

Figure 11. Recruitment dynamics of XRCC1 after laser induced DNA damage.

XRCC1 transfected Cos7 cells were laser irradiated with 100ms per FRAP point on one line through the nucleus. XRCC1 localization was monitored over time. **A)** before irradiation, **B)** directly after irradiation, **C)** 10s, **D)** 30s, **E)** 60s, **F)** 10min, **G)** 30min, **H)** 60min

4.1.4. Additional experimental procedures

4.1.4.1. Comet assay

For discrimination between central and peripheral cells, ES-1 human primary fibroblasts were seeded 24h before ELF-EMF exposure in DMEM onto 10cm Petri dishes containing 24x26mm cover slips in the center and at the periphery. After 15h intermittent (5min on/10min off) exposure with 50Hz, 1mT ELF-EMF cells from the different cover slips of sham and exposed cultures were harvested for comet analysis as described in the Appendix 7.1.

For the continuous pre-exposure experiments, cells were exposed for 4h continuously at 50Hz, 1mT and then left to recover/adapt for 24h. Then they were subjected to 50Hz, 1mT intermittent (5min on/10min off) ELF-EMF exposure for 15h h. This is the only exposure protocol, where we could not use blinded conditions. After the second exposure period comet assay was performed as described in Appendix 7.1.

In the PARP inhibition experiments 10mM 3ABA (Sigma) was added directly before ELF-EMF exposure. In the case of AZT survival assays were performed to adjust the appropriate concentration by seeding 1500 cells per well in triplicates into a 96well plate 16h before AZT addition. Cells were incubated 48h with the indicated concentrations of AZT (Sigma). 10µl of WST-8 [2-(2-methoxy-4-nitrophenyl)-3-(4-nitrophenyl)-5-(2,4-disulfophenyl)-2H-tetrazolium, monosodium salt] ("Cell Counting Kit 8", Dojindo Laboratories, Kumamoto, Japan) was added. The converted product was measured at 450nm in an ELISA plate reader after 2-4h. In the ELF-EMF exposure experiments, appropriate concentrations of AZT were added to the cultures immediately before exposure.

4.1.4.2. Immunofluorescence

Cells were seeded in DMEM and grown on cover slips for 24h. Cells were then exposed to a 50Hz, 1mT intermittent (5/10) ELF-EMF for 15h, then washed twice in PBS and fixed for 15 min with PF-buffer (PBS, 2% paraformaldehyde) at RT. After four washing steps of 10 min in PBS at RT, cells were permeabilized in ice cold P-buffer (PBS, 0.2% TritonX100) for 5 min. To reduce autofluorescence, the coverslips were incubated for another 5 min in ice-cold P-buffer containing 0.2% $NaBH_4$. After blocking twice in H-buffer for 10 min (PBS, 1% BSA) and once in D-buffer for 10 min (PBS, 1:20 donkey serum), samples were hybridized with anti-XRCC1 antibody (#ab1838, Abcam, Cambridge, UK, dilution 1:50 in H-buffer) or anti γH2AX antibody (#05-636, Upstate, NY, USA, dilution 1:500 in H-buffer) for 1h at RT. Following four washing steps of 10 min in H-buffer, the samples were hybridized with secondary antibody (anti-mouse IgG Cy2, dilution 1:500 in H-buffer) for 1 h at RT. After four washing steps of 10 min in PBS, the coverslips were dried and embedded in Mowiol (*Mowiol* 4.88, Calbiochem #475904). XRCC1 signals were visualized on an Axiovert 200M microscope (Zeiss, Germany) using a FITC filter (exitation 492 nm, emission 520 nm).

4.1.4.3. Construction and validation of expression vectors

Table 1: Primers for amplification of target genes from cDNA

RPA2	P1 5´-CGGACTCGAGGGGCCGCCATGTGGAACAGTGGATTCGAAAG-3´ P2 5´-TACCAAGCTTACGGATCCGA TTCTGCATCTGTGGATTTAAAATGG-3´
H2B	P1 5´- TTATCTCGAGGCGCCGCCATGCCAGAGCCAGCGAAGTC-3´ P2 5´- TGCAAAGCTTACGGATCCGACTTAGCGCTGGTGTACTTGG-3´
PCNA	P1 5´- TGTTCTCGAGGCGCCACCATGTTCGAGGCGCGCCTGG-3´ P2 5´- CTTGAAAGCTTACGGATCCGAAGATCCTTCTTCATCCTCG-3´
OGG1	P1 5´- GCGGCTCGAGGTGCCGCCATGCCTGCCCGCGCGCTTCTGC-3´ P2 5´- TGTCAAGCTTACGGATCCGAGCCTTCCGGCCCTTTGGAACC-3´
seqPN	5´- CGCCGTCCAGCTCGACCAG-3´
seqPN1	5´- CGTGTACGGTGGGAGGTC -3´
seqPC	5´- CATGGTCCTGCTGGAGTTCG-3´
seqPC1	5´- TCTACAAATGTGGTATGGCTGA-3´

5µg of total RNA from HeLa cells was reverse transcribed using the "RevertAid™ H Minus First Strand cDNA Synthesis Kit" (#K1631, Fermentas, St. Leon-Rot, Germany) according to the manufacturer´s instructions. cDNA was PCR amplified with Phusion polymerase (Finnzymes, Finland) and primers P1 (forward) and P2 (reverse) for the four genes RPA2, H2B, PCNA and OGG1 respectively (see Table 1), thereby introducing XhoI, HindIII and BamHI restriction sites at the ends (see Figure 8). PCR conditions were as follows: 98°C, 30s (1x), 98°C, 10s – 62°C, 10s – 72°C, 10s (35x), 72°C, 30s (1x). PCR fragments were purified with "peq gold Cycle-Pure Kit" (peqlab, Erlangen, Germany) according to the manufacturers instructions. Restriction digest was carried out using HindIII and XhoI (New England Biolabs, USA) enzymes followed by ligation using 1U Ligase T4 and transfection of DH5α competent bacteria by electroporation. MiniPreps were carried out with "peqgold Plasmid Mini Prep Kit" (peqlab) according to the given instructions. After a test digest positive clones were used for sequencing with the BigDye Terminator sequencing kit according to the manufacturer´s instructions using primer PC or PC1. Reaction program was as follows: 96°C, 10s – 50°C, 5s – 60°C, 4min (35x). For subcloning into pEYFP-N1 vector (clontech), targets and vector were restriction digested with XhoI and BamHI and ligated into the new vector as before.

Transfection-grade DNA was obtained by extraction with “QIAfilter endofree plasmid Midi Kit” (Qiagen) according to the instructions.

For transient transfection Cos7 (SV40 immortalized African green monkey kidney fibroblasts) cells were grown in DMEM (dulbeccos modified eagle´s medium, Sigma) supplemented with 10% FCS and 1% L-Glutamine. 50% confluent cultures in 6well plates were transfected with 0.5µg DNA using 1µl Transfectin (BioRad). Cells were harvested after 48h for GFP western blot analysis. For microscopic analysis cells were seeded in 12well plates onto cover slips and transfected with corresponding amounts of DNA and transfectin. Analysis was done after 24h with a Leica DMI6000B life cell imaging microscope using a Ludin chamber (Life Imaging Services). For FRAP analysis cells were irradiated partially with a laser at 355nm to induce DNA damage and followed over time to analyse recruitment and dynamics of proteins.

For Western blot cells were lysed directly on the plate by adding 100µl 2xSDS buffer (100mM NaCl, 500mM Tris [ph=8], 10% wt/vol SDS). After 5min at 95°C, 20µl of the lysates were separated in a 10% SDS-polyacrylamide gel and transferred to a nitrocellulose membrane (Millipore, USA). After blocking membranes with TBS buffer (100 mM Tris/HCl, 150 mM NaCl, pH 8.0) with 5% dry milk for 1h at RT, they were incubated with the first antibody (mouse anti-GFP # 11-814-460-001, Roche, Switzerland, 1:1000) in the blocking buffer for 1h at RT, followed by three 10min washing steps with TBS at RT. Secondary antibody (#926-32220, goat anti-mouse IRDye 680, LI-COR, Lincoln, USA) was diluted 1:10 000 in blocking buffer and hybridized to the membranes for 1h at RT. After three washing steps of 10 min at RT detection of the signals was carried out using the Odyssey Infrared Imaging system (LI-COR).

4.2. Involvement of Thymine DNA Glycosylase in DNA based cytotoxicity of 5-fluorouracil (Appendix III)

5-fluorouracil (5-FU) has been in use as chemotherapeutic substance since decades, but its exact mode of action is still poorly understood. Inhibition of the thymidilate synthase by 5-FU increases the dUMP (or FdUMP) level on the expense of dTMP, which, upon conversion to dUTP (or dFdUTP) can get incorporated into genomic DNA. This DNA directed action of 5-FU has been proposed to generate toxic DNA damage through excision repair processes. The pathway generating this lethal DNA damage has not been defined yet. In biochemical assays, uracil and 5-FU in DNA represent substrates for the Thymine DNA Glycosylase (TDG). The

aim of this study was to evaluate a possible role of TDG dependent BER in the response to 5-FU treatment. In a genetic approach we discovered that mouse embryonic fibroblast cells with a targeted disruption of the TDG gene show significantly reduced sensitivity towards 5-FU treatment compared to wild type cells. This phenotype could be complemented by expression of a catalytically active TDG.

Therefore I addressed the question, if TDG dependent DNA strand breaks can be seen in 5-FU treated cells making use of the highly sensitive comet assay I established in the laboratory. Thereby I saw increased levels of DNA fragmentation in wild type cells compared to knock out cells. Analysing the cell cycle of these cells, I found that wild type cells accumulate more in S-phase than knock out cells upon 5-FU treatment. This correlated with the loss of activation of an intra S-phase DNA damage checkpoint. Altogether, these findings suggest a rate limiting role for TDG in mediating the DNA directed cytotoxicity of 5-FU.

4.3. Cell cycle regulation of the uracil DNA glycosylases TDG and UNG (Appendix IV)

TDG is a member of the uracil DNA glycosylase (UDG) superfamily of proteins, which all excise uracil from DNA. Hence, the uracil processing activity of TDG is not unique, at least three additional proteins (UNG, SMUG and MBD4) with such properties are present in mammalian cells. The co-evolution of these apparently redundant enzymes implies the existence of non-redundant biological functions that must be coordinated. In this study, we addressed the role of gene regulation in the functional separation of the DNA glycosylases UNG and TDG. We found that UNG is present mainly in S-phase, while TDG is detectable from G2 to the next G1 phase and absent in S-phase. As part of this study I provided cytological support for counter-regulation of these two DNA glycosylases. For this purpose, I stainied HeLa cells with antibodies against TDG and the S-phase marker PCNA to do immunofluorescence. I counted cells for single and double staining and showed, that PCNA positive (and therefore S-phase) cells do not stain for TDG and vice versa. We also showed, that regulation of TDG occurs at the protein level, as mRNA levels are constant throughout the cell cycle and that the protein is ubiquitinated and degraded by the proteasome.

4.4. Arginine Methylation Regulates DNA Polymerase β (Appendix V)

In this study, we addressed the function of a newly discovered arginine methylation in DNA Polymerase β, the DNA polymerase involved in DNA BER. Pol β was found to form a complex with the protein arginine methyltransferase 6 (PRMT6) and to be specifically methylated at arginine *in vitro* and *in vivo*. In biochemical assays, methylation of Pol β by PRMT6 strongly stimulated DNA polymerase activity by enhancing DNA binding and processivity, while single nucleotide insertion and dRP-lyase activity were not affected. Two residues, R83 and R152, were identified in DNA Pol β as the sites of methylation by PRMT6. I contributed to the genetic complementation experiments of this study, which confirmed, that the amino acid residues targeted by PRMT6 *in vitro* are indeed important for the cellular resistance to DNA alkylating agents. Making use of differentially complemented mouse embryonic fibroblast cell lines with a genomic DNA Pol β knock out, I investigated DNA fragmentation levels following MMS (methyl methanesulfonate) treatment. This showed, that DNA Pol β knock out cells complemented with a mutated form of DNA Pol β, not able to be methylated, exhibit a higher level of DNA fragmentation upon induced DNA damage than cell complemented with wild type DNA Pol β. Together with reduced survival rates and an increased subG1 fraction in cells challenged with a DNA damaging agent, this established the *in vivo* relevance of DNA Pol β methylation.

5. Discussion and Outlook

5.1. Biologic effects of electromagnetic fields

Genotoxicity of 50Hz electromagnetic fields

Genotoxicity studies with 50Hz electromagnetic fields in the past produced conflicting conclusions. Independent confirmation of results was not possible in some cases. This study was aimed at the validation of previous work reporting ELF-EMF derived genotoxicity, and at the clarification of discrepancies between different studies. Using identical exposure equipment and conditions (50Hz, 1mT, 15h) and the same cell line (ES-1) and comet analysis method as published previously [1], I could reproduce evidence for increased DNA fragmentation in comet analysis following ELF-EMF exposure. This comet effect was less pronounced than previously published, but nevertheless statistically significant. I observed increased levels of comet tail DNA under intermittent but not under continuous exposure conditions. This excludes thermal effects as a cause. I tested, if cells are able to adapt under continuous exposure conditions, but did not find evidence in support of such a scenario. Hence, the reason for the difference between intermittent and continuous exposure remains unclear. As the visual method of comet scoring used in the original study was criticized, I compared side by side visual and automated computerized analysis and showed, that the observed DNA fragmentation was in the same range, irrespective of the scoring method. I then expanded the study to other cell lines. ELF-EMF induced DNA fragmentation was more pronounced in a fibroblast cell line from an older donor and absent in the cancer cell line HeLa. This could be due to altered DNA repair, cell cycle control or apoptosis capacities in the cancer cell line.

I addressed whether cells in different stages of the cell cycle are affected differently by ELF-EMF exposure. Cells blocked in G1 phase did not show a significant comet tailfactor increase, suggesting, that cells undergoing DNA replication show the ELF-EMF effect more readily than non-replicating cells. This could have influenced outcomes of other studies, as the fraction of S-phase cells varies with different cell lines and culture conditions. For instance, the previously reported influence of EMFs on the iron pool of the cell [75], which I did not find in

my experiments, might be due to the use of iron-chelators, which are known to induce G1 arrest.

Effects of ELF-EMF exposure on cell cycle and apoptosis

Results with G1 blocked cells suggested, that ELF-EMF directed effects are detectible mainly in S-phase cells. DNA of S-phase cells is known to migrate into the comet tail and therefore contributes to the outcome of the assay [187, 188]. It was therefore not clear from the previous studies, if the observed comet tailfactor differences upon ELF-EMF exposure were due to direct DNA damage or due to an increase of the fraction of S-phase cells. Interference of electromagnetic fields with cell cycle progression was shown before, whereby inhibition of proliferation was observed [27, 28] as well as acceleration [24, 26]. However, cell cycle analyses in my study after intermittent 50Hz, 1mT exposure for 15h revealed no significant differences between exposed and non-exposed cells, indicating that an accumulation of cells in S-phase is not responsible for the increased comet tailfactor. The number of replicating cells however, was slightly but significantly reduced in the cell line showing higher DNA fragmentation in the comet assay. This suggests that ELF-EMF exposure disturbed DNA replication or entering of S-phase in a subpopulation of cells.

Apoptotic cells were also suggested to account for the comet tailfactor increase after ELF-EMF exposure [188, 189]. In this study the cell line, that showed the higher comet tailfactor increase, also had increased levels of apoptotic cells after ELF-EMF exposure (4.5% versus 3%), suggesting that apoptotic cells might contribute to the comet effects. Cells entering S-phase, which, as shown before, encounter replication problems, might be driven into apoptosis. But as about 2.4% more cells are found in comet stage E, the stage, that would contain apoptotic cells, after ELF-EMF exposure and the increase of apoptosis was measured to be 1.5%, apoptosis can only partially account for the comet effect.

Type of possible DNA lesions induced by ELF-EMF exposure

The comet tailfactor increase seems to be partially due to increased apoptosis, but the remaining part must be of other origin. The hypothesis of an influence of EMFs on the free radical pool [190-193] and the generation of oxidative DNA damage due to Fenton reactions was not supported by monitoring unrepaired oxidative damage in ELF-EMF exposed cells. The data cannot definitely rule out the generation of a small amount of oxidative DNA

damage upon ELF-EMF exposure, but they argue against a major contribution of such damage. The apparent discrepancy to previous studies might be due to cell line specific responses.

γH2AX is a widely used marker for the visualization of DSBs, but also highlights stalled replication forks. As I found no change in γH2AX foci numbers and distribution after intermittent 50Hz, 1mT exposure for 15h, the generation of significant levels of DSBs can be excluded. There is a report of increased γH2AX foci formation in mouse preimplantation embryos [18] after ELF-EMF exposure with 0.3-0.5mT for 24h. These developing cells could respond more sensitively to ELF-EMF exposure, possibly due to high proliferation rates and, hence, the presence of a large fraction of replicating cells.

I also studied the influence of inhibition of the DNA SSB sensor PARP on ELF-EMF effects. Usage of the inhibitor increased background DNA fragmentation, possibly because of increased steady state levels of DNA repair intermediates. When applying both inhibitor and EMF, the comet tailfactor did not increase further, indicating no direct SSBs as a result from ELF-EMF exposure. Both treatments might be epistatic, indicating that PARP inhibition and ELF-EMF exposure affect the same processes. Hence, the result might suggest that ELF-EMF exposure might affect SSB repair efficiency rather than inducing DNA damage itself.

The pathway responsible for the removal of small lesions is DNA BER, critical components of which are XRCC1 and DNA Pol β. I could not find evidence for an engagement of XRCC1 following ELF-EMF exposure. When inhibiting DNA Pol β, cells exhibited increased comet assay tailfactors, which is probably due to an accumulation of cells in S-phase, as confirmed by cell cycle analysis. The subG1 fraction, which was not increased with ELF-EMF or inhibitor treatment alone, was significantly increased upon application of both treatments. As subG1 might represent apoptotic cells, this finding indicates an involvement of BER. It thus appears that, if repair synthesis is inhibited, some cells start to execute apoptosis. This could either be due to the generation of BER relevant DNA lesions induced by ELF-EMF exposure, or to inhibition of BER of endogenous DNA damage upon ELF-EMF exposure.

Radiofrequency electromagnetic fields

Whether or not RF fields also have an influence on biological systems is unclear. The majority of studies do not support adverse health effects like cancer promotion. Nevertheless there is *in vivo* and *in vitro* evidence suggesting genotoxic effects on biological

systems. Using the same exposure setup and conditions (intermittent exposure, GSM talk modulated field, SAR 1 or 2W/kg, 16h), applied to the same cell line (ES-1), I could not reproduce the genotoxic effects obtained in a former study. I did find a small comet tailfactor increase in another fibroblast cell line (HR-1d), when applying the same exposure conditions. This effect was significant within a SAR range below the official threshold for RF exposure of the population (2W/kg). Importantly, differences in comet tail DNA were only seen when applying a modulated RF field, which, as described in the introduction, has different low frequency components. Therefore, as carrier wave exposure did not lead to a significant increase of the comet tailfactor, thermal effects can be excluded and low frequency components might be responsible for the described effects.

Possible mechanisms

Comet tail DNA changes are generally related to changes in steady-state levels of DNA strand breaks. This can be due to DNA damage, to an increased S-phase population, or to apoptosis. I showed that S-phase-differences and apoptosis indeed play a role, but they cannot explain the full extent of the comet assay effects. As DNA BER inhibition led to increased apoptosis upon ELF-EMF exposure, small DNA base lesions or single strand breaks appear to occur, either directly or indirectly. But what are the events that lead to S-phase-alterations and apoptosis and what lesions could be resulting from exposure to electromagnetic fields?

A well established consequence of electromagnetic field exposure is alteration of calcium homeostasis of the cells. As calcium is an important regulator of cellular processes including proliferation, gene expression and apoptosis, it might be that the effects on DNA replication and apoptosis and the proposed impairment of DNA repair capacity are based on changes in calcium distribution within the cell. A recent report showed that calcium levels influence DNA replication by enhancing the binding of negative regulators to Cdc6 (cell division control protein 6), an essential component of the pre-replication complex [194]. Calcium also plays a role in apoptosis [40] and is an important component of many signalling pathways that induce changes in gene expression, cell cycle or apoptosis. It has also been shown that the functions of membrane channels can be altered due to ELF-EMF exposure, which could affect signalling cascades [195]. Hence, changes in intracellular calcium concentration and distribution may play a role in the effects observed in this study.

Small amounts of oxidative DNA damage might arise due to alteration of the redox status of the cell. My results, however, indicate that these effects cannot be significant. Another possibility is that cells are affected in repairing endogenous DNA damage or in cellular processes like DNA replication due to an influence of the field on the enzymes involved. Alterations of enzyme turnover rates upon ELF-EMF exposure have been shown (e.g. [82]), although not yet with regard to DNA metabolism. It was suggested that EMFs interact with moving electrons in enzymes [196], which could also affect DNA repair enzymes, that often contain metal ions. Along the same lines, it is possible that EMFs interact with electrons in DNA and either directly cause oxidative damage or, as shown by others, alter specific gene expression [197]. Moreover, interactions of EMFs with membrane bound proteins could lead to signalling cascades that influence gene expression. The gene expression changes reported after EMF exposure comprise heat shock proteins, pointing to a stress response of the cell. There are also cell cycle regulating genes like cyclin D, p21CIP1 and p16INK4a [28] and proliferation related genes like c-myc [37]. Altered regulation of the cell cycle could be responsible for the decreased replication efficiency rates observed here. Furthermore it was shown that there can be altered expression of apoptosis-related genes like bcl-2, bax and c-myc [36]. So, besides the decreased replication efficiency, a direct influence on apoptosis-related genes could be responsible for the increased fraction of apoptotic cells induced by ELF-EMF exposure.

Taken together these results suggest an indirect influence of the ELF-EMF on essential cellular processes like DNA repair, replication or gene expression, rather than the induction of DNA damage.

Future directions

The current evidence suggests that DNA transactions rather than the DNA itself are affected by EMF exposure. Hence, the activity of enzymes processing DNA might be altered. Therefore, a future approach could be to use *in vitro* reconstituted enzymatic systems to address, if EMF exposure affects DNA repair and replication processes in a quantitative or qualitative manner.

Another approach will be the monitoring of cells during exposure. The current analyses are limited in that they only monitor endpoints after exposure, but the cellular responses might well be transient. Therefore, we already started to develop a small ELF-EMF exposure

chamber, which can be placed under a live cell imaging microscope to allow real time assessment of possible ELF-EMF effects. For this purpose, I started to establish fluorophore tagged proteins of interest. Important proteins to study are components of the DNA BER pathway like XRCC1 and APE1, which can give further hints with regard to the engagement of DNA repair following EMF exposure. Additionally, the human 8-oxoG glycosylase OGG1 will provide further insights into whether oxidative damage is involved, and the damage sensing protein PARP will identify putative DNA SSB repair processes. The inclusion of RPA2, a damage sensor, will allow the monitoring of ssDNA regions. With this set of diagnostic proteins, it will be interesting to assess repair dynamics of induced DNA damage. The damage in this context can be induced e.g. by H_2O_2 or by a micro-laser and differences in recruitment dynamics of DNA repair proteins can be measured. As a cell cycle marker, I established GFP-tagged PCNA, which is also involved in DNA repair. Another question to be addressed is, if electromagnetic fields also have an influence on the epigenome of the cell. There is preliminary evidence, suggesting that low dose ionozing radiation may induce DNA methylation changes. To answer this question, the methyl-binding protein domain of MBD1 was chosen to reveal DNA methylation pattern differences as a consequence of EMF exposure.

5.2. Involvement of TDG in the toxicity mechanism of 5-FU (Appendix III)

5-fluorouracil (5-FU) is a widely used anti-cancer drug, but its mode of action has not been solved. We show in this work, that TDG knock out cells display hyperresistance to 5-FU and this phenotype can be reverted by complementation. This suggests an involvement of TDG, but not other uracil DNA glycosylases, in 5-FU mediated cytotoxicity. Importantly, this establishes for the first time a functional separation between uracil DNA glycosylases. Whereas TDG mediates toxicity of 5-FU, SMUG, was reported to protect cells from the cytotoxic effects of 5-FU, and UNG does not seem to contribute significantly to the processing of 5-FU derived DNA lesions.

Interestingly, it has been shown that there can be a correlation between reduced BER capacity and better survival rates of patients upon combination therapy with 5-FU [198]. Therefore it will be of great interest, to examine, if TDG levels in tumor cells of patients correlate with response of the cancers to the 5-FU treatment.

5.3. Cell cycle regulation of Thymine DNA Glycosylase (TDG) (Appendix IV)

This study established the temporal separation of function of the otherwise redundant uracil DNA glycosylases TDG and UNG. The two enzymes are present in different cell cycle phases, UNG in S-phase and TDG in all other phases of the cell cycle. TDG and UNG have different substrate affinity spectra. While UNG processes uracil opposite adenine with high efficiency, TDG has a low affinity to this substrate. During DNA replication, misincorporation of uracil mostly happens opposite adenine, making UNG the more suitable enzyme for repair. TDG, however, could interfere with DNA replication processes following base excision, as it binds to AP sites with high affinity. TDG might also interfere with the postreplicative mismatch repair system, because it also binds to and processes G:T mismatches, a relatively frequent product of base misincorporation of replicative DNA polymerases. In non-replicating cells, G:U and G:T mismatches mainly occur by deamination of cytosine and 5-methyl-cytosine, respectively, and therefore require a mismatch specific damage directed DNA glycosylase for non-mutagenic repair. Hence, the cell cycle regulation of TDG makes perfect biological sense.

This work establishes a novel regulatory mechanism for DNA repair. The fact that the ubiquitin-proteasome system is involved in cell cycle controlled degradation of TDG suggests this pathway as an important coordinator of BER, especially of uracil repair. It will therefore be of interest, if other repair processes are also regulated in this way.

5.4. A new regulatory mechanism for DNA Polymerase β (Appendix V)

This work established protein arginine methylation as a novel regulatory modification of DNA Pol β. The data shows a functional interaction of DNA Pol β with the protein arginine methyltransferase PRMT6 and an influence of the methylation on DNA binding and processivity of DNA Pol β *in vitro,* and on the DNA repair capacity of cells *in vivo*. Hence, methylation of DNA Pol β seems to be a biologically significant regulatory mechanism of DNA BER. Methylated DNA Pol β could more efficiently protect cells from DNA damage due to the higher affinity of the enzyme to DNA repair intermediates generated in BER. Furthermore, DNA Pol β-specific protein complexes could be stabilized or weakened due to methylation.

Another interesting question to be resolved will be, if PRMT6 interacts also with other BER proteins and if protein arginine methylation is more general regulatory mechanism in DNA repair.

6. References

1 **Ivancsits, S., Diem, E., Jahn, O. and Rudiger, H. W.,** Intermittent extremely low frequency electromagnetic fields cause DNA damage in a dose-dependent way. *Int Arch Occup Environ Health* 2003. **76**: 431-436.

2 **Ivancsits, S., Diem, E., Pilger, A., Rudiger, H. W. and Jahn, O.,** Induction of DNA strand breaks by intermittent exposure to extremely-low-frequency electromagnetic fields in human diploid fibroblasts. *Mutat Res* 2002. **519**: 1-13.

3 **Winker, R., Ivancsits, S., Pilger, A., Adlkofer, F. and Rudiger, H. W.,** Chromosomal damage in human diploid fibroblasts by intermittent exposure to extremely low-frequency electromagnetic fields. *Mutat Res* 2005. **585**: 43-49.

4 **Hoeijmakers, J. H.,** Genome maintenance mechanisms for preventing cancer. *Nature* 2001. **411**: 366-374.

5 Guidelines for limiting exposure to time-varying electric, magnetic, and electromagnetic fields (up to 300 GHz). International Commission on Non-Ionizing Radiation Protection. *Health Phys* 1998. **74**: 494-522.

6 **Ahlbom, A., Day, N., Feychting, M., Roman, E., Skinner, J., Dockerty, J., Linet, M., McBride, M., Michaelis, J., Olsen, J. H., Tynes, T. and Verkasalo, P. K.,** A pooled analysis of magnetic fields and childhood leukaemia. *Br J Cancer* 2000. **83**: 692-698.

7 **Feychting, M., Forssen, U. and Floderus, B.,** Occupational and residential magnetic field exposure and leukemia and central nervous system tumors. *Epidemiology* 1997. **8**: 384-389.

8 **Greenland, S., Sheppard, A. R., Kaune, W. T., Poole, C. and Kelsh, M. A.,** A pooled analysis of magnetic fields, wire codes, and childhood leukemia. Childhood Leukemia-EMF Study Group. *Epidemiology* 2000. **11**: 624-634.

9 **Feychting, M. and Forssen, U.,** Electromagnetic fields and female breast cancer. *Cancer Causes Control* 2006. **17**: 553-558.

10 **Forssen, U. M., Lonn, S., Ahlbom, A., Savitz, D. A. and Feychting, M.,** Occupational magnetic field exposure and the risk of acoustic neuroma. *Am J Ind Med* 2006. **49**: 112-118.

11 **McCann, J., Dietrich, F. and Rafferty, C.,** The genotoxic potential of electric and magnetic fields: an update. *Mutat Res* 1998. **411**: 45-86.

12 **Olive, P. L., Banath, J. P. and Durand, R. E.,** Heterogeneity in radiation-induced DNA damage and repair in tumor and normal cells measured using the "comet" assay. *Radiat Res* 1990. **122**: 86-94.

13 **Lai, H. and Singh, N. P.,** Acute exposure to a 60 Hz magnetic field increases DNA strand breaks in rat brain cells. *Bioelectromagnetics* 1997. **18**: 156-165.

14 **Svedenstal, B. M., Johanson, K. J. and Mild, K. H.,** DNA damage induced in brain cells of CBA mice exposed to magnetic fields. *In Vivo* 1999. **13**: 551-552.

15 **Scarfi, M. R., Sannino, A., Perrotta, A., Sarti, M., Mesirca, P. and Bersani, F.,** Evaluation of genotoxic effects in human fibroblasts after intermittent exposure to 50 Hz electromagnetic fields: a confirmatory study. *Radiat Res* 2005. **164**: 270-276.

16 **Wahab, M. A., Podd, J. V., Rapley, B. I. and Rowland, R. E.,** Elevated sister chromatid exchange frequencies in dividing human peripheral blood lymphocytes exposed to 50 Hz magnetic fields. *Bioelectromagnetics* 2007. **28**: 281-288.

17 **Nordenson, I., Mild, K. H., Andersson, G. and Sandstrom, M.,** Chromosomal aberrations in human amniotic cells after intermittent exposure to fifty hertz magnetic fields. *Bioelectromagnetics* 1994. **15**: 293-301.

18 **Luo, Q., Yang, J., Zeng, Q. L., Zhu, X. M., Qian, Y. L. and Huang, H. F.,** 50-Hertz electromagnetic fields induce gammaH2AX foci formation in mouse preimplantation embryos in vitro. *Biol Reprod* 2006. **75**: 673-680.

19 **Juutilainen, J., Kumlin, T. and Naarala, J.,** Do extremely low frequency magnetic fields enhance the effects of environmental carcinogens? A meta-analysis of experimental studies. *Int J Radiat Biol* 2006. **82**: 1-12.

20 **Stronati, L., Testa, A., Villani, P., Marino, C., Lovisolo, G. A., Conti, D., Russo, F., Fresegna, A. M. and Cordelli, E.,** Absence of genotoxicity in human blood cells exposed to 50 Hz magnetic fields as assessed by comet assay, chromosome aberration, micronucleus, and sister chromatid exchange analyses. *Bioelectromagnetics* 2004. **25**: 41-48.

21 **Hintenlang, D. E.,** Synergistic effects of ionizing radiation and 60 Hz magnetic fields. *Bioelectromagnetics* 1993. **14**: 545-551.

22 **Cantoni, O., Sestili, P., Fiorani, M. and Dacha, M.,** The effect of 50 Hz sinusoidal electric and/or magnetic fields on the rate of repair of DNA single/double strand breaks in oxidatively injured cells. *Biochem Mol Biol Int* 1995. **37**: 681-689.

23 **Fiorani, M., Cantoni, O., Sestili, P., Conti, R., Nicolini, P., Vetrano, F. and Dacha, M.,** Electric and/or magnetic field effects on DNA structure and function in cultured human cells. *Mutat Res* 1992. **282**: 25-29.

24 **Cadossi, R., Bersani, F., Cossarizza, A., Zucchini, P., Emilia, G., Torelli, G. and Franceschi, C.,** Lymphocytes and low-frequency electromagnetic fields. *Faseb J* 1992. **6**: 2667-2674.

25 **Rosenthal, M. and Obe, G.,** Effects of 50-hertz electromagnetic fields on proliferation and on chromosomal alterations in human peripheral lymphocytes untreated or pretreated with chemical mutagens. *Mutat Res* 1989. **210**: 329-335.

26 **Katsir, G., Baram, S. C. and Parola, A. H.,** Effect of sinusoidally varying magnetic fields on cell proliferation and adenosine deaminase specific activity. *Bioelectromagnetics* 1998. **19**: 46-52.

27 **Conti, P., Gigante, G. E., Cifone, M. G., Alesse, E., Ianni, G., Reale, M. and Angeletti, P. U.,** Reduced mitogenic stimulation of human lymphocytes by extremely low frequency electromagnetic fields. *FEBS Lett* 1983. **162**: 156-160.

28 **Lange, S., Richard, D., Viergutz, T., Kriehuber, R., Weiss, D. G. and Simko, M.,** Alterations in the cell cycle and in the protein level of cyclin D1, p21CIP1, and p16INK4a after exposure to 50 Hz MF in human cells. *Radiat Environ Biophys* 2002. **41**: 131-137.

29 **Yoshizawa, H., Tsuchiya, T., Mizoe, H., Ozeki, H., Kanao, S., Yomori, H., Sakane, C., Hasebe, S., Motomura, T., Yamakawa, T., Mizuno, F., Hirose, H. and Otaka, Y.,** No effect of extremely low-frequency magnetic field observed on cell growth or initial response of cell proliferation in human cancer cell lines. *Bioelectromagnetics* 2002. **23**: 355-368.

30 **Harris, P. A., Lamb, J., Heaton, B. and Wheatley, D. N.,** Possible attenuation of the G2 DNA damage cell cycle checkpoint in HeLa cells by extremely low frequency (ELF) electromagnetic fields. *Cancer Cell Int* 2002. **2**: 3.

31 **Kumlin, T., Heikkinen, P., Kosma, V. M., Alhonen, L., Janne, J. and Juutilainen, J.,** p53-independent apoptosis in UV-irradiated mouse skin: possible inhibition by 50 Hz magnetic fields. *Radiat Environ Biophys* 2002. **41**: 155-158.

32 **De Nicola, M., Cordisco, S., Cerella, C., Albertini, M. C., D'Alessio, M., Accorsi, A., Bergamaschi, A., Magrini, A. and Ghibelli, L.,** Magnetic fields protect from apoptosis via redox alteration. *Ann N Y Acad Sci* 2006. **1090**: 59-68.

33 **Narita, K., Hanakawa, K., Kasahara, T., Hisamitsu, T. and Asano, K.,** Induction of apoptotic cell death in human leukemic cell line, HL-60, by extremely low frequency electric magnetic fields: analysis of the possible mechanisms in vitro. *In Vivo* 1997. **11**: 329-335.

34 **Blumenthal, N. C., Ricci, J., Breger, L., Zychlinsky, A., Solomon, H., Chen, G. G., Kuznetsov, D. and Dorfman, R.,** Effects of low-intensity AC and/or DC electromagnetic fields on cell attachment and induction of apoptosis. *Bioelectromagnetics* 1997. **18**: 264-272.

35 **Mangiacasale, R., Tritarelli, A., Sciamanna, I., Cannone, M., Lavia, P., Barberis, M. C., Lorenzini, R. and Cundari, E.,** Normal and cancer-prone human cells respond differently to extremely low frequency magnetic fields. *FEBS Lett* 2001. **487**: 397-403.

36 **Czyz, J., Nikolova, T., Schuderer, J., Kuster, N. and Wobus, A. M.,** Non-thermal effects of power-line magnetic fields (50 Hz) on gene expression levels of pluripotent embryonic stem cells-the role of tumour suppressor p53. *Mutat Res* 2004. **557**: 63-74.

37 **Lin, H., Goodman, R. and Shirley-Henderson, A.,** Specific region of the c-myc promoter is responsive to electric and magnetic fields. *J Cell Biochem* 1994. **54**: 281-288.

38 **Nikolova, T., Czyz, J., Rolletschek, A., Blyszczuk, P., Fuchs, J., Jovtchev, G., Schuderer, J., Kuster, N. and Wobus, A. M.,** Electromagnetic fields affect transcript levels of apoptosis-related genes in embryonic stem cell-derived neural progenitor cells. *Faseb J* 2005. **19**: 1686-1688.

39 **Verheyen, G. R., Pauwels, G., Verschaeve, L. and Schoeters, G.,** Effect of coexposure to 50 Hz magnetic fields and an aneugen on human lymphocytes, determined by the cytokinesis block micronucleus assay. *Bioelectromagnetics* 2003. **24**: 160-164.

40 **Santini, M. T., Ferrante, A., Rainaldi, G., Indovina, P. and Indovina, P. L.,** Extremely low frequency (ELF) magnetic fields and apoptosis: a review. *Int J Radiat Biol* 2005. **81**: 1-11.

41 **Tokalov, S. V. and Gutzeit, H. O.,** Weak electromagnetic fields (50 Hz) elicit a stress response in human cells. *Environ Res* 2004. **94**: 145-151.

42 **Bernardini, C., Zannoni, A., Turba, M. E., Bacci, M. L., Forni, M., Mesirca, P., Remondini, D., Castellani, G. and Bersani, F.,** Effects of 50 Hz sinusoidal magnetic fields on Hsp27, Hsp70, Hsp90 expression in porcine aortic endothelial cells (PAEC). *Bioelectromagnetics* 2007. **28**: 231-237.

43 **Malagoli, D., Lusvardi, M., Gobba, F. and Ottaviani, E.,** 50 Hz magnetic fields activate mussel immunocyte p38 MAP kinase and induce HSP70 and 90. *Comp Biochem Physiol C Toxicol Pharmacol* 2004. **137**: 75-79.

44 **Lin, H., Opler, M., Head, M., Blank, M. and Goodman, R.,** Electromagnetic field exposure induces rapid, transitory heat shock factor activation in human cells. *J Cell Biochem* 1997. **66**: 482-488.

45 **Lin, H., Blank, M., Rossol-Haseroth, K. and Goodman, R.,** Regulating genes with electromagnetic response elements. *J Cell Biochem* 2001. **81**: 143-148.

46 **Manikonda, P. K., Rajendra, P., Devendranath, D., Gunasekaran, B., Channakeshava, Aradhya, R. S., Sashidhar, R. B. and Subramanyam, C.,** Influence of extremely low frequency magnetic fields on Ca2+ signaling and NMDA receptor functions in rat hippocampus. *Neurosci Lett* 2007. **413**: 145-149.

47 **Guo, H., Xing, L., Zheng, M., Fan, C., Li, Y., Wang, J., Zhang, X. and Yan, W.,** Effects of 50Hz Homogeneous Ferromagnetic Field on the Concentrations of Intracellular Calcium-ion of SNU Cells and Lymphma Cells In Vitro. *Conf Proc IEEE Eng Med Biol Soc* 2005. **5**: 4874-4877.

48 **Liboff, A. R., Cherng, S., Jenrow, K. A. and Bull, A.,** Calmodulin-dependent cyclic nucleotide phosphodiesterase activity is altered by 20 microT magnetostatic fields. *Bioelectromagnetics* 2003. **24**: 32-38.

49 **Lindstrom, E., Lindstrom, P., Berglund, A., Mild, K. H. and Lundgren, E.,** Intracellular calcium oscillations induced in a T-cell line by a weak 50 Hz magnetic field. *J Cell Physiol* 1993. **156**: 395-398.

50 **Korzh-Sleptsova, I. L., Lindstrom, E., Mild, K. H., Berglund, A. and Lundgren, E.,** Low frequency MFs increased inositol 1,4,5-trisphosphate levels in the Jurkat cell line. *FEBS Lett* 1995. **359**: 151-154.

51 **Sandblom, J. and Theander, S.,** The effect of microwave radiation on the stability and formation of gramicidin-A channels in lipid bilayer membranes. *Bioelectromagnetics* 1991. **12**: 9-20.

52 **Liburdy, R. P., Callahan, D. E., Harland, J., Dunham, E., Sloma, T. R. and Yaswen, P.,** Experimental evidence for 60 Hz magnetic fields operating through the signal transduction cascade. Effects on calcium influx and c-MYC mRNA induction. *FEBS Lett* 1993. **334**: 301-308.

53 **Mattsson, M. O., Lindstrom, E., Still, M., Lindstrom, P., Mild, K. H. and Lundgren, E.,** [Ca2+](i) rise in Jurkat E6-1 cell lines from different sources as a response to 50 Hz magnetic field exposure as a reproducible effect and independent of poly-L-lysine treatment. *Cell Biol Int* 2001. **25**: 901-907.

54 **Kristupaitis, D., Dibirdik, I., Vassilev, A., Mahajan, S., Kurosaki, T., Chu, A., Tuel-Ahlgren, L., Tuong, D., Pond, D., Luben, R. and Uckun, F. M.,** Electromagnetic field-induced stimulation of Bruton's tyrosine kinase. *J Biol Chem* 1998. **273**: 12397-12401.

55 **Dibirdik, I., Kristupaitis, D., Kurosaki, T., Tuel-Ahlgren, L., Chu, A., Pond, D., Tuong, D., Luben, R. and Uckun, F. M.,** Stimulation of Src family protein-tyrosine kinases as a proximal and mandatory step for SYK kinase-dependent phospholipase Cgamma2 activation in lymphoma B cells exposed to low energy electromagnetic fields. *J Biol Chem* 1998. **273**: 4035-4039.

56 **Uckun, F. M., Kurosaki, T., Jin, J., Jun, X., Morgan, A., Takata, M., Bolen, J. and Luben, R.,** Exposure of B-lineage lymphoid cells to low energy electromagnetic fields stimulates Lyn kinase. *J Biol Chem* 1995. **270**: 27666-27670.

57 **Nuccitelli, S., Cerella, C., Cordisco, S., Albertini, M. C., Accorsi, A., De Nicola, M., D'Alessio, M., Radogna, F., Magrini, A., Bergamaschi, A. and Ghibelli, L.,** Hyperpolarization of plasma membrane of tumor cells sensitive to antiapoptotic effects of magnetic fields. *Ann N Y Acad Sci* 2006. **1090**: 217-225.

58 **Auvinen, A., Toivo, T. and Tokola, K.,** Epidemiological risk assessment of mobile phones and cancer: where can we improve? *Eur J Cancer Prev* 2006. **15**: 516-523.

59 **Adey, W. R., Byus, C. V., Cain, C. D., Higgins, R. J., Jones, R. A., Kean, C. J., Kuster, N., MacMurray, A., Stagg, R. B. and Zimmerman, G.,** Spontaneous and nitrosourea-induced primary tumors of the central nervous system in Fischer 344 rats exposed to frequency-modulated microwave fields. *Cancer Res* 2000. **60**: 1857-1863.

60 **Chagnaud, J. L., Moreau, J. M. and Veyret, B.,** No effect of short-term exposure to GSM-modulated low-power microwaves on benzo(a)pyrene-induced tumours in rat. *Int J Radiat Biol* 1999. **75**: 1251-1256.

61 **Lai, H. and Singh, N. P.,** Acute low-intensity microwave exposure increases DNA single-strand breaks in rat brain cells. *Bioelectromagnetics* 1995. **16**: 207-210.

62 **Lai, H. and Singh, N. P.,** Single- and double-strand DNA breaks in rat brain cells after acute exposure to radiofrequency electromagnetic radiation. *Int J Radiat Biol* 1996. **69**: 513-521.

63 **Malyapa, R. S., Ahern, E. W., Bi, C., Straube, W. L., LaRegina, M., Pickard, W. F. and Roti Roti, J. L.,** DNA damage in rat brain cells after in vivo exposure to 2450 MHz electromagnetic radiation and various methods of euthanasia. *Radiat Res* 1998. **149**: 637-645.

64 **Repacholi, M. H., Basten, A., Gebski, V., Noonan, D., Finnie, J. and Harris, A. W.,** Lymphomas in E mu-Pim1 transgenic mice exposed to pulsed 900 MHZ electromagnetic fields. *Radiat Res* 1997. **147**: 631-640.

65 **Utteridge, T. D., Gebski, V., Finnie, J. W., Vernon-Roberts, B. and Kuchel, T. R.,** Long-term exposure of E-mu-Pim1 transgenic mice to 898.4 MHz microwaves does not increase lymphoma incidence. *Radiat Res* 2002. **158**: 357-364.

66 **Vijayalaxmi, Leal, B. Z., Szilagyi, M., Prihoda, T. J. and Meltz, M. L.,** Primary DNA damage in human blood lymphocytes exposed in vitro to 2450 MHz radiofrequency radiation. *Radiat Res* 2000. **153**: 479-486.

67 **Stronati, L., Testa, A., Moquet, J., Edwards, A., Cordelli, E., Villani, P., Marino, C., Fresegna, A. M., Appolloni, M. and Lloyd, D.,** 935 MHz cellular phone radiation. An in vitro study of genotoxicity in human lymphocytes. *Int J Radiat Biol* 2006. **82**: 339-346.

68 **Diem, E., Schwarz, C., Adlkofer, F., Jahn, O. and Rudiger, H.,** Non-thermal DNA breakage by mobile-phone radiation (1800 MHz) in human fibroblasts and in transformed GFSH-R17 rat granulosa cells in vitro. *Mutat Res* 2005. **583**: 178-183.

69 **Speit, G., Schutz, P. and Hoffmann, H.,** Genotoxic effects of exposure to radiofrequency electromagnetic fields (RF-EMF) in cultured mammalian cells are not independently reproducible. *Mutat Res* 2007. **626**: 42-47.

70 **Heynick, L. N., Johnston, S. A. and Mason, P. A.,** Radio frequency electromagnetic fields: cancer, mutagenesis, and genotoxicity. *Bioelectromagnetics* 2003. **Suppl 6**: S74-100.

71 **Krewski, D., Glickman, B. W., Habash, R. W., Habbick, B., Lotz, W. G., Mandeville, R., Prato, F. S., Salem, T. and Weaver, D. F.,** Recent advances in research on radiofrequency fields and health: 2001-2003. *J Toxicol Environ Health B Crit Rev* 2007. **10**: 287-318.

72 **Nylund, R. and Leszczynski, D.,** Mobile phone radiation causes changes in gene and protein expression in human endothelial cell lines and the response seems to be genome- and proteome-dependent. *Proteomics* 2006. **6**: 4769-4780.

73 **Cotgreave, I. A.,** Biological stress responses to radio frequency electromagnetic radiation: are mobile phones really so (heat) shocking? *Arch Biochem Biophys* 2005. **435**: 227-240.

74 **Vogel, G.,** Scientific misconduct. Fraud charges cast doubt on claims of DNA damage from cell phone fields. *Science* 2008. **321**: 1144-1145.

75 **Lai, H. and Singh, N. P.,** Magnetic-field-induced DNA strand breaks in brain cells of the rat. *Environ Health Perspect* 2004. **112**: 687-694.

76 **Zmyslony, M., Palus, J., Jajte, J., Dziubaltowska, E. and Rajkowska, E.,** DNA damage in rat lymphocytes treated in vitro with iron cations and exposed to 7 mT magnetic fields (static or 50 Hz). *Mutat Res* 2000. **453**: 89-96.

77 **Porath, D., Bezryadin, A., de Vries, S. and Dekker, C.,** Direct measurement of electrical transport through DNA molecules. *Nature* 2000. **403**: 635-638.

78 **Wan, C., Fiebig, T., Schiemann, O., Barton, J. K. and Zewail, A. H.,** Femtosecond direct observation of charge transfer between bases in DNA. *Proc Natl Acad Sci U S A* 2000. **97**: 14052-14055.

79 **Giese, B.,** Electron transfer through DNA and peptides. *Bioorg Med Chem* 2006. **14**: 6139-6143.

80 **Ravera, S., Falugi, C., Calzia, D., Pepe, I. M., Panfoli, I. and Morelli, A.,** First cell cycles of sea urchin Paracentrotus lividus are dramatically impaired by exposure to extremely low-frequency electromagnetic field. *Biol Reprod* 2006. **75**: 948-953.

81 **Sahebjamei, H., Abdolmaleki, P. and Ghanati, F.,** Effects of magnetic field on the antioxidant enzyme activities of suspension-cultured tobacco cells. *Bioelectromagnetics* 2007. **28**: 42-47.

82 **Blank, M. and Soo, L.,** Optimal frequencies for magnetic acceleration of cytochrome oxidase and Na,K-ATPase reactions. *Bioelectrochemistry* 2001. **53**: 171-174.

83 **Blank, M. and Soo, L.,** Electromagnetic acceleration of the Belousov-Zhabotinski reaction. *Bioelectrochemistry* 2003. **61**: 93-97.

84 **Belyaev, I. Y., Hillert, L., Protopopova, M., Tamm, C., Malmgren, L. O., Persson, B. R., Selivanova, G. and Harms-Ringdahl, M.,** 915 MHz microwaves and 50 Hz magnetic field affect chromatin conformation and 53BP1 foci in human lymphocytes from hypersensitive and healthy persons. *Bioelectromagnetics* 2005. **26**: 173-184.

85 **Lindahl, T.,** Instability and decay of the primary structure of DNA. *Nature* 1993. **362**: 709-715.

86 **Chaudhuri, J., Tian, M., Khuong, C., Chua, K., Pinaud, E. and Alt, F. W.,** Transcription-targeted DNA deamination by the AID antibody diversification enzyme. *Nature* 2003. **422**: 726-730.

87 **Davies, K. J.,** The broad spectrum of responses to oxidants in proliferating cells: a new paradigm for oxidative stress. *IUBMB Life* 1999. **48**: 41-47.

88 **Wardman, P. and Candeias, L. P.,** Fenton chemistry: an introduction. *Radiat Res* 1996. **145**: 523-531.

89 **Burney, S., Caulfield, J. L., Niles, J. C., Wishnok, J. S. and Tannenbaum, S. R.,** The chemistry of DNA damage from nitric oxide and peroxynitrite. *Mutat Res* 1999. **424**: 37-49.

90 **Saran, M. and Bors, W.,** Radical reactions in vivo--an overview. *Radiat Environ Biophys* 1990. **29**: 249-262.

91 **Breen, A. P. and Murphy, J. A.,** Reactions of oxyl radicals with DNA. *Free Radic Biol Med* 1995. **18**: 1033-1077.

92 **Goodhead, D. T.,** The initial physical damage produced by ionizing radiations. *Int J Radiat Biol* 1989. **56**: 623-634.

93 **Varghese, A. J.,** Photochemistry of nucleic acids and their constituents. *Photophysiology* 1972: 207-274.

94 **Lober, G. and Kittler, L.,** Selected topics in photochemistry of nucleic acids. Recent results and perspectives. *Photochem Photobiol* 1977. **25**: 215-233.

95 **Duker, N. J. and Gallagher, P. E.,** Purine photoproducts. *Photochem Photobiol* 1988. **48**: 35-39.

96 **Lawley, P. D. and Phillips, D. H.,** DNA adducts from chemotherapeutic agents. *Mutat Res* 1996. **355**: 13-40.

97 **Phillips, D. H.,** Fifty years of benzo(a)pyrene. *Nature* 1983. **303**: 468-472.

98 **Smela, M. E., Currier, S. S., Bailey, E. A. and Essigmann, J. M.,** The chemistry and biology of aflatoxin B(1): from mutational spectrometry to carcinogenesis. *Carcinogenesis* 2001. **22**: 535-545.

99 **Beranek, D. T.,** Distribution of methyl and ethyl adducts following alkylation with monofunctional alkylating agents. *Mutat Res* 1990. **231**: 11-30.

100 **Hearst, J. E., Isaacs, S. T., Kanne, D., Rapoport, H. and Straub, K.,** The reaction of the psoralens with deoxyribonucleic acid. *Q Rev Biophys* 1984. **17**: 1-44.

101 **Ferguson, L. R. and Baguley, B. C.,** Mutagenicity of anticancer drugs that inhibit topoisomerase enzymes. *Mutat Res* 1996. **355**: 91-101.

102 **Bennett, R. A., Swerdlow, P. S. and Povirk, L. F.,** Spontaneous cleavage of bleomycin-induced abasic sites in chromatin and their mutagenicity in mammalian shuttle vectors. *Biochemistry* 1993. **32**: 3188-3195.

103 **Rich, T. A., Shepard, R. C. and Mosley, S. T.,** Four decades of continuing innovation with fluorouracil: current and future approaches to fluorouracil chemoradiation therapy. *J Clin Oncol* 2004. **22**: 2214-2232.

104 **Heidelberger, C., Chaudhuri, N. K., Danneberg, P., Mooren, D., Griesbach, L., Duschinsky, R., Schnitzer, R. J., Pleven, E. and Scheiner, J.,** Fluorinated pyrimidines, a new class of tumour-inhibitory compounds. *Nature* 1957. **179**: 663-666.

105 **Longley, D. B., Harkin, D. P. and Johnston, P. G.,** 5-fluorouracil: mechanisms of action and clinical strategies. *Nat Rev Cancer* 2003. **3**: 330-338.

106 **Christmann, M., Tomicic, M. T., Roos, W. P. and Kaina, B.,** Mechanisms of human DNA repair: an update. *Toxicology* 2003. **193**: 3-34.

107 **Bergstralh, D. T. and Sekelsky, J.,** Interstrand crosslink repair: can XPF-ERCC1 be let off the hook? *Trends Genet* 2008.

108 **Taylor, A. M.,** Chromosome instability syndromes. *Best Pract Res Clin Haematol* 2001. **14**: 631-644.

109 **Masih, P. J., Kunnev, D. and Melendy, T.,** Mismatch Repair proteins are recruited to replicating DNA through interaction with Proliferating Cell Nuclear Antigen (PCNA). *Nucleic Acids Res* 2008. **36**: 67-75.

110 **Wang, H. and Hays, J. B.,** Human DNA mismatch repair: coupling of mismatch recognition to strand-specific excision. *Nucleic Acids Res* 2007. **35**: 6727-6739.

111 **Scherer, S. J., Maier, S. M., Seifert, M., Hanselmann, R. G., Zang, K. D., Muller-Hermelink, H. K., Angel, P., Welter, C. and Schartl, M.,** p53 and c-Jun functionally synergize in the regulation of the DNA repair gene hMSH2 in response to UV. *J Biol Chem* 2000. **275**: 37469-37473.

112 **Rustgi, A. K.,** The genetics of hereditary colon cancer. *Genes Dev* 2007. **21**: 2525-2538.

113 **Parrilla-Castellar, E. R., Arlander, S. J. and Karnitz, L.,** Dial 9-1-1 for DNA damage: the Rad9-Hus1-Rad1 (9-1-1) clamp complex. *DNA Repair (Amst)* 2004. **3**: 1009-1014.

114 **Lehmann, A. R., Niimi, A., Ogi, T., Brown, S., Sabbioneda, S., Wing, J. F., Kannouche, P. L. and Green, C. M.,** Translesion synthesis: Y-family polymerases and the polymerase switch. *DNA Repair (Amst)* 2007. **6**: 891-899.

115 **Hanawalt, P. C.,** Subpathways of nucleotide excision repair and their regulation. *Oncogene* 2002. **21**: 8949-8956.

116 **Shuck, S. C., Short, E. A. and Turchi, J. J.,** Eukaryotic nucleotide excision repair: from understanding mechanisms to influencing biology. *Cell Res* 2008. **18**: 64-72.

117 **Vermeulen, W., de Boer, J., Citterio, E., van Gool, A. J., van der Horst, G. T., Jaspers, N. G., de Laat, W. L., Sijbers, A. M., van der Spek, P. J., Sugasawa, K., Weeda, G., Winkler, G. S., Bootsma, D., Egly, J. M. and Hoeijmakers, J. H.,** Mammalian nucleotide excision repair and syndromes. *Biochem Soc Trans* 1997. **25**: 309-315.

118 **Yang, L. Y., Jiang, H. and Rangel, K. M.,** RNA polymerase II stalled on a DNA template during transcription elongation is ubiquitinated and the ubiquitination facilitates displacement of the elongation complex. *Int J Oncol* 2003. **22**: 683-689.

119 **Ljungman, M. and Zhang, F.,** Blockage of RNA polymerase as a possible trigger for u.v. light-induced apoptosis. *Oncogene* 1996. **13**: 823-831.

120 **Spivak, G.,** UV-sensitive syndrome. *Mutat Res* 2005. **577**: 162-169.

121 **Pegg, A. E., Dolan, M. E. and Moschel, R. C.,** Structure, function, and inhibition of O6-alkylguanine-DNA alkyltransferase. *Prog Nucleic Acid Res Mol Biol* 1995. **51**: 167-223.

122 **Aas, P. A., Otterlei, M., Falnes, P. O., Vagbo, C. B., Skorpen, F., Akbari, M., Sundheim, O., Bjoras, M., Slupphaug, G., Seeberg, E. and Krokan, H. E.,** Human and bacterial oxidative demethylases repair alkylation damage in both RNA and DNA. *Nature* 2003. **421**: 859-863.

123 **Nilsen, H. and Krokan, H. E.,** Base excision repair in a network of defence and tolerance. *Carcinogenesis* 2001. **22**: 987-998.

124 **Scharer, O. D. and Jiricny, J.,** Recent progress in the biology, chemistry and structural biology of DNA glycosylases. *Bioessays* 2001. **23**: 270-281.

125 **Sobol, R. W., Horton, J. K., Kuhn, R., Gu, H., Singhal, R. K., Prasad, R., Rajewsky, K. and Wilson, S. H.,** Requirement of mammalian DNA polymerase-beta in base-excision repair. *Nature* 1996. **379**: 183-186.

126 **Deterding, L. J., Prasad, R., Mullen, G. P., Wilson, S. H. and Tomer, K. B.,** Mapping of the 5'-2-deoxyribose-5-phosphate lyase active site in DNA polymerase beta by mass spectrometry. *J Biol Chem* 2000. **275**: 10463-10471.

127 **Matsumoto, Y., Kim, K., Hurwitz, J., Gary, R., Levin, D. S., Tomkinson, A. E. and Park, M. S.,** Reconstitution of proliferating cell nuclear antigen-dependent repair of apurinic/apyrimidinic sites with purified human proteins. *J Biol Chem* 1999. **274**: 33703-33708.

128 **Wilson, D. M., 3rd and Thompson, L. H.,** Life without DNA repair. *Proc Natl Acad Sci U S A* 1997. **94**: 12754-12757.

129 **Zhou, J., Ahn, J., Wilson, S. H. and Prives, C.,** A role for p53 in base excision repair. *Embo J* 2001. **20**: 914-923.

130 **Kenny, M. K., Mendez, F., Sandigursky, M., Kureekattil, R. P., Goldman, J. D., Franklin, W. A. and Bases, R.,** Heat shock protein 70 binds to human apurinic/apyrimidinic endonuclease and stimulates endonuclease activity at abasic sites. *J Biol Chem* 2001. **276**: 9532-9536.

131 **Gu, Y., Parker, A., Wilson, T. M., Bai, H., Chang, D. Y. and Lu, A. L.,** Human MutY homolog, a DNA glycosylase involved in base excision repair, physically and functionally interacts with mismatch repair proteins human MutS homolog 2/human MutS homolog 6. *J Biol Chem* 2002. **277**: 11135-11142.

132 **Bessho, T.,** Nucleotide excision repair 3' endonuclease XPG stimulates the activity of base excision repairenzyme thymine glycol DNA glycosylase. *Nucleic Acids Res* 1999. **27**: 979-983.

133 **Shimizu, Y., Iwai, S., Hanaoka, F. and Sugasawa, K.,** Xeroderma pigmentosum group C protein interacts physically and functionally with thymine DNA glycosylase. *Embo J* 2003. **22**: 164-173.

134 **Hoege, C., Pfander, B., Moldovan, G. L., Pyrowolakis, G. and Jentsch, S.,** RAD6-dependent DNA repair is linked to modification of PCNA by ubiquitin and SUMO. *Nature* 2002. **419**: 135-141.

135 **Hardeland, U., Steinacher, R., Jiricny, J. and Schar, P.,** Modification of the human thymine-DNA glycosylase by ubiquitin-like proteins facilitates enzymatic turnover. *Embo J* 2002. **21**: 1456-1464.

136 **Gocke, C. B., Yu, H. and Kang, J.,** Systematic identification and analysis of mammalian small ubiquitin-like modifier substrates. *J Biol Chem* 2005. **280**: 5004-5012.

137 **Jaiswal, M., LaRusso, N. F., Nishioka, N., Nakabeppu, Y. and Gores, G. J.,** Human Ogg1, a protein involved in the repair of 8-oxoguanine, is inhibited by nitric oxide. *Cancer Res* 2001. **61**: 6388-6393.

138 **Hasan, S., Stucki, M., Hassa, P. O., Imhof, R., Gehrig, P., Hunziker, P., Hubscher, U. and Hottiger, M. O.,** Regulation of human flap endonuclease-1 activity by acetylation through the transcriptional coactivator p300. *Mol Cell* 2001. **7**: 1221-1231.

139 **Neddermann, P. and Jiricny, J.,** The purification of a mismatch-specific thymine-DNA glycosylase from HeLa cells. *J Biol Chem* 1993. **268**: 21218-21224.

140 **Hardeland, U., Bentele, M., Jiricny, J. and Schar, P.,** The versatile thymine DNA-glycosylase: a comparative characterization of the human, Drosophila and fission yeast orthologs. *Nucleic Acids Res* 2003. **31**: 2261-2271.

141 **Gallinari, P. and Jiricny, J.,** A new class of uracil-DNA glycosylases related to human thymine-DNA glycosylase. *Nature* 1996. **383**: 735-738.

142 **Cortazar, D., Kunz, C., Saito, Y., Steinacher, R. and Schar, P.,** The enigmatic thymine DNA glycosylase. *DNA Repair (Amst)* 2007. **6**: 489-504.

143 **Barrett, T. E., Savva, R., Panayotou, G., Barlow, T., Brown, T., Jiricny, J. and Pearl, L. H.,** Crystal structure of a G:T/U mismatch-specific DNA glycosylase: mismatch recognition by complementary-strand interactions. *Cell* 1998. **92**: 117-129.

144 **Hardeland, U., Bentele, M., Jiricny, J. and Schar, P.,** Separating substrate recognition from base hydrolysis in human thymine DNA glycosylase by mutational analysis. *J Biol Chem* 2000. **275**: 33449-33456.

145 **Waters, T. R., Gallinari, P., Jiricny, J. and Swann, P. F.,** Human thymine DNA glycosylase binds to apurinic sites in DNA but is displaced by human apurinic endonuclease 1. *J Biol Chem* 1999. **274**: 67-74.

146 **Steinacher, R. and Schar, P.,** Functionality of human thymine DNA glycosylase requires SUMO-regulated changes in protein conformation. *Curr Biol* 2005. **15**: 616-623.

147 **Melchior, F., Schergaut, M. and Pichler, A.,** SUMO: ligases, isopeptidases and nuclear pores. *Trends Biochem Sci* 2003. **28**: 612-618.

148 **Um, S., Harbers, M., Benecke, A., Pierrat, B., Losson, R. and Chambon, P.,** Retinoic acid receptors interact physically and functionally with the T:G mismatch-specific thymine-DNA glycosylase. *J Biol Chem* 1998. **273**: 20728-20736.

149 **Chevray, P. M. and Nathans, D.,** Protein interaction cloning in yeast: identification of mammalian proteins that react with the leucine zipper of Jun. *Proc Natl Acad Sci U S A* 1992. **89**: 5789-5793.

150 **Chen, D., Lucey, M. J., Phoenix, F., Lopez-Garcia, J., Hart, S. M., Losson, R., Buluwela, L., Coombes, R. C., Chambon, P., Schar, P. and Ali, S.,** T:G mismatch-specific thymine-DNA glycosylase potentiates transcription of estrogen-regulated genes through direct interaction with estrogen receptor alpha. *J Biol Chem* 2003. **278**: 38586-38592.

151 **Tini, M., Benecke, A., Um, S. J., Torchia, J., Evans, R. M. and Chambon, P.,** Association of CBP/p300 acetylase and thymine DNA glycosylase links DNA repair and transcription. *Mol Cell* 2002. **9**: 265-277.

152 **Fremont, M., Siegmann, M., Gaulis, S., Matthies, R., Hess, D. and Jost, J. P.,** Demethylation of DNA by purified chick embryo 5-methylcytosine-DNA glycosylase requires both protein and RNA. *Nucleic Acids Res* 1997. **25**: 2375-2380.

153 **Jost, J. P. and Jost, Y. C.,** Mechanism of active DNA demethylation during embryonic development and cellular differentiation in vertebrates. *Gene* 1995. **157**: 265-266.

154 **Li, Y. Q., Zhou, P. Z., Zheng, X. D., Walsh, C. P. and Xu, G. L.,** Association of Dnmt3a and thymine DNA glycosylase links DNA methylation with base-excision repair. *Nucleic Acids Res* 2007. **35**: 390-400.

155 **Beard, W. A. and Wilson, S. H.,** Structural design of a eukaryotic DNA repair polymerase: DNA polymerase beta. *Mutat Res* 2000. **460**: 231-244.

156 **Moon, A. F., Garcia-Diaz, M., Batra, V. K., Beard, W. A., Bebenek, K., Kunkel, T. A., Wilson, S. H. and Pedersen, L. C.,** The X family portrait: structural insights into biological functions of X family polymerases. *DNA Repair (Amst)* 2007. **6**: 1709-1725.

157 **Idriss, H. T., Al-Assar, O. and Wilson, S. H.,** DNA polymerase beta. *Int J Biochem Cell Biol* 2002. **34**: 321-324.

158 **Tokui, T., Inagaki, M., Nishizawa, K., Yatani, R., Kusagawa, M., Ajiro, K., Nishimoto, Y., Date, T. and Matsukage, A.,** Inactivation of DNA polymerase beta by in vitro phosphorylation with protein kinase C. *J Biol Chem* 1991. **266**: 10820-10824.

159 **Hasan, S., El-Andaloussi, N., Hardeland, U., Hassa, P. O., Burki, C., Imhof, R., Schar, P. and Hottiger, M. O.,** Acetylation regulates the DNA end-trimming activity of DNA polymerase beta. *Mol Cell* 2002. **10**: 1213-1222.

160 **Nicholls, A., Sharp, K. A. and Honig, B.,** Protein folding and association: insights from the interfacial and thermodynamic properties of hydrocarbons. *Proteins* 1991. **11**: 281-296.

161 **Momand, J., Wu, H. H. and Dasgupta, G.,** MDM2--master regulator of the p53 tumor suppressor protein. *Gene* 2000. **242**: 15-29.

162 **Bartek, J. and Lukas, J.,** Pathways governing G1/S transition and their response to DNA damage. *FEBS Lett* 2001. **490**: 117-122.

163 **Nakayama, K. I., Hatakeyama, S. and Nakayama, K.,** Regulation of the cell cycle at the G1-S transition by proteolysis of cyclin E and p27Kip1. *Biochem Biophys Res Commun* 2001. **282**: 853-860.

164 **Coleman, T. R. and Dunphy, W. G.,** Cdc2 regulatory factors. *Curr Opin Cell Biol* 1994. **6**: 877-882.

165 **Kastan, M. B. and Bartek, J.,** Cell-cycle checkpoints and cancer. *Nature* 2004. **432**: 316-323.

166 **Yang, J., Xu, Z. P., Huang, Y., Hamrick, H. E., Duerksen-Hughes, P. J. and Yu, Y. N.,** ATM and ATR: sensing DNA damage. *World J Gastroenterol* 2004. **10**: 155-160.

167 **Stewart, G. S., Wang, B., Bignell, C. R., Taylor, A. M. and Elledge, S. J.,** MDC1 is a mediator of the mammalian DNA damage checkpoint. *Nature* 2003. **421**: 961-966.

168 **Paull, T. T., Rogakou, E. P., Yamazaki, V., Kirchgessner, C. U., Gellert, M. and Bonner, W. M.,** A critical role for histone H2AX in recruitment of repair factors to nuclear foci after DNA damage. *Curr Biol* 2000. **10**: 886-895.

169 **Durocher, D. and Jackson, S. P.,** DNA-PK, ATM and ATR as sensors of DNA damage: variations on a theme? *Curr Opin Cell Biol* 2001. **13**: 225-231.

170 **Kim, M. Y., Zhang, T. and Kraus, W. L.,** Poly(ADP-ribosyl)ation by PARP-1: 'PAR-laying' NAD+ into a nuclear signal. *Genes Dev* 2005. **19**: 1951-1967.

171 **Pleschke, J. M., Kleczkowska, H. E., Strohm, M. and Althaus, F. R.,** Poly(ADP-ribose) binds to specific domains in DNA damage checkpoint proteins. *J Biol Chem* 2000. **275**: 40974-40980.

172 **Miyashita, T. and Reed, J. C.,** Tumor suppressor p53 is a direct transcriptional activator of the human bax gene. *Cell* 1995. **80**: 293-299.

173 **Oda, E., Ohki, R., Murasawa, H., Nemoto, J., Shibue, T., Yamashita, T., Tokino, T., Taniguchi, T. and Tanaka, N.,** Noxa, a BH3-only member of the Bcl-2 family and candidate mediator of p53-induced apoptosis. *Science* 2000. **288**: 1053-1058.

174 **Nakano, K. and Vousden, K. H.,** PUMA, a novel proapoptotic gene, is induced by p53. *Mol Cell* 2001. **7**: 683-694.

175 **Zhou, M., Gu, L., Li, F., Zhu, Y., Woods, W. G. and Findley, H. W.,** DNA damage induces a novel p53-survivin signaling pathway regulating cell cycle and apoptosis in acute lymphoblastic leukemia cells. *J Pharmacol Exp Ther* 2002. **303**: 124-131.

176 **Mihara, M., Erster, S., Zaika, A., Petrenko, O., Chittenden, T., Pancoska, P. and Moll, U. M.,** p53 has a direct apoptogenic role at the mitochondria. *Mol Cell* 2003. **11**: 577-590.

177 **Konishi, A., Shimizu, S., Hirota, J., Takao, T., Fan, Y., Matsuoka, Y., Zhang, L., Yoneda, Y., Fujii, Y., Skoultchi, A. I. and Tsujimoto, Y.,** Involvement of histone H1.2 in apoptosis induced by DNA double-strand breaks. *Cell* 2003. **114**: 673-688.

178 **Yang, S., Kuo, C., Bisi, J. E. and Kim, M. K.,** PML-dependent apoptosis after DNA damage is regulated by the checkpoint kinase hCds1/Chk2. *Nat Cell Biol* 2002. **4**: 865-870.

179 **Li, H., Kolluri, S. K., Gu, J., Dawson, M. I., Cao, X., Hobbs, P. D., Lin, B., Chen, G., Lu, J., Lin, F., Xie, Z., Fontana, J. A., Reed, J. C. and Zhang, X.,** Cytochrome c release and apoptosis induced by mitochondrial targeting of nuclear orphan receptor TR3. *Science* 2000. **289**: 1159-1164.

180 **Komatsu, K., Miyashita, T., Hang, H., Hopkins, K. M., Zheng, W., Cuddeback, S., Yamada, M., Lieberman, H. B. and Wang, H. G.,** Human homologue of S. pombe Rad9 interacts with BCL-2/BCL-xL and promotes apoptosis. *Nat Cell Biol* 2000. **2**: 1-6.

181 **Erwig, L. P. and Henson, P. M.,** Clearance of apoptotic cells by phagocytes. *Cell Death Differ* 2008. **15**: 243-250.

182 **Schwarz, C., Kratochvil, E., Pilger, A., Kuster, N., Adlkofer, F. and Rudiger, H. W.,** Radiofrequency electromagnetic fields (UMTS, 1,950 MHz) induce genotoxic effects in vitro in human fibroblasts but not in lymphocytes. *Int Arch Occup Environ Health* 2008. **81**: 755-767.

183 **Takao, M., Aburatani, H., Kobayashi, K. and Yasui, A.,** Mitochondrial targeting of human DNA glycosylases for repair of oxidative DNA damage. *Nucleic Acids Res* 1998. **26**: 2917-2922.

184 **Kobayakawa, S., Miike, K., Nakao, M. and Abe, K.,** Dynamic changes in the epigenomic state and nuclear organization of differentiating mouse embryonic stem cells. *Genes Cells* 2007. **12**: 447-460.

185 **Kanda, T., Sullivan, K. F. and Wahl, G. M.,** Histone-GFP fusion protein enables sensitive analysis of chromosome dynamics in living mammalian cells. *Curr Biol* 1998. **8**: 377-385.

186 **Leonhardt, H., Rahn, H. P., Weinzierl, P., Sporbert, A., Cremer, T., Zink, D. and Cardoso, M. C.,** Dynamics of DNA replication factories in living cells. *J Cell Biol* 2000. **149**: 271-280.

187 **Olive, P. L. and Banath, J. P.,** Induction and rejoining of radiation-induced DNA single-strand breaks: "tail moment" as a function of position in the cell cycle. *Mutat Res* 1993. **294**: 275-283.

188 **Vijayalaxmi, McNamee, J. P. and Scarfi, M. R.,** Comments on: "DNA strand breaks" by Diem et al. [Mutat. Res. 583 (2005) 178-183] and Ivancsits et al. [Mutat. Res. 583 (2005) 184-188]. *Mutat Res* 2006. **603**: 104-106; author reply 107-109.

189 **Olive, P. L. and Banath, J. P.,** Sizing highly fragmented DNA in individual apoptotic cells using the comet assay and a DNA crosslinking agent. *Exp Cell Res* 1995. **221**: 19-26.

190 **Scaiano, J. C., Cozens, F. L. and Mohtat, N.,** Influence of combined AC-DC magnetic fields on free radicals in organized and biological systems. Development of a model and application of the radical pair mechanism to radicals in micelles. *Photochem Photobiol* 1995. **62**: 818-829.

191 **Brocklehurst, B. and McLauchlan, K. A.,** Free radical mechanism for the effects of environmental electromagnetic fields on biological systems. *Int J Radiat Biol* 1996. **69**: 3-24.

192 **Regoli, F., Gorbi, S., Machella, N., Tedesco, S., Benedetti, M., Bocchetti, R., Notti, A., Fattorini, D., Piva, F. and Principato, G.,** Pro-oxidant effects of extremely low frequency electromagnetic fields in the land snail Helix aspersa. *Free Radic Biol Med* 2005. **39**: 1620-1628.

193 **Lai, H. and Singh, N. P.,** Melatonin and a spin-trap compound block radiofrequency electromagnetic radiation-induced DNA strand breaks in rat brain cells. *Bioelectromagnetics* 1997. **18**: 446-454.

194 **Davis, A. J., Yan, Z., Martinez, B. and Mumby, M. C.,** Protein phosphatase 2A is targeted to the cell division control protein 6 by a calcium-regulated regulatory subunit. *J Biol Chem* 2008.

195 **Simko, M. and Mattsson, M. O.,** Extremely low frequency electromagnetic fields as effectors of cellular responses in vitro: possible immune cell activation. *J Cell Biochem* 2004. **93**: 83-92.

196 **Blank, M.,** Do electromagnetic fields interact with electrons in the Na,K-ATPase? *Bioelectromagnetics* 2005. **26**: 677-683.

197 **Blank, M. and Goodman, R.,** Electromagnetic fields may act directly on DNA. *J Cell Biochem* 1999. **75**: 369-374.

198 **Jaremko, M., Justenhoven, C., Schroth, W., Abraham, B. K., Fritz, P., Vollmert, C., Illig, T., Simon, W., Schwab, M. and Brauch, H.,** Polymorphism of the DNA repair enzyme XRCC1 is associated with treatment prediction in anthracycline and cyclophosphamide/methotrexate/5-fluorouracil-based chemotherapy of patients with primary invasive breast cancer. *Pharmacogenet Genomics* 2007. **17**: 529-538.

7. Acknowledgements

I am deeply grateful to Prof. Primo Schär for accepting me as a member of his lab and introducing me to this exciting project, for always being willing to talk about scientific problems, for his constant support and both scientific interest and guidance during my PhD project.

I thank Christophe Kunz and David Schürmann for their scientific support and Daniel Cortazar for adding some colour to the daily lab routine and for encouraging me during hard times of the project.

I am also thankful to all other members of the Schär lab (Yusuke, Olivier, Mirco, Roland, Sanja, Patric, Basia, Ueli, Marcel, Claudia, Stefan, Angelika, Faiza) for the warm and open welcome, for their help and friendship and for providing a stimulating and joyful lab atmosphere.

I am very grateful to my family, which paved the way for me to a good education and always supported me in realising my dreams.

I am also thankful to all my friends, which made up the social network that is needed for such a project.

Special thanks go to Martin, for his love, friendship, support and encouragement through this time.

Appendices

Appendix I: Manuscript: DNA Fragmentation in Human Fibroblasts Under Extremely Low Frequency Electromagnetic Field Exposure

Frauke Focke, Niels Kuster, Primo Schär

Appendix II: Manuscript: Genotoxic Effects From Radiofrequency Electromagnetic Fields: Revisiting a Controversial Issue

Frauke Focke, Niels Kuster, Primo Schär

Appendix III: Submitted Manuscript: Base Excision by Thymine DNA Glycosylase Mediates DNA-Directed Cytotoxicity of 5-Fluorouracil

Christophe Kunz, **Frauke Focke**, Yusuke Saito, David Schürmann, Jim Selfridge, Adrian Bird and Primo Schär

Appendix IV: Cell cycle regulation as a mechanism for functional separation of the apparently redundant uracil DNA glycosylases TDG and UNG2

Ulrike Hardeland, Christophe Kunz, **Frauke Focke**, Marta Szadkowski, and Primo Schär

Nucleic Acids Res. 2007;35(11):3859-67. Epub 2007 May 25.

Appendix V: Arginine Methylation Regulates DNA Polymerase β

Nazim El-Andaloussi, Taras Valovka, Magali Toueille, Roland Steinacher, **Frauke Focke**, Peter Gehrig, Marcela Covic, Paul O. Hassa, Primo Schär, Ulrich Hübscher and Michael O. Hottiger

Mol Cell. 2006 Apr 7;22(1):51-62.

Appendix I:

DNA Fragmentation in Human Fibroblasts Under Extremely Low Frequency Electromagnetic Field Exposure

Frauke Focke[1], Niels Kuster[2], and Primo Schär[1*]

[1] Department of Biomedicine
University of Basel
Mattenstrasse 28
4058 Basel
Switzerland

[2] IT'IS Foundation
Zeughausstrasse 43
8004 Zurich
Switzerland

DNA Fragmentation in Human Fibroblasts Under Extremely Low Frequency Electromagnetic Field Exposure

Running title: ELF-EMF effects on DNA

Frauke Focke[1], Niels Kuster[2], and Primo Schär[1*]

[1] Department of Biomedicine
University of Basel
Mattenstrasse 28
4058 Basel
Switzerland

[2] IT'IS Foundation
Zeughausstrasse 43
8004 Zurich
Switzerland

* Corresponding author: primo.schaer@unibas.ch
Phone: +41 61 267 0767
Fax: +41 61 267 3566

Characters including spaces: 58687

ABSTRACT

Electromagnetic fields in the extremely low frequency range (ELF-EMF) were reported to cause DNA fragmentation as inferred from “comet” analyses of human cell lines. These findings were heavily debated on the grounds of theoretical considerations but also because of the lack of reproducibility in replication studies. We revisited this issue with the aim to clarify some of the discrepancies and uncertainties associated with previous studies. We analysed DNA fragmentation using ELF-EMF exposure and comet assay conditions as well as human cell lines identical to those used in a previous study. We then expanded the study to include additional cell lines and to address possible confounder effects; i.e. cell proliferation and apoptosis as well as mode of comet analyses. We found that human primary fibroblasts but not HeLa cells show slightly but significantly increased DNA fragmentation in comet assays following 15 hours intermittent (but not continuous) exposure to 50 Hz EFL-EMF. This effect was apparent in proliferating cells but not in starvation-induced G1-arrested cultures, suggesting that processes in DNA replication may be targeted by the exposure. We did not find evidence for an ELF-EMF dependent induction of oxidative DNA base damage. In the cell line showing the highest ELF-EMF induced DNA fragmentation, however, ELF-EMF exposure slightly reduced the fraction of actively replicating cells while increasing the apoptotic fraction, and this effect contributed mildly to the comet tailfactor increase. Hence, our data confirm that ELF-EMF exposure can induce comet tailfactor increases in primary human fibroblasts, and these implicate increased steady-state levels of DNA strand-breaks. The data further suggest that these DNA breaks are unlikely due to ELF-EMF induced oxidative DNA damage but can be accounted for by the disturbance of S-phase processes and, marginally, by inductions of apoptosis.

INTRODUCTION

During the past decades, the exposure of humans to extremely low frequency electromagnetic fields (ELF-EMFs) has grown considerably, mainly because of an ever increasing transmission and use of electric power at a frequency of 50 Hz in Europe. Consequently, public concern about adverse health impacts of ELF-EMFs, also directed to genetic integrity and cancer promotion, has been raising. Numerous investigations into biological effects of ELF-EMF exposure with epidemiological, molecular and biophysical approaches yielded inconsistent, sometimes conflicting, information. Conclusive evidence allowing an assessment of the risk of magnetic fields for human health has not been produced. Yet, epidemiology studies have correlated the exposure to EMFs of electric power lines with an increased incidence of childhood leukaemia (1-3) but not with other types of cancer (4,5). Since there is a well-established relationship between radiation induced genotoxicity and carcinogenicity, it was hypothesized that ELF-EMFs, similar to ultraviolet light or ionizing radiation, may induce DNA damage with the mutagenic potential to increase the risk of carcinogenesis. Laboratory studies addressing genome integrity under ELF-EMF exposure conditions have been conducted in different model systems. These, however, produced inconsistent results, some revealing the occurrence of DNA aberrations under certain conditions (6-11), others not (12-15). However, the application of non-standardized exposure equipment and conditions as well as the use of different cell types or cell lines of different origin in these studies makes a direct comparison difficult. Additionally, the studies that produced positive results were heavily criticized with regard to conceptional and experimental shortcomings like the analysis method they used and the failure to exclude confounder effects from apoptosis or cell cycle changes (16).

It seems counterintuitive that the energy transmitted with low frequency magnetic or electromagnetic fields is powerful enough to challenge the chemical integrity of the DNA, and it is generally accepted that ELF-EMFs do not damage DNA directly (17). Consequently, ELF-EMFs are not considered direct genotoxic agents. Nevertheless, several hypotheses for how they might affect the DNA structure have been put forward. EMFs might influence DNA stability

by inducing secondary currents in the body (18) leading to a movement of electrons. If this happens in DNA, temporary guanine radicals may form that, upon reaction with water, will be converted to oxidative damage. Induction of electric currents in DNA was shown *in vitro*, using short dsDNA oligonucleotides (19,20), and electron migration was shown to occur over long distances, whereby guanines may act as electron sinks (21). Alternatively, it was proposed that EMFs may alter cellular processes that could indirectly affect DNA integrity or transactions (22,23). These include free radical production through an influence on the iron pool of the cell (24-26), modulation of enzymatic activities (27-29), acceleration of cellular proliferation (30-33), or perturbation of the cell cycle (34).

The aim of this study was to revisit experiments by Ivancsits *et. al*. (11,35), which produced evidence for increased DNA strand breaks, micronuclei and chromosomal aberrations in cells intermittently exposed to 50 Hz ELF-EMF, and to expand the study to address some imminent conceptual, experimental, and mechanistic questions associated with these findings. Applying experimental conditions identical to those of Ivancsits *et. al*. (11), we were able to reproduce their finding of an ELF-EMF exposure dependent increase in the comet tail DNA, albeit at a lower level and with higher variability. This effect of DNA fragmentation was small but statistically significant and cell line dependent, implicating modulation by a genetic or physiological component. Our data further suggests that the impact of ELF-EMF exposure is unlikely due to reactive oxygen species (ROS) mediated induction of oxidative DNA damage but can be accounted for mainly by disturbance of S-phase associated processes and a small amount of apoptosis.

MATERIALS AND METHODS

Cell lines and culture

Human primary fibroblasts (ES-1, male, 6 years old; HR-1d, male, 42 years old) kindly provided by Prof. Rüdiger (Vienna) and HeLa cells were grown in Dulbecco´s modified Eagle´s medium (DMEM), supplemented with 10% FCS, 100 U/mL penicillin, 100 µg/mL streptomycin and 2 mM L-glutamine (Sigma-Aldrich, St. Louis, MO, USA). MRC-5 cells (human primary fetal lung fibroblasts) were grown in Minimum Essential Medium Eagle supplemented with 10% FCS, 2 mM L-glutamine, 100 U/mL penicillin, 100 µg/mL streptomycin and 1% Non-essential Amino Acids (Sigma-Aldrich). Cells were grown in 15-cm Petri dishes (Falcon 353025) at 37°C in a humified atmosphere containing 5% CO_2 and were supplied with fresh medium every 48 h.

24 h before exposure to EMF, cells were seeded into 10-cm Petri dishes (Falcon 353003) to a confluency of about 30%. G1 blocked cells were obtained by culturing them in DMEM supplemented with 0.5% FCS (starving medium) for 48 h before as well as during exposure. In iron supplementation experiments, starving medium was supplemented with 653.7 µg/L $FeCl_2$. H_2O_2 treatment was done directly after harvesting of cells by centrifugation, keeping them in PBS supplemented with the indicated amounts of H_2O_2 on ice for 15 min. For cell survival experiments after ELF-EMF exposure, cells were cultured for 7 d, passaging them at day 2 after treatment. Finally, cells were counted with CASY Cell Counter (Model TT, Schärfe Systems GmbH, Reutlingen), according to the manufacturer's instructions.

ELF-EMF exposure

The exposure system was built and provided by the Foundation for Information Technologies in Society (IT'IS foundation, Zurich, Switzerland), matching the one used in the comparative studies (11,35) . It is described in detail in (36). The setup consisted of two four-coil systems each of which was placed inside a µ-metal box chamber. The currents in the bi-filar coils could be switched parallel for field exposure or non-parallel for control (sham-exposure) and allowed magnetic fields up to 2.3 mT in the frequency range from DC to 1.5 kHz. Constant

environmental conditions (37°C, 5% CO_2, 95% humidity) were ensured by two fans in both µ-metal boxes and by placing them inside a commercial incubator (BBD 6220, Kendro). During exposure, the current of the coils and the temperature at the location of dishes was continuously monitored and data were stored in an encoded file. The temperature was maintained between 36.5 and 37.5°C and never exceeded 0.5°C difference between the two chambers. Except for sham-sham control, all exposure experiments were done under blind condition: the computer randomly determined which of the two chambers was exposed and decoding was done after analysis of the experiment by the IT'IS foundation.

Comet assay

Alkaline comet assay was performed basically as described by Singh *et. al.* (37). 10^4 cells were harvested and resuspended in 0.5% low melting point agarose (Cambrex) at 37°C. The cell/agarose suspension is laid onto microscope slides precoated with 1.5% normal melting point agarose (BioRad, Hercules, CA, USA), spread with a cover slip and let solidify for about 15 min. Slides then were immersed in freshly prepared ice-cold lysis buffer (2.5 M NaCl, 100 mM Na_2EDTA, 10 mM Tris-HCl pH 10, 1% Triton X-100, 10% DMSO, pH 10) for 90 min, washed in ddH_2O, drained and placed side by side in a gel electrophoresis tank. Slides were submerged with freshly made electrophoresis buffer (1 mM Na_2EDTA, 300 mM NaOH, pH>13) and incubated for 30 min to allow DNA unwinding prior to electrophoresis at 25 V/ 300 mA for 20 min. All steps after exposure were performed under dimmed light at 4°C. After electrophoresis slides were washed three times with 0.4 mM Tris-HCl pH 7.5 for 10 min, followed by fixation with EtOH absolute (2x 5 min) and air drying. Finally, nuclear DNA was stained with 20µg/mL ethidium bromide and analysed with a fluorescent microscope at 400x magnification.

For the modified comet assay according to Pouget *et. al.(38)*, the bacterial formamidopyrimidine DNA glycosylase (Fpg, New England BioLabs) was additionally added after cell lysis for 1 h. Slides were washed three times with 0.4 M Tris-HCl, pH 7.5 to remove

remaining lysis buffer and twice with Fpg reaction buffer (20 mM Tris-HCl pH 8, 0.2 mg/mL BSA, 0.5 mM Na_2EDTA, 0.1 M KCl, pH 8). Then 100 µL of either Fpg (0.04 U per slide in Fpg buffer) or Fpg buffer alone as control was laid on every slide. Cover slips were mounted and slides were incubated at 37°C for 45 min followed by DNA unwinding and electrophoresis as described above.

Comet data collection and statistical analyses

Data collection was done according to Anderson *et. al.* (39) with minor modifications by Ivancsits *et.al.* (11). For each individual exposure condition, two slides were subjected to the comet assay. Nuclei of 500 cells per slide were visually scored and classified into five categories corresponding to their amount of DNA in the tail (Figure 2c). Tailfactors (tf) were calculated with the following formula: tf (%) = ((A*F(A) + B*F(B) + C*F(C) + D*F(D) + E*F(E))/1000, where A is the number of cells classified to group A, F(A) the average of group A (2.5% of fragmented DNA), B the number of cells classified to group B, F(B) the average of group B (12.5%), C the number of cells classified to group C, F(C) the average of group C (30%), D the number of cells classified to group D, F(D) is the average of group D (67.5%), E the number of cells classified to group E, and F(E) the average of group E (97.5%). For automated comet analysis, slides were stained with Propidium Iodide and 100 cells per slide were analysed according to Frieauff *et. al.* (40), revealing tail moments (the product from tail length and % of DNA in tail). The two slides from each exposure condition were pooled.

Each visually scored EMF exposure experiment was repeated 1-13 times and differences between sham and exposed cells were statistically analysed by the Student´s *t*-test applying it to percentage of cells in each category and to the tailfactors of all experimental replica. Additionally, the statistical significance of the difference between sham and exposed cells was tested by applying the chi-square test to the whole distribution of cells for each single experiment. The indicated numbers are mean p-values of all experiments. For automatically analyzed comet assays, the average and median tail moment of 100 nuclei per slide from 3

slides per condition of three independent experiments were calculated and statistically analyzed by the Student´s *t*-test.

FACS analysis

Propidium Iodide (PI) staining: $5x10^4$ to $5x10^5$ cells were harvested and fixed in cold 70% EtOH overnight (can be stored up to one week). Cells were collected by centrifugation with 800 g for 5 min and resuspended in 300 µL RNase A (Qiagen, Venlo, The Netherlands 0.5 mg/mL in 0.1 M Tris-HCl pH 7.5, 0.1 M NaCl). After 30min incubation at 37°C, 300 µL pepsin (Fluka) was added (1 mg/mL in 0.4% HCl) and samples were incubated at 37°C for 15 min. 600 µL PI solution (20 µg/mL in PBS pH 7.4) was added followed by an incubation on ice for at least 30 min. DNA content of cells was measured by a FACScan Cytometer (Beckton Dickinson) in the FL2 channel (575 nm). Raw data was quantitatively analysed for cell cycle phases (G1, S, G2 and subG1) with the FlowJo analysing program (TreeStar, , Ashland, OR, USA). Statistics analysis was done by comparing percentage of cells in each cell cycle stage from sham and exposed cultures of 3-7 independent experiments with Student´s *t*-test.

Bromodeoxyuridin (BrdU) incorporation and staining: Replicating cells were labelled with 10 µM BrdU within the last two hours of ELF-EMF exposure, then harvested and fixed in cold 70% EtOH overnight. Samples were centrifuged at 800 g for 5 min, resuspended in 2 M HCl and incubated at RT for 30 min, occasionally mixing. After centrifugation at 400 g for 15 min, they were washed in PBS-T (Phosphate buffered saline + 0.5% BSA + 0.2% Tween-20, pH 7.4). 100 µL of 1:100 diluted FITC-labelled BrdU-antibody (Invitrogen, Carlsbad, CA, USA) was added and samples were incubated at RT for 45 min. After washing with PBS, samples were resuspended in 300 µL RNase A (Qiagen, 0.5 mg/mL in 0.1 M Tris-HCl pH 7.5, 0.1 M NaCl) and incubated at 37°C for 30min. 600 µL PI solution (20 µg/mL in PBS, pH 7.4) was added followed by an incubation on ice for at least 30min. Samples were analysed with FACS Cantoll Cytometer (Beckton Dickinson). The relative number of FITC-positive cells in exposed and sham replica was statistically analysed by the Student´s *t*-test.

Apoptosis measurement: $3x10^5$ to $6x10^5$ cells were harvested and resuspended in 30-60 µL of Annexin-V labeling solution according to the manufacturer's instruction (Annexin-V-FLUOS staining kit, Roche; 2 µL PI and 1.4 µL Annexin-V-FITC per 100 µL incubation buffer). After incubation at RT for 15 min, 500 µL incubation buffer was added and samples were analysed for PI and FITC signals by the FACS Cantoll Cytometer (Beckton Dickinson). According to their fluorescence signals, cells were categorized into: living (FITC negative, PI negative), early apoptotic (FITC positive, PI negative), late apoptotic (FITC positive, PI positive) and necrotic (FITC negative, PI positive). Discrimination of the categories was done with non-stained and single-dye stained positive controls (MMS treated cells). The relative number of apoptotic cells (early + late) of replica were statistically analysed by the Student´s *t*-test.

RESULTS

Intermittent ELF-EMF exposure induces DNA fragmentation in primary human cells

The ambiguous outcome of previous studies investigating the genotoxic impact of 50 Hz ELF-EMFs on human cells prompted us to replicate key ELF-EMF exposure experiments, applying identical exposure conditions, cell lines, and comet assay procedures for DNA fragmentation analysis as published by Ivancsits *et. al*. (11). To start with, we thus measured possible DNA fragmentation by the comet assay, applying visual scoring (39), in four different cell lines: two human primary fibroblasts ES-1 and HR-1d (derived from a 6 years and 42 years old male, respectively), the primary fetal lung fibroblast cell line MRC-5 and the cervical carcinoma cell line HeLa.

We exposed exponentially growing cells to a 50 Hz ELF-EMF at 1 mT for 15 hours. The field was alternating on for 5 min and off for 10 min because such intermittent exposure was shown to have the greatest impact in the comet assay (35). All experiments were done under strictly blinded conditions at least 2 times independently and in each experiment at least 400 cells on 2 individual slides were scored. For all three primary human cell lines tested, we found a significant decrease in the fraction of cells falling into the comet stage A, representing undamaged nuclear DNA, and a corresponding increase in cells in one or more of the comet stages B to E, representing increasingly higher levels of DNA fragmentation (Figure 1A, Supplementary Table 1). By contrast, the ELF-EMF exposure did not change significantly the comet stage distribution of the HeLa cancer cells. Accordingly, the comparison of the relative distribution of cells in all comet stages by the chi-square test yielded significant differences between sham exposed and exposed cells for the primary fibroblast cell lines but not for the cancer cell line. Moreover, the comet tailfactors, a measure for the degree of DNA fragmentation in the population, were slightly but significantly increased by a factor of 1.6, 1.4 and 1.7 in the human primary fibroblast HR-1d, ES-1 and MRC-5, respectively, but not so in HeLa cells. Note that in all three responding cell lines, stage E cells are significantly increased upon ELF-EMF exposure. Besides highly damages cells, stage E may contain apoptotic cells

at an early stage of DNA fragmentation (41). We also performed the continuous exposure experiments (50 Hz, 1 mT, 15 h) with the field on for the entire period of exposure (15 h). As observed before (11), this mode of exposure yielded no significant DNA fragmentation effects in the comet assay in all cell lines tested (Figure 1A).

To exclude that the observed comet effects of ELF-EMF exposure originate from differences of the two exposure chambers, we performed sham-sham exposure experiments. When both ELF-EMF coils were set to sham exposure, differences in comet tailfactors and stage distribution disappeared for all cell lines (Figure 2A and data not shown), confirming that the comet effects measured upon ELF-EMF exposure are not due to chamber bias. To validate the visual scoring and staging of comets, we also performed fully automated comet analyses. For this purpose, HR-1d cells were intermittently (5'/10') exposed to 50 Hz ELF-EMF at 1 mT for 15 h and analysed in parallel in comet assays with visual scoring and with fully automated analysis using a robotic system based on the Leitz MIAS image analysis system (40). Since the read-out of the two analyses, i.e. the tailfactor and the tail moment, are based on different scoring parameters and calculation algorithms, their absolute values are not directly comparable. However, the relative changes resulting from genotoxic insult should be similar. In these experiments, we measured a statistically significant 1.47-fold increased average tailfactor by the visual scoring method and an equally significant 1.33-fold increase of the median tail moment (1.58 fold average) in the automated analysis (Figure 2C). Our findings, thus, substantiate the previously reported increase of DNA fragmentation, as assessed by the comet assay, of human primary cell lines under intermittent ELF-EMF exposure. Controls that were not included in previous studies further establish that these comet effects are not due to a bias in the parallel exposure chambers or the visual scoring of comet events. Interestingly enough, this EMF effect is absent in an immortalized cell line and under continuous exposure of the same field strength (50 Hz, 1 mT for 15 h) in all tested cell lines.

Oxidative DNA damage by ELF-EMF exposure is unlikely the cause for the DNA fragmentation effect observed in comet assays

Magnetic field exposure was proposed to affect the free radical pool in cells, leading to an increase of oxidative damage and, hence, to the observed DNA fragmentation (25). To test this hypothesis, we compared the comet effects resulting from the exposure of cells to ELF-EMF and to H_2O_2, in particularly stage distributions at doses producing similar tailfactor changes. As expected, exposure to the oxidizing agent H_2O_2 resulted in a dose dependent increase in the comet tailfactor in both HR-1d and HeLa cells, although more pronounced in the primary cell line HR-1d (Figure 2B). When treated with 150 µM H_2O_2, most of the HR-1d cells produced stage E comets, most likely reflecting early apoptotic responses of cells. Apoptosis is impaired in the p53 deficient immortalized HeLa cell line, and this might explain the absence of stage E comets in this cells line. The relative increase of tailfactors after ELF-EMF exposure in the HR-1d cell line (1.6) best matches that of a 10 µM H_2O_2 treatment (1.3) (Figure 1A and Figure 2B). In terms of comet stage distribution, however, the two treatments differ significantly: 10 µM H_2O_2 increases almost exclusively stage B comets, indicating a relatively high number of cells with low amounts of damage, while ELF-EMF exposure mainly affects stages C and E, representing a smaller cell population with high amounts of damage or apoptosis.

To address the proposed involvement of oxidative DNA damage in ELF-EMF dependent comet effects from another angle, we combined the comet assay with a treatment with a bacterial purine glycosylase (Fpg), which excises a variety of oxidized guanine lesions including 8-oxo-G, the predominant form of oxidative DNA damage (38). This allows visualization of transiently unrepaired damage to purine bases that is otherwise not detectable in the comet assay. We first generated oxidative DNA damage using 10 µM H_2O_2 and found a 1.7-fold increase of the comet tailfactor with the Fpg treatment (Figure 3). This shows that unrepaired oxidative purine damage exists following treatment of cells with doses of H_2O_2, that generate a comet tailfactor change comparable to that of 15 hours intermittent ELF-EMF exposure at 1 mT. We thus performed the Fpg comet assay after ELF-EMF exposure and

observed a relative increase of the tailfactor by 1.3-fold compared to the sham control. This increase is not different from 1.4-fold measured in the comet assay without Fpg (Figure 3). The data therefore suggests that the amount of unrepaired oxidative DNA damage in ELF-EMF exposed cells is not higher than in sham controls. So, if EMF exposure induces oxidative DNA damage, it must be below the detection limit of our assay, meaning that it does not contribute to the comet tailfactor changes observed. Altogether, these data do not support the hypothesis of increased oxidative DNA damage due to ELF-EMF exposure.

DNA fragmentation upon ELF-EMF appears in proliferating cells only

Replicating cells naturally contribute to the comet tailfactor, because they harbour DNA fragments at replication forks, which migrate into the tail (42). S-phase cells are also particularly sensitive to DNA damage, mainly due to the increased vulnerability of the DNA while it is being replicated. Hence, to address the role of DNA replication in the ELF-EMF induced comet tailfactor changes, we examined cells synchronized in G1 of the cell cycle. To exclude secondary effects of cell cycle blocking agents on DNA metabolism, we used serum starvation with 0.5% FCS to enrich for cells in G1. Comparing cycling and serum starved cells, the G1-phase population of HR-1d and ES-1 primary fibroblast cells increased from about 75% and 70% to about 90% and 80%, respectively, an the S-phase fractions dropped from 11.5% to 1.6% and from 11.5% to 2.6% respectively (compare Figures 4A and 5A). While maintaining the cells in G1-phase, they were intermittently exposed to an ELF-EMF of 50 Hz, 1 mT for 15 h and subsequently analysed for DNA fragmentation by comet assays. For both cell lines, we did not find significant changes under EMF exposure, neither for the tailfactor nor in the relative distribution of cells into comet stages (Figure 4B). Hence, unlike asynchronous cultures of HR-1d and ES-1 cells (Figure 1A), G1-arrested cultures do not show ELF-EMF induced DNA fragmentation in the comet assay anymore, suggesting that the EMF affects predominantly replicating cells.

The synchronisation of cells in G1-phase by serum starvation, however, goes together with lowering the iron concentration of the medium. To rule out that the loss of DNA fragmentation following serum starvation is accounted for by the iron depletion, we supplemented serum-starved HR-1d cells with iron concentrations typically present in full FCS medium. In the iron supplemented G1-arrested cultures, we measured increased DNA fragmentation in the comet assay compared to non-supplementation cultures. ELF-EMF exposure however, did not produce a significant comet tailfactor or stage changes in the iron supplemented culture (Supplementary Figure 2). It was not possible here to do a complementary approach using an iron chelator in FCS rich medium, because these compounds interfere with cell cycle progression (43,44). We therefore conclude that cycling of the cells is necessary to produce the comet effect of the electromagnetic field.

ELF-EMF exposure slightly alters cell cycle profiles

Our data show that ELF-EMF exposure induces DNA fragmentation in replicating cells only. Because unwound DNA at replication forks also migrates into the comet tail (42), we reasoned that the small effects of EMFs might in fact reflect an accumulation of exposed cells in S-phase. Therefore, we assessed the cell cycle distribution of asynchronous ES-1 and HR-1d cultures after ELF-EMF exposure (50 Hz, 1 mT, intermittent for15h) by FACS analysis of PI-stained cells. We did not measure notable difference in G1, S, and G2 populations between exposed and sham-exposed cells (Figure 5A). However, we noticed a small but still not significant increase in the subG1 population for both fibroblast cell lines, indicating that the fraction of apoptotic cells might increase during exposure.

We then used BrdU incorporation to directly monitor DNA synthesis during the last 2 hours of ELF-EMF exposure (50 Hz, 1 mT, intermittent for15h). In both fibroblast lines tested, the fraction of BrdU incorporating cells was slightly reduced but the reduction was statistically significant only for HR-1d, the cell line showing slightly higher DNA fragmentation in the comet assay following ELF-EMF exposure (Figure 5B). Although only about 1% of cells are

concerned, these data may indicate that a proportion of cells under EMF exposure have difficulties to enter S-phase, to initiate efficient DNA replication.

Apoptosis contributes to the increase of comet tail DNA following ELF-EMF exposure

We observed that ELF-EMF exposure (50 Hz, 1 mT, intermittent for15h) of the human fibroblast cell lines causes a small increase of the fraction of cells with a subG1 content of nuclear DNA (Figure 5A) as well as an increase in stage E comets (Figure 1A), representing cells with highly fragmented DNA. Because early stages of apoptotic DNA fragmentation are detectable as highly damaged cells in comet assays (45), the two findings might indicate that ELF-EMF exposure indeed induces apoptosis in a small fraction of cells. We addressed the question directly by Annexin-V and PI co-staining of cells following ELF-EMF exposure. Annexin-V binds to phosphatidylserine, which is externalized to the outer leaflet of the (still intact) plasma membrane early in apoptosis, preceding DNA fragmentation (46). Hence, flow cytometric analysis of these cells allows intact, early- and late apoptotic, and necrotic cells to be distinguished from each other. For ES-1 cells, we found only an insignificant increase of apoptotic cells (early apoptotic (Annexin-V positive, PI negative) plus late apoptotic (Annexin-V positive, PI positive) cells) following ELF-EMF exposure, while the apoptotic fraction in the HR-1d cell line was significantly increased by about 1.5% (Figure 5C). This is a small fraction but nevertheless contributes to stage E comet events (1.5% of 2.4% cells in comet stage E) arising in the ELF-EMF exposed HR-1d population.

Since we detected a small increase of apoptotic cells shortly after exposure to EMF, we also investigated possible long-term effects on cell survival and proliferation. For ES-1 and HR-1d cells, we counted the number of cells before, directly after and 24, 48, 72, 96 hours and 7 days after intermitted exposure to ELF-EMF of 50Hz, 1 mT for 15 h. There was no statistically significant difference between sham and exposed cells for both cell lines at any time point (Supplementary Figure 1). We conclude that exposure to ELF-EMF may provoke apoptosis in

some cells, and this accounts partially for the comet tailfactor increases observed. Further cell death or proliferation arrest upon prolonged culturing following exposure is not observed.

DISCUSSION

Whether or not ELF-EMFs affect genome integrity in human cells is heavily debated in the scientific community as well as in the public, largely provoked by the conflicting experimental evidence available. Discrepant observations in different studies are difficult to interpret, mainly due the lack of standardized experimental procedures, making direct comparisons generally difficult. The aim of this work was therefore to replicate a previous study by Ivancsits *et. al* (35), the results of which revealed increased DNA fragmentation in a comet assay with ELF-EMF exposed human primary fibroblasts. Using an identical primary human fibroblast cell line (ES-1), identical ELF-EMF exposure equipment and conditions (intermittent, 50 Hz, 1 mT, 15 h), and identical comet assay procedures, we were able to independently reproduce evidence for increased DNA fragmentation. We observed increased levels of comet tail DNA under intermittent but not under continuous EMF exposure. Generally, our comet effects were less pronounced and more variable than those reported previously but the differences between exposed and sham-exposed cultures were nevertheless statistically significant.

Exactly why the ELF-EMF induced comet effects depend on intermittent exposure remains unclear. We tested the hypothesis that cells adapt to the field under continuous exposure. The results from an experiment with pre-exposed cells, however, indicate that adaptation does not occur. Regardless the reason, the absence of an increase in DNA fragmentation under continuous exposure clearly excludes thermal effects as cause.

Increased DNA breaks were found in two additional human primary fibroblast cell lines (HR-1d and MRC-5), which excludes a cell line-specific response to ELF-EMF exposure. It appears that a fibroblast cell line originating from an older donor is more susceptible to the EMF than one from a younger donor, being in line with an age of donor-dependent EMF response previously observed (47). In contrast to the primary fibroblasts, the cancer cell line

HeLa does not show an increase in comet tail DNA under EMF exposure. This could be due to acquired physiological or genetic features such as increased repair capacities or the loss of apoptosis.

Apoptotic cells indeed seem to contribute to the comet tailfactor increases observed under ELF-EMF exposure. The proportion of apoptotic cells rises from about 3% to 4.5% in the highly responsive HR-1d line under ELF-EMF exposure and the cell cycle profiles of exposed cells revealed a slightly increased subG1 population, presumably reflecting apoptotic or necrotic cells with a reduced DNA content. Supporting our findings, other studies reported more apoptosis (48-50) or altered expression of apoptosis-related genes like bcl-2, bax and c-myc (51) after exposure to 50 Hz ELF-EMFs. But other studies did not find evidence for a direct effect of ELF-EMFs on apoptosis (52). Our results thus suggest that the increased DNA fragmentation of EMF responsive cells is partially due to the induction of apoptosis also explaining why immortalized cell lines like HeLa do not respond the same way as primary cells do. A contribution of apoptosis is also congruent with the relative changes in comet stages observed under exposure. The most pronounced increase is found for comet stage E, representing fragmented nuclear DNA, into which also apoptotic cells would be assigned to. In the HR-1d cell line, 2.4% increase in stage E is found and Annexin-V staining reveals, that 1.5% of them could be apoptotic cells.

Previous studies were criticized for the lack of a sham-sham control, or the visual scoring of the comets. Our sham-sham control shows that the exposure setup does not generate an experimental bias (e.g. intrinsic difference between the coils), hence, the comet effects measured under exposure depend on the EMF applied. Also, fully automated comet evaluation following ELF-EMF exposure reproduces a comet tail moment increase for the HR-1d cell line in a range similar to the visual scoring. Hence, visual comet scoring in our hands did not introduce an experimental bias, and the same was found previously (53-55). We nevertheless decided to use visual scoring because this method allows a higher number of cells to be analyzed (1000 compared to about 50-100) per experiment, which provides a better

statistical representation of the relatively small numbers of damaged cells and allows a direct assessment of the type of biological responses involved on the basis of patterns of comet stage changes.

Apoptosis could be induced by a critical amount of DNA damage saturating the cellular repair capacity. Although the energy deposited by ELF-EMFs is not sufficient to directly damage DNA, it was proposed that the field might enhance levels of bio-molecular or free radicals in cells and, thereby, indirectly provoke increased formation of oxidative DNA damage (24-26). EMF-induced radicals would be expected to randomly damage the cellular DNA and, thus, to lead to a gradual and dose-dependent shift of comet stages towards more DNA fragmentation. This is what we observed upon exposure of cells to H_2O_2, a well characterized oxidizing agent, but not upon ELF-EMF exposure, which typically induced a disproportional increase of comet stage E nuclei at comparable comet tailfactor effects. This difference suggests that the DNA directed effects of H_2O_2 and EMF exposure are of a different nature. In the same context, we also investigated the accumulation of unrepaired oxidative DNA damage making use of the combined Fpg comet assay, which processes the most prevalent oxidative base lesions into DNA strand breaks (38). Fpg pre-digestion did show the expected sensitivity enhancement of the comet assay, but no specific increase of the ELF-EMF induced effect. These data cannot definitely rule out the generation of a small amount oxidative DNA damage upon ELF-EMF exposure, but they argue strongly against a major contribution of such damage. However, others found that radical scavengers reduced ELF-EMF effects on DNA migration in the comet assay (56). This discrepancy might be due to cell type-specific responses or to influences of scavengers on cellular mechanisms such as cell cycle progression.

EMFs were previously shown to affect the cell cycle, both in an inhibitory (57,58) and in a stimulatory way (31,33). A slight accumulation of S-phase cells upon ELF-EMF exposure could account for the increase of the comet tailfactor observed. We could not detect any significant differences in the cell cycle profiles of sham and field-exposed cells. The number of

cells actively synthesizing DNA during the last two hours of exposure, however, was slightly reduced, indicating that a fraction of cells is either disturbed in entering S-phase or in replicating DNA. Interestingly, this reduction correlated with the magnitude of the ELF-EMF induced comet effect. We therefore conclude that an accumulation of S-phase cells under field exposure does not account for the increased comet tailfactor. On the other hand, G1 arrested cultures do not show the comet effect, and the loss of the effect correlates with the reduction of S-phase cells. This clearly suggests that it is the S-phase fraction of cells that is responsible for the comet tailfactor increase. This may, at least partially, explain the varying outcomes in different studies, as the fraction of S-phase cells in a population is determined by the culture conditions and the cell lines used, and these parameters may vary between laboratories. For instance, the previously reported dependency of EMF effects on the cellular iron pool, which we did not observe in our experiments, might be due to the use of iron-chelators, which are known to induce G1 arrests.

In conclusion, we confirmed the previously reported increase in nuclear DNA fragmentation in comet assays upon exposure of cells to ELF-EMFs. For the primary human fibroblasts analyzed here, this genotoxic effect depends on cell proliferation, most likely the passage of cells through S-phase, rather than on radical mediated induction of oxidative DNA damage. Direct DNA damage induction by EMFs seems unlikely but cannot be ruled out definitely at this point. Our data suggests that cells entering S-phase under EMF exposure may encounter replication problems, which might increase the steady-state level of DNA fragmentation and eventually lead to the induction of apoptosis. Both would then contribute to an increased comet tailfactor. Exactly why ELF-EMFs affect S-phase cells more than non-replicating cells remains speculative. It is possible though that the efficiency of enzymatic DNA transactions that occur during S-phase is slightly affected, which altogether increases the number of DNA replication and repair intermediates that will be scored as DNA fragmentation events in the comet assay.

ACKNOWLEDGEMENTS

We thank Melanie Struwe and Dr. Martin Schneider from the “Novartis Institutes for BioMedical Research” for the help with the automated computerized analysis of comet assays. This study was supported by grants from the Forschungsstiftung Mobilfunk (Zürich) and the NFP57 program of the Swiss National Science Foundation.

REFERENCES

1. Ahlbom, A., Day, N., Feychting, M., Roman, E., Skinner, J., Dockerty, J., Linet, M., McBride, M., Michaelis, J., Olsen, J.H. *et al.* (2000) A pooled analysis of magnetic fields and childhood leukaemia. *Br J Cancer*, **83,** 692-698.
2. Feychting, M., Forssen, U. and Floderus, B. (1997) Occupational and residential magnetic field exposure and leukemia and central nervous system tumors. *Epidemiology*, **8,** 384-389.
3. Greenland, S., Sheppard, A.R., Kaune, W.T., Poole, C. and Kelsh, M.A. (2000) A pooled analysis of magnetic fields, wire codes, and childhood leukemia. Childhood Leukemia-EMF Study Group. *Epidemiology*, **11,** 624-634.
4. Feychting, M. and Forssen, U. (2006) Electromagnetic fields and female breast cancer. *Cancer Causes Control*, **17,** 553-558.
5. Forssen, U.M., Lonn, S., Ahlbom, A., Savitz, D.A. and Feychting, M. (2006) Occupational magnetic field exposure and the risk of acoustic neuroma. *Am J Ind Med*, **49,** 112-118.
6. Winker, R., Ivancsits, S., Pilger, A., Adlkofer, F. and Rudiger, H.W. (2005) Chromosomal damage in human diploid fibroblasts by intermittent exposure to extremely low-frequency electromagnetic fields. *Mutat Res*, **585,** 43-49.
7. Lai, H. and Singh, N.P. (1997) Acute exposure to a 60 Hz magnetic field increases DNA strand breaks in rat brain cells. *Bioelectromagnetics*, **18,** 156-165.
8. Svedenstal, B.M., Johanson, K.J. and Mild, K.H. (1999) DNA damage induced in brain cells of CBA mice exposed to magnetic fields. *In Vivo*, **13,** 551-552.
9. Wahab, M.A., Podd, J.V., Rapley, B.I. and Rowland, R.E. (2007) Elevated sister chromatid exchange frequencies in dividing human peripheral blood lymphocytes exposed to 50 Hz magnetic fields. *Bioelectromagnetics*, **28,** 281-288.

10. Nordenson, I., Mild, K.H., Andersson, G. and Sandstrom, M. (1994) Chromosomal aberrations in human amniotic cells after intermittent exposure to fifty hertz magnetic fields. *Bioelectromagnetics*, **15,** 293-301.

11. Ivancsits, S., Diem, E., Pilger, A., Rudiger, H.W. and Jahn, O. (2002) Induction of DNA strand breaks by intermittent exposure to extremely-low-frequency electromagnetic fields in human diploid fibroblasts. *Mutat Res*, **519,** 1-13.

12. Stronati, L., Testa, A., Villani, P., Marino, C., Lovisolo, G.A., Conti, D., Russo, F., Fresegna, A.M. and Cordelli, E. (2004) Absence of genotoxicity in human blood cells exposed to 50 Hz magnetic fields as assessed by comet assay, chromosome aberration, micronucleus, and sister chromatid exchange analyses. *Bioelectromagnetics*, **25,** 41-48.

13. Cantoni, O., Sestili, P., Fiorani, M. and Dacha, M. (1995) The effect of 50 Hz sinusoidal electric and/or magnetic fields on the rate of repair of DNA single/double strand breaks in oxidatively injured cells. *Biochem Mol Biol Int*, **37,** 681-689.

14. Fiorani, M., Cantoni, O., Sestili, P., Conti, R., Nicolini, P., Vetrano, F. and Dacha, M. (1992) Electric and/or magnetic field effects on DNA structure and function in cultured human cells. *Mutat Res*, **282,** 25-29.

15. Scarfi, M.R., Sannino, A., Perrotta, A., Sarti, M., Mesirca, P. and Bersani, F. (2005) Evaluation of genotoxic effects in human fibroblasts after intermittent exposure to 50 Hz electromagnetic fields: a confirmatory study. *Radiat Res*, **164,** 270-276.

16. Vijayalaxmi, McNamee, J.P. and Scarfi, M.R. (2006) Comments on: "DNA strand breaks" by Diem et al. [Mutat. Res. 583 (2005) 178-183] and Ivancsits et al. [Mutat. Res. 583 (2005) 184-188]. *Mutat Res*, **603,** 104-106; author reply 107-109.

17. Adair, R.K. (1998) Extremely low frequency electromagnetic fields do not interact directly with DNA. *Bioelectromagnetics*, **19,** 136-138.

18. Valberg, P.A., Kavet, R. and Rafferty, C.N. (1997) Can low-level 50/60 Hz electric and magnetic fields cause biological effects? *Radiat Res*, **148,** 2-21.

19. Porath, D., Bezryadin, A., de Vries, S. and Dekker, C. (2000) Direct measurement of electrical transport through DNA molecules. *Nature*, **403,** 635-638.

20. Wan, C., Fiebig, T., Schiemann, O., Barton, J.K. and Zewail, A.H. (2000) Femtosecond direct observation of charge transfer between bases in DNA. *Proc Natl Acad Sci U S A*, **97,** 14052-14055.

21. Giese, B. (2006) Electron transfer through DNA and peptides. *Bioorg Med Chem*, **14,** 6139-6143.

22. Juutilainen, J. and Lang, S. (1997) Genotoxic, carcinogenic and teratogenic effects of electromagnetic fields. Introduction and overview. *Mutat Res*, **387,** 165-171.

23. McCann, J., Dietrich, F. and Rafferty, C. (1998) The genotoxic potential of electric and magnetic fields: an update. *Mutat Res*, **411,** 45-86.

24. Brocklehurst, B. and McLauchlan, K.A. (1996) Free radical mechanism for the effects of environmental electromagnetic fields on biological systems. *Int J Radiat Biol*, **69,** 3-24.

25. Lai, H. and Singh, N.P. (2004) Magnetic-field-induced DNA strand breaks in brain cells of the rat. *Environ Health Perspect*, **112,** 687-694.

26. Zmyslony, M., Palus, J., Jajte, J., Dziubaltowska, E. and Rajkowska, E. (2000) DNA damage in rat lymphocytes treated in vitro with iron cations and exposed to 7 mT magnetic fields (static or 50 Hz). *Mutat Res*, **453,** 89-96.

27. Blank, M. and Goodman, R. (1999) Electromagnetic fields may act directly on DNA. *J Cell Biochem*, **75,** 369-374.

28. Blank, M. (2005) Do electromagnetic fields interact with electrons in the Na,K-ATPase? *Bioelectromagnetics*, **26,** 677-683.

29. Sahebjamei, H., Abdolmaleki, P. and Ghanati, F. (2007) Effects of magnetic field on the antioxidant enzyme activities of suspension-cultured tobacco cells. *Bioelectromagnetics*, **28,** 42-47.

30. De Mattei, M., Caruso, A., Traina, G.C., Pezzetti, F., Baroni, T. and Sollazzo, V. (1999) Correlation between pulsed electromagnetic fields exposure time and cell proliferation

increase in human osteosarcoma cell lines and human normal osteoblast cells in vitro. *Bioelectromagnetics*, **20,** 177-182.

31. Cadossi, R., Bersani, F., Cossarizza, A., Zucchini, P., Emilia, G., Torelli, G. and Franceschi, C. (1992) Lymphocytes and low-frequency electromagnetic fields. *Faseb J*, **6,** 2667-2674.
32. Rosenthal, M. and Obe, G. (1989) Effects of 50-hertz electromagnetic fields on proliferation and on chromosomal alterations in human peripheral lymphocytes untreated or pretreated with chemical mutagens. *Mutat Res*, **210,** 329-335.
33. Katsir, G., Baram, S.C. and Parola, A.H. (1998) Effect of sinusoidally varying magnetic fields on cell proliferation and adenosine deaminase specific activity. *Bioelectromagnetics*, **19,** 46-52.
34. Harris, P.A., Lamb, J., Heaton, B. and Wheatley, D.N. (2002) Possible attenuation of the G2 DNA damage cell cycle checkpoint in HeLa cells by extremely low frequency (ELF) electromagnetic fields. *Cancer Cell Int*, **2,** 3.
35. Ivancsits, S., Diem, E., Jahn, O. and Rudiger, H.W. (2003) Intermittent extremely low frequency electromagnetic fields cause DNA damage in a dose-dependent way. *Int Arch Occup Environ Health*, **76,** 431-436.
36. Schuderer, J., Oesch, W., Felber, N., Spat, D. and Kuster, N. (2004) In vitro exposure apparatus for ELF magnetic fields. *Bioelectromagnetics*, **25,** 582-591.
37. Singh, N.P., Tice, R.R., Stephens, R.E. and Schneider, E.L. (1991) A microgel electrophoresis technique for the direct quantitation of DNA damage and repair in individual fibroblasts cultured on microscope slides. *Mutat Res*, **252,** 289-296.
38. Pouget, J.P., Douki, T., Richard, M.J. and Cadet, J. (2000) DNA damage induced in cells by gamma and UVA radiation as measured by HPLC/GC-MS and HPLC-EC and Comet assay. *Chem Res Toxicol*, **13,** 541-549.

39. Anderson, D., Yu, T.W., Phillips, B.J. and Schmezer, P. (1994) The effect of various antioxidants and other modifying agents on oxygen-radical-generated DNA damage in human lymphocytes in the COMET assay. *Mutat Res*, **307,** 261-271.

40. Frieauff, W., Hartmann, A. and Suter, W. (2001) Automatic analysis of slides processed in the Comet assay. *Mutagenesis*, **16,** 133-137.

41. Wilkins, R.C., Kutzner, B.C., Truong, M., Sanchez-Dardon, J. and McLean, J.R. (2002) Analysis of radiation-induced apoptosis in human lymphocytes: flow cytometry using Annexin V and propidium iodide versus the neutral comet assay. *Cytometry*, **48,** 14-19.

42. Olive, P.L. and Banath, J.P. (1993) Induction and rejoining of radiation-induced DNA single-strand breaks: "tail moment" as a function of position in the cell cycle. *Mutat Res*, **294,** 275-283.

43. Chenoufi, N., Baffet, G., Drenou, B., Cariou, S., Desille, M., Clement, B., Brissot, P., Lescoat, G. and Loreal, O. (1998) Deferoxamine arrests in vitro the proliferation of porcine hepatocyte in G1 phase of the cell cycle. *Liver*, **18,** 60-66.

44. Brodie, C., Siriwardana, G., Lucas, J., Schleicher, R., Terada, N., Szepesi, A., Gelfand, E. and Seligman, P. (1993) Neuroblastoma sensitivity to growth inhibition by deferrioxamine: evidence for a block in G1 phase of the cell cycle. *Cancer Res*, **53,** 3968-3975.

45. Olive, P.L. and Banath, J.P. (1995) Sizing highly fragmented DNA in individual apoptotic cells using the comet assay and a DNA crosslinking agent. *Exp Cell Res*, **221,** 19-26.

46. van Genderen, H., Kenis, H., Lux, P., Ungeth, L., Maassen, C., Deckers, N., Narula, J., Hofstra, L. and Reutelingsperger, C. (2006) In vitro measurement of cell death with the annexin A5 affinity assay. *Nat Protoc*, **1,** 363-367.

47. Ivancsits, S., Diem, E., Jahn, O. and Rudiger, H.W. (2003) Age-related effects on induction of DNA strand breaks by intermittent exposure to electromagnetic fields. *Mech Ageing Dev*, **124,** 847-850.

48. Narita, K., Hanakawa, K., Kasahara, T., Hisamitsu, T. and Asano, K. (1997) Induction of apoptotic cell death in human leukemic cell line, HL-60, by extremely low frequency electric magnetic fields: analysis of the possible mechanisms in vitro. *In Vivo*, **11,** 329-335.

49. Blumenthal, N.C., Ricci, J., Breger, L., Zychlinsky, A., Solomon, H., Chen, G.G., Kuznetsov, D. and Dorfman, R. (1997) Effects of low-intensity AC and/or DC electromagnetic fields on cell attachment and induction of apoptosis. *Bioelectromagnetics*, **18,** 264-272.

50. Mangiacasale, R., Tritarelli, A., Sciamanna, I., Cannone, M., Lavia, P., Barberis, M.C., Lorenzini, R. and Cundari, E. (2001) Normal and cancer-prone human cells respond differently to extremely low frequency magnetic fields. *FEBS Lett*, **487,** 397-403.

51. Nikolova, T., Czyz, J., Rolletschek, A., Blyszczuk, P., Fuchs, J., Jovtchev, G., Schuderer, J., Kuster, N. and Wobus, A.M. (2005) Electromagnetic fields affect transcript levels of apoptosis-related genes in embryonic stem cell-derived neural progenitor cells. *Faseb J*, **19,** 1686-1688.

52. Verheyen, G.R., Pauwels, G., Verschaeve, L. and Schoeters, G. (2003) Effect of coexposure to 50 Hz magnetic fields and an aneugen on human lymphocytes, determined by the cytokinesis block micronucleus assay. *Bioelectromagnetics*, **24,** 160-164.

53. Chaubey, R.C. (2005) Computerized image analysis software for the comet assay. *Methods Mol Biol*, **291,** 97-106.

54. Anderson, D., Yu, T.W., Dobrzynska, M.M., Ribas, G. and Marcos, R. (1997) Effects in the Comet assay of storage conditions on human blood. *Teratog Carcinog Mutagen*, **17,** 115-125.

55. Speit, G., Schutz, P. and Hoffmann, H. (2007) Genotoxic effects of exposure to radiofrequency electromagnetic fields (RF-EMF) in cultured mammalian cells are not independently reproducible. *Mutat Res*, **626,** 42-47.

56. Lai, H. and Singh, N.P. (1997) Melatonin and N-tert-butyl-alpha-phenylnitrone block 60-Hz magnetic field-induced DNA single and double strand breaks in rat brain cells. *J Pineal Res*, **22,** 152-162.

57. Conti, P., Gigante, G.E., Cifone, M.G., Alesse, E., Ianni, G., Reale, M. and Angeletti, P.U. (1983) Reduced mitogenic stimulation of human lymphocytes by extremely low frequency electromagnetic fields. *FEBS Lett*, **162,** 156-160.

58. Lange, S., Richard, D., Viergutz, T., Kriehuber, R., Weiss, D.G. and Simko, M. (2002) Alterations in the cell cycle and in the protein level of cyclin D1, p21CIP1, and p16INK4a after exposure to 50 Hz MF in human cells. *Radiat Environ Biophys*, **41,** 131-137.

FIGURE LEGENDS

Figure 1. Intermittent ELF-EMF exposure results in an increased DNA fragmentation in primary human cell lines. HR-1d, ES-1, MRC-5 and HeLa cells were intermittently (5 min on / 10 min off) (**A**) or continuously (**B**) exposed to EMFs of 50 Hz, 1 mT, for 15 h. Nuclear DNA fragmentation was analysed with the alkaline comet assay and visual scoring. Each nucleus was assigned to comet stages A-E: stage A represents cells without DNA migration into the tail and stages B-E cells with increasing amounts of DNA in tail and tail length (see Figure 2C). The percentages of cells in comet stages A-E are displayed and statistically analysed. (n) is the number of experiments, error bars indicate standard errors of the mean and asterisks represent the significance levels of Student´s *t*-test comparing individual comet stage categories (***** $p<0.05$; ****** $p<0.01$; ******* $p<0.005$). The horizontal line and p(c) show the mean significance of the chi-square tests analysing the comet stage distribution of sham and EMF-exposed nuclei of individual experiments. The upper right boxes show the mean tailfactor values for sham and exposed cells as well as the significance level of the Student´s *t*-test on the tailfactors (p(s)).

Figure 2. Control experiments for exposure equipment, data evaluation and DNA fragmentation by oxidative DNA damage confirm the impact of ELF-EMF exposure on genome integrity. (**A**) Alkaline comet assay of HR-1d and ES-1 fibroblasts after sham exposure in both coils with a 50 Hz, 1 mT intermittent (5/10) exposure for 15 h, comet stage distribution (stages A-E) and corresponding standard errors of the mean for coil 1 and coil 2. The upper right boxes contain mean tailfactor values for coil1 and coil2 cells and the significance level of the tailfactors by Student´s *t*-test (p(s)). The horizontal bar and p(c) show the mean significance of the chi-square tests analysing the comet stage distribution of sham and EMF-exposed nuclei of individual experiments. (**B**) HR-1d and HeLa cells were exposed to increasing

concentrations of H_2O_2, which induces oxidative DNA damage, and the extend of DNA fragmentation was analysed by the alkaline comet assay. For the indicated H_2O_2 concentration, the percentages of cells in comet stages A-E are displayed and the mean tailfactor values are indicated in the upper right box. Error bars indicated the SEM of (n) experiments. (**C**) Visual and automated data analysis of alkaline comet assays were directly compared in HR-1d cells, intermittently exposed to an ELF-EMF of 50 Hz and 1 mT for 15 h. Cells of three independent experiments were analysed with a computer based fully automated analysis to obtain tail moments (right panels) and with the manual analysis used for the other experiments by assigning nuclei into the five different comet stages A-E and calculating tailfactors (left panels). Asterisks represent significance levels of the Student´s *t*-test applied on the tailfactor and tail moment of replica: * $p<0.05$; ** $p<0.01$; *** $p<0.005$.

Figure 3. DNA fragmentation under EMF exposure condition is not caused by oxidative damage. HR-1d cells exposed to 50 Hz, 1 mT intermittent (5/10) ELF-EMF for 15 h were analysed for their tailfactors of standard (control) or of the modified alkaline comet assay (Fpg) including an enzymatic DNA nicking step at sites of unrepaired oxidative damage by the bacterial 8-oxoG glycosylase Fpg. Error bars indicate SEM. The mean tailfactors of two independent experiments were statistically analysed by the Student's *t*-test. As positive control, cells treated with 10 µM H_2O_2 were included.

Figure 4. Increased DNA fragmentation upon ELF-EMF exposure is detectable in proliferating cell only. The human primary fibroblast cell lines HR-1d and ES-1 were arrested in G1 phase by serum starvation prior and during exposure to an intermittent ELF-EMF of 50 Hz, 1 mT for 15 h. Cells were harvested and subjected to cell cycle analysis by flow cytometry of propidium iodide-stained nuclei (**A**) as well as to DNA fragmentation analysis by the comet assay (**B**). (**A**) Cell cycle profiles of PI-stained cells after ELF-EMF exposure. Mean percentage of cells in the

different phases of the cell cycle with SEM. (**B**) Alkaline comet assay: each nucleus was assigned to comet stages A-E: stage A represents cells without DNA migration into the tail and stages B-E cells with increasing amounts of DNA in tail and tail length (see Figure 2C). The percentages of cells in comet stages A-E are displayed and statistically analysed. (n) is the number of experiments, error bars indicate standard errors of the mean. The horizontal bar and p(c) show the mean significance of the chi-square tests analysing the comet stage distribution of sham and EMF-exposed nuclei of individual experiments. The upper right boxes show the mean tailfactor values for sham and exposed cells as well as the significance level of the Student´s *t*-test on the tailfactors (p(s)).

Figure 5. A slight reduction of DNA synthesis in S-phase and an increase of the apoptotic fraction are observed in a human fibroblast cell line. HR-1d and ES-1 cells were exposed to 50 Hz, 1 mT intermittent (5/10) ELF-EMF for 15 h, stained for the respective molecular markers and analysed for the cell cycle profile, DNA synthesis and apoptotic index. (**A**) Cell cycle profiles of PI-stained cells after ELF-EMF exposure. Mean percentage of cells in the different cell cycle phases with SEM. (**B**) Relative number of cells with BrdU incorporation during the last two hours of ELF-EMF exposure. Mean percentage of BrdU positive cells with SEM and p-value of Student´s *t*-test are shown. (**C**) The percentage of apoptotic cells (Annexin-V positive cells, Q2+Q4) after ELF-EMF exposure of HR-1d and ES-1 cells (left panel). Representative pictures of FACS-sorted cells stained with PI and FITC-Annexin-V after sham- or EMF-exposure or MMS-treatment as positive control (right panel). Cells in quadrant 4 (Q4, FITC positive) are recognized as early apoptotic, cells in Q2 (FITC/PI positive) as late apoptotic and PI-only cells (Q1) as necrotic, while cells in Q3 (double negative) are living cells. Cells in Q2 and Q4 were counted together as apoptotic cells. Results are presented as average percentage of Q2+Q4 cells. Statistical analysis was done by Student´s *t*-test.

Supplementary Figure 1. Cell survival and proliferation after ELF-EMF exposure is not altered. HR-1d and ES-1 cells were exposed to intermittent ELF-EMF of 50 Hz, 1 mT for 15 h and cell proliferation was followed over time. Relative cell numbers were calculated by normalization to cell number prior to exposure. Shown are relative cell numbers t_0 (directly before exposure) with standard errors.

Supplementary Figure 2. DNA fragmentation induced by the exposure to ELF-EMF depends on cell cycling but not on presence of iron. HR-1d cells were serum starved for 48h before and during 15h intermittent (5/10) ELF exposure including iron supplementation. After harvest they were analysed by alkaline comet assay and assigned to comet stages A-E: stage A represents cells without DNA migration into the tail and stages B-E cells with increasing amounts of DNA in tail and tail length (see Figure 2C). The percentages of cells in comet stages A-E are displayed and statistically analysed. (n) is the number of experiments, error bars indicate standard errors of the mean. The horizontal bar and p(c) show the mean significance of the chi-square tests analysing the comet stage distribution of sham and EMF-exposed nuclei of individual experiments. The upper right boxes show the mean tailfactor values for sham and exposed cells as well as the significance level of the Student´s *t*-test on the tailfactors (p(s)).

Focke et. al., Figure 1

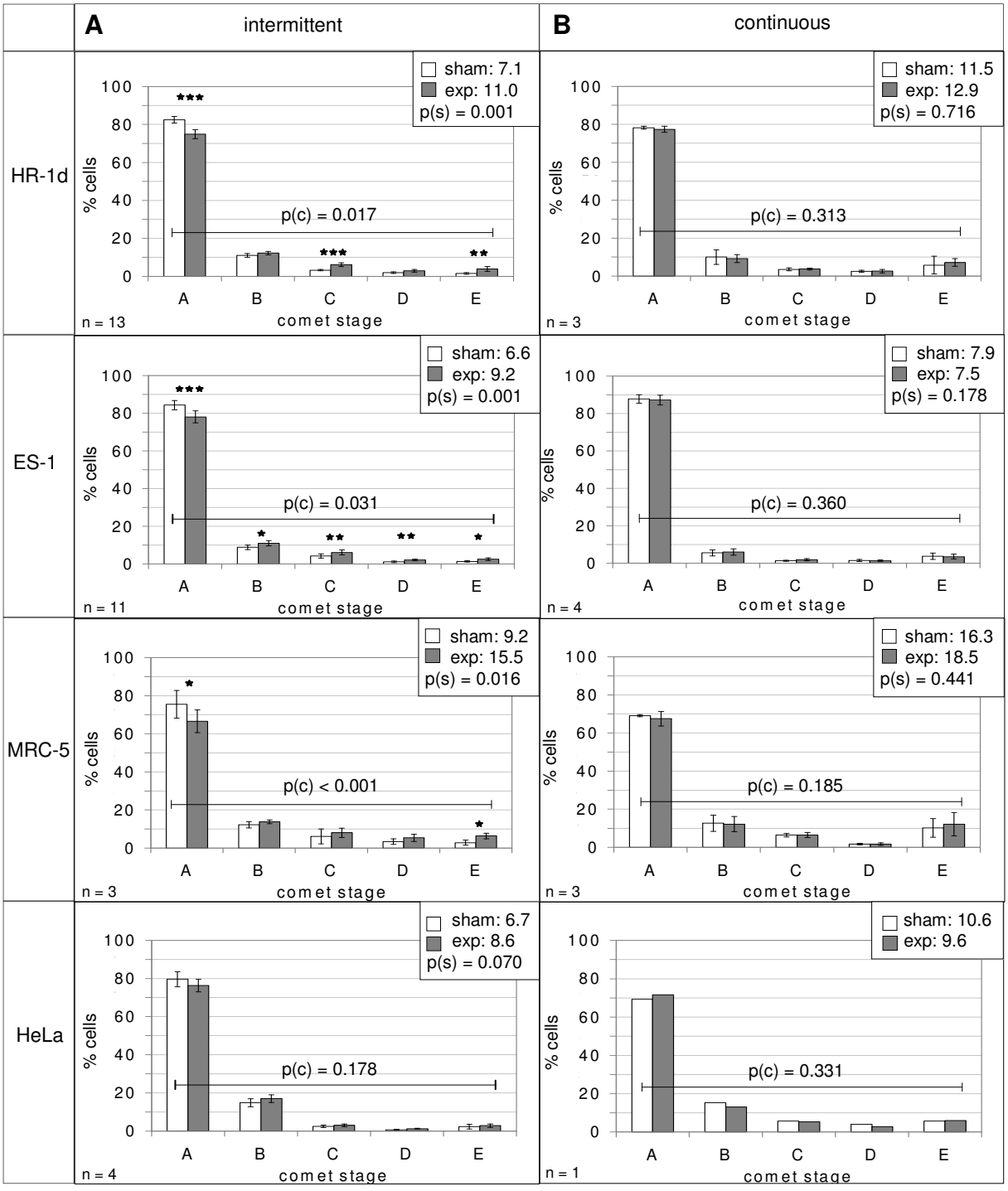

Focke et. al., Figure 2

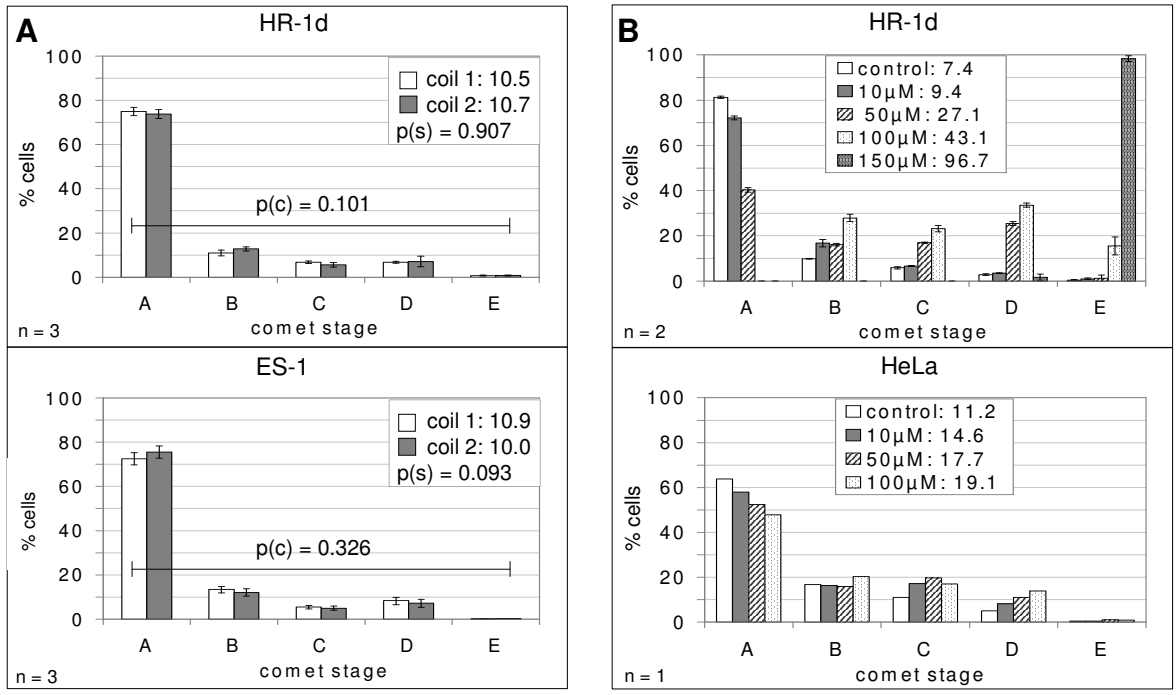

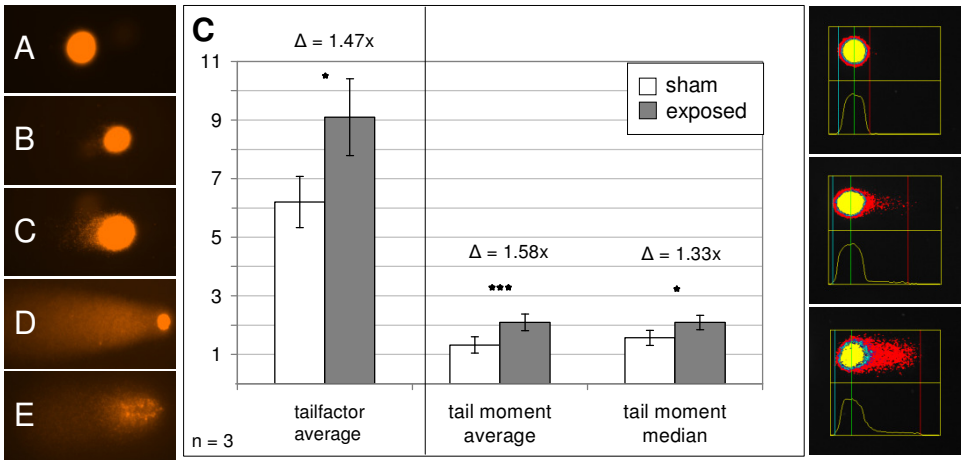

Focke et. al., Figure 3

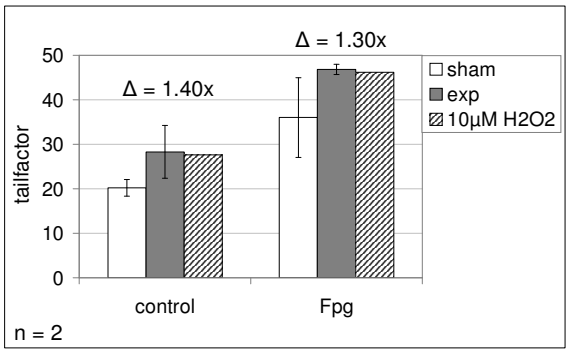

Focke et. al., Figure 4

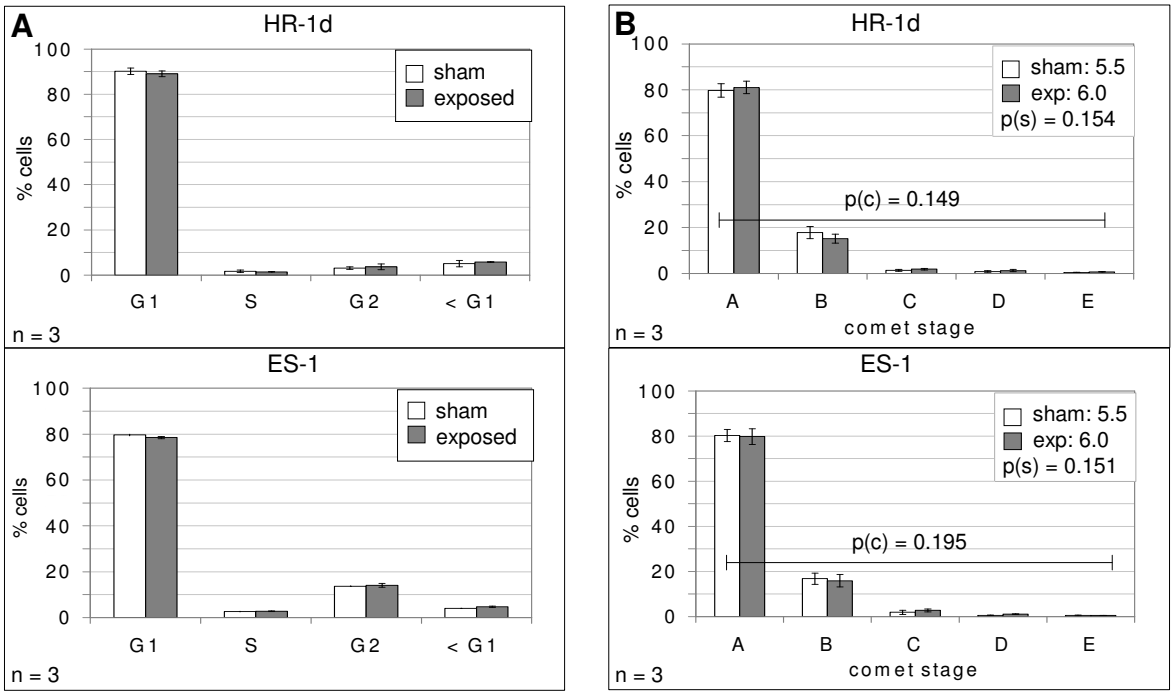

Focke et. al., Figure 5

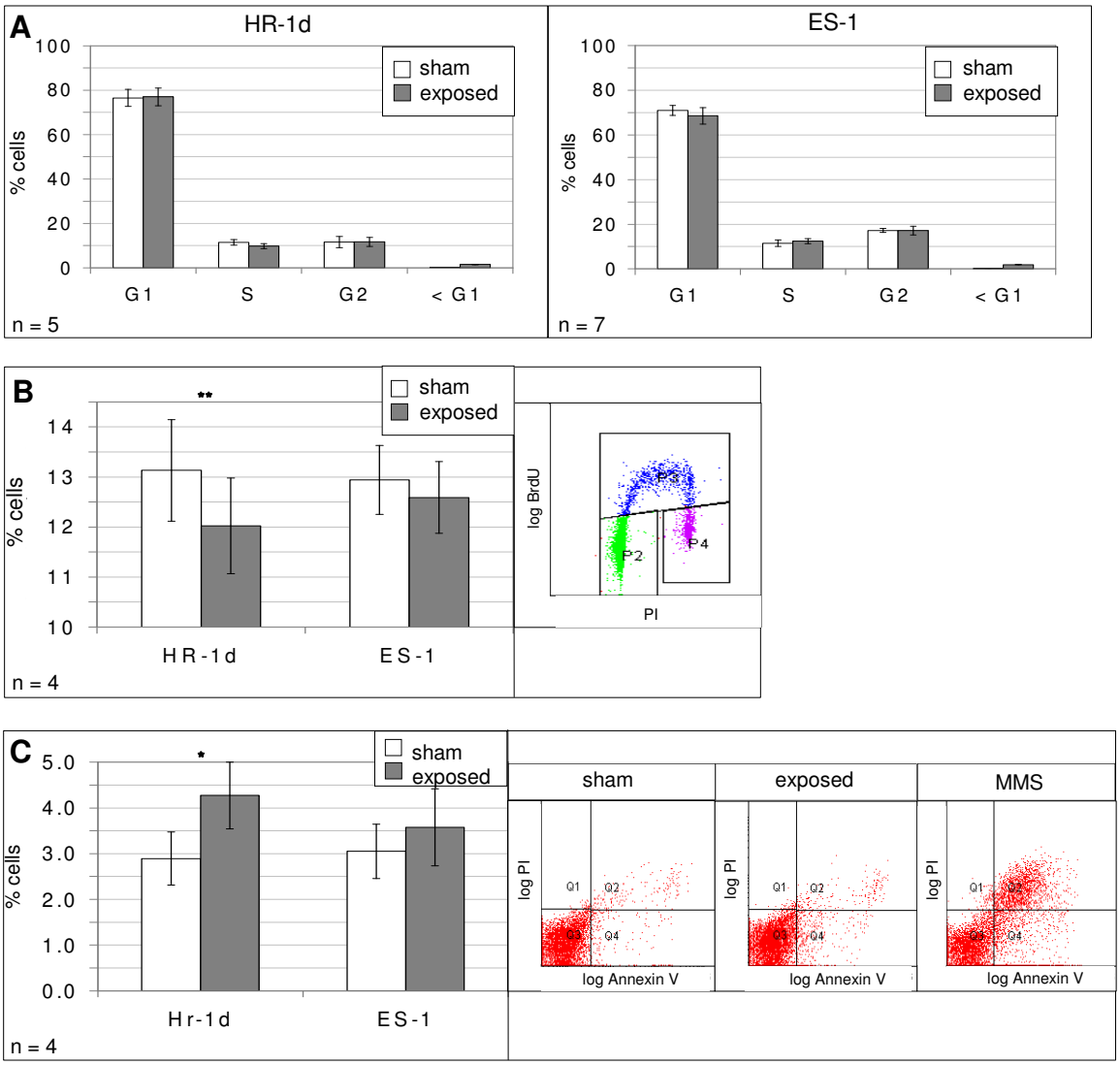

Focke et. al., supplementary Figure 1

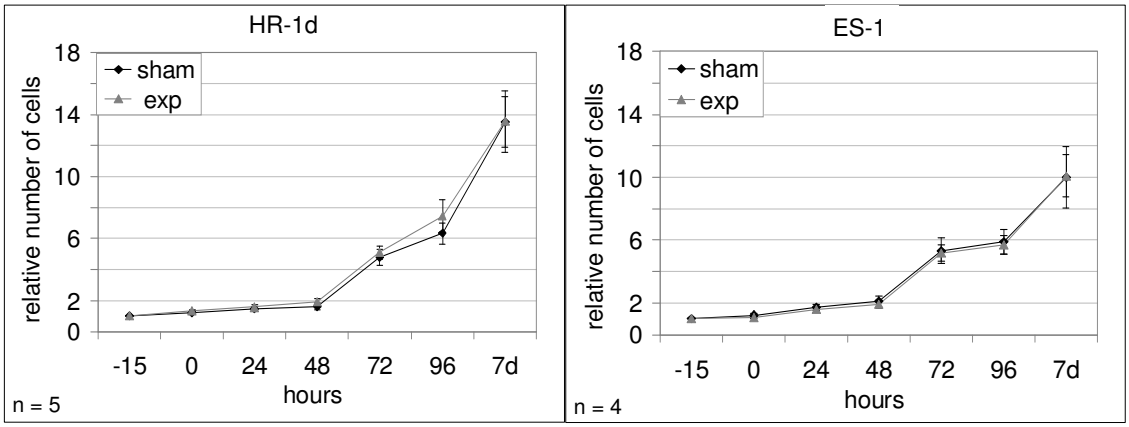

Focke et. al., supplementary Figure 2

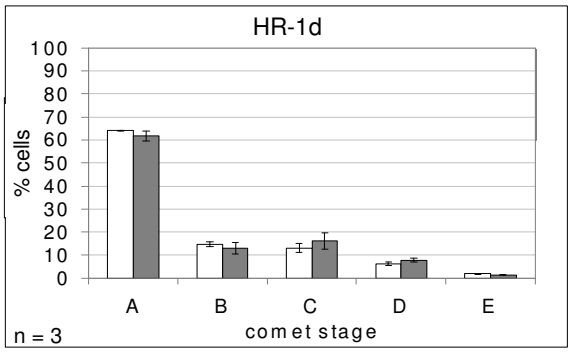

Focke et. al., supplementary Table 1:

comet stage scores intermittent exposure

		A	B	C	D	E	total	tailfactor
HR-1d								
1	sham	847	131	33	13	32	1056	8.3
	exposed	657	178	62	18	90	1005	15.6
2	sham	971	42	5	1	4	1023	3.5
	exposed	1079	115	23	13	51	1281	8.3
3	sham	628	106	39	26	26	825	10.1
	exposed	251	44	32	34	31	392	19.0
4	sham	365	67	10	10	27	479	11.2
	exposed	631	118	88	23	155	1015	22.0
5	sham	738	42	18	3	0	801	3.9
	exposed	700	58	35	3	4	800	5.1
6	sham	844	109	29	14	5	1001	5.8
	exposed	931	113	54	16	10	1124	6.6
7	sham	781	149	40	14	18	1002	7.7
	exposed	712	163	110	70	12	1067	12.2
8	sham	1173	194	83	31	19	1500	7.9
	exposed	1144	209	106	62	42	1563	10.8
9	sham	1351	117	39	3	2	1512	4.2
	exposed	1266	204	19	7	7	1503	5.0
10	sham	800	113	42	55	5	1015	8.7
	exposed	803	117	46	55	26	1047	10.6
11	sham	823	105	44	33	5	1010	7.3
	exposed	807	96	147	31	22	1103	10.8
12	sham	777	159	31	26	11	1004	7.7
	exposed	736	186	55	23	21	1021	9.2
13	sham	854	103	24	12	9	1002	5.8
	exposed	902	130	40	16	25	1113	7.7

Focke et. al., supplementary Table 1:

comet stage scores intermittent exposure

ES-1								
1	sham	1081	80	4	1	1	1167	3.4
	exposed	951	100	19	7	7	1084	4.9
2	sham	695	151	44	49	25	964	11.1
	exposed	455	121	55	32	45	708	15.3
3	sham	872	60	17	16	39	1004	8.3
	exposed	687	123	73	35	59	977	13.9
4	sham	765	156	41	14	25	1001	8.5
	exposed	569	162	52	23	49	855	13.3
5	sham	897	78	16	4	6	1001	4.5
	exposed	768	88	25	6	15	902	6.3
6	sham	467	24	16	0	3	510	4.4
	exposed	501	73	22	5	9	610	6.6
7	sham	933	45	21	3	12	1014	4.8
	exposed	904	66	24	8	8	1010	5.1
8	sham	745	135	146	16	25	1067	10.7
	exposed	729	191	215	43	18	1196	12.8
9	sham	947	109	55	14	1	1126	5.7
	exposed	807	72	50	36	12	977	8.2
10	sham	703	53	37	4	3	800	5.1
	exposed	711	35	42	9	5	802	5.7
11	sham	426	36	32	4	2	500	5.9
	exposed	405	36	36	7	13	497	8.6

Focke et. al., supplementary Table 1:

comet stage scores intermittent exposure

MRC-5								
1	sham	971	101	14	5	2	1093	4.2
	exposed	794	134	48	18	38	1032	9.7
2	sham	456	90	20	28	25	619	11.6
	exposed	385	73	38	43	37	576	16.5
3	sham	543	110	117	43	36	849	14.9
	exposed	428	119	96	53	67	763	20.4
HeLa								
1	sham	952	128	10	3	8	1101	4.8
	exposed	899	118	15	9	18	1059	6.2
2	sham	686	204	37	11	59	997	11.9
	exposed	767	210	46	19	59	1101	11.8
3	sham	844	116	21	10	9	1000	5.7
	exposed	778	182	24	10	16	1010	7.1
4	sham	481	95	21	1	12	610	7.0
	exposed	367	100	21	8	14	510	9.2

Focke et. al., supplementary Table 2:

comet stage scores continuous exposure

		A	B	C	D	E	total	tailfactor
HR-1d								
1	sham	790	137	44	22	21	1014	8.4
	exposed	499	73	27	27	51	677	14.4
2	sham	854	46	29	40	153	1122	18.9
	exposed	791	57	28	18	127	1021	16.8
3	sham	781	120	35	18	15	969	7.4
	exposed	774	108	41	19	14	956	7.5
ES-1								
1	sham	918	113	23	29	20	1103	7.5
	exposed	883	114	37	19	33	1086	8.5
2	sham	890	44	13	7	88	1042	11.7
	exposed	931	66	10	18	72	1097	10.7
3	sham	805	23	13	22	37	900	8.6
	exposed	815	18	23	16	38	910	8.5
4	sham	939	53	7	1	5	1005	3.8
	exposed	931	56	8	1	4	1000	3.7
MRC-5								
1	sham	508	68	49	7	106	738	19.5
	exposed	690	98	48	10	155	1001	20.2
2	sham	710	76	48	19	159	1012	20.7
	exposed	567	64	86	30	194	941	27.4
3	sham	677	210	77	22	5	991	8.7
	exposed	750	204	56	9	3	1022	6.9
HeLa								
1	sham	707	156	58	42	58	1021	13.7
	exposed	763	139	57	31	64	1054	13.0

Focke et. al., supplementary Table 3:

comet stage scores sham-sham exposure

		A	B	C	D	E	total	tailfactor
HR-1d								
1	coil 1	727	128	75	50	10	990	10.1
	coil 2	777	118	68	35	12	1010	8.9
2	coil 1	588	93	56	58	6	801	11.0
	coil 2	568	117	29	83	5	802	12.3
3	coil 1	794	85	57	70	4	1010	9.8
	coil 2	728	119	64	84	5	1000	11.4
ES-1								
1	coil 1	778	110	57	55	0	1000	8.7
	coil 2	810	87	67	35	2	1001	7.7
2	coil 1	572	114	33	80	3	802	11.9
	coil 2	578	107	37	76	2	800	11.5
3	coil 1	683	153	67	96	1	1000	12.2
	coil 2	805	154	39	93	4	1095	10.8

Focke et. al., supplementary Table 4:

comet stage scores H_2O_2 treatment

		A	B	C	D	E	total	tailfactor
HR-1d								
1	control	406	49	29	14	2	500	7.3
	10µM H2O2	293	68	27	14	4	406	9.2
	50µM H2O2	171	68	72	108	5	424	26.5
	100µM H2O2	0	167	139	201	93	600	41.9
	150µM H2O2	0	0	0	10	592	602	97
2	control	437	52	35	18	1	543	7.6
	10µM H2O2	366	72	34	18	7	497	9.5
	50µM H2O2	221	96	94	138	19	568	27.7
	100µM H2O2	0	172	144	198	56	570	44.4
	150µM H2O2	0	0	0	18	485	503	96.4
HeLa								
1	control	438	115	76	35	3	667	11.2
	10µM H2O2	348	98	103	49	3	601	14.6
	50µM H2O2	357	108	135	75	7	682	17.7
	100µM H2O2	313	133	111	91	6	654	19.1

Focke et. al., supplementary Table 5:

comet stage scores Fpg, intermittent exposure

		A	B	C	D	E	total	tailfactor
HR-1d								
1	sham	147	410	72	64	9	702	18.3
	exposed	174	357	72	96	26	725	22.2
	sham Fpg	14	368	197	111	10	700	27.2
	exp Fpg	4	146	177	252	44	623	45.7
	H2O2	96	355	146	138	28	763	27.7
	H2O2 Fpg	0	127	366	404	24	921	46.2
2	sham	183	377	158	81	34	833	22.1
	exposed	103	307	159	183	71	823	34.0
	sham Fpg	6	199	196	181	108	690	45.1
	exp Fpg	2	174	224	199	128	727	47.9

Focke et. al., supplementary Table 6:

comet stage scores for G1 starved cells (+iron supplementation)

		A	B	C	D	E	total	tailfactor
HR-1d								
1	sham	801	170	22	3	6	1002	5.6
	exposed	820	157	16	8	8	1009	5.8
2	sham	857	261	15	16	1	1150	6.1
	exposed	764	183	25	22	7	1001	7.1
3	sham	845	138	5	8	3	999	4.8
	exposed	910	122	16	9	7	1064	5.2
ES-1								
1	sham	912	242	10	5	10	1179	5.9
	exposed	726	173	34	8	6	947	6.5
2	sham	794	181	39	6	1	1021	5.8
	exposed	760	190	32	13	5	1000	6.6
3	sham	857	121	10	7	5	1000	4.9
	exposed	867	104	14	12	3	1000	5.0

		A	B	C	D	E	total	tailfactor
HR-1d								
1	sham	698	179	131	57	23	1088	12.9
	exposed	605	138	215	71	18	1047	15.5
2	sham	687	137	181	60	14	1079	13.2
	exposed	664	89	189	71	12	1025	14.1
3	sham	695	162	115	85	24	1081	14.1
	exposed	668	185	99	104	13	1069	14.3

Appendix II:

Genotoxic Effects From Radiofrequency Electromagnetic Fields: Revisiting a Controversial Issue

Comment to the "News of the Week" article: Fraud Charges Cast Doubt on Claims of DNA Damage From Cell Phone Fields. SCIENCE Vol. 321. pp. 1144f. [74]

Frauke Focke[1], Niels Kuster[2], and Primo Schär[1*]

[1] Department of Biomedicine
University of Basel
Mattenstrasse 28
4058 Basel
Switzerland

[2] IT'IS Foundation
Zeughausstrasse 43
8004 Zurich
Switzerland

Genotoxic Effects From Radiofrequency Electromagnetic Fields: Revisiting a Controversial Issue

Running title: RF-EMF effects on DNA

Frauke Focke[1], Niels Kuster[2], and Primo Schär[1*]

[1] Department of Biomedicine
University of Basel
Mattenstrasse 28
4058 Basel
Switzerland

[2] IT'IS Foundation
Zeughausstrasse 43
8004 Zurich
Switzerland

* Corresponding author: primo.schaer@unibas.ch
Phone: +41 61 267 0767
Fax: +41 61 267 3566

Comment to the “News of the Week” article: Fraud Charges Cast Doubt on Claims of DNA Damage From Cell Phone Fields. SCIENCE Vol. 321. pp. 1144f.

Characters including spaces: 10630

Scientific misconduct and fraud allegations were recently raised against a study that showed DNA breakage in primary human fibroblasts following exposure to mobile-phone radiation. We aimed to clarify the issue by replicating and expanding this study, using identical experimental procedures and conditions. We were able to reproduce weak genotoxic effects of radiofrequency magnetic field exposure for one human fibroblast cell line but not for the cell line reported in the study under debate.

Conflicting results have been published about genotoxic effects resulting from radiofrequency electromagnetic fields (RF-EMFs). Although a majority of studies produced negative evidence, genotoxicity was shown in a few cases (reviewed in [1, 2]). Two recent scientific publications received considerable public attention and concern, because they reported enhanced DNA fragmentation in different human cell lines (ES-1, IH-9 and HW-2 fibroblasts) following exposure to unmodulated and talk-modulated RF-EMF signals [3, 4]. These studies came under massive criticism on the ground of statistical considerations, culminating in allegations of data fabrication and scientific misconduct [5]. Indeed, a first partial replication study failed to reproduce genotoxic effects in human ES-1 fibroblasts, although these analyses focused on the 1.8 GHz carrier wave only, and did not systematically address effects of modulated signals [6]. Therefore, it remains unclear whether or not RF-EMFs have a genotoxic potential. We aimed to clarify the issue in a replication study.

In the original study, ES-1 human primary fibroblasts were exposed to a 1800 MHz RF-EMF at a SAR (specific absorption rate) of 2 W/kg (legal exposure threshold for the general population) for 4, 16 and 24 h and analysed with the comet assay [7]. Comet events were scored visually and nuclei classified into five categories representing increasing amounts of DNA fragmentation. A comet tailfactor was then

calculated to assess the average level of DNA fragmentation in the cell population. Continuous and intermittent (5´field on/10´field off) exposure to the carrier wave increased the comet tailfactor after 16 h and 24 h by about 1.6 to 2-fold. Exposure to a pulse modulated field as well as to a GSM talk modulated field (simulating a mobile phone conversation with the “Global System for Mobile Communication” standard net) also significantly increased the comet tailfactor by about 2-fold. Later, the effect of the RF-EMF carrier wave (intermittent exposure for 1, 4 and 24 h) could not be reproduced independently for the ES-1 cell line [6]. Unlike before, however, the comets in the latter study were scored with a computerized system, a method that analyzes smaller numbers of nuclei and yields a comet tail moment (product of comet tail length and percentage of DNA in tail) as a measure for DNA fragmentation.

Here, we first exposed the ES-1 cell line to a GSM talk modulated intermittent RF-EMF at SAR values of 1 W/kg and 2 W/kg for 16 h. We then assessed DNA fragmentation by the comet assay, applying visual scoring Fig. 1A) as in [3] as well as fully automated, computerized analyses (Fig. 1B) [7]. We measure no statistically significant differences between sham and exposed ES-1 cells with either method of comet scoring (Fig. 1A, 1B). We noticed a trend towards more DNA fragmentation in exposed cells at a SAR value of 1 W/kg exposure, though, but not at a SAR of 2W/kg. Given the absence of statistical significance, however, we interpret these data to mean that the RF-EMF exposure conditions applied do not induce DNA fragmentation in the ES-1 cell line.

We then used a second human primary fibroblast cell line, HR-1d, which we found previously to show higher comet effects than ES-1 following extremely low frequency EMF exposure. With this cell line, we found a small but significant increase of the tailfactor (1.5 fold) after intermittent exposure to RF-EMF at a SAR of 1 W/kg and GSM talk modulation (Fig. 2A). The visual comet scoring revealed a decrease of

almost 7% of cells in comet stage A, representing undamaged cells. When exposing these cells intermittently to RF-ELF at a SAR of 2 W/kg, the tailfactor change was smaller (1.3 fold) but still statistically significant. Intermittent exposure to the unmodulated carrier wave (5´/10´) at a SAR value of 1 W/kg for 16 h did not produce significant differences between sham and exposed cells, although a trend towards more DNA fragmentation in exposed cells in discernible. Using fully automated comet analysis, we confirmed statistically significant differences after exposure of HR-1d cells to a GSM-talk modulated field at 1 W/kg, but not at 2 W/kg. These analyses also revealed no effect of the carrier wave exposure (Fig. 2B). Hence, these result support the visually scored data partially, i.e. for the condition that produced a slightly more robust tail factor differences (1 W/kg GSM talk modulated RF-EMFs). Applying the stringent requirement that a genotoxic effect is genuine only if both comet scoring techniques produce statistically significant differences, we conclude the RF-EMF exposure at 1W/kg slightly increases the steady-state level of DNA strand breaks in the HR1-d cell line.

In conclusion, we are not able to reproduce results obtained in a previously published study showing RF-EMF induced DNA fragmentation in the ES-1 fibroblast cell line. A different human fibroblasts cell line (HR-1d), derived from an older donor, shows a small but significant increase of both, the comet tailfactor obtained by visual scoring and the tail moment obtained by fully automated computerized analysis, following exposure to a talk modulated field at a SAR value of 1W/kg. There are notable trends in other exposure conditions tested, which could still be biologically relevant although statistically not significant.

References and Notes

1 **Heynick, L. N., Johnston, S. A. and Mason, P. A.,** Radio frequency electromagnetic fields: cancer, mutagenesis, and genotoxicity. *Bioelectromagnetics* 2003. **Suppl 6**: S74-100.

2 **Krewski, D., Glickman, B. W., Habash, R. W., Habbick, B., Lotz, W. G., Mandeville, R., Prato, F. S., Salem, T. and Weaver, D. F.,** Recent advances in research on radiofrequency fields and health: 2001-2003. *J Toxicol Environ Health B Crit Rev* 2007. **10**: 287-318.

3 **Diem, E., Schwarz, C., Adlkofer, F., Jahn, O. and Rudiger, H.,** Non-thermal DNA breakage by mobile-phone radiation (1800 MHz) in human fibroblasts and in transformed GFSH-R17 rat granulosa cells in vitro. *Mutat Res* 2005. **583**: 178-183.

4 **Schwarz, C., Kratochvil, E., Pilger, A., Kuster, N., Adlkofer, F. and Rudiger, H. W.,** Radiofrequency electromagnetic fields (UMTS, 1,950 MHz) induce genotoxic effects in vitro in human fibroblasts but not in lymphocytes. *Int Arch Occup Environ Health* 2008. **81**: 755-767.

5 **Vogel, G.,** Scientific misconduct. Fraud charges cast doubt on claims of DNA damage from cell phone fields. *Science* 2008. **321**: 1144-1145.

6 **Speit, G., Schutz, P. and Hoffmann, H.,** Genotoxic effects of exposure to radiofrequency electromagnetic fields (RF-EMF) in cultured mammalian cells are not independently reproducible. *Mutat Res* 2007. **626**: 42-47.

7 Materials and methods plus comet stage scores of individual experiments are available on *Science* Online.

8 We thank Melanie Struwe and Dr. Martin Schneider from the “Novartis Institutes for BioMedical Research” for the help with the automated computerized analysis of comet assays. This study was supported by grants

from the Forschungsstiftung Mobilfunk (Zürich) and the NFP57 program of the Swiss National Science Foundation.

Figure legends

Fig. 1. Comet analysis of RF-EMF exposed ES-1 fibroblasts. (**A**) Visual comet stage analysis with percentages of cells in comet stages A-E. Primary measurements for each single experiment are shown in supplementary Tables 1-3. (n) is the number of experiments, error bars indicate SEMs and asterisks represent the significance levels by the Student´s *t*-test comparing fraction of cell in individual comet stage: ***** $p<0.05$; ****** $p<0.01$; ******* $p<0.005$. The horizontal bar and p(c) show the mean significance of the chi-square tests, analysing the comet stage distribution of sham and EMF-exposed nuclei of individual experiments. The upper right boxes show the mean tailfactor values for sham and exposed cells as well as the significance level of the Student´s *t*-test on the tailfactors (p(s)). (**B**) Automated analysis: pooled tail moment values from 300 cells (100 cells from 3 slides) per condition for 3 independent experiments per exposure type are displayed together with median, interquartile range (boxes) and 10-90 percentile range (whiskers). Significance was tested with Student´s *t*-test comparing the medians of each single experiment. Mean medians for each exposure condition are given on the x-axis.

Fig. 2. Comet assay results of RF-EMF exposed HR-1d fibroblasts. (**A**) Visual comet stage analysis with percentages of cells in comet stages A-E. Primary measurements for each single experiment are shown in supplementary Tables 1-3. (n) is the number of experiments, error bars indicate SEMs and asterisks represent the significance

levels of Student´s *t*-test comparing fraction of cells in individual comet stages: * $p<0.05$; ** $p<0.01$; *** $p<0.005$. The horizontal bar and p(c) show the mean significance of the chi-square tests, analysing the comet stage distribution of sham and EMF-exposed nuclei of individual experiments. The upper right boxes show the mean tailfactor values for sham and exposed cells as well as the significance level of the Student´s *t*-test on the tailfactors (p(s)). (**B**) Automated analysis, pooled tail moment values from 100 cells of 3 slides per condition for 3 independent experiments per exposure type are displayed together with median, interquartile range (boxes) and 10-90 percentile range (whiskers). Significance was tested with Student´s *t*-test comparing the medians of each single experiment. Mean medians for each exposure condition are given on the x-axis.

Focke et. al., Figure 1

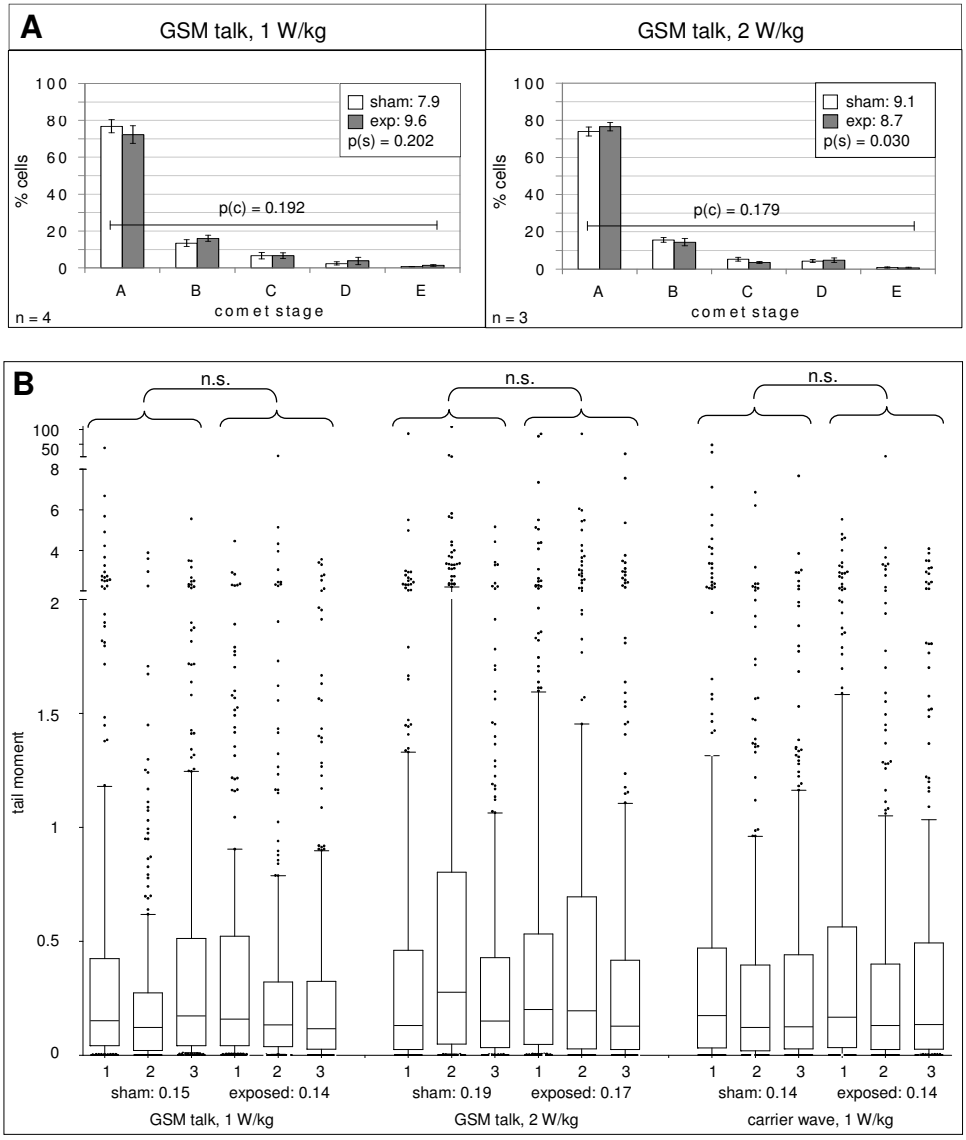

Focke et. al., Figure 2

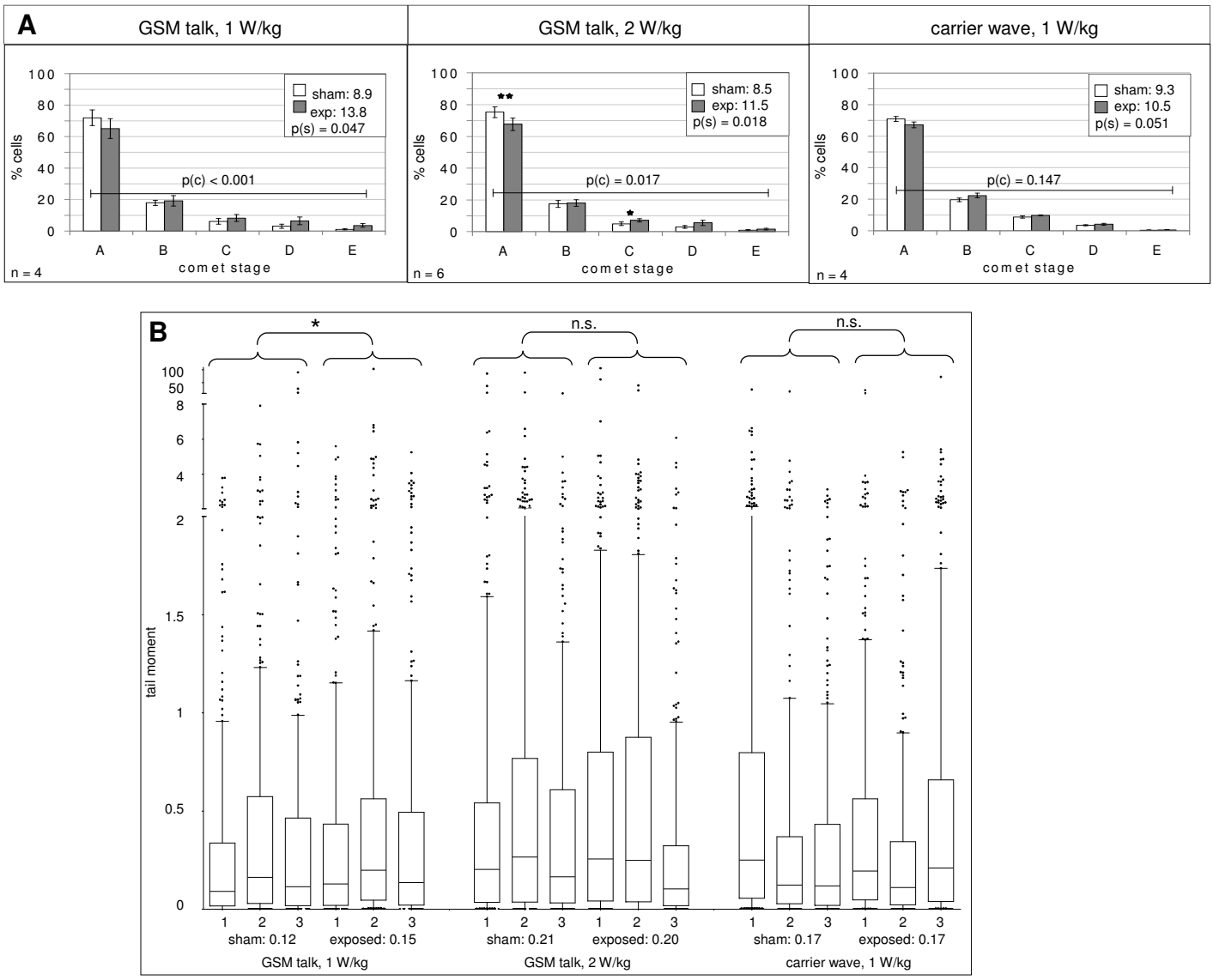

Supplementary Information

Materials and Methods

Radio frequency exposure system and exposure conditions. The RF-ELF exposure system sXcUMTS was built and provided by the Foundation for Information Technologies in Society (IT'IS foundation), Zurich, Switzerland and is described in detail on http://www.itis.ethz.ch/index/index_sxc1950.html. The setup is based on two R18 waveguides operating at 1950 MHz. Two waveguides (exposed, sham-exposed) were placed inside a commercial incubator to ensure constant environmental conditions (37°C, 5% CO_2, 95% humidity). Six 35mm Petri dishes can be exposed simultaneously and are placed in the H-field maxima. The system provides an efficiency of > 50 W/kg per Watt input power, deviations from SAR uniformity of < 30%, variability of < 6% and a temperature load of < 0.03°C per W/kg average SAR. A computer-controlled signal and monitoring unit was developed (1) to generate complex modulated GSM and UMTS signals, (2) to continuously monitor the field and environmental conditions (air temperature, fan cooling system) and (3) to realize blinded exposure protocols.

The field was either applied without modulation of the signal (=carrier wave) or with modulation: GSM signals were amplitude-modulated by rectangular pulses with a repetition frequency of 217 Hz and a duty cycle of 1:8, yielding frames of a length of 4.61 ms each including a 576 µs burst. Since every 26^{th} frame is idle, an 8 Hz modulation component is integrated into the signal. In order to save battery power during active periods without speaking into the phone the number of active frames is reduced (=discontinuous transmission mode, DTX). GSM talk modulation simulates a

mobile-phone conversation by alternating between GSM mode and DTX at an average rate of 97 and 50 s.

Cell lines and culture. Human primary fibroblasts (ES-1, male, 6 years old; HR-1d, male, 42 years old) kindly provided by Prof. Rüdiger (Vienna) were grown in Dulbecco´s modified Eagle´s medium (DMEM), supplemented with 10% FCS, 100 U/mL penicillin, 100 µg/mL streptomycin and 2 mM L-glutamine (Sigma-Aldrich, St. Louis, MO, USA). Cells were grown in 15-cm Petri dishes (Falcon 353025) at 37°C in a humified atmosphere containing 5% CO_2 and were supplied with fresh medium every 48 h. 24 h before exposure to EMF, cells were seeded into 3-cm Petri dishes (Nunc) to a confluency of about 30%.

Comet assay procedure and analysis. Alkaline comet assay was performed basically as described by Singh *et. al.* [1]. 10^4 cells were harvested and resuspended in 0.5% low melting point agarose (Cambrex) at 37°C. The cell/agarose suspension is laid onto microscope slides precoated with 1.5% normal melting point agarose (BioRad, Hercules, CA, USA), spread with a cover slip and let solidify for about 15 min. Slides then were immersed in freshly prepared ice-cold lysis buffer (2.5 M NaCl, 100 mM Na_2EDTA, 10 mM Tris-HCl pH 10, 1% Triton X-100, 10% DMSO, pH 10) for 90 min, washed in ddH_2O, drained and placed side by side in a gel electrophoresis tank. Slides were submerged with freshly made electrophoresis buffer (1 mM Na_2EDTA, 300 mM NaOH, pH>13) and incubated for 30 min to allow DNA unwinding prior to electrophoresis at 25 V/ 300 mA for 20 min. All steps after exposure were performed under dimmed light at 4°C. After electrophoresis slides were washed three times with 0.4 mM Tris-HCl pH 7.5 for 10 min, followed by fixation with EtOH absolute (2x 5 min) and air drying.

For visual analysis nuclear DNA was stained with 20 µg/ml ethidium bromide and analysed with a fluorescent microscope at 400x magnification. Data collection was done according to Anderson *et. al.* [2] with minor modifications by Ivancsits *et.al.* [3]. For each individual exposure condition, two slides were subjected to the comet assay. Nuclei of at least 450 cells per slide were visually scored and classified into five categories corresponding to their amount of DNA in the tail (Figure 2c). Tailfactors (tf) were calculated with the following formula: tf (%) = ((A*F(A) + B*F(B) + C*F(C) + D*F(D) + E*F(E))/1000, where A is the number of cells classified to group A, F(A) the average of group A (2.5% of fragmented DNA), B the number of cells classified to group B, F(B) the average of group B (12.5%), C the number of cells classified to group C, F(C) the average of group C (30%), D the number of cells classified to group D, F(D) is the average of group D (67.5%), E the number of cells classified to group E, and F(E) the average of group E (97.5%). For automated comet analysis, slides were stained with Propidium Iodide and 100 cells per slide were analysed with a coputerized automated system according to Frieauff *et. al.* [4].

Each visually scored EMF exposure experiment was repeated 3-6 times and differences between sham and exposed cells were statistically analysed by the Student´s *t*-test applying it to percentage of cells in each category and to the tailfactors of all experimental replica. Additionally, the statistical significance of the difference between sham and exposed cells was tested by applying the chi-square test to the whole distribution of cells for each single experiment. The indicated numbers are mean p-values of all experiments. For automatically analyzed comet assays, the median tail moments of 100 nuclei per slide from 3 slides per condition of

three independent experiments were calculated and statistically analyzed by the Student´s *t*-test.

References

1 **Singh, N. P., Tice, R. R., Stephens, R. E. and Schneider, E. L.,** A microgel electrophoresis technique for the direct quantitation of DNA damage and repair in individual fibroblasts cultured on microscope slides. *Mutat Res* 1991. **252**: 289-296.

2 **Anderson, D., Yu, T. W., Phillips, B. J. and Schmezer, P.,** The effect of various antioxidants and other modifying agents on oxygen-radical-generated DNA damage in human lymphocytes in the COMET assay. *Mutat Res* 1994. **307**: 261-271.

3 **Ivancsits, S., Diem, E., Pilger, A., Rudiger, H. W. and Jahn, O.,** Induction of DNA strand breaks by intermittent exposure to extremely-low-frequency electromagnetic fields in human diploid fibroblasts. *Mutat Res* 2002. **519**: 1-13.

4 **Frieauff, W., Hartmann, A. and Suter, W.,** Automatic analysis of slides processed in the Comet assay. *Mutagenesis* 2001. **16**: 133-137.

Focke et. al.,

supplementary Table 1: 1W/kg

		A	B	C	D	E	total	tailfactor
HR-1d								
1	sham	633	213	74	58	22	1000	12.5
	exposed	548	169	116	92	75	1000	20.5
2	sham	666	203	113	51	8	1041	11.3
	exposed	551	331	145	141	24	1192	18.2
3	sham	1272	208	36	5	10	1531	5.3
	exposed	1113	199	48	19	31	1410	7.8
4	sham	966	213	49	12	7	1247	6.4
	exposed	943	190	58	27	24	1242	8.6
ES-1								
1	sham	750	115	87	42	6	1000	9.3
	exposed	698	151	84	41	26	1000	11.5
2	sham	748	127	84	35	9	1003	9.2
	exposed	626	183	86	94	11	1000	13.9
3	sham	1303	162	20	5	10	1500	4.8
	exposed	1281	176	32	5	6	1500	4.9
4	sham	849	228	99	18	7	1201	8.2
	exposed	870	232	89	15	15	1221	8.4

Focke et. al.,

supplementary Table 2: 2W/kg

		A	B	C	D	E	total	tailfactor
HR-1d								
1	sham	697	217	94	50	6	1064	10.6
	exposed	486	198	98	106	17	905	17.1
2	sham	761	243	65	18	16	1103	8.8
	exposed	652	246	55	32	16	1001	10.1
3	sham	785	74	10	1	0	870	3.7
	exposed	836	108	51	2	3	1000	5.4
4	sham	700	156	60	62	2	980	10.1
	exposed	628	130	89	52	6	905	11.0
5	sham	768	168	25	28	18	1007	8.4
	exposed	714	224	60	45	40	1083	12.3
6	sham	649	171	43	21	12	896	8.5
	exposed	685	161	60	86	18	1010	13.0
ES-1								
1	sham	762	178	77	30	8	1055	8.8
	exposed	771	193	45	30	12	1051	8.5
2	sham	783	129	39	43	2	996	7.9
	exposed	845	122	28	46	3	1044	7.5
3	sham	697	168	47	55	14	981	10.5
	exposed	754	134	39	70	6	1003	10.0

Focke et. al.,

supplementary Table 3: CW

		A	B	C	D	E	total	tailfactor
HR-1d								
1	sham	770	168	107	40	5	1090	9.6
	exposed	737	193	103	55	8	1096	10.8
2	sham	763	237	85	38	5	1128	9.3
	exposed	693	224	94	53	8	1072	10.9
3	sham	839	244	111	47	6	1247	9.8
	exposed	775	307	127	34	5	1248	9.9
4	sham	824	237	90	32	3	1186	8.6
	exposed	765	266	109	39	5	1184	9.8

Appendix III:

Base Excision by Thymine DNA Glycosylase Mediates DNA-Directed Cytotoxicity of 5-Fluorouracil

Christophe Kunz[1], Frauke Focke[1], Yusuke Saito[1], David Schürmann[1], Jim Selfridge[2], Adrian Bird[2] and Primo Schär[1*]

[1] Centre for Biomedicine, Department of Biomedicine, University of Basel, Mattenstrasse 28, 4058 Basel, Switzerland

Base Excision by Thymine DNA Glycosylase Mediates DNA-Directed Cytotoxicity of 5-Fluorouracil

Running foot: TDG mediated 5-FU toxicity

Christophe Kunz[1], Frauke Focke[1], Yusuke Saito[1], David Schürmann[1], Jim Selfridge[2], and Primo Schär[1*]

[1] Department of Biomedicine
University of Basel
Mattenstrasse 28
CH-4058 Basel
Switzerland

[2] Wellcome Trust Centre for Cell Biology
Institute of Cell and Molecular Biology
University of Edinburgh
Michael Swann Building, King's Buildings
Mayfield Road
Edinburgh EH9 3JR
Scotland U.K.

* Corresponding author: Prof. Dr. Primo Schär[1]
primo.schaer@unibas.ch
Phone: +41 61 267 0767
Fax: +41 61 267 3566

Abstract

Background: 5-Fluorouracil (5-FU), a chemotherapeutic drug commonly used in cancer treatment, imbalances nucleotide pools, favoring misincorporation of uracil and 5-FU into genomic DNA. The processing of these bases by DNA repair activities was proposed to account for the DNA-directed cytotoxicity of the drug, but underlying mechanisms have not been resolved. *Methodology/Principle Findings*: In this study, we investigated an unexpected role of thymine DNA glycosylase (TDG), one of four mammalian uracil DNA glycosylases (UDG), in the cellular response to 5-FU. Using mouse genetic and biochemical tools, we found that inactivation of TDG significantly increases resistance of cells towards 5-FU, and that excision of DNA-incorporated 5-FU by TDG generates persistent DNA strand-breaks, delays S-phase progression, and activates DNA damage signaling. In the absence of TDG, repair of 5-FU induced DNA strand-breaks is more efficient. *Conclusions/Significance*: Hence, excision of 5-FU by TDG but not by other UDGs (UNG2, SMUG1) prevents efficient downstream processing of the repair intermediate, thereby mediating DNA-directed cytotoxicity. The status of TDG expression in a cancer is therefore likely to determine its response to 5-FU based chemotherapy.

Introduction

The antimetabolite 5-fluorouracil (5-FU) is an analogue of uracil with a fluorine substitution at the C_5 position. Developed as an inhibitor of thymidylate synthase (TS) [1], it has become an important compound in the first-line treatment of a range of human cancers, most prominently colorectal carcinomas [2]. Inside cells, 5-FU is converted to different active metabolites, including fluorodeoxyuridine monophosphate (FdUMP), fluorodeoxyuridine triphosphate (FdUTP), and fluorouridine triphosphate (FUTP) [2]. These metabolites have been implicated in both, global RNA metabolism due to incorporation of the ribonucleotide FUMP into RNA, and DNA metabolism due to TS inhibition or direct incorporation of FdUMP into DNA. The therapeutic importance of the DNA-directed actions is emphasized by a direct correlation of TS activity with the response rate of tumors or cancer cell lines to the treatment with 5-FU [3,4,5]. TS converts deoxyuridine monophosphate (dUMP) to deoxythymidine monophosphate (dTMP), but FdUMP inactivates the enzyme irreversibly upon docking to the nucleotide binding site and formation of a stable complex with TS and its cofactor 5,10-methylenetetrahydrofolate [6,7]. Thus, TS inhibition deprives the cell of its capacity to synthesize dTMP from dUMP and, thereby, elevates deoxyuridine triphosphate (dUTP) levels at the expense of deoxythymidine triphosphate (dTTP). The resulting dUTP/dTTP imbalance then favors the misincorporation of dUMP during DNA replication, giving rise to a dose dependent increase in the steady-state level of DNA uracil [8,9].

It has been argued that the therapeutic effects of TS inhibition base on the fragmentation of genomic DNA as a result of massive uracil excision by the replication associated uracil DNA glycosylase (UDG) UNG2 and/or of futile cycles of base excision repair (BER) [2,10,11]. This, however, is not entirely consistent with the

experimental evidence available. Although UNG2 constitutes a major activity against the accumulation of uracil in genomic DNA [12], its expression status does not affect the cellular resistance towards TS inhibition [13] and, hence, the survival of 5-FU treated cells [14]. Thus, uracil excision by UNG2 unlikely accounts for the DNA-directed cytotoxicity of 5-FU. In light of a recent report, however, showing that FdUMP gets itself incorporated into genomic DNA in 5-FU treated cells, with levels even exceeding those of misincorporated uracil [9], it may be that the 5-FU rather than the uracil in the DNA is cell toxic.

While UNG is the most efficient and specific UDG present in mammalian cells, it is not the only one. Single-strand-selective monofunctional uracil-DNA glycosylase 1 (Smug1) [15], thymine DNA glycosylase (TDG) [16] and methyl-CpG-binding domain protein 4 (MBD4) [17,18] represent additional activities. All these enzymes are capable of processing uracil as well as 5-FU in DNA, albeit with different kinetic properties. Smug1 was shown to provide resistance to 5-FU exposed cells [9], whereas MBD4 may contribute to the toxicity of the drug, arguably through DNA damage signaling [19]. Human TDG, originally discovered as a G•T mismatch-specific thymine DNA glycosylase [20], processes a broad range of substrates, including uracil and 5-FU. Although its has a strong preference for bases mispaired with a guanine, TDG excises 5-FU with a high efficiency irrespective of whether the opposite base is a guanine or an adenine [16,21,22]. Consistently, plasmid based *in vitro* repair assays with immunodepleted cell lysates have revealed a significant contribution of TDG to 5-FU excision [23].

Due to the redundancy of UDG activities that can contribute to 5-FU processing in cells, it is difficult to predict in which way and to what extent one or the other contributes to the cellular response to 5-FU, and thus to the efficacy of cancer therapies including 5-FU. Moreover, recent evidence from *in vitro* repair studies has

implicated the postreplicative mismatch repair system (MMR) in the processing of 5-FU•G base pairs [23]. In part, this account for the increased resistance of MMR deficient cells to treatment with fluoropyrimidines [24,25,26]. Given the general nucleotide imbalance induced by TS inhibition, however, the MMR dependent toxicity of 5-FU is best explained by excessive formation and repair of DNA mispairs during replication [25,27]. Hence, the DNA-directed effects of 5-FU may reflect two lines of responses; the excision 5-FU or U from DNA (5-FU/U•A, 5-FU/U•G) mainly by UDGs and the excision of mismatched nucleotides mainly by MMR.

The objective of this study was to clarify the role of TDG in this context. We examined cellular and molecular responses to 5-FU exposure of matched *Tdg* proficient and deficient mouse embryonic fibroblasts and stem cells. We show that TDG, of all UDGs, is responsible for the accumulation of DNA strand-breaks, a delay in S-phase progression and a persistent activation of DNA damage signaling upon treatment of cells with 5-FU, and that inactivation of *Tdg* by mutation causes hyperresistance towards the drug. We conclude that TDG, unlike UNG2 and Smug1, mediates the DNA-directed cytotoxic effects of 5-FU.

Results

TDG deficiency confers hyper-resistance towards 5-FU

To investigate the role of TDG during 5-FU treatment of cells in culture, we established SV40 immortalized mouse embryonic fibroblasts (MEFs) with homozygous or heterozygous *Tdg* disruptions ($Tdg^{+/+}$, $Tdg^{+/-}$, $Tdg^{-/-}$) from embryos (ED 9.5) of heterozygous matings. The *Tdg* knockout allele, generated by classical gene targeting, had a replacement of exons 6 and 7, encoding parts of the catalytic core of TDG, with a neomycin resistance cassette (Lettieri et al., unpublished data). We then used litter-matched MEF lines for phenotypic examination. Western blotting with a polyclonal anti-mouse TDG antibody confirmed that neither full-length nor truncated versions of TDG were present in whole cell extracts of the homozygous knockout MEFs, while heterozygous cells produced about half endogenous levels of the protein (Figure 1A, data not shown). Continuous exposure of these MEFs to 5-FU for 48 hours reduced living cell counts in a dose-dependent manner. However, compared to wildtype, TDG deficient cells displayed a remarkable hyperresistance (Figure 1B), and heterozygous cells showed an intermediate 5-FU sensitivity (suppl. Figure 1). These findings implicated a rate limiting contribution of TDG to 5-FU mediated cytotoxicity. A differential response of TDG proficient and deficient MEFs to 5-FU treatment was also observed in a real-time assessment of growth behavior. Whereas TDG proficient MEFs started to die after 36 hours of 5-FU exposure, TDG deficient cells responded with a dose dependent growth retardation only (suppl. Figure 2).

Since immortalization by the SV40 large-T antigen (LTA) occurs through inactivation of antiproliferative proteins such as p53 or pRb and, thus, can affect the cellular DNA damage response [28,29], we also included spontaneously

immortalized MEF cell lines in our analysis. To this end, we set up isogenic *Tdg* proficient and deficient MEF lines by stable transfection of a single clone with either a complementing *Tdg* transgene under the control of an SV40 promoter or the corresponding expression vector only (Figure 1A). Survival tests then showed that *Tdg* expression sensitized the *Tdg* deficient cells to treatment with 5-FU to a level comparable to *Tdg* proficient MEFs (Figure 1B). This confirmed that the 5-FU hyperresistance of *Tdg* knockout cells is a direct consequence of the loss of TDG rather than of unspecific effects by SV40 LTA immortalization or other differences in clonal backgrounds.

To validate the hyperresistance phenotype in cells that are naturally immortal, we examined the 5-FU response of $Tdg^{+/-}$ and $Tdg^{-/-}$ mouse embryonic stem (ES) cells generated in our laboratory (Figure 1A) (Y. Saito, et al., unpublished data). Also there, the loss of TDG was associated with a remarkable increase in resistance towards 5-FU (Figure 1B). Hence, the mechanism by which TDG mediates cytotoxicity of 5-FU is active in very divergent cell-types, including immortalized differentiated cells as well as undifferentiated stem cells.

Finally, to examine the drug specificity of the phenotype, we assessed the sensitivities of TDG proficient and deficient MEFs towards the monofunctional DNA alkylating agent MMS methyl methansulfonate (MMS) (Figure 1C). At MMS concentrations yielding ≥10% cell survival, the TDG status did not significantly affect cellular sensitivity. At higher concentrations (≤ 5% survival), however, TDG deficient cells were slightly hypersensitive. This indicated that, although TDG may contribute to the repair of MMS induced DNA lesions, it does not mediate cytotoxicity as it does in the case of 5-FU.

TDG contributes to A•FU repair in nuclear extracts

Biochemical studies revealed that the human TDG acts on a rather broad range of substrates, including G•U and G•FU mispairs but also 5-FU base-paired with adenine. 5-FU in fact turned out to be the only base that is efficiently processed by TDG in normal base pairing configuration or even in single-stranded DNA [21]. We thus reasoned that the excision of 5-FU and/or uracil from genomic DNA by TDG might be the source of 5-FU mediated killing in wildtype cells. To test this hypothesis, we first validated the 5-FU and uracil processing abilities of purified mouse TDG in base release assays. This showed that, like its human counterpart, the mouse protein excises thymine, uracil and 5-FU opposite guanine but also 5-FU paired with adenine, all with comparable efficiencies (Figure 2A). A•U containing homoduplex DNA, however, was hardly processed, suggesting that mouse TDG does not contribute significantly to the repair of A•U base pairs.

To assess the contribution of the endogenous mouse TDG to overall uracil and 5-FU processing, we analyzed the activities present in nuclear extracts of *Tdg* wildtype, heterozygous and null mutant MEFs. G•T processing served as a control and was detectable in extracts from wildtype cells but not from homozygous *Tdg* knockout cells (Figure 2A). Heterozygous *Tdg* knockout cells showed reduced thymine excision activity compared to homozygous wildtype cells, which is in line with the reduced levels of TDG in these cells (Figures 2B, 1A). Thus, TDG constitutes the major and rate-limiting mismatch-specific thymine excision activity in these cells, suggesting that MBD4, another G•T processing DNA glycosylase [30,31], is not or only poorly active. Since a lack of MBD4 activity was also observed with protein extracts from mouse ES cells (data not shown) and in previous studies with different cell systems [23,32], the role of this DNA glycosylase in mismatch processing remains uncertain. Considerably higher amounts of nicked DNA products were detected for all uracil and 5-FU containing substrates. Removal of uracil and 5-FU

from G•U, G•FU and A•U was equally efficient irrespective of the TDG status. Excision of 5-FU from an A•FU substrate, however, was significantly reduced in extracts from *Tdg*$^{-/-}$ MEFs (Figure 2B). The remaining activity on A•FU, but also the efficient processing of A•U, G•U and G•FU in extracts from *Tdg* knockout MEFs is most likely attributed to the presence of other UDGs with overlapping substrate spectra. As the highly efficient, replicative UNG2 was inhibited by addition of saturating amounts of UGI peptide in these assays (data not shown), and MBD4 activity was not detected, Smug1 most likely represents the redundant uracil and 5-FU processing activity observed here. The data therefore suggest that, under conditions of low UNG2 activity in cells, such as outside of S-phase when UNG2 is downregulated [32,33,34], TDG constitutes a major and rate-limiting A•5-FU processing activity.

This is consistent with measurements of 5-FU incorporation into genomic DNA following 5-FU treatment. The genomic levels of uracil and 5-FU upon treatment with 10 μM 5-FU for 48 hours were four and eleven times higher in TDG knockout MEFs (3.4×10^5 U-residues; 1.7×10^6 5-FU residues) than in wildtype cells (8.2×10^4; U residues; 1.5×10^5 5-FU residues), respectively, and this compares to the levels measured in 5-FU treated *Smug1 knockdown* cells (D. Barnes, personal communication; [9]). Not only do these data confirm that 5-FdUMP gets incorporated into genomic DNA, they also establish that both TDG and Smug1 constitute the major activities processing these lesions, whereas UNG2 does not appear to contribute significantly as also implicated by incorporation measurements and sensitivity tests with *Ung-/-* knockout cells (2.1×10^5 U; 1.5×10^5 5-FU) [9,14].

5-FU treatment induces TDG dependent DNA strand-breaks

5-FU treatment has been associated with the generation of DNA strand-breaks [2,10,11]. In the light of our biochemical evidence implicating TDG in processing genomic A•FU base pairs, this might be accounted for by an accumulation apyrimidinic/apurinic sites (AP-site) in DNA. Through further processing by the BER system (APE1), spontaneous breakage or stalling of DNA polymerases, these could give rise to increased levels of single-stranded DNA breaks (SSBs) in cells. To test this hypothesis, we applied alkaline Comet analyses to assess 5-FU induced AP-site and/or SSB formation in TDG proficient and deficient MEFs, as well as in complemented knockout cells stably expressing an ectopic wildtype or catalytic mutant *Tdg* (Figure 3A). To avoid *Tdg* over-expression artifacts in the latter [32], we made use of constructs that drive *Tdg* expression from its endogenous promoter (Schürmann et al., unpublished results). Automated analyses of Comet tail moments then showed similar background levels of DNA strand-breaks in all untreated cell populations. Following treatment with 5 μM 5-FU for 24 hours and a recovery of another 24 hours, however, the tail moments increased significantly above background in TDG proficient populations, whereas no significant increase was detected for TDG deficient cells (Figure 3B). Remarkably, cells complemented with the catalytic inactive mutant form of TDG did not show significantly elevated tail moments after 5-FU treatment. These data indicate that base excision by TDG accounts for the increase in steady-state levels of DNA strand-breaks observed upon treatment of cells with 5-FU.

Base excision generates single-stranded DNA breaks, feeding into a SSB repair pathway whereby XRCC1 plays a central role [35]. To address a possible engagement of SSB repair following 5-FU treatment, we quantified nuclear XRCC1 foci by immunofluorescence detection of the endogenous protein with specific mono- and polyclonal antibodies [36]. This showed indeed that the median number of

XRCC1 foci per cell increased after 24 hours of low dose 5-FU treatment and a recovery of 24 hours in the absence of the drug (Figure 3C). We therefore conclude that uracil/5-FU excision from genomic DNA activates SSB repair processes at the site of the lesion. Remarkably, 5-FU treatment induced significantly more XRCC1 foci in *Tdg* knockout cells, indicating higher SSB repair activity in these cells, most probably downstream of uracil/5-FU excision by the remaining UDG activities. Thus, in wildtype cells TDG may compete with these glycosylases for the 5-FU substrates, generate AP-sites, but then prevent efficient downstream processing of the repair intermediates by the SSB repair pathway.

5-FU arrests MEFs in S-phase and actives DNA damage responses

5-FU treatment was shown to delay or even arrest S-phase progression in HeLa and DT40 cells [37,38]. To address the role of TDG in this context, we determined the cell cycle profiles of TDG proficient and deficient MEFs following 5-FU treatment. Relative to the mock control, treatment for 24 hours with 5 μM 5-FU and subsequent cultivation in drug-free medium for additional 24 hours resulted in a significant enrichment of *Tdg* wildtype cells in the S (2-fold) and G2/M phases (1.3-fold) of the cell cycle (Figure 4A). This enrichment occurred at the expense of the G1 cell population, which was reduced by a factor of three. By contrast, the 5-FU induced changes in cell cycle distribution of TDG deficient MEFs were less pronounced and not statistically significant (Figure 4A). Since treatment with hydroxyurea (HU) impeded S-phase progression equally in both cell lines (data not shown), the lack of a cell cycle response to 5-FU of TDG deficient MEFs was unlikely the result of a defect in the intra-S phase DNA damage checkpoint in these cells. To corroborate the TDG dependence of the 5-FU mediated S-phase delay, we compared the response of *Tdg* knockout cells complemented by stable expression of endogenous

levels of wildtype *Tdg* with that of a vector control. Also in this setting, the S-phase delay induced by 5-FU treatment was significantly more pronounced in the *Tdg* expressing cell line (1.7-fold vs. 1.2 fold) (Figure 4B). Thus, TDG contributes to cell cycle responses following 5-FU treatment.

5-FU induced cell cycle arrest in early S-phase was shown previously to depend on Chk1, a DNA damage and replication checkpoint effector kinase [37,38] that gets activated through ATR dependent phosphorylation at serine residues 317 and 345 (Chk1-p) [39]. We examined the role of TDG in checkpoint activation following treatment of cells with 10 μM 5-FU for 24 hours and a recovery in drug-free medium for another 24 hours. Immunoblotting of whole cell extracts with a S345 phospho-specific Chk1 antibody confirmed significant activation of the kinase in *Tdg* wildtype cells (Figure 5A). In extracts of 5-FU treated *Tdg* knockout cells, however, 5-FU induced Chk1 phosphorylation was hardly detectable. This was not due to an absence of Chk1 or an inability to phosphorylate the kinase in these cells; immunodetection of total Chk1 protein confirmed similar levels in wildtype and knockout extracts (Figure 5A), and the replication inhibitor hydroxyurea (HU) induced Chk1 phosphorylation in both cell types (Figure 5C). The reduced TDG protein levels detected in the extracts of 5-FU treated wildtype MEFs (Figure 5A) reflected the accumulation of the cells in S-phase, where TDG is not expressed [32]. Finally, stable transfection of a TDG expressing plasmid restored 5-FU inducible Chk1 phosphorylation in the Tdg knockout cells (Figure 5B).

To address the dynamics of Chk1 activation, we monitored S345 phosphorylation during a 24 hour treatment with 10 μM 5-FU and an additional recovery time of 24 hours in the absence of 5-FU. Weak Chk1 phosphorylation became detectable after 16 hours of treatment both in *Tdg* wildtype and knockout MEFs. This initial signal persisted throughout a treatment period of 24 hours (Figure 5C), but declined

gradually during the subsequent recovery period. Strikingly, however, in TDG proficient cells, Chk1 phosphorylation reappeared at 40 hours into the time course, which is 16 hours after removal of the drug (Figure 5C). Thus, 5-FU elicits an early checkpoint response that is independent of TDG and a late response that depends on TDG.

Another readout of ATM or ATR dependent DNA damage responses is the formation of nuclear foci containing a phosphorylated variant of histone H2AX [40]. γH2AX is considered a marker of DNA damage, including DNA double strand-breaks that may occur during DNA replication when moving forks encounter damage in the parental strands. We thus measured changes in the steady state levels of γH2AX foci in TDG proficient and deficient MEF populations upon treatment with 5 μM 5-FU for 24 hours and additional recovery for 24 hours in drug-free medium. Although both mock treated cell lines showed similar levels of γH2AX foci, the wildtype MEFs accumulated significantly higher numbers of γH2AX foci than the TDG deficient cells during 5-FU treatment (Figure 5D). This corroborates that 5-FU treatment induces DNA strand-breaks and consequently DNA damage signaling in a TDG dependent manner.

Discussion

Despite many years of clinical application, the mode of action underlying the therapeutic efficacy of the antimetabolite 5-FU has remained elusive. Circumstantial evidence, however, has suggested that a significant part of its cancer directed cytotoxicity is mediated through the excision of misincrorporated uracil or 5-FU from genomic DNA, saturating the cellular SSB repair capacity [2]. Such a scenario clearly implicates a critical role for UDGs in mediating the cytotoxicity. However, Smug1 was reported to protect cells from the cytotoxic effects of 5-FU, and the status of UNG2, the catalytically most efficient UDG of all, does not seem to affect cellular sensitivity at all [9,13,14]. MBD4 deficient cells were shown to have a survival benefit on 5-FU [19], but this may not be linked to its DNA glycosylase activity since immunodepletion of the enzyme did not alter the 5-FU repair capacity of nuclear extracts [23]. Thus, whether or not and to what extent UDG activities are responsible for the DNA directed 5-FU toxicity remained unclear.

Our data now establish a significant contribution of TDG to 5-FU cytotoxicity. We show that inactivation of TDG in MEFs but also in ES cells results in a marked cellular hyperresistance towards 5-FU, which can be complemented by expression of wildtype *Tdg*. This phenotype is specific to 5-FU as the TDG deficient MEFs showed no hyperresistance when treated with MMS. Recently, An et al. [9] demonstrated the accumulation of appreciable amounts of FdUMP in genomic DNA following 5-FU treatment of cells, and presented genetic data consistent with 5-FU rather than uracil in DNA being the toxic lesion. Our data show that nuclear extracts from TDG deficient cells excise 5-FU from A•5-FU base pairs with significantly reduced efficiency when compared to wildtype extracts. Although this difference is detectable only upon inhibition of the highly active UNG2 by the UGI peptide, it nevertheless implicates a

rate limiting contribution of TDG to the excision of 5-FU in non S-phase cells, where UNG2 activity is down regulated [32,33,34]. In agreement with this, we found TDG deficient MEFs to accumulate significantly higher levels of 5-FU in their DNA than TDG proficient cells following 5-FU exposure. Hence, TDG processes 5-FU in genomic DNA and may thus contribute to the cytotoxicity of the drug. Given the inability of TDG to excise U from A•U base pair on the one hand [20,21], and the comparably high contribution of TDG to A•5-FU processing in nuclear extracts on the other hand, we argue that the primary TDG relevant cytotoxic DNA lesion is the A•5-FU base pair.

Consistent with a concept of DNA repair generating lethal DNA strand-breaks upon 5-FU treatment [2], our comet data show an increase of the tailmoment in 5-FU treated MEFs, and this effect is largely dependent on the presence of a catalytically active TDG. At the same time, we observed a significant increase of the number of XRCC1 foci per cell, suggesting that 5-FU treatment triggers DNA SSB repair [35]. Strikingly, after 5-FU treatment, *Tdg* knockout cells produced significantly higher levels of XRCC1 foci than their wildtype counterparts, suggesting that the loss of TDG enhances overall SSB repair activity while reducing lethal 5-FU processing.

Why then is the excision of 5-FU (or uracil) by TDG cytotoxic, whereas excision by other UDGs, particularly Smug1, protects against cell death [9]. The difference may relate to the distinct modes of action of these enzymes. Both, TDG and Smug1 bind AP-sites in DNA, albeit with different affinities. The dissociation of the glycosylases from these repair intermediates is therefore rate limiting for further processing [22,41]. However, whereas Smug1 can be made to turnover in the presence of APE1, the downstream acting endonuclease competing for the AP-site [41], efficient AP-site release (and stimulation by APE1) of TDG requires a SUMO modification induced conformational change that reduces its DNA binding affinity

[42,43]. Thus, base excision by Smug1 may connect to a straightforward downstream repair process, while base excision by TDG may be associated with delayed repair of the AP-site, possibly due to saturation of the SUMOylation system. Some AP-sites generated by TDG would thus escape repair until they eventually interfere with DNA replication, leading to fork stalling and collapse and activation of replication stress or DNA damage checkpoints [44]. Indeed, we and others found 5-FU treatment to affect the progression of cells through S-phase [38,45], and this effect was associated with activation of the Chk1 kinase that contributes to S and G2/M checkpoints [46]. Both, an accumulation of cells in S-phase and the activation Chk1 upon 5-FU exposure was virtually absent in TDG deficient MEFs, and was in line with reduced levels of 5-FU-induced DNA strand-breaks and γH2AX foci in these cells.

We reported previously that TDG is absent from S-phase cells due to programmed degradation by the proteasome system at the G1-S boundary [32]. This is consistent with the dynamics of Chk1 activation and cell death in our experiments, both indicating that the TDG dependent cytotoxic action is temporally separated from the incorporation of 5-FU (and U) into DNA. On the basis of these findings, we can now put forward a model for how temporally separated 5-FU/uracil misincorporation and repair processes can determine the cellular responses to 5-FU (Figure 6). Upon exposure to 5-FU, 5-FU/uracil will be misincrorporated into DNA during DNA replication in S-phase of the cell cycle. In this context, UNG2 will act efficiently on uracil (A•U and G•U) but less so on 5-FU [9], whereas Smug1 (and MBD4) may process the same lesions but with lower efficiencies. These repair events will activate the first wave of checkpoint response that is TDG independent. Due to saturation of uracil repair, considerable amounts of A•5-FU base pairs will persist in the DNA into the subsequent phases of the cell cycle, where UNG2 is down-regulated and they will be attacked mainly by TDG and Smug1. AP-sites generated by TDG will be protected

from repair due to rate limiting dissociation of the glycosylases and, hence, accumulate and interfere with the replication machinery in the subsequent S-phase. This will give rise to a second wave checkpoint activation (Chk1 phosphorylation, formation of γH2AX), this time TDG dependent, which is correlated with the occurrence of DNA stand-breaks, even if the cells are no longer cultivated in the presence of 5-FU.

Notably, according to a recent report, breast cancer patients carrying a specific polymorphism in XRCC1 have a significantly reduced risk of recurrence and show better long time survival following a combination therapy with cyclophosphamide-methotrexate-5-FU [47]. The same polymorphism was previously reported to reduce DNA repair activity of XRCC1 [47,48], suggesting that inactivation of DNA single strand-break repair can improve the efficacy 5-FU treatment. The data presented here for TDG and previously for Smug1 [9] is consistent with 5-FU excision being responsible for the generation of a significant fraction of AP-sites and DNA single strand-breaks following 5-FU treatment. It is now becoming clear that the efficiency of coupling downstream repair with base excision, presumably through XRCC1, depends on the biochemical properties of the DNA glycosylase engaged and critically determines the cellular responses to the drug. It will therefore be important to examine to what extent the status of TDG activity correlates with the response of tumors to 5-FU based chemotherapy.

Materials and methods

Reagents, antibodies and *Tdg* expression constructs

Chemicals and reagents were purchased from Sigma (Switzerland), Complete™ protease inhibitor from Roche (Switzerland), RNase from Qiagen (Switzerland) and UGI from New England Biolabs (USA). LIF was from Chemicon-Millipore (USA), sodium pyruvate from Invitrogen (USA) and all other supplements or cell culture media from Sigma (Switzerland). The polyclonal rabbit anti-mTDG antiserum was newly generated by immunization with recombinant full length mouse TDGa (Primm Labs, UK). Rabbit anti-Chk1 (#2345) and rabbit anti-Chk1-Ser345p (#2341) antibodies were from Cell Signaling (USA), the mouse anti-β-actin (ab8226) antibody was from Abcam (UK), the rabbit anti-XRCC1 (X0629) was from Sigma (Switzerland) and the mouse anti-γH2AX (#05-636) was from Chemicon-Millipore (USA). The secondary horse-radish-peroxidase conjugated antibodies against mouse (NXA931) or rabbit (NA934V) were purchased from GE Healthcare Life Sciences (Germany), the secondary Cy2 conjugated donkey anti-mouse IgG (715-225-151) and anti-rabbit IgG (711-225-152) antibodies and donkey serum (017-000-001) were from Jackson ImmunoResearch Laboratories (USA).

For bacterial expression of an N-terminally 6xHis tagged mouse TDG, the murine *TdgA* cDNA (GenBank: NM_172552) was cloned into pET28c (Novagen-Merck, Germany). Mammalian expression constructs were obtained by PCR cloning of the mouse *TdgA* sequence into pSG5-HH25 [43] or pTCO4 (unpublished results) for expression controlled by the SV40 or the authentic *Tdg* promoter, respectively. *In vitro* mutagenesis of mouse *Tdg* was performed using the QuikChange site-directed mutagenesis kit (Stratagene, USA). PCR primer sequences and vector maps are available on request.

Cell culturing

For immortalization of cell lines see Supplemental data. Immortal MEFs were cultivated in growth medium (DMEM, 10% FCS, 2 mM L-glutamine) containing penicillin/streptomycin (pen/strep) at 37°C with 5% CO_2. For complementation, *Tdg*$^{-/-}$ cell lines were transfected at 70% confluency with 1 µg of plasmid DNA and the Transfectin reagent (BioRad, USA). Puromycin-resistant cells were selected and further maintained in medium supplemented with 1.5 µg/ml puromycin. For protein extraction, comet assays or FACS analysis, 1 x 10^6 (mock) or 2 x 10^6 (Fu) cells were seeded into 10 cm culture dishes and incubated for 24 h. Cells were treated with indicated 5-FU concentrations for 24 h and washed with PBS. After additional incubation for 24 h in drug-free medium, cells were harvested by trypsinization. Mouse embryonic stem cells (ES) with a homozygous disruption of the *Tdg* gene were selected with increasing concentrations of neomycin from ES cells heterozygous for *Tdg*. ES cells were passaged in ES medium (DMEM, 15% heat-inactived FCS, 2 mM L-glutamine, 0.1 mM β-mercaptoethanol, 1 mM sodium pyruvate, 1x non-essential amino acids, 1x pen/strep, 1'000 U/ml LIF) in the presence of γ-ray inactivated feeder cells, which were removed prior to sensitivity assays.

Protein extraction and western blotting

Cells were washed with ice-cold PBS and lysed for 30 min on ice in lysis buffer (50 mM Na-phosphate pH 8.0, 125 mM NaCl, 1% NP-40, 0.5 mM EDTA, 1 mM PMSF, 1 mM DTT, 1x Complete™ protease inhibitors, 2x phosphatase inhibitor cocktail 1 and 2). Extracts were clarified by centrifugation (15 min, 20'000g, 4°C). Protein concentrations were determined using the Bradford reagent (BioRad, USA). 50 µg of soluble protein was separated in 10% SDS-polyacrylamide gels and

transferred to a nitrocellulose membrane (Millipore, USA). Membranes were washed once with TBS-T (100 mM Tris/HCl pH 8.0, 150 mM NaCl, 0.1% Tween20) and incubated with blocking buffer (TBS-T, 5% dry milk) for 1 h at room temperature (RT). Blocked membranes were washed once with TBS-T for 5 min before incubation with the primary antibody for 1 h at 33°C (anti-mTDG) or RT (anti-β-actin) in blocking buffer or overnight at 4°C in TBS-T containing 5% BSA (anti-Chk1, anti-Chk1-Ser345p). Dilutions were: 1:10'000 for the rabbit anti-mTDG antibody and the mouse anti-β-actin, 1:1'000 for the rabbit anti-Chk1 and the rabbit anti-Chk1-Ser345p. The washing steps after hybridization were: once at 33°C and twice at RT for 15 min (anti-mTDG), three times at RT for 10 min (anti-β-actin) and three times for 5 min at RT (anti-Chk1, anti-Chk1-Ser345p). Both secondary horse-radish-peroxidase conjugated antibodies were diluted 1:5'000 in blocking buffer and hybridized to the membranes for 1 h at RT. After three washing steps of 10 min at RT, detection of the signals was carried out using the Immobilon Western Chemiluminescent HRP Substrate (Millipore, USA).

Cell sensitivity assays

Cell viability was measured by the Cell Counting Kit-8 (Dojindo, Japan). Triplicate cultures of each cell line were plated in 96-well plates at 1 x 10^3 cells per well and pre-incubated in the respective growth medium. 5-FU or MMS was added to final concentrations as indicated. Cells were exposed for 48 h to 5-FU (1 h to MMS and additional 47 hours in normal growth medium), washed with PBS before incubation in medium containing the WST-8 substrate at 37°C. After incubation for 2 h (MEF) or 4 h (ES) the cell density was measured indirectly by quantification of the solubilized formazan product at 450 nm with a SpectraMax340 microplate spectrophotometer (Molecular Devices, USA).

Purification of recombinant mTDGa

For expression of mTDGa, 2 L of Superbroth containing 50 µg/ml kanamycin were inoculated with an overnight culture of E. coli BL21(DE3) transformed with pET-28c-m*TdgA*. The culture was grown to an A_{600} of 0.6 and cooled to 15°C. TDG expression was induced by the addition of 200 µM IPTG and incubation was allowed to proceed at 15°C for 23 h. Cells were collected by centrifugation (Sorvall SLC-6000, 5000 rpm, 4°C, 30 min), and the pellets were resuspended in 3 ml/g sonication buffer (50 mM Na-phosphate pH 8.0, 750 mM NaCl, 20% glycerol, 1 mM imidazole, 10 mM β-mercaptoethanol, 1 mM phenylmethylsulfonyl fluoride). After shock freezing in liquid nitrogen cells were stored at -80°C. Crude extracts were prepared by sonication (12 times for 30s on ice with intermittent chilling), and clarified by centrifugation (Sorvall SS34, 18'000 rpm, 4°C). All steps were performed at 4°C. The supernatant was applied to a disposable column packed with 1.5 ml preequilibrated Ni-NTA agarose (Qiagen) at a flow rate of 15 ml/h. After washing with 120 ml sonication buffer, bound proteins were eluted with 10 ml sonication buffer containing 500 mM imidazole and dialyzed against buffer H50 (50 mM Na-phosphate pH 8.0, 50 mM NaCl, 20% glycerol, 10 mM β-mercaptoethanol, 1 mM phenylmethylsulfonyl fluoride). After loading the dialyzed fraction onto a 5 ml HiTrap Heparin HP column (GE Healthcare, Germany) at a flow rate of 1 ml/min and washing with 10 ml H50, bound protein was eluted with a liner gradient of 50-800 mM NaCl in 50 ml. Purest fractions were pooled, dialysed against buffer Q20 (50 mM Na-phosphate pH 8.5, 20 mM NaCl, 10% glycerol, 10 mM β-mercaptoethanol, 1 mM phenylmethylsulfonyl fluoride), and loaded on a 1 ml HiTrap Q HP at a flow rate of 1 ml/min. After washing with 10 ml Q20 buffer, bound proteins were eluted with a linear gradient of 20-500 mM NaCl in 15 ml. The fractions containing TDG with >98% homogeneity were

pooled, dialyzed against storage buffer (50 mM Na-phosphate pH 8.0, 50 mM NaCl, 10% glycerol, 10 mM β-mercaptoethanol, 1 mM phenylmethylsulfonyl fluoride), frozen in liquid nitrogen and stored at -80°C.

Base release assays

Nuclear protein extracts were prepared according to [32]. For base release assays 20 µg of nuclear proteins were incubated with 1 pmol of a fluorescein labeled homoduplex or mismatched DNA substrate (2) in reaction buffer (50 mM Tris-HCl pH 8.0, 1 mM EDTA, 1 mM DTT, 1mg/ml BSA, 2 U UGI) for 20 h at 37°C. Generated AP-sites were cleaved by the addition of NaOH to a final concentration of 100 mM and heating to 95°C for 10 min. Subsequently, DNA was ethanol precipitated overnight at -20°C in 0.3 M Na-acetate pH 5.2 and in the presence of 0.4 mg/ml carrier tRNA. The DNA was collected by centrifugation (20 min, 20'000g, 4°C) and washed in 80% ethanol. Air-dried pellets were resuspended in loading buffer (1x TBE, 90% formamide), heated at 95°C for 5 min and immediately chilled on ice. Reaction products were separated on 15% denaturing polyacrylamide gels in 1x TBE. The fluorescein-labeled DNA was visualized with a Typhoon 9400 (GE Healthcare, Germany) and quantified using the ImageQuant TL software (GE Healthcare, Germany).

Alkaline comet assays

Comet assays were performed according to [49] with minor modifications described by [50]. After treatment, cells were trypsinized, collected by centrifugation (5 min, 450g, RT) and washed with PBS. 10'000 cells were resuspended in 100 µl low-melting-point agarose (PBS, 0.5% LMPA; Lonza, Switzerland) at 37°C, and casted onto microscope slides precoated with 1.5% normal melting agarose (BioRad,

USA). After gelling, cells were lysed by immersion of the slides in freshly prepared ice-cold lysis buffer (2.5 M NaCl, 100 mM EDTA, 10 mM Tris/HCl pH 10, 1% TritonX-100, 10% DMSO) for 90 min at 4°C. Slides were then washed with ddH_2O and covered with fresh electrophoresis buffer in an electrophoresis tank (1 mM EDTA, 300 mM NaOH, pH>13). After DNA unwinding for 30 min at 4°C, electrophoresis was performed at 25 V and 300 mA for 20 minutes. All above steps were done under dimmed light. Neutralization was carried out by three washings of 10 minutes with 0.4 M Tris/HCl pH 7.5 at RT. After two fixation steps of 5 minutes in 100% EtOH at RT, slides were air-dried and stained with 50 µl PI solution (Vectashield, 2.5 µg/ml propidium iodide). Comet tail moments of 100 to 150 cells per slide were analysed by automated analysis [51] using a Leitz MIAS image analyzer (Leitz Messtechnik, Germany) together with a Leica DM RBE microscope (Leica Microsystems, Germany).

FACS analysis

5×10^5 to 5×10^6 cells were fixed overnight in 5 ml 70% ethanol at 4°C, collected by centrifugation (5 min, 800g, 4°C) and resuspended in 0.3 ml RNase solution (100 mM Tris/HCl pH 7.5, 100 mM NaCl, RNase 0.5mg/ml,). RNA digestion was performed at 37°C for 45 min. 0.3 ml of PE-solution (0.4% HCl, pepsin 1mg/ml) were added to the samples during the last 15 min of incubation. The DNA was stained by the addition of 0.6 ml PI solution (PBS, 50µg/ml propidium iodide) on ice for 30 min. Samples were analyzed by flow cytometry with a FACS Canto II cytometer (Beckton Dickinson, USA). Cell cycle distribution was analyzed using the FlowJo software (TreeStar, USA).

Immunofluorescence

MEFs were cultivated on cover slips for 24h. Cells were then treated with 5 µM 5-FU for 24 h followed by cultivation in drug free medium for another 24 h. Cover slips were then washed twice in PBS and the cells fixed for 15 min with PF-buffer (PBS, 2% paraformaldehyde) at RT, washed 4 time 10 min in PBS at RT, and permeabilized in ice cold P-buffer (PBS, 0.2% TritonX100) for 5 min. Coverslips were incubated for another 5 min in ice-cold P-buffer containing 0.2% $NaBH_4$. After blocking twice in H-buffer for 10 min (PBS, 1% BSA) and once in D-buffer for 10 min (PBS, 1:20 donkey serum), samples were hybridized with the anti-XRCC1 (1:100 dilution in H-buffer) or the anti-γH2AX (1:500 dilution in H-buffer) antibody for 1 h at RT. Following four washes of 10 min in H-buffer the samples were hybridized with the respective Cy2 conjugated secondary antibody at a dilution of 1:500 (XRCC1) or 1:200 (γH2AX) in H-buffer for 1 h at RT. After four washes of 10 min in PBS, the cover slips were dried and embedded in Mowiol (Calbiochem, Germany). XRCC1 or γH2AX signals were visualized on an Axiovert 200M microscope (Zeiss, Germany) using a FITC filter (exitation 492 nm, emission 520 nm).

Statistical analysis

Statistical analyses were done using the Prism 5 software (GraphPad Software, Inc., USA). Comet tail moments data were analyzed according to P. Duez et al., 2003 by two-way ANOVA of medians and 75% percentiles obtained from 3 independent experiments, followed by the Bonferroni post test. XRCC1 and γH2AX foci distributions were tested for normality by the Shapiro-Wilk test and further evaluated by one-way ANOVA using the non-parametric Kruskal-Wallis test followed by the Dunn’s multiple comparison analysis comparing treated with untreated samples. Analysis of cell cycle data was done by the Fisher's exact test from contingency tables comparing the distributions of G1-, S- and G2-cells.

References

1. Heidelberger C, Chaudhuri NK, Danneberg P, Mooren D, Griesbach L, et al. (1957) Fluorinated pyrimidines, a new class of tumour-inhibitory compounds. Nature 179: 663-666.

2. Longley DB, Harkin DP, Johnston PG (2003) 5-fluorouracil: mechanisms of action and clinical strategies. Nat Rev Cancer 3: 330-338.

3. Copur S, Aiba K, Drake JC, Allegra CJ, Chu E (1995) Thymidylate synthase gene amplification in human colon cancer cell lines resistant to 5-fluorouracil. Biochem Pharmacol 49: 1419-1426.

4. Johnston PG, Drake JC, Trepel J, Allegra CJ (1992) Immunological quantitation of thymidylate synthase using the monoclonal antibody TS 106 in 5-fluorouracil-sensitive and -resistant human cancer cell lines. Cancer Res 52: 4306-4312.

5. Peters GJ, Backus HH, Freemantle S, van Triest B, Codacci-Pisanelli G, et al. (2002) Induction of thymidylate synthase as a 5-fluorouracil resistance mechanism. Biochim Biophys Acta 1587: 194-205.

6. Santi DV, McHenry CS, Sommer H (1974) Mechanism of interaction of thymidylate synthetase with 5-fluorodeoxyuridylate. Biochemistry 13: 471-481.

7. Sommer H, Santi DV (1974) Purification and amino acid analysis of an active site peptide from thymidylate synthetase containing covalently bound 5-fluoro-2'-deoxyuridylate and methylenetetrahydrofolate. Biochem Biophys Res Commun 57: 689-695.

8. Ingraham HA, Tseng BY, Goulian M (1982) Nucleotide levels and incorporation of 5-fluorouracil and uracil into DNA of cells treated with 5-fluorodeoxyuridine. Mol Pharmacol 21: 211-216.

9. An Q, Robins P, Lindahl T, Barnes DE (2007) 5-Fluorouracil incorporated into DNA is excised by the Smug1 DNA glycosylase to reduce drug cytotoxicity. Cancer Res 67: 940-945.

10. van der Wilt CL, Smid K, Aherne GW, Noordhuis P, Peters GJ (1997) Biochemical mechanisms of interferon modulation of 5-fluorouracil activity in colon cancer cells. Eur J Cancer 33: 471-478.

11. Peters GJ, van Triest B, Backus HH, Kuiper CM, van der Wilt CL, et al. (2000) Molecular downstream events and induction of thymidylate synthase in mutant and wild-type p53 colon cancer cell lines after treatment with 5-fluorouracil and the thymidylate synthase inhibitor raltitrexed. Eur J Cancer 36: 916-924.

12. Nilsen H, Rosewell I, Robins P, Skjelbred CF, Andersen S, et al. (2000) Uracil-DNA glycosylase (UNG)-deficient mice reveal a primary role of the enzyme during DNA replication. Mol Cell 5: 1059-1065.

13. Welsh SJ, Hobbs S, Aherne GW (2003) Expression of uracil DNA glycosylase (UDG) does not affect cellular sensitivity to thymidylate synthase (TS) inhibition. European Journal of Cancer 39: 378-387.

14. Andersen S, Heine T, Sneve R, Konig I, Krokan HE, et al. (2005) Incorporation of dUMP into DNA is a major source of spontaneous DNA damage, while excision of uracil is not required for cytotoxicity of fluoropyrimidines in mouse embryonic fibroblasts. Carcinogenesis 26: 547-555.

15. Kavli B, Sundheim O, Akbari M, Otterlei M, Nilsen H, et al. (2002) hUNG2 Is the Major Repair Enzyme for Removal of Uracil from U:A Matches, U:G Mismatches, and U in Single-stranded DNA, with hSMUG1 as a Broad Specificity Backup. J Biol Chem 277: 39926-39936.

16. Cortazar D, Kunz C, Saito Y, Steinacher R, Schar P (2007) The enigmatic thymine DNA glycosylase. DNA Repair (Amst) 6: 489-504.

17. Petronzelli F, Riccio A, Markham GD, Seeholzer SH, Stoerker J, et al. (2000) Biphasic kinetics of the human DNA repair protein MED1 (MBD4), a mismatch-specific DNA N-glycosylase. J Biol Chem 275: 32422-32429.

18. Turner DP, Cortellino S, Schupp JE, Caretti E, Loh T, et al. (2006) The DNA N-glycosylase MED1 exhibits preference for halogenated pyrimidines and is involved in the cytotoxicity of 5-iododeoxyuridine. Cancer Res 66: 7686-7693.

19. Cortellino S, Turner D, Masciullo V, Schepis F, Albino D, et al. (2003) The base excision repair enzyme MED1 mediates DNA damage response to antitumor drugs and is associated with mismatch repair system integrity. Proc Natl Acad Sci U S A 100: 15071-15076.

20. Neddermann P, Jiricny J (1993) The purification of a mismatch-specific thymine-DNA glycosylase from HeLa cells. J Biol Chem 268: 21218-21224.

21. Hardeland U, Bentele M, Jiricny J, Schar P (2003) The versatile thymine DNA-glycosylase: a comparative characterization of the human, Drosophila and fission yeast orthologs. Nucleic Acids Res 31: 2261-2271.

22. Hardeland U, Bentele M, Jiricny J, Schar P (2000) Separating substrate recognition from base hydrolysis in human thymine DNA glycosylase by mutational analysis. J Biol Chem 275: 33449-33456.

23. Fischer F, Baerenfaller K, Jiricny J (2007) 5-Fluorouracil is efficiently removed from DNA by the base excision and mismatch repair systems. Gastroenterology 133: 1858-1868.

24. Meyers M, Wagner MW, Mazurek A, Schmutte C, Fishel R, et al. (2005) DNA mismatch repair-dependent response to fluoropyrimidine-generated damage. J Biol Chem 280: 5516-5526.

25. Meyers M, Wagner MW, Hwang HS, Kinsella TJ, Boothman DA (2001) Role of the hMLH1 DNA mismatch repair protein in fluoropyrimidine-mediated cell death and cell cycle responses. Cancer Res 61: 5193-5201.

26. Carethers JM, Chauhan DP, Fink D, Nebel S, Bresalier RS, et al. (1999) Mismatch repair proficiency and in vitro response to 5-fluorouracil. Gastroenterology 117: 123-131.

27. Aebi S, Fink D, Gordon R, Kim HK, Zheng H, et al. (1997) Resistance to cytotoxic drugs in DNA mismatch repair-deficient cells. Clin Cancer Res 3: 1763-1767.

28. Ozer HL, Banga SS, Dasgupta T, Houghton J, Hubbard K, et al. (1996) SV40-mediated immortalization of human fibroblasts. Exp Gerontol 31: 303-310.

29. Chang F, Syrjanen S, Kurvinen K, Syrjanen K (1993) The p53 tumor suppressor gene as a common cellular target in human carcinogenesis. Am J Gastroenterol 88: 174-186.

30. Bellacosa A (2001) Role of MED1 (MBD4) Gene in DNA repair and human cancer. J Cell Physiol 187: 137-144.

31. Hendrich B, Hardeland U, Ng HH, Jiricny J, Bird A (1999) The thymine glycosylase MBD4 can bind to the product of deamination at methylated CpG sites. Nature 401: 301-304.

32. Hardeland U, Kunz C, Focke F, Szadkowski M, Schar P (2007) Cell cycle regulation as a mechanism for functional separation of the apparently redundant uracil DNA glycosylases TDG and UNG2. Nucleic Acids Res 35: 3859-3867.

33. Haug T, Skorpen F, Aas PA, Malm V, Skjelbred C, et al. (1998) Regulation of expression of nuclear and mitochondrial forms of human uracil-DNA glycosylase. Nucleic Acids Res 26: 1449-1457.

34. Fischer JA, Muller-Weeks S, Caradonna S (2004) Proteolytic degradation of the nuclear isoform of uracil-DNA glycosylase occurs during the S phase of the cell cycle. DNA Repair (Amst) 3: 505-513.

35. Caldecott KW (2003) XRCC1 and DNA strand break repair. DNA Repair (Amst) 2: 955-969.

36. El-Khamisy SF, Masutani M, Suzuki H, Caldecott KW (2003) A requirement for PARP-1 for the assembly or stability of XRCC1 nuclear foci at sites of oxidative DNA damage. Nucleic Acids Res 31: 5526-5533.

37. Robinson HM, Jones R, Walker M, Zachos G, Brown R, et al. (2006) Chk1-dependent slowing of S-phase progression protects DT40 B-lymphoma cells

against killing by the nucleoside analogue 5-fluorouracil. Oncogene 25: 5359-5369.

38. Xiao Z, Xue J, Sowin TJ, Rosenberg SH, Zhang H (2005) A novel mechanism of checkpoint abrogation conferred by Chk1 downregulation. Oncogene 24: 1403-1411.

39. Zhao H, Piwnica-Worms H (2001) ATR-Mediated Checkpoint Pathways Regulate Phosphorylation and Activation of Human Chk1. Mol Cell Biol 21: 4129-4139.

40. Fernandez-Capetillo O, Lee A, Nussenzweig M, Nussenzweig A (2004) H2AX: the histone guardian of the genome. DNA Repair (Amst) 3: 959-967.

41. Pettersen HS, Sundheim O, Gilljam KM, Slupphaug G, Krokan HE, et al. (2007) Uracil-DNA glycosylases SMUG1 and UNG2 coordinate the initial steps of base excision repair by distinct mechanisms. Nucl Acids Res 35: 3879-3892.

42. Steinacher R, Schär P (2005) Functionality of human thymine DNA glycosylase requires SUMO-regulated changes in protein conformation. Curr Biol 15: 616-623.

43. Hardeland U, Steinacher R, Jiricny J, Schar P (2002) Modification of the human thymine-DNA glycosylase by ubiquitin-like proteins facilitates enzymatic turnover. Embo J 21: 1456-1464.

44. Nyberg KA, Michelson RJ, Putnam CW, Weinert TA (2002) Toward maintaining the genome: DNA damage and replication checkpoints. Annu Rev Genet 36: 617-656.

45. Xiao Z, Xue J, Semizarov D, Sowin TJ, Rosenberg SH, et al. (2005) Novel indication for cancer therapy: Chk1 inhibition sensitizes tumor cells to antimitotics. Int J Cancer 115: 528-538.

46. Chen Y, Sanchez Y (2004) Chk1 in the DNA damage response: conserved roles from yeasts to mammals. DNA Repair (Amst) 3: 1025-1032.

47. Jaremko M, Justenhoven C, Schroth W, Abraham BK, Fritz P, et al. (2007) Polymorphism of the DNA repair enzyme XRCC1 is associated with treatment prediction in anthracycline and cyclophosphamide/methotrexate/5-fluorouracil-based chemotherapy of patients with primary invasive breast cancer. Pharmacogenet Genomics 17: 529-538.

48. Lunn RM, Langlois RG, Hsieh LL, Thompson CL, Bell DA (1999) XRCC1 polymorphisms: effects on aflatoxin B1-DNA adducts and glycophorin A variant frequency. Cancer Res 59: 2557-2561.

49. Ostling O, Johanson KJ (1984) Microelectrophoretic study of radiation-induced DNA damages in individual mammalian cells. Biochem Biophys Res Commun 123: 291-298.

50. Singh NP, Tice RR, Stephens RE, Schneider EL (1991) A microgel electrophoresis technique for the direct quantitation of DNA damage and repair in individual fibroblasts cultured on microscope slides. Mutat Res 252: 289-296.

51. Frieauff W, Hartmann A, Suter W (2001) Automatic analysis of slides processed in the Comet assay. Mutagenesis 16: 133-137.

Acknowledgements

We are grateful to Deborah Barnes and Tomas Lindahl for measuring 5-FU and uracil levels in our cell lines, Josef Jiricny and Franziska Fischer for helpful discussions and communication of unpublished data. We thank the laboratory of toxicology and pathology at Novartis Pharma AG for providing access to the automated Comet analysis.

Funding

This study was funded by a grant from the Swiss Cancer League.

Figure legends

Figure 1. TDG deficient mouse cells are hyperresistant to 5-FU. (A) Western blot analysis of whole cell protein extracts derived from SV40 immortalized mouse embryonic fibroblast lines (MEFs, left panel), spontaneously immortalized MEFs (middle panel), and embryonic stem cell lines (right panel) used. *Tdg* genotypes were as indicated. A highly specific polyclonal anti-mouse TDG antibody (TDG_{ab}) was used to detect TDG and beta-actin staining served as loading control ($\beta\text{-}act_{ab}$). TDG is undetectable in extracts from $Tdg^{-/-}$ cells and levels are reduced in heterozygous MEFs. Stable transfection of a *Tdg* expression construct (p*Tdg*) restores TDG levels in knockout MEFs. (B) TDG deficient MEF and ES cells exhibit increased 5-FU resistance, and ectopic expression of wildtype *Tdg* in knockout MEFs restores 5-FU sensitivity. The sensitivity to increasing amounts of 5-FU was measured for the different cell lines after a continuous treatment of 48 hours. Shown are survival curves as percentages of mock-treated cells. (C) TDG deficient MEFs are not generally hyper-resistant to induced DNA base damage. Sensitivity to MMS was measured after a treatment for one hour with increasing concentrations of MMS. Shown are survival curves as percentages of mock-treated cells. Data are presented as means ± SEM from at least three independent experiments. pC, vector control; p*Tdg*, *Tdg* expressing vector.

Figure 2. Involvement of TDG in processing of uracil and 5-FU. (A) Base release activities of purified recombinant mouse TDG (mTDG) and nuclear protein extracts of TDG wildtype ($Tdg^{+/+}$), heterozygous ($Tdg^{+/-}$) and knockout ($Tdg^{-/-}$) MEFs on uracil, 5-FU and G•T containing synthetic 60-mer DNA duplexes. Shown are representative results of base release assays with the intact substrate DNA strands (S) and the

cleaved products (P) resolved on denaturing polyacrylamid gels. All reactions were performed in the presence of the UNG inhibitory UGI peptide. Purified TDG processes thymine, uracil and 5-FU when opposite guanine as well as 5-FU paired with adenine, but only inefficiently uracil opposite adenine. (B) Quantitation of base release activities in nuclear extracts. G•T processing activity is reduced in protein extracts of heterozygous cells and absent form knockout extracts. *Tdg* knockout extracts also show a significant reduction of A•5-FU processing. All other uracil and 5-FU containing substrates were processed with similar efficiencies by all three nuclear extracts. Data are presented as means ± SD from three independent experiments. *, 5'-Fluorescein-labelled strand.

Figure 3. 5-FU induced DNA strand-breaks are reduced in TDG deficient cells while overall repair activity is increased.

(A) Complementation of *Tdg* knockout MEFs with wildtype and catalytically deficient TDG. Stable transfectants of $Tdg^{-/-}$ MEFs ectopically expressing either TDG variant from the native promoter show about endogenous TDG levels as detected by Western blotting. (B) Reduced levels of 5-FU induced DNA strand-break in cells lacking active TDG. Steady-state levels of DNA single and double strand-breaks in the cell lines indicated were assessed by the alkaline comet assay using automated comet tail moment analysis. 5-FU treatment resulted in a significant tail moment increase in wildtype but not in *Tdg* knockout MEFs. The generation of 5-FU specific DNA strand breaks in *Tdg* knockout cells was restored by complementation with wildtype *Tdg* but not with the catalytically inactive mutant. Shown are boxplots with individual moments per cell, medians, interquartile ranges (boxes), 2.5 – 97.5 % percentiles (whiskers) and outliers (dots) of pooled data (600 to 900 cells) obtained from three independent experiments. (C) 5-FU treatment triggers DNA single-strand

break repair in TDG wildtype and knockout cells. The top panel shows nuclei of *Tdg* proficient and deficient cells stained with a polyclonal anti-XRCC1 antibody ($XRCC1_{ab}$) after 5-FU treatment. The statistical analysis of XRCC1 foci per cell across the populations analyzed (n ≥ 100 cells per population) is shown as scatter plot with medians and the interquartile ranges. pC, empty vector; p*Tdg*, vector expressing TDG; pTdg_{cat}, vector expressing a catalytic variant of TDG.

Figure 4. 5-FU treatment induces a TDG dependent S-phase delay. The histograms show the effect of the 5-FU treatment on the relative cell cycle distribution (% cells) of TDG proficient and deficient MEFs (A), and of TDG knockout cell lines stably transfected with a plasmid expressing *Tdg* from its authentic promoter (B). 5-FU treatment of TDG proficient cells results in a significant accumulation cells in S-phase at the expense of G1 cells, whereas TDG deficient cells show only insignificant changes in cell cycle distribution. Expression of wildtype *Tdg* in knockout MEFs partially restored the 5-FU dependent S-phase delay. The data shown represent averages of three independent experiments with fold changes upon 5-FU treatment. pC, empty vector; p*Tdg*, vector expressing TDG.

Figure 5. TDG dependent activation of DNA damage responses upon 5-FU treatment. (A-C) TDG mediates late Chk1 activation following 5-FU treatment. Activation of Chk1 in TDG proficient and deficient MEFs (A) as well as in complemented knockout cells (B) was determined by Western blotting with an S345 phospho-specific antibody against Chk1 (Chk1-P_{ab}). After treatment with 10 µM 5-FU, wildtype but not TDG deficient MEFs show a strong accumulation of S345 phosphorylated Chk1. Total Chk1 protein is the same in both MEF lines before and after 5-FU treatment ($Chk1_{ab}$). TDG levels in wildtype cells, detected with a specific

anti-mTDG antibody (TDG_{ab}), are reduced in 5-FU exposed cells, reflecting an accumulation of cells in S-phase where TDG is absent. *Tdg* knockout MEFs stably expressing an ectopic copy of *Tdg* (B) contain low levels of TDG, which is sufficient to induce Chk1 activation upon 5-FU treatment. (C) Dynamics of Chk1 activation in TDG proficient and deficient MEFs during and after exposure to 5-FU or hydroxyurea (HU). The drug containing medium was exchanged after treatment with 10 μM 5-FU or 2.5 mM HU for 24 or 16 hours, respectively. Samples were taken at the timepoints indicated and analyzed for Chk1 S345 phoshorylation by Western blotting. After 16 hours into treatment, activated Chk1 appears equally in extracts from 5-FU and HU treated cells; at 24 hours, the Chk1-p signal is undetectable in the HU treated samples and significantly reduced in 5-FU treated cells; at 40 hours, significant levels of phosphorylated Chk1 reappear in 5-FU exposed TDG proficient MEFs but not in TDG deficient MEFs. (D) The induction of γH2AX foci by 5-FU treatment is significantly reduced in TDG deficient MEFs. The top panels show examples of MEFs immuno-stained with a monoclonal antibody against γH2AX ($\gamma H2AX_{mab}$) after treatment with 5 μM 5-FU. The statistical analysis of γH2AX foci per cell across the populations analyzed (n > 95 cells per population) is depicted in the lower panel as scatter plot with medians and the interquartile ranges. pC, empty vector; p*Tdg*, vector expressing TDG; TDG-S, TDG modified with SUMO; *, unspecific cross-reaction of the secondary antibody

Figure 6. TDG dependent 5-FU cytotoxicity. Illustrated are the cell cycle distribution of the three relevant UDGs, TDG, UNG2 and Smug1 (top), together with expected levels of genomic 5-FU, uracil, AP-sites and the observed Chk1 activation following 5-FU treatment (bottom). TDG is present during the G2/M and G1 phases but is degraded prior to and absent from S-phase. UNG2 shows a strictly inverse

regulation whereas Smug1 is expressed throughout the entire cell cycle. Treatment with 5-FU for 24 hours gives rise to misincorporation of appreciable levels of 5-FU and uracil during S-phase (S1), resulting in Chk1 activation by ongoing replication associated UNG2 and Smug1-dependent BER. Although Smug1 and UNG2 will initiate faithful repair of uracil and 5-FU bases directly after DNA synthesis, these pathways will become saturated under 5-FU exposure and, in addition, are relatively inefficient in processing the 5-FU•A base pairs. Hence, some of them will persist in the DNA into the subsequent G2 and G1 phases of the cell cycle. There TDG will initiate repair but turnover with a low rate, leading to an accumulation of AP-sites and/or DNA single strand-breaks. During the subsequent S-phase, these repair intermediates will interfere with DNA replication, causing replication fork stalling, fork collapse, DNA double strand breaks and a second round of Chk1 activation. Due to genome fragmentation cells will then induce apoptosis.

Figure 1 Kunz *et al.*

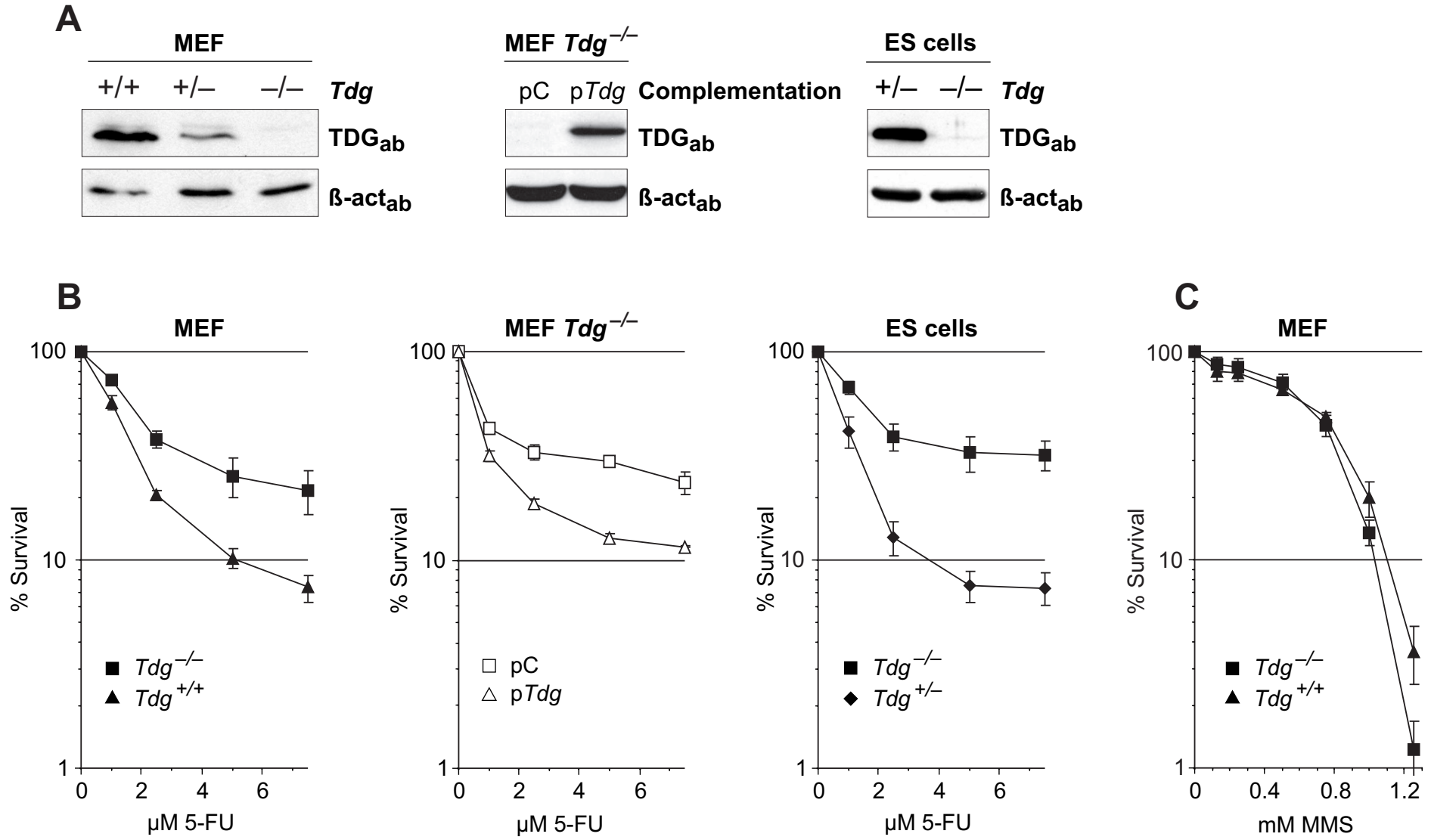

Figure 2 Kunz *et al.*

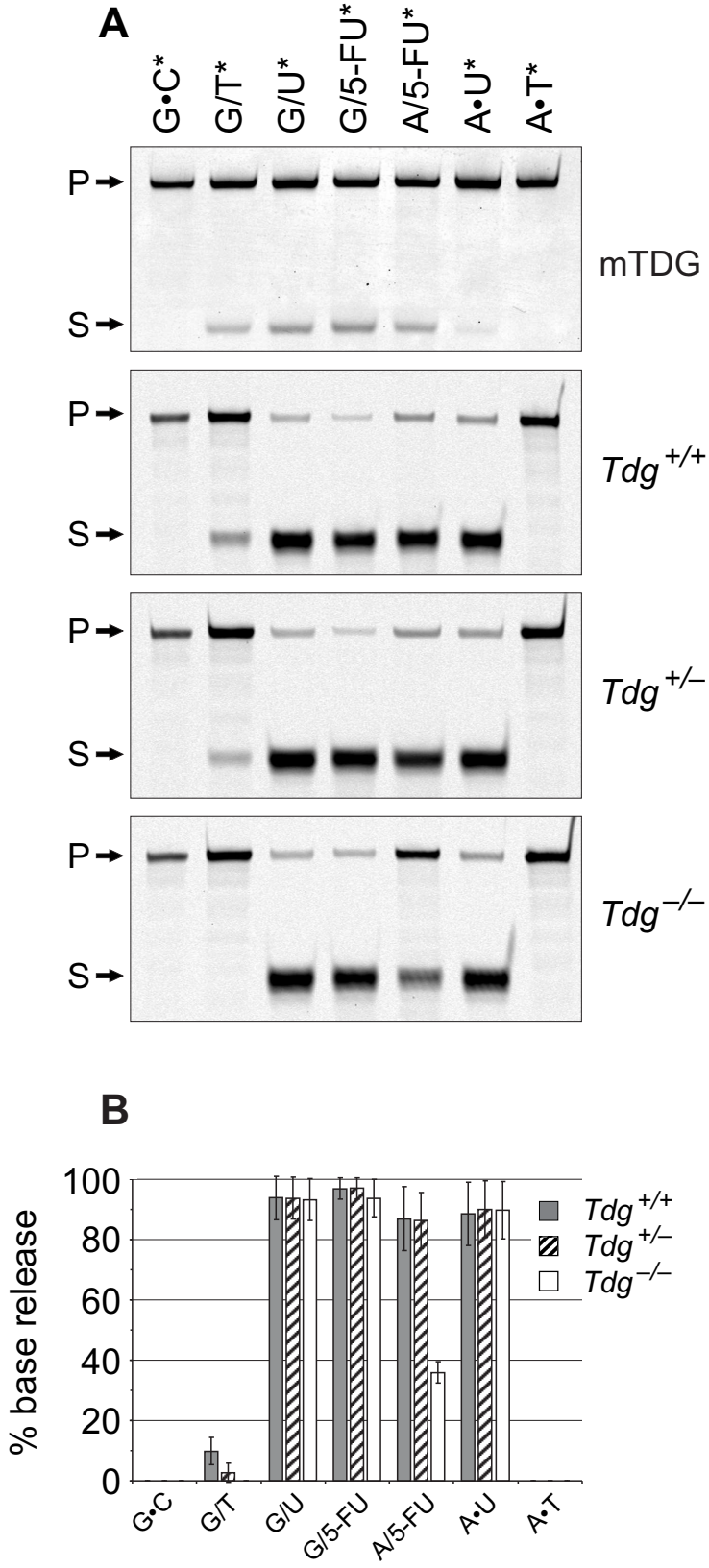

Figure 3 Kunz *et al.*

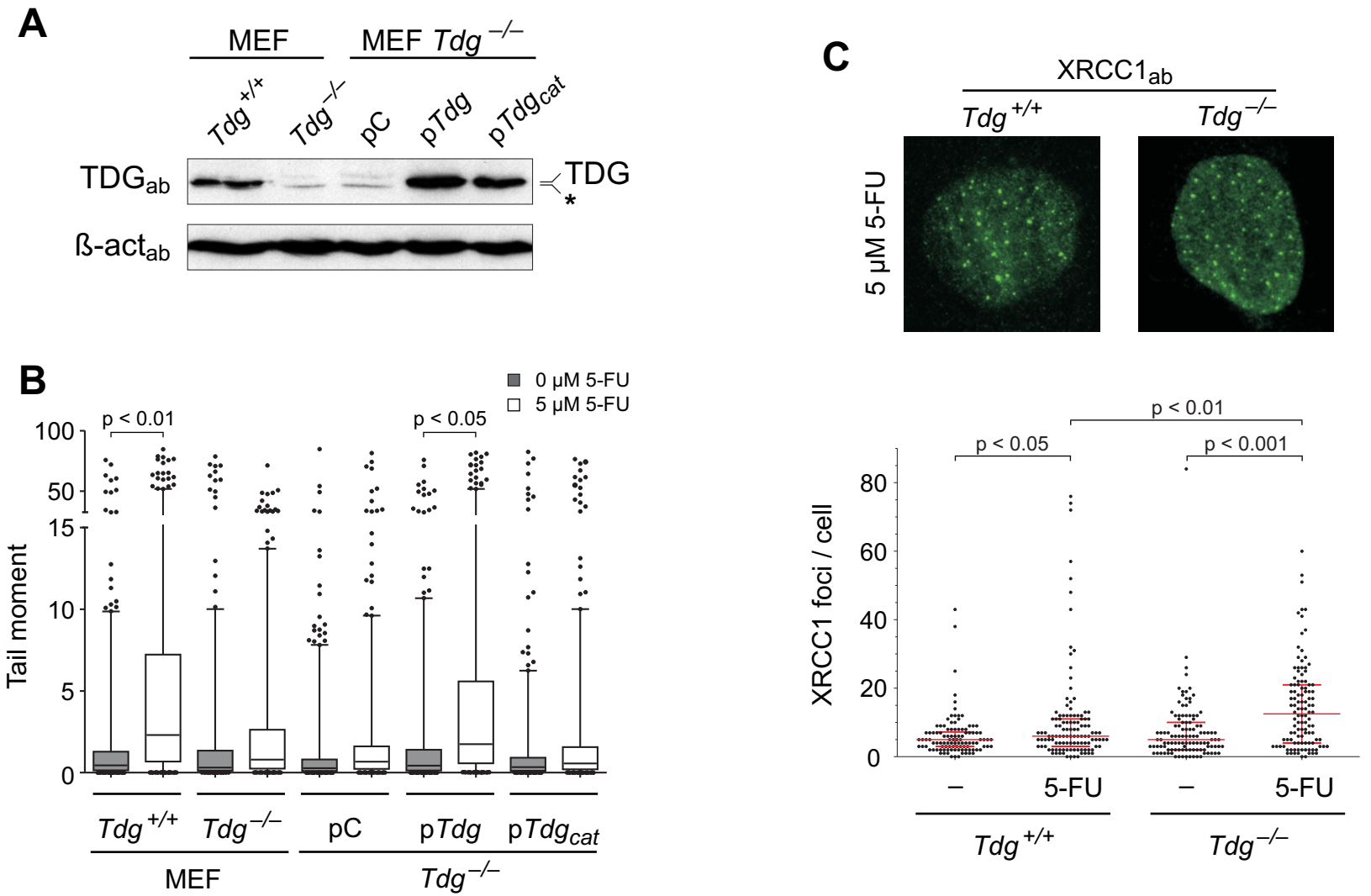

Figure 4 Kunz *et al.*

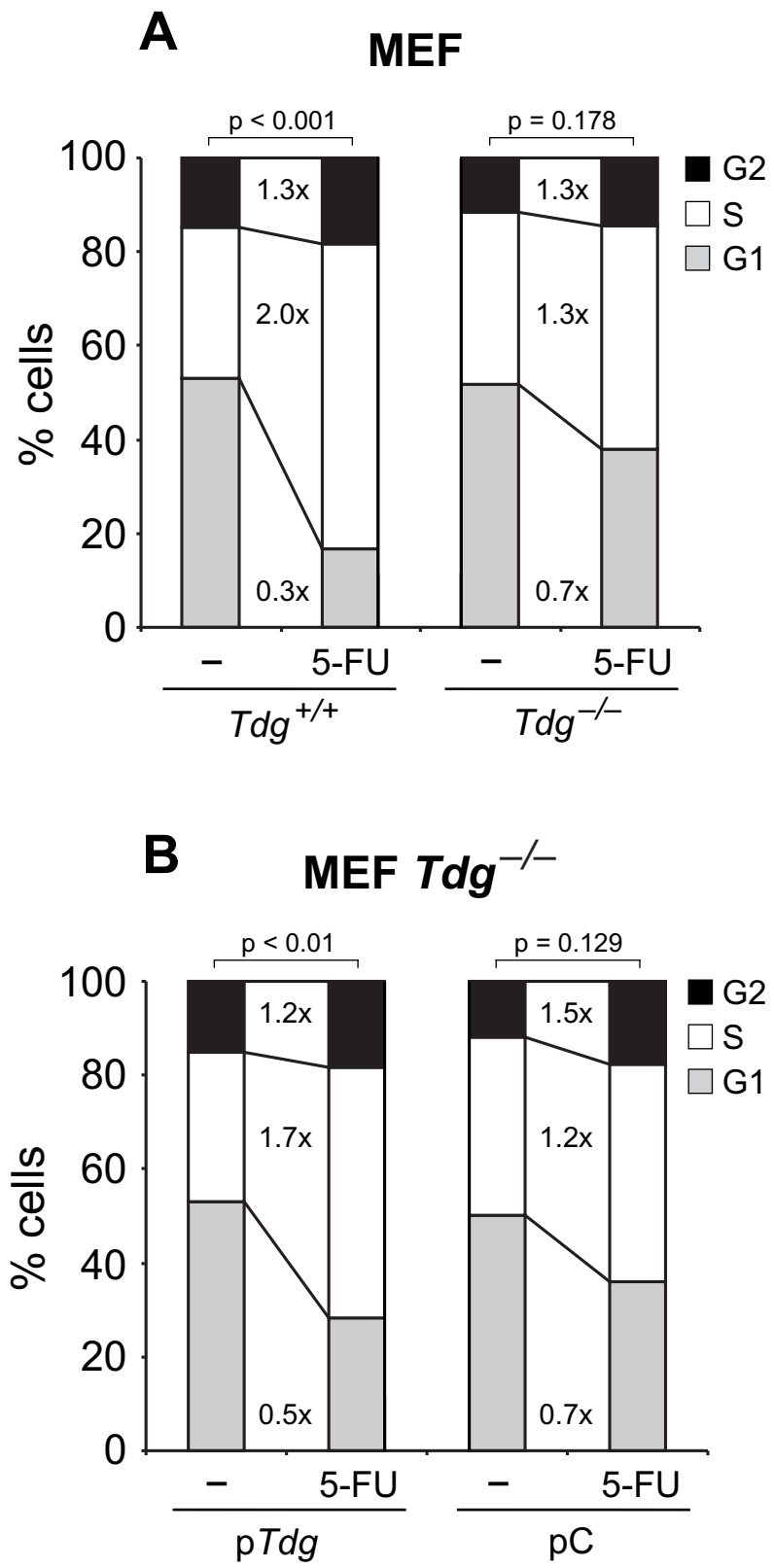

Figure 5 Kunz *et al.*

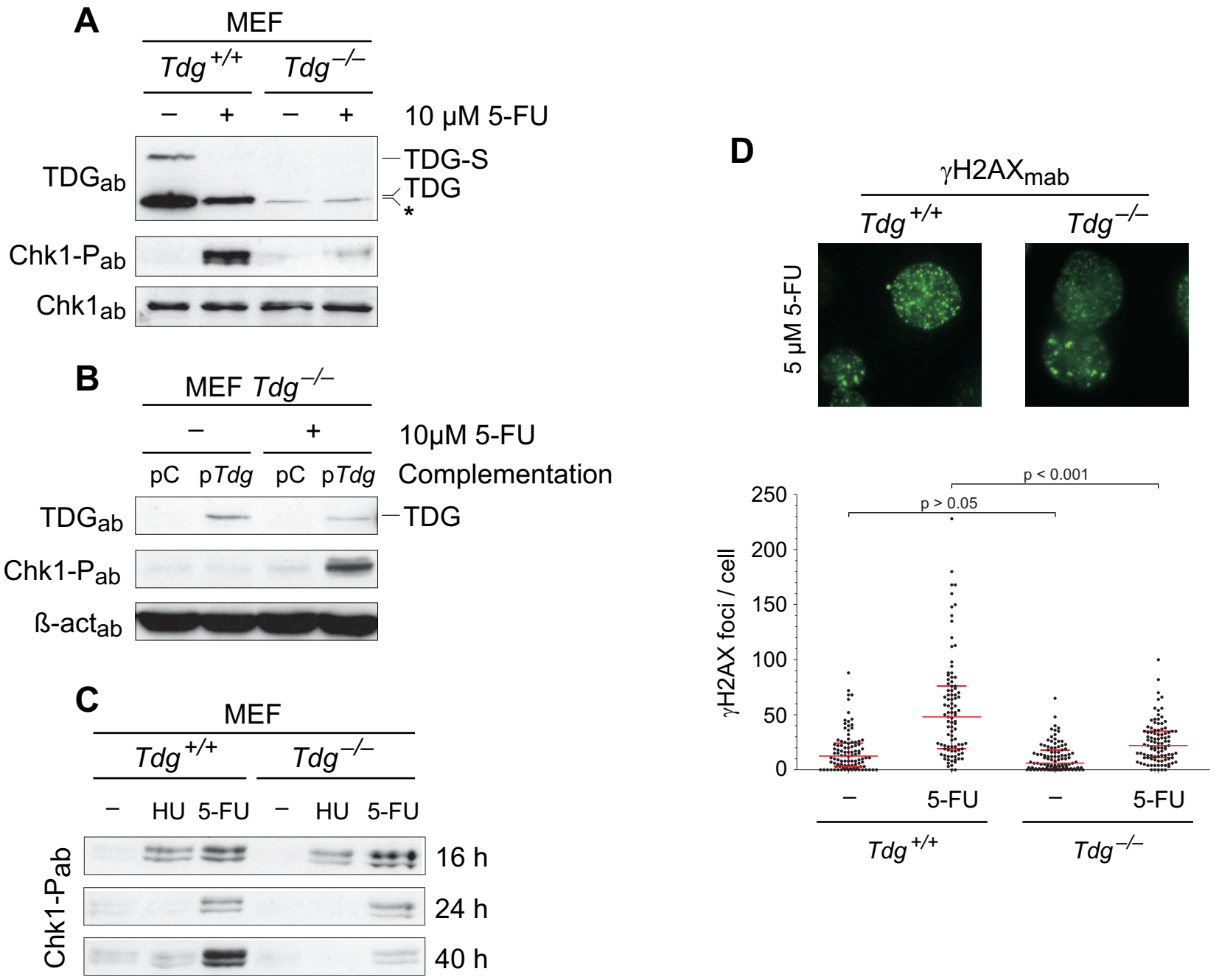

Figure 6 Kunz *et al.*

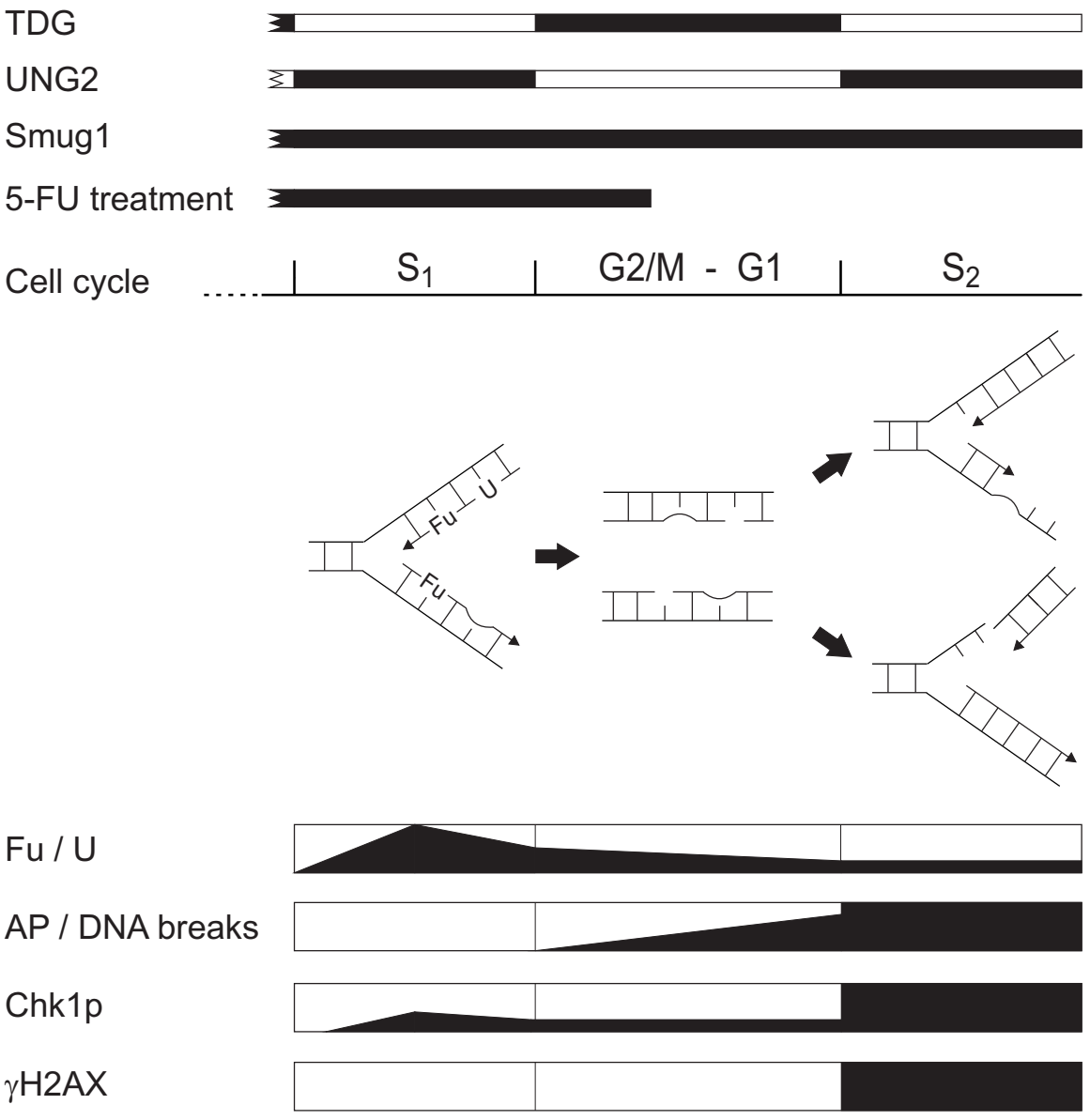

Supplemental Data

Base Excision by Thymine DNA Glycosylase Mediates DNA-Directed Cytotoxicity of 5-Fluorouracil

Running title: TDG mediated 5-FU toxicity

Christophe Kunz[1], Frauke Focke[1], Yusuke Saito[1], David Schürmann[1], Jim Selfridge[2], Adrian Bird[2] and Primo Schär[1*]

[1] Department of Biomedicine
University of Basel
Mattenstrasse 28
4058 Basel
Switzerland

[2] Wellcome Trust Centre for Cell Biology
Institute of Cell and Molecular Biology
University of Edinburgh
Michael Swann Building, King's Buildings
Mayfield Road
Edinburgh EH9 3JR
Scotland U.K.

* Corresponding author: Prof. Dr. Primo Schär[1]
primo.schaer@unibas.ch
Phone: +41 61 267 0767
Fax: +41 61 267 3566

Supplemental experimental procedures

Analysis of growth

For real-time analysis of cell growth during 5-Fu treatment, cells were seeded in 12-well plates at ~5% confluence. Following a preincubation of 24 hours, the growth medium was exchanged with medium containing 5-FU concentrations as indicated in the figure. The assessment of cell growth was performed with automated IncuCyte™ microscope (Essen Instruments, USA) by taking nine pictures per well and hour. The calculation of confluence and further analysis was performed with the IncuCyte™ software interface.

Supplemental figure legends

Figure S1. MEFs heterozygous for TDG display an intermediate Fu sensitivity. The sensitivity of $TDG^{+/+}$, $TDG^{+/-}$ and $TDG^{-/-}$cell lines to increasing amounts of Fu was measured after a continuous treatment of 48 hours. The panel shows cell survival as percent of untreated cells averaged from three independent experiments. When compared to wt MEF cells carrying a homozygous disruption of the TDG gene were hyperresistant to Fu treatment. The sensitivity of a cell line with heterozygous TDG genotype was in between the sensitivities measured for wt and knockout MEF. Error bars represent standard deviations.

Figure S2. Different effects of 5-Fu treatment on cell growth of TDG proficient and deficient MEFs. The growth of asynchronic TDG wildtype (*Tdg*$^{+/+}$) and knockout (*Tdg*$^{-/-}$) MEF cultures was monitored in real-time during treatment with different concentrations of 5-FU. Whereas 5-FU treatment resulted in cell toxicity for wildtype cells, it only caused slow growth in the case of knockout MEF cultures. Curves

represent the mean confluence at the respective time points and error bars represent standard deviations of 3 independent cultures.

Figure S1 Kunz *et al.*

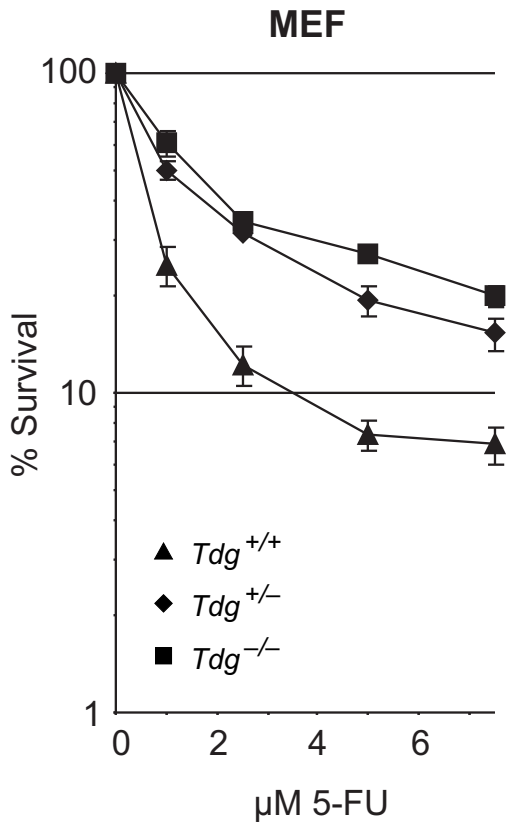

Figure S2 Kunz *et al.*

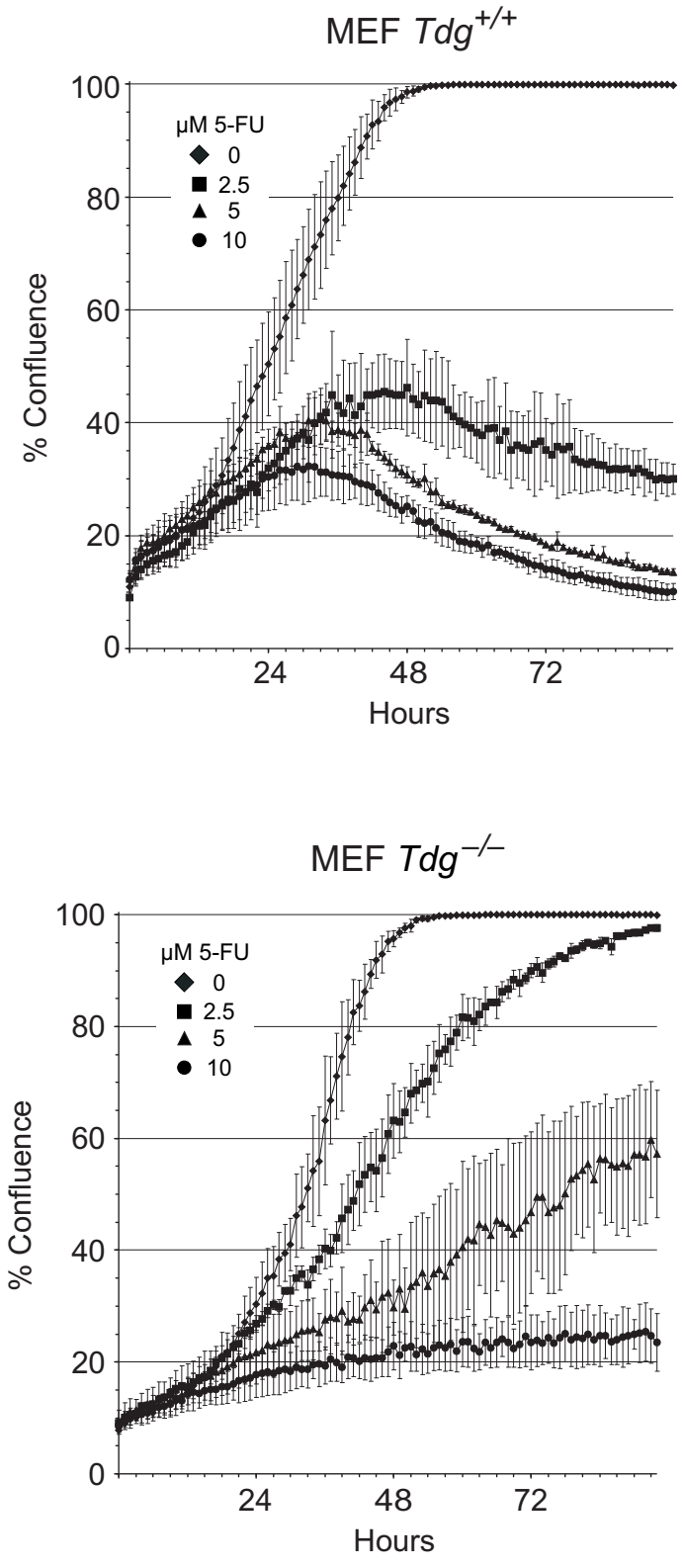

Appendix IV:

Cell cycle regulation as a mechanism for functional separation of the apparently redundant uracil DNA glycosylases TDG and UNG2

Nucleic Acids Res. 2007;35(11):3859-67. Epub 2007 May 25.

Ulrike Hardeland,[2†] Christophe Kunz,[1†] Frauke Focke,[1] Marta Szadkowski,[3] and Primo Schär[1*]

[1]Centre for Biomedicine, DKBW, University of Basel, Mattenstrasse 28, CH-4058 Basel, Switzerland, [2]Molecular Metabolic Control, DKFZ, Im Neuenheimer Feld 280, D-69120 Heidelberg, Germany and [3]KuDOS Pharmaceuticals Ltd., 327 Cambridge Science Park, Milton Road, Cambridge, CB4 0WG, UK

Published online 25 May 2007

Nucleic Acids Research, 2007, Vol. 35, No. 11 ***3859–3867***
doi:10.1093/nar/gkm337

Cell cycle regulation as a mechanism for functional separation of the apparently redundant uracil DNA glycosylases TDG and UNG2

Ulrike Hardeland[2,†], Christophe Kunz[1,†], Frauke Focke[1], Marta Szadkowski[3] and Primo Schär[1,*]

[1]Centre for Biomedicine, DKBW, University of Basel, Mattenstrasse 28, CH-4058 Basel, Switzerland, [2]Molecular Metabolic Control, DKFZ, Im Neuenheimer Feld 280, D-69120 Heidelberg, Germany and [3]KuDOS Pharmaceuticals Ltd., 327 Cambridge Science Park, Milton Road, Cambridge, CB4 0WG, UK

Received March 5, 2007; Revised April 18, 2007; Accepted April 19, 2007

ABSTRACT

Human Thymine-DNA Glycosylase (TDG) is a member of the uracil DNA glycosylase (UDG) superfamily. It excises uracil, thymine and a number of chemical base lesions when mispaired with guanine in double-stranded DNA. These activities are not unique to TDG; at least three additional proteins with similar enzymatic properties are present in mammalian cells. The successful co-evolution of these enzymes implies the existence of non-redundant biological functions that must be coordinated. Here, we report cell cycle regulation as a mechanism for the functional separation of apparently redundant DNA glycosylases. We show that cells entering S-phase eliminate TDG through the ubiquitin–proteasome system and then maintain a TDG-free condition until G2. Incomplete degradation of ectopically expressed TDG impedes S-phase progression and cell proliferation. The mode of cell cycle regulation of TDG is strictly inverse to that of UNG2, which peaks in and throughout S-phase and then declines to undetectable levels until it appears again just before the next S-phase. Thus, TDG- and UNG2-dependent base excision repair alternates throughout the cell cycle, and the ubiquitin–proteasome pathway constitutes the underlying regulatory system.

INTRODUCTION

Uracil (U) arises in DNA either by erroneous incorporation of dUMP opposite adenine (A) during DNA synthesis or by deamination of cytosine (C), which generates a U mispaired with guanine (G). To what extent A•U base pairs affect the function of DNA is unclear; G•U mispairs, however, give rise to C → T mutations if a DNA polymerase replicates across. Uracil DNA glycosylases (UDGs) (1) have evolved to eliminate this irregular base from the DNA. They hydrolyze the *N*-glycosidic bond linking the U to the sugar moiety of the nucleotide, thereby initiating a base excision repair (BER) process (2) that restores the canonical Watson–Crick base pair. Mammalian cells posses at least four enzymes with UDG activity, namely UNG, TDG, SMUG1 and MBD4 (3–6), and the successful co-evolution of these enzymes implies that each of them fulfils specific non-redundant biological functions. The question then is how cells achieve the functional separation of these enzymatically redundant activities. One way would be to control their spatial and temporal distribution as exemplified by the UNG proteins. Differential expression of the human *UNG* gene from two alternative promoters generates two isoforms, UNG1 and UNG2, that localize to mitochondria and to nuclei, respectively (7). Moreover, *UNG2* expression is up-regulated during S-phase of the cell cycle where the protein associates with PCNA and RPA at replication foci, implicating a role for this UDG in the removal of misincorporated U during DNA replication (8,9). Whether similar forms of regulation apply to other UDGs and, thus, could provide a cellular mechanism for functional coordination of uracil repair is not known. Here, we report that Thymine-DNA Glycosylase (TDG), a mismatch-specific UDG, underlies strict cell cycle regulation. TDG has a comparably broad substrate spectrum including the deamination product of 5-methylcytosine, i.e. a T mispaired with a G, but its most efficiently processed physiological substrate is a G•U mispair (6). Cells entering S-phase eliminate this glycosylase through the ubiquitin–proteasome pathway and

*To whom correspondence should be addressed. Tel: +41 0 61 267 0767; Fax: +41 0 61 267 3566; Email: primo.schaer@unibas.ch

†The authors wish it to be known that, in their opinion, the first two authors should be regarded as joint First Authors.

maintain a TDG free state until DNA replication is completed. Degradation of TDG is critical for S-phase progression and cell proliferation, implicating that this UDG interferes negatively with vital processes of DNA replication. Strikingly, TDG levels decline just when UNG2 expression comes up and *vice versa*, suggesting that uracil repair is handled by distinct pathways throughout the cell cycle that are coordinated by the ubiquitin–proteasome system.

MATERIAL AND METHODS

Reagents and antibodies and expression constructs

The complete^{TM} protease inhibitor tablets were purchased from Roche (Switzerland). All other chemicals and reagents were from Sigma (Germany). All media and supplements used for cell culture were purchased from Gibco BRL (Invitrogen, UK). The polyclonal and monoclonal (99) anti-TDG antibodies were described earlier (Hardeland *et al.*, 2002), anti-ubiquitin (P4D1) and anti-cyclin B1 (GNS 1) antibodies were from Santa Cruz Biotechnology, Inc. (CA, USA), anti-HA (3F10) antibody from Roche (Switzerland), anti cyclin A (BF 683) from Milliporee (MA, USA) and anti-cyclin E (Ab-1, Ab-2) antibodies from Labvision (CA, USA), and anti-UNG (ab23926) and anti MBD4 (ab12187) antibodies from Abcam (UK). The anti-β-tubulin antibody (N37) and the secondary horse-radish-peroxidase conjugated antibodies were purchased from GE Healthcare Life Sciences (Germany). The plasmid constructs expressing HA-TDG or HA-TDG^{N140A} have been previously described (10).

Cell culturing, cell cycle synchronizations, protein extractions

MRC5 cells were cultured in Nutrition Mix Ham's F-10 medium with Glutamax I, HeLa, HeLa S3 and 293T cells were grown in Dulbecco's modified Eagle's (DMEM) medium containing 2 mM L-glutamine, both supplemented with 10% fetal calf serum and antibiotics (penicillin/streptomycin). For HeLa cells stably or transiently transfected with TDG expression constructs, the medium was supplemented with 0.8 or 0.2 μg/ml puromycin, respectively. Stably transfected 293T cells were grown in the presence of 1.5 μg/ml puromycin. All cultures were incubated at 37°C in a humidified atmosphere containing 5% CO_2. All transfections were done at 30% confluency with 1 μg (HeLa cells) or 8 μg (293T cells) of vector DNA using the Fugene reagent (Roche, Switzerland). The efficiency of plasmid delivery was estimated by transfection of pEGFP-N1 (Clontech, USA) under identical conditions and quantitation of EGFP positive cells by fluorescence microscopy. Transiently transfected cells were cultured for 48 h unless stated otherwise.

For cell cycle analysis, 293T cells were seeded onto microscope slides at a confluency of 50% and allowed to attach for 7 h in medium at 37°C. The slides were then washed three times in PBS and cells fixed in acetone for 2 min at −20°C. After short rehydration with PBS, the slides were covered with staining solution (50 μg/ml propidium iodide, 200 μg/ml RNaseA) and incubated for 30 min at 37°C in a humidified chamber. After quick rinsing in PBS, the slides were covered with 50% glycerol in PBS and a coverslip and their DNA content analysed on a laser scanning cytometer, LSC-1 (LSC® CompuCyte, USA). In parallel, cell cycle analyses were done by standard flow cytometry.

Cell cycle arrest experiments were performed by treatment of 5×10^6 HeLa cells at 50% confluency with either 2.5 mM hydroxyurea (HU, 2 M stock in H_2O), 0.8 μg/ml nocodazole (NO, 1 mg/ml stock in DMSO) or respective amounts of DMSO only. After 16 h, denaturing extracts were prepared by scraping cells from the culture plates in 400 μl of lysis buffer I (8 M urea, 200 mM DTT, 120 mM Tris/HCl pH 6.8, 4% SDS, 20% glycerol, 0.01% bromphenolblue) and heating for 10 min at 95°C. Equal sample volumes were then analysed by 10% SDS–polyacrylamide-gel-electrophoresis (SDS-PAGE) and western blotting. HeLa S3 cells were synchronized by harvesting and reseeding detached mitotic cells as follows. Cells were first cultured to 70% confluency in 8 flasks of 175 cm^2 size. To remove all loosely attaching cells, the cultures were extensively washed with pre-warmed medium. The washing procedure was repeated after another 2 h of incubation. After further 2 h, the medium containing detached mitotic cells was removed and cells collected by centrifugation. 1.3×10^6 cells per time point were replated and grown for the times indicated. At each time point, cells were washed with 1× PBS pH 7.4 on the plate and the proteins extracted by direct lysis in 200 μl lysis buffer I. Equal amounts of extract were then analysed by SDS-PAGE and western blotting. MRC5 cells were synchronized by serum starvation followed by mimosine treatment as described in (11). After release, samples were taken at different time points and cell extracts prepared for western blotting (11).

For proteasome inhibition 5×10^6 HeLa cells at 50% confluency were treated for 12 h with 20 μM MG132 (20 mM stock in DMSO) or an equivalent of DMSO only. The cells were then washed with PBS and directly lysed by addition of 400 μl lysis buffer I. For the preparation of soluble and insoluble protein fractions 2.5×10^7 MG132 treated cells were lysed with 2 ml of lysis buffer II (50 mM Na-phosphate pH 8.0, 125 mM NaCl, 1% NP-40, 0.5 mM EDTA, 1 mM PMSF, 1× complete^{TM} protease inhibitors). Soluble and insoluble proteins were then separated by centrifugation for 15 min at 14 000 r.p.m., 4°C. After removal of the supernatant (soluble proteins) the pellet (insoluble proteins) was resuspended in the same volume. Equal amounts of both fractions were separated by SDS-PAGE and analysed by western blotting. Denaturing extracts of MG132 treated cells were obtained by scraping cells from culture dishes in lysis buffer III (50 mM Tris/HCl pH 7.5, 1% SDS, 5 mM DTT) and heating the suspensions for 10 min at 95°C.

Immunoprecipitation and western blotting

M-280 tosylactivated Dynabeads (Invitrogen, UK) were coated with affinity purified rabbit polyclonal anti-TDG antibody or BSA according to the manufacturer's protocol. An aliquot of 400 μl of the denaturing extracts of MG132 treated HeLa cells was diluted 1:10 in dilution

buffer (50 mM Tris/HCl pH 7.5, 120 mM NaCl, 5% glycerol, 1% NP-40, 1 mM EDTA, 1 mM PMSF and 1× complete™ protease inhibitors) before the addition of equilibrated Dynabeads (~2.4×10^7 beads/assay). After incubation for 4 h at 4°C under rotation, unbound proteins were removed and the beads washed three times with dilution buffer at 4°C. Bound proteins were then eluted in 40 µl of 2× SDS-sample-buffer (200 mM DTT, 120 mM Tris/HCl pH 6.8, 4% SDS, 20% glycerol, 0.01% bromphenolblue) and incubation at 95°C for 5 min. Following protein separation by 8 or 10% SDS-PAGE, western blotting was done with antibodies against TDG and ubiquitin following standard procedures. All antibodies were diluted in TBS-T (100 mM Tris/HCl pH 8.0, 150 mM NaCl, 0.1% Tween20) containing 5% dry milk as blocking reagent; the polyclonal anti-TDG antiserum was diluted 1:10 000, the monoclonal anti-TDG and anti-ubiquitin antibodies 1:1000. Detection of the signals was carried out using the enhanced chemiluminescent (ECL™) substrate system (GE Healthcare Life Sciences, Germany).

Immunofluorescence

HeLa cells were grown on coverslips to a confluency of 30%. After washing extensively in PBS, the cells were fixed for 5 min in pre-chilled methanol (−20°C), re-hydrated for 4 times 10 min at room temperature (rT) in PBS, and permeabilized for 5 min in ice-cold P-buffer (PBS, 0.2% TritonX100). To reduce autofluorescence, the coverslips were incubated for another 5 min in ice-cold P-buffer containing 0.2% $NaBH_4$. Soluble protein was then washed out by gently shaking the coverslips in PBS for 10 min at rT. After blocking for 10 min at rT in hybridization buffer (PBS, 1% BSA), samples were hybridized with affinity-purified polyclonal rabbit anti-TDG- (1:100 dilution) and a FITC coupled anti-PCNA (1:500, Leinco Technologies, MO, USA) antibodies at 4°C overnight. After four washing steps of 10 min in hybridization buffer at rT, samples were hybridized with an anti-rabbit IgG Alexa-546 conjugated secondary antibody (1:200, Invitrogen, UK) at rT for 1 h. After four washing steps of 10 min in PBS, the coverslips were dried and embedded in Mowiol containing 1 µg/ml DAPI. TDG and PCNA signals were visualized on a Axiovert 200M microscope (Zeiss, Germany) using TRITC (exitation 560 nm, emission 580 nm) and FITC (exitation 490, emission 520 nm) filters, respectively.

Northern blot analyses

Total RNA was isolated from MRC5 cells using the TRIzol reagent. RNA concentrations were determined by A_{260} measurement and the quality was checked by electrophoresis on 1% formaldehyde agarose gels. Twenty microgram of total RNA in formamide loading buffer were separated in a 1% agarosegel containing formaldehyde. After washing the gel twice for 10 min in 8 mM NaOH, the RNA was transferred to a Zeta Probe membrane (BioRad, CA, USA) overnight in 8 mM NaOH. After a brief washing step with 2× SSC the transferred RNA was fixed by baking at 80°C. Following pre-hybridization of the membrane at 65°C in hybridization buffer (0.5 M Na_2PO_4 pH 7.2, 7% SDS) for 5 min, hybridization with probe was done for 20 h at 65°C. A ^{32}P-labeled PCR fragment (Megaprime Kit, GE Healthcare Life Sciences, Germany), representing the 5′ part of the TDG cDNA served as specific probe. After hybridization the membrane was washed twice with wash buffer I (40 mM Na_2PO_4 pH 7.2, 5% SDS) for 20 min at 65°C, followed by one washing steps with wash buffer II (40 mM Na_2PO_4 pH 7.2, 1% SDS) at 65°C for 10 min. After exposition of the membrane to a phosphoimager screen, signals were visualized on a Storm phosphoimager (GE Healthcare Life Sciences, Germany).

Ubiquitylation *in vitro*

In vitro ubiquitylation reactions were performed with the ubiquitin conjugation Enzyme Kit (Biotrend, Germany) according to the manufacturer's instructions. An aliquot of 20 µl reactions contained 1× MgATP, 5 µg conjugating fraction I, 5 µg conjugation fraction II, 26 µg ubiquitin (Biotrend), 200 ng ubiquitin-aldehyde and 10 ng of recombinant TDG protein. The reactions were incubated at 37°C for 0 and 2 h and stopped by the addition of 4 µl 6× SDS-sample buffer (600 mM DTT, 360 mM Tris/HCl pH 6.8, 12% SDS, 60% glycerol, 0.03% bromphenolblue). After heating at 95°C for 5 min the reaction products were analysed by 7.5% SDS-PAGE and western blotting with the polyclonal anti-TDG antibody.

Base release assays

Nuclear extracts were prepared from 10^8 HeLa cells harvested after HU (or mock) treatment. Cells were resuspended in ice-cold hypotonic buffer (20 mM HEPES pH 8.0, 5 mM KCl, 1.5 mM $MgCl_2$, 0.5 mM PMSF, 1 mM DTT, 1× complete™ protease inhibitors) at a cell density of 1×10^8 cells/ml and allowed to swell for 20 min on ice. Cells were broken up in a Dounce homogenizer on ice to achieve >80% lysis and the liberated nuclei were harvested by centrifugation at 3000*g* and 4°C. After estimation of the packed nuclear volume (pnv) the pellet was resuspended in 1/2 pnv low salt buffer (20 mM HEPES pH 8.0, 25% glycerol, 1.5 mM $MgCl_2$, 20 mM KCl, 0.2 mM EDTA, 0.5 mM PMSF, 0.5 mM DTT, 1× complete™ protease inhibitors). Nuclear proteins were extracted by the addition of 1/2 pnv high salt buffer (low salt buffer but 0.8 M KCl) and incubation at 4°C under constant mixing for 30 min. The extracted nuclei were pelleted for 20 min at 20 000*g* and 4°C. The supernatant was dialyzed against storage buffer (20 mM HEPES pH 8.0, 10% glycerol, 1.5 mM $MgCl_2$, 5 mM KCl, 0.2 mM EDTA, 0.5 mM PMSF, 0.5 mM DTT, 0.25× complete™ protease inhibitors). The dialyzed extracts were clarified by centrifugation for 20 min at 20 000*g* and 4°C and stored in aliquots at −80°C. Protein concentrations were estimated by the Bradford method (BioRad) using BSA as standard. Base release assays were then done according to (12) with slight modifications. An aliquot of 40 µl reactions contained 25 µg nuclear extracts and 1 pmol of either double-stranded homoduplex or mismatched DNA substrate (12). The reactions were incubated for 24 h at 37°C in reaction buffer (50 mM Tris-HCl

pH 8.0, 1 mM EDTA, 1 mM DTT, 1mg/ml BSA) containing 2 U UGI. Quantitative cleavage of AP sites was achieved by the addition of 100 mM NaOH and heating at 95°C for 10 min. Subsequently, DNA was ethanol precipitated overnight at −20°C in 0.3 M sodium acetate pH 5.2 and in the presence of 0.4 mg/ml carrier tRNA. The DNA was then pelleted by centrifugation (20 min, 20 000*g*, 4°C), washed once in 80% ethanol, air-dried, resuspended in formamide loading buffer (1× TBE, 90% formamide), heated at 95°C for 5 min and immediately chilled on ice. The reaction products were separated by electrophoresis in preheated 15% denaturing polyacrylamide gels and 1× TBE buffer. Visualization of the fluorescein labelled DNA was carried out on a Typhoon 9400 (GE Healthcare, Germany) and the data were quantified using the ImageQuant TL software (GE Healthcare, Germany).

RESULTS

S-phase progression requires cell cycle regulation of TDG-mediated BER

We found in different human cell models (HeLa, 293T, MRC5) that expression of high levels of TDG is incompatible with cell proliferation. Although transfection of various constructs designed for stable TDG expression produced transiently up to 30-fold the endogenous level, any attempt to maintain expression at levels above 5-fold in culture was unsuccessful. Cell cycle analyses then revealed that, following transfection with a TDG expressing construct, a fraction of cells accumulated specifically in S-phase of the cell cycle. This, however, was not observed in cell populations transfected with a catalytically inactive variant of TDG (Figure 1A), although transient expression levels were equally high. As previously observed (13), overexpressed TDG localized strictly to the cell nucleus (data not shown). Upon cultivation of the cells under conditions selecting for stable TDG expression, this cell cycle effect disappeared concomitantly with the drop of TDG protein to <5-fold the endogenous level (Figure 1B). These observations indicated that high levels of TDG lead to a disturbance of S-phase progression, thus conferring a selective advantage to low TDG expressing cells, i.e. the loss of high expressing cells, in the culture.

These findings prompted us to examine whether TDG expression underlies cell cycle regulation. To this end, we made use of two stably transfected HeLa cell populations, one expressing an N-terminally HA-tagged TDG from an SV40 promoter at ~5-fold the level of the endogenous protein (10), the other serving as a vector control and, thus, producing endogenous TDG only. We treated these cells with hydroxyurea (HU) or nocodazole (NO) to induce S- or G2/M-phase arrests, respectively, and then assessed TDG protein levels in denaturing cell extracts by immunoblotting with anti-TDG or anti-HA antibodies. To monitor the cell cycle status, we probed the membranes additionally with antibodies against cyclin E or cyclin B1 (Figure 2A). This showed that endogenous (Figure 2B) as well as ectopically expressed (Figure 2C) TDG was

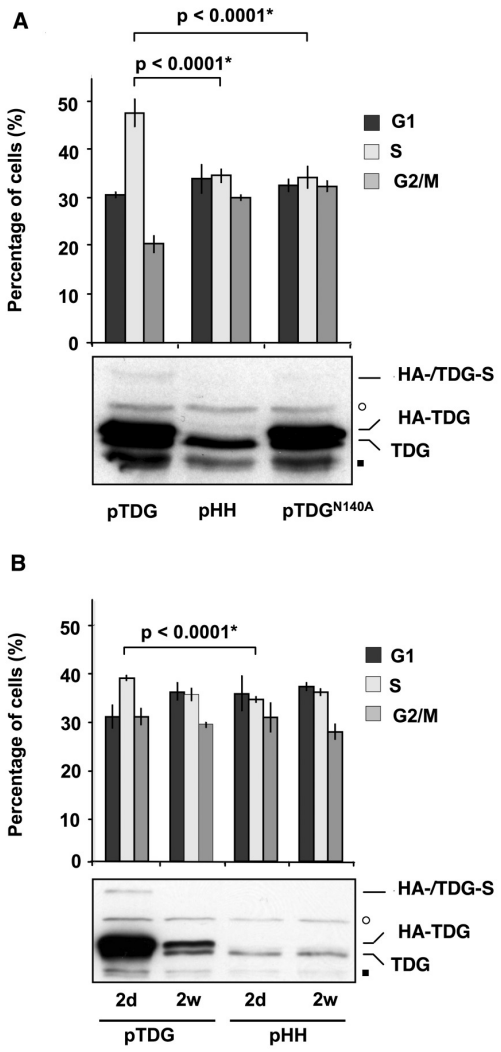

Figure 1. 293T cells expressing high levels of TDG accumulate in S-phase. (**A**) 293T cells were transiently co-transfected with a plasmid overexpressing either active HA-TDG (pTDG), the catalytically inactive variant HA-TDG/N140A (pTDG^{N140A}), or a vector control (pHH), and a EGFP expressing plasmid at a 10:1 ratio. The histogram shows the cell cycle distribution of transfected cells gated for EGFP positive cells, as determined by flow cytometry. The bottom panel documents TDG protein levels of the respective total cell population as determined by western blotting. TDG levels in cell populations carrying the overexpression construct were elevated by 20–30-fold. High levels of HA-TDG expression significantly increased the fraction of S-phase cells. This change in cell cycle distribution required TDG to be active, as overexpression of HA-TDG/N140A failed to produce the same effect. (**B**) The histogram shows the cell cycle distribution of 293T cells expressing active HA-TDG (pTDG) two days after transfection (2d) or after two weeks of selection for stable expression (2w). A vector control was also included (pHH). TDG expression levels are documented by western blots in the bottom panel. Shortly after transfection, TDG protein levels were 20–30 times higher than normal, but dropped to about three times the amount of endogenous TDG after selection. Concomitantly, the cell cycle effect seen after transfection disappeared. *P*-values (asterisk) were obtained by the Fisher's exact test from contingency tables comparing the distributions of G1-, S- and G2-cells. (Open circle) Unspecific cross-reaction of the primary antibody. (Filled square) Faster migrating forms of TDG. HA-/TDG-S: SUMO-modified HA-TDG and endogenous TDG, respectively.

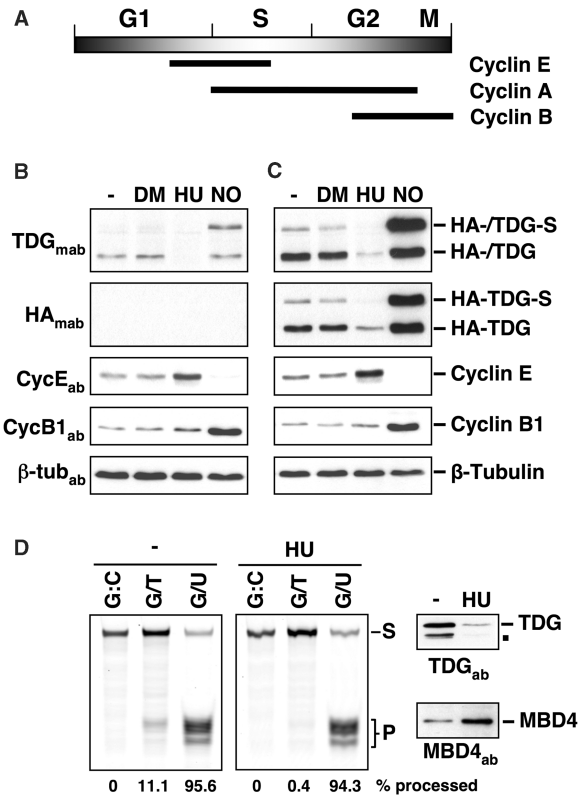

Figure 2. TDG is absent in S-phase arrested HeLa cells. (**A**) Schematic illustration of expression of cyclin E, cyclin A and cyclin B during the cell cycle. (**B** and **C**) HeLa cells expressing endogenous *TDG* alone or together with *HA-TDG* were blocked in S-phase with hydroxyurea (HU) or in G2/M with nocodazole (NO). Untreated asynchronous cells (-) and DMSO (DM) mock-treated cells were analysed in parallel. Denaturing cell extracts were examined by western blotting with antibodies against TDG or the HA-tag as indicated. Antibodies against Cyclin E and Cyclin B1 were applied to monitor the cell cycle arrest; β-tubulin staining served as a loading control. A monoclonal anti-TDG antibody (TDG_{mab}) detected endogenous TDG in extracts of untreated, mock treated or G2/M arrested cells, but none in extracts from S-phase arrested cells (B). Ectopically expressed HA-TDG also declined in HU arrested cells, although faint TDG (TDG_{mab}) and HA- (HA_{mab}) -specific signals were still discernible (C). (**D**) Base release assays with a fluorescent-labelled synthetic 60-mer DNA duplex document a significant reduction of G•T processing activity in nuclear extracts from HU-arrested HeLa cells. The assay was done with 25 μg of nuclear extract supplemented with 2 U of UNG2 inhibitory UGI peptide. A denaturing polyarcylamide gel with the intact DNA strand migrating at the top (S) and the cleaved products occurring as a consequence of G•T processing (P) are shown. Immunoblots of the corresponding cell extracts with TDG and MBD4-specific antibodies are shown on the right. (Filled square) Faster migrating forms of TDG. HA-/TDG-S: SUMO-modified HA-TDG and endogenous TDG, respectively.

virtually undetectable in S-phase arrested cells. Residual TDG signals likely reflected traces of protein from contaminating G2/M cells, as indicated by the low amounts of cyclin B1 in these extracts. Base excision assays with nuclear extracts (12) then revealed a >25-fold reduction of G•T glycosylase activity in HU-arrested HeLa cells (Figure 2D), and this correlated directly with the decline of TDG protein. MBD4, another mismatch-specific thymine-DNA glycosylase (5), did not contribute notably to G•T processing in these extracts (Figure 2D). Given the slight enrichment of the enzyme in S-phase arrested cells and that recombinant MBD4 is active under identical experimental conditions (data not shown), this must be interpreted to mean that G•T processing by BER is largely TDG dependent and does not occur during S-phase. By contrast, G•U processing did not correlate with TDG protein levels. Considering that these base release reactions were done in the presence of a 4-fold saturating amount of the UNG-inhibitory UGI peptide and that MBD4 appears to be poorly active in these extracts, the uracil processing observed in the S-phase arrested cells most likely reflected the activity of SMUG1. In the absence of the UGI-peptide, however, UNG2 was clearly the predominant uracil processing activity in these extracts (data not shown). Together, these experiments showed that HeLa cells down-regulate TDG protein and activity during S-phase and are able to do so even when it is stably expressed from an SV40 promoter at levels up to five times higher than normal.

To exclude that the HU treatment itself affects TDG stability, we examined its levels in synchronously cycling cell populations. Mitotic shake off experiments with HeLaS3 cells confirmed that TDG protein peaks during G1 and drops in S-phase (Figure 3A). Here, the disappearance of TDG coincided with the appearance of cyclin A (14), suggesting that downregulation occurs at the G1/S boundary. This experiment also confirmed the strict cell cycle regulation of the nuclear form of the highly efficient UNG (8,9) and thus, established that the expression of TDG and UNG2 is perfectly anti-cyclic with at most two short phases of overlap in late G1 and early G2 of the cell cycle.

Next, we performed immunofluorescence (IF) microscopy to correlate TDG expression with the PCNA status in an asynchronous HeLa cell population. This confirmed the absence of TDG from nuclei with focal PCNA pattern, i.e. from S-phase nuclei (Figure 3B). Ninety-two percent of cells with PCNA foci were TDG negative, whereas 96% of cells with diffuse PCNA staining had a strong nuclear TDG signal. Moreover, more than two-thirds of the nuclei with PCNA foci were in an early stage of DNA replication (15) and the vast majority of them (89%) were TDG negative. Together, these data establish that the decline of TDG in HeLa cells occurs at the G1–S transition, the latest in early S-phase.

Finally, we ascertained the cell cycle regulation of TDG in human primary fibroblasts. We synchronized MRC5 cells in early S-phase by serum starvation and mimosine treatment (16) and extracted protein and RNA from cells harvested at different time points following release into S-phase. Examination of the protein extracts by immunoblotting then showed that TDG was virtually undetectable at the mimosine block and for 10 h post-release (Figure 4A). According to the cyclin E and B1 expression patterns, this time period represented the progression of the cell population through S-phase. In G2, the TDG levels started to increase until they reached a maximum in the subsequent G1-phase. Examination of the steady-state levels of the *TDG* transcript by northern blotting showed only marginal fluctuations throughout

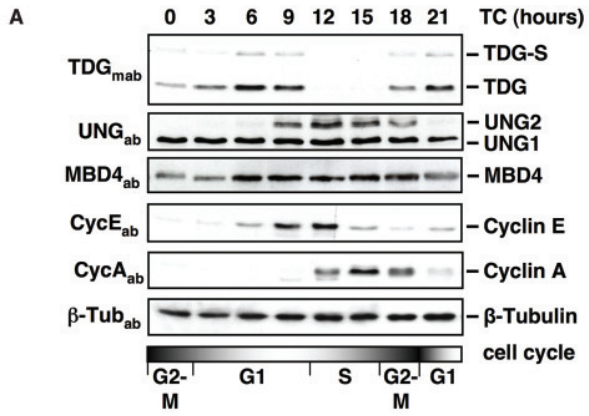

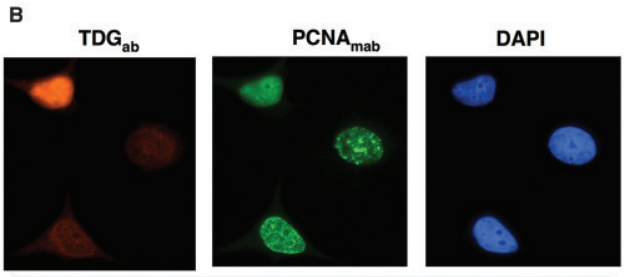

PCNA statu s	TDG positive		TDG negative		Total
	Cells	%	Cells	%	Cells
Diffuse PCNA (G1,G2/M)	320*	96.1	13*	3.9	333
Focal PCNA (S)	14*	8.4	153*	91.6	167
early S	13	11	104	89	117
mid S	0	0	40	100	40
late S	1	10	9	90	10

Figure 3. Cell cycle regulation of TDG in non-arrested cells. (**A**) HeLa S3 cells were synchronized by mitotic shake off. Following re-plating, TDG, UNG2 and MBD4 expression was examined in a time course (TC) of 21 h. At the time point indicated, cell extracts were prepared under denaturing conditions and analysed by western blotting with specific antibodies as indicated on the left. The cell cycle phases indicated at the bottom were deduced from the expression of cyclin A (S–G2/M) and E (G1–S). β-tubulin detection served as loading control. The monoclonal anti-TDG antibody detected TDG in mitotic and G1 cells (TC 0-9) and in G2/M cells (TC 18). No TDG was detectable in S-phase cells (TC 12,15). The disappearance of TDG at 12 h coincided with the *de novo* expression of cyclin A, indicating a downregulation of TDG at the G1/S boundary. By contrast, nuclear UNG2 was detectable between 9 and 18 h with a peak at 12 h, representing cells in S-phase. Mitochondrial UNG1 did not fluctuate throughout the cell cycle, nor did MBD4, which shows only slightly increased expression around S-phase. (**B**) Immunofluorescence staining of endogenous TDG and PCNA illustrate the absence of TDG from S-phase nuclei. Upper cell, TDG positive cell with diffuse PCNA staining; lower cell, TDG negative cell with PCNA staining indicating early to mid S-phase; middle cell, TDG negative cell with fewer and larger PCNA foci indicating late S-phase. Shown are typical events of 500 randomly chosen cells scored and classified as indicated in the table at the bottom. Asterisk: statistically significant difference, $P<0.0001$ by contingency tables and Fisher's exact test; TDG-S: endogenous TDG modified with SUMO.

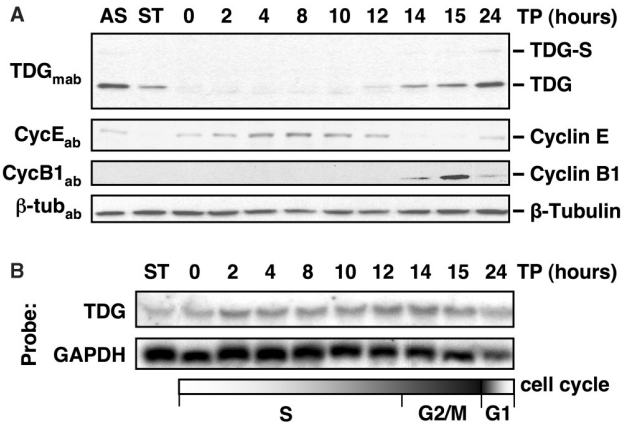

Figure 4. TDG protein levels fluctuate during the cell cycle in primary cells but mRNA is constitutively transcribed. MRC5 primary fibroblasts were synchronized in early S-phase by serum starvation and mimosine treatment. (**A**) Western blot analyses of protein extracts prepared from asynchronous cells (AS), serum starved cells (ST) and cells harvested at indicated times (TP hours) after release from the mimosine block. Proteins examined were endogenous TDG, Cyclin E, Cyclin B1 and β-tubulin as a loading control. TDG-specific signals appeared at 12 h after release into S-phase and increased gradually to the levels found in the asynchronous culture. Expression of cyclin E and cyclin B1 coincided with the lack or the presence of TDG, respectively. (**B**) Northern blot analysis of TDG and GAPDH mRNAs (loading control) at corresponding time points, showing that TDG-specific mRNA was detectable throughout the cell cycle. TDG-S: endogenous TDG modified with SUMO.

the cell cycle (Figure 4B), which cannot account for the dramatic changes seen at the protein level. Hence, cell-cycle-dependent expression of TDG applies to different human cell types and does not involve regulation at the levels of promoter activity or mRNA stability.

TDG is targeted by ubiquitin for proteasomal degradation

We then addressed a possible role of posttranslational modifications in the regulation of TDG. To examine whether the glycosylase is subject to degradation by the ubiquitin–proteasome system (17), we measured the effect of MG132, a reversible inhibitor of the 26S proteasome, on the TDG protein level in asynchronously proliferating HeLa cells. Cells treated with MG132 had clearly elevated steady-state levels of TDG (Figure 5A). This effect, however, was only apparent when extracts were prepared under denaturing conditions, the reason being a change in TDG solubility upon proteasome inhibition. While TDG extracted predominantly in the soluble protein fraction in untreated cells, a substantial amount became insoluble after MG132 treatment (Figure S1A), just like the majority of ubiquitin-conjugated proteins (Figure S2B). Following these indications for ubiquitylation of TDG, we prepared denaturing extracts from HeLa cells, again expressing either endogenous TDG alone or together with HA-TDG, for immunoprecipitation (IP). IP with an affinity-purified polyclonal TDG antibody then led to the expected enrichment of the glycosylase as evident from immunoblotting with a monoclonal TDG antibody (Figure 5B, left panel). The same antibody, however,

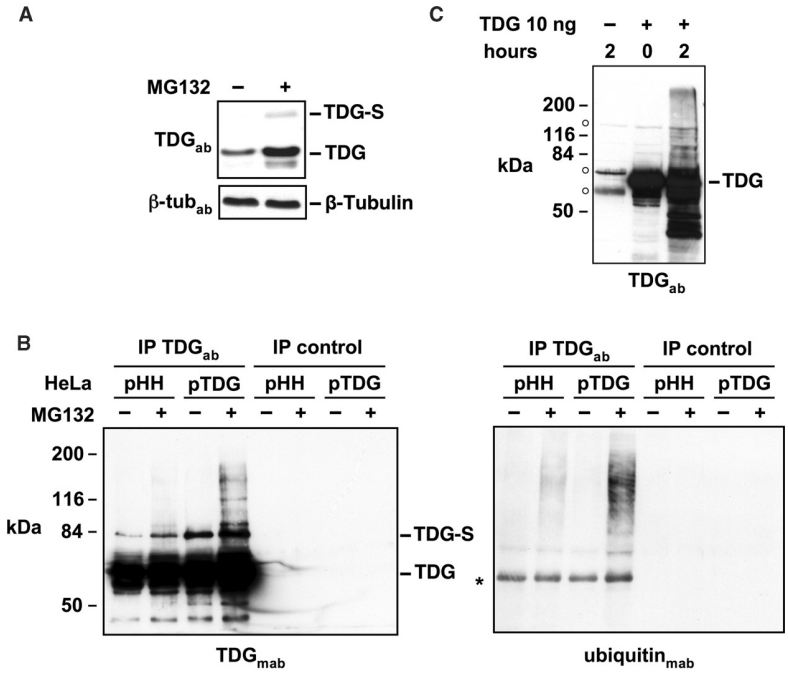

Figure 5. TDG is polyubiquitylated and stabilized by proteasome inhibition. (**A**) Asynchronous HeLa cultures were treated with the proteasome inhibitor MG132 (20 μM) or DMSO. Cell extracts prepared under denaturing conditions were analysed by western blotting with a polyclonal anti-TDG (TDG$_{ab}$) and an anti-β-tubulin antibody (β-tub$_{ab}$). SUMOylated and unmodified TDG increased after proteasome inhibition. (**B**) HeLa cells stably transfected with a HA-TDG (pTDG) expression construct or the vector (pHH) were treated with MG132 or DMSO. Cell extracts prepared under denaturing conditions were subjected to TDG-IP with an affinity purified polyclonal anti-TDG antibody (TDG$_{ab}$). Bound protein fractions were analysed by western blotting with the monoclonal anti-TDG (TDG$_{mab,}$ left panel) or an anti-ubiquitin antibody (ubiquitin$_{ab}$, right panel). Strong signals appeared in the TDG-IPs but none in the IP-controls. TDG-specific signals smearing towards higher molecular weights indicated an accumulation of modified TDG in extracts of MG132 treated cells. The anti-ubiquitin antibody detected proteins with comparable migration properties in the corresponding TDG-IP protein fractions. (**C**) 10 ng of purified recombinant TDG were subjected to *in vitro* ubiquitylation. Shown is a western blot with the polyclonal anti-TDG antibody of aliquots taken at 0 and 2 h of incubation, and of a control reaction lacking TDG. The appearance of TDG-dependent high molecular weight bands after 2 h indicates ubiquitylation of TDG. (Asterisk), protein co-precipitating in TDG-IP and cross-reacting with the secondary antibody used; (Open circle) Components of the ubiquitylation system cross-reacting with the anti-TDG antibody.

also detected a smear of high molecular weight proteins in the TDG-IP's from extracts of proteasome inhibited cells. These signals were more pronounced in the extracts containing additional HA-TDG. Probing of the membrane with a specific anti-ubiquitin antibody revealed proteins at high molecular weight, resembling the pattern observed with the TDG antibody (Figure 5B, right panel). Thus, polyubiquitylated protein species co-precipitated with a TDG-specific antibody from extracts of proteasome inhibited cells. Unspecific binding of ubiquitylated proteins to the beads did not occur (see control IP), and, given the denaturing conditions applied for extract preparation, unspecific binding of ubiquitylated proteins to TDG can also be virtually excluded. We therefore conclude that the proteins recognized by the anti-ubiquitin antibody must be TDG isoforms carrying polyubiquitin chains of different lengths. To formally prove its susceptibility to ubiquitin conjugation, we subjected bacterially produced TDG to ubiquitylation in an *in vitro* reconstituted assay. This indeed produced TDG isoforms of increased molecular weight (Figure 5C). The reaction, however, was inefficient, indicating that ubiquitylation *in vivo* may require priming of TDG, possibly by phosphorylation, to stimulate its interaction with an E3 ubiquitin ligase (18). Taken together, our data strongly suggest that polyubiquitylation and proteasomal degradation is the mechanism underlying the disappearance of TDG at the G1/S boundary of the cell cycle. TDG was also shown to be target for SUMO conjugation in cells (10). To address whether SUMO modification contributes to the cell cycle regulation of TDG, we examined the behaviour of an ectopically expressed SUMOylation-deficient TDG variant (HA-TDG^{K330A}) upon HU or NO treatment of the cells. The protein was absent from S-phase cells and enriched at the G2/M stage, exactly as the wild-type control (Figure S1C), establishing that SUMO modification neither positively nor negatively interferes with TDG ubiquitylation and proteasome degradation.

DISCUSSION

Our data establish that two prominent members of the UDG family, TDG and UNG2, underlie strict anticyclic cell cycle regulation. While TDG is highly expressed throughout the G2-M and G1 phases its levels rapidly

decline at the G1–S transition just when UNG2 starts to rise above background. The UNG2 protein then peaks at the beginning of S-phase and gradually declines towards termination of DNA replication (see also reference 9), when TDG expression resumes. This implicates that the two biochemically redundant UDGs control non-redundant, cell cycle stage-specific pathways for uracil repair; while UNG2 is active during DNA replication, TDG functions in non-replicating DNA, notably, when U arises mainly through deamination of cytosine. Strikingly, although the pattern of cell cycle regulation of the two UDGs is diametrically opposed, the underlying mechanism appears to be the same. As shown here for TDG and reported previously for UNG2 (9), both are subject to cell cycle controlled ubiquitylation and proteasome degradation. Thus, the ubiquitin–proteasome system appears to be at the heart of the coordination of redundant BER pathways, which would be an as yet unrecognized function. Whether this interesting concept of coordination is a feature restricted to TDG and UNG2 only, or whether it applies more generally to DNA repair remains to be resolved.

We wanted to get some insight into why TDG needs to be eliminated before S-phase from ectopically expressing the glycosylase to levels saturating its degradation. TDG expression at >30-fold the endogenous level could readily be obtained by transient transfection, and such amounts were indeed saturating in the sense that low amounts of the protein remained detectable in S-phase arrested cell populations. Yet, attempts to maintain high expression in culture failed; upon selection of stable clones, TDG expression declined to levels <5-fold that were compatible with complete degradation of the protein in S-phase. Thus, the presence of TDG in S-phase seems incompatible with cell cycle progression and proliferation, and this is in line with the observation that 293T cells transiently expressing high levels of wild-type TDG accumulate in S-phase.

Interference with S-phase progression might occur at the level of U excision (1). If misincorporated, U must be eliminated from newly synthesized DNA in a way that is coordinated with the replication process. Given its enzymatic properties, TDG would be totally unsuited for this task; by processing A•U only inefficiently (19) and binding to AP sites with high affinity (10,20), it would perturb the replication process. By contrast, UNG2 would be the glycosylase of choice here; it processes U•A with a comparably high rate, and it associates with replication factors at the replication fork. Consistently, UNG was shown to keep genomic uracil levels low (1,8,21,22).

Considering the rather broad substrate spectrum of TDG (19), however, its presence in S-phase might cause other forms of interference. TDG could induce the formation of DNA double-strand breaks either directly, if it removed substrate bases close to each other in opposite DNA strands, or indirectly, through the generation of replication blocking lesions such as AP sites or single-strand breaks. The latter would be aided by the inability of TDG to dissociate freely from AP sites (12,20). *In vitro*, AP-site release is facilitated by a SUMOylation-induced conformational change in TDG, a rate-limiting step that appears useful for a temporary protection of the labile intermediate in the repair process (10,23). The protective nature of this dissociation delay, however, may turn into a disadvantage in the context of DNA replication; it might generate situations where TDG is bound to AP sites in front of an approaching replication fork where it acts as a road block, causing fork stalling and eventually collapse.

A special case of mutagenic interference during S-phase may relate to TDG's ability to remove T from G•T mismatches. While this feature provides an excellent means to counter mutagenesis by deamination of 5-meC, it may represent a disadvantage during DNA replication, where G•T mispairs arise predominantly by DNA polymerase errors. The inability of TDG to discriminate between parental and newly synthesized DNA strands would fix C to T transition mutations in cases where the T is in the parental strand. In addition, TDG induced postreplicative G•T repair in the parental DNA strand, particularly in the parental lagging strand, could destabilize the replication fork and thereby impede the replication process. Thus, G•T correction during DNA synthesis should be left to the postreplicative mismatch repair system, which is designed to correct the error in the newly synthesized DNA strand.

SUPPLEMENTARY DATA

Supplementary Data are available at NAR Online.

ACKNOWLEDGEMENTS

Thanks go to Josef Jiricny, Stefano Ferrari, Giancarlo Marra and Teresa Lettieri for stimulating discussions and support, and to Margaret Fäsi for excellent technical assistance. This study was funded by grants from the Swiss National Science Foundation (U.H., C.K) and the Schweizerische Krebsliga (U.H.). Funding to pay the Open Access publication charges for this article was provided by the University of Basel.

Conflict of interest statement. None declared.

REFERENCES

1. Krokan,H.E., Drablos,F. and Slupphaug,G. (2002) Uracil in DNA – occurrence, consequences and repair. *Oncogene*, **21**, 8935–8948.
2. Barnes,D.E. and Lindahl,T. (2004) Repair and genetic consequences of endogenous DNA base damage in mammalian cells. *Annu. Rev. Genet.*, **38**, 445–476.
3. Slupphaug,G., Eftedal,I., Kavli,B., Bharati,S., Helle,N.M., Haug,T., Levine,D.W. and Krokan,H.E. (1995) Properties of a recombinant human uracil-DNA glycosylase from the UNG gene and evidence that UNG encodes the major uracil-DNA glycosylase. *Biochemistry*, **34**, 128–138.
4. Haushalter,K.A., Todd Stukenberg,M.W., Kirschner,M.W. and Verdine,G.L. (1999) Identification of a new uracil-DNA glycosylase family by expression cloning using synthetic inhibitors. *Curr. Biol.*, **9**, 174–185.
5. Hendrich,B., Hardeland,U., Ng,H.H., Jiricny,J. and Bird,A. (1999) The thymine glycosylase MBD4 can bind to the product of deamination at methylated CpG sites. *Nature*, **401**, 301–304.

6. Hardeland,U., Bentele,M., Lettieri,T., Steinacher,R., Jiricny,J. and Schär,P. (2001) Thymine DNA glycosylase. *Prog. Nucleic Acid Res. Mol. Biol.*, **68**, 235–253.
7. Nilsen,H., Otterlei,M., Haug,T., Solum,K., Nagelhus,T.A., Skorpen,F. and Krokan,H.E. (1997) Nuclear and mitochondrial uracil-DNA glycosylases are generated by alternative splicing and transcription from different positions in the UNG gene. *Nucleic Acids Res.*, **25**, 750–755.
8. Otterlei,M., Warbrick,E., Nagelhus,T.A., Haug,T., Slupphaug,G., Akbari,M., Aas,P.A., Steinsbekk,K., Bakke,O. *et al.* (1999) Post-replicative base excision repair in replication foci. *EMBO J.*, **18**, 3834–3844.
9. Fischer,J.A., Muller-Weeks,S. and Caradonna,S. (2004) Proteolytic degradation of the nuclear isoform of uracil-DNA glycosylase occurs during the S phase of the cell cycle. *DNA Repair (Amst.)*, **3**, 505–513.
10. Hardeland,U., Steinacher,R., Jiricny,J. and Schär,P. (2002) Modification of the human thymine-DNA glycosylase by ubiquitin-like proteins facilitates enzymatic turnover. *EMBO J.*, **21**, 1456–1464.
11. Szadkowski,M. and Jiricny,J. (2002) Identification and functional characterization of the promoter region of the human MSH6 gene. *Genes Chromosomes Cancer*, **33**, 36–46.
12. Hardeland,U., Bentele,M., Jiricny,J. and Schär,P. (2000) Separating substrate recognition from base hydrolysis in human thymine DNA glycosylase by mutational analysis. *J. Biol. Chem.*, **275**, 33449–33456.
13. Mohan,R.D., Rao,A., Gagliardi,J. and Tini,M. (2007) SUMO-1-dependent allosteric regulation of thymine DNA glycosylase alters subnuclear localization and CBP/p300 recruitment. *Mol. Cell. Biol.*, **27**, 229–243.
14. Yam,C.H., Fung,T.K. and Poon,R.Y. (2002) Cyclin A in cell cycle control and cancer. *Cell. Mol. Life Sci.*, **59**, 1317–1326.
15. Leonhardt,H., Rahn,H.P., Weinzierl,P., Sporbert,A., Cremer,T., Zink,D. and Cardoso,M.C. (2000) Dynamics of DNA replication factories in living cells. *J. Cell. Biol.*, **149**, 271–280.
16. Gilbert,D.M., Neilson,A., Miyazawa,H., DePamphilis,M.L. and Burhans,W.C. (1995) Mimosine arrests DNA synthesis at replication forks by inhibiting deoxyribonucleotide metabolism. *J. Biol. Chem.*, **270**, 9597–9606.
17. Nandi,D., Tahiliani,P., Kumar,A. and Chandu,D. (2006) The ubiquitin-proteasome system. *J. Biosci.*, **31**, 137–155.
18. Gao,M. and Karin,M. (2005) Regulating the regulators: control of protein ubiquitination and ubiquitin-like modifications by extracellular stimuli. *Mol. Cell*, **19**, 581–593.
19. Hardeland,U., Bentele,M., Jiricny,J. and Schär,P. (2003) The versatile thymine DNA-glycosylase: a comparative characterization of the human, Drosophila and fission yeast orthologs. *Nucleic Acids Res.*, **31**, 2261–2271.
20. Waters,T.R., Gallinari,P., Jiricny,J. and Swann,P.F. (1999) Human thymine DNA glycosylase binds to apurinic sites in DNA but is displaced by human apurinic endonuclease 1. *J. Biol. Chem.*, **274**, 67–74.
21. Akbari,M., Otterlei,M., Pena-Diaz,J., Aas,P.A., Kavli,B., Liabakk,N.B., Hagen,L., Imai,K., Durandy,A. *et al.* (2004) Repair of U/G and U/A in DNA by UNG2-associated repair complexes takes place predominantly by short-patch repair both in proliferating and growth-arrested cells. *Nucleic Acids Res.*, **32**, 5486–5498.
22. Nilsen,H., Rosewell,I., Robins,P., Skjelbred,C., Andersen,S., Slupphaug,G., Daly,G., Krokan,H.E., Lindahl,T. *et al.* (2000) Uracil-DNA glycosylase (UNG)-deficient mice reveal a primary role of the enzyme during DNA replication. *Mol. Cell*, **5**, 1059–1065.
23. Steinacher,R. and Schär,P. (2005) Functionality of human thymine DNA glycosylase requires SUMO-regulated changes in protein conformation. *Curr. Biol.*, **15**, 616–623.

Appendix V:

Arginine Methylation Regulates DNA Polymerase β

Mol Cell. 2006 Apr 7;22(1):51-62.

Nazim El-Andaloussi[1, 4], Taras Valovka[1, 4], Magali Toueille[1], Roland Steinacher[2], Frauke Focke[2], Peter Gehrig[3], Marcela Covic[1], Paul O. Hassa[1], Primo Schär[2], Ulrich Hübscher[1] and Michael O. Hottiger[1,]

[1]Institute of Veterinary Biochemistry and Molecular Biology, University of Zurich, Winterthurerstrasse 190, 8057 Zurich, Switzerland

[2]Center for Biomedicine, Department of Clinical Biological Research, University of Basel, Mattenstrasse 28, CH-4058 Basel, Switzerland

[3]Functional Genomics Center Zurich, Winterthurerstrasse 190, 8057 Zurich, Switzerland

Molecular Cell 22, 51–62, April 7, 2006 ©2006 Elsevier Inc. DOI 10.1016/j.molcel.2006.02.013

Arginine Methylation Regulates DNA Polymerase β

Nazim El-Andaloussi,[1,4] Taras Valovka,[1,4] Magali Toueille,[1] Roland Steinacher,[2] Frauke Focke,[2] Peter Gehrig,[3] Marcela Covic,[1] Paul O. Hassa,[1] Primo Schär,[2] Ulrich Hübscher,[1] and Michael O. Hottiger[1,*]

[1] Institute of Veterinary Biochemistry and Molecular Biology
University of Zurich
Winterthurerstrasse 190
8057 Zurich
Switzerland

[2] Center for Biomedicine
Department of Clinical Biological Research
University of Basel
Mattenstrasse 28
CH-4058 Basel
Switzerland

[3] Functional Genomics Center Zurich
Winterthurerstrasse 190
8057 Zurich
Switzerland

Summary

Alterations in DNA repair lead to genomic instability and higher risk of cancer. DNA base excision repair (BER) corrects damaged bases, apurinic sites, and single-strand DNA breaks. Here, a regulatory mechanism for DNA polymerase β (Pol β) is described. Pol β was found to form a complex with the protein arginine methyltransferase 6 (PRMT6) and was specifically methylated in vitro and in vivo. Methylation of Pol β by PRMT6 strongly stimulated DNA polymerase activity by enhancing DNA binding and processivity, while single nucleotide insertion and dRP-lyase activity were not affected. Two residues, R83 and R152, were identified in Pol β as the sites of methylation by PRMT6. Genetic complementation of Pol β knockout cells with R83/152K mutant revealed the importance of these residues for the cellular resistance to DNA alkylating agent. Based on our findings, we propose that PRMT6 plays a role as a regulator of BER.

Introduction

Mammalian cells developed multiple mechanisms for the maintenance of their genome integrity (Hoeijmakers, 2001). DNA base excision repair (BER) corrects damaged bases, apurinic sites, and single-strand DNA breaks (Nilsen and Krokan, 2001). In mammalian cells, BER can proceed through at least two pathways, designated as "short-patch" and "long-patch" BER (Hoeijmakers, 2001). The two pathways are distinguished not only by the repair patch sizes but also by the contribution of factors involved (Biade et al., 1998; Klungland and Lindahl, 1997).

*Correspondence: hottiger@vetbio.unizh.ch

[4] These authors contributed equally to this work.

Mammalian DNA polymerase β (Pol β) is a small, constitutively expressed DNA polymerase (Hubscher et al., 2002) implicated in BER (Idriss et al., 2002; Sobol et al., 1996). The multifunctional, single polypeptide enzyme consists of 335 amino acids that build two functional domains connected by a protease-sensitive hinge region (Idriss et al., 2002). The N-terminal 8 kDa domain harbors the dRP-lyase activity, whereas the 31 kDa C-terminal domain constitutes the nucleotidyltransferase function (Casas-Finet et al., 1991; Matsumoto and Kim, 1995; Prasad et al., 1998). Structurally, the 31 kDa domain is composed of the fingers, palm, and thumb subdomains arranged to form a DNA binding channel reminiscent of the architecture of the Klenow fragment of *Escherichia coli* Pol I (Sawaya et al., 1994) and many other pols (Steitz, 1999). Pol β has the ability to fill in short single-stranded DNA gaps up to 12 nucleotides (Singhal and Wilson, 1993) but lacks an associated exonuclease or proofreading activity. Furthermore, it catalyzes the β elimination of 5′ dRP residues generated by the AP-endonuclease during BER (Matsumoto and Kim, 1995). Knockout (−/−) mice deficient in Pol β are nonviable, and fibroblast cell lines derived from Pol $\beta^{-/-}$ embryos display marked hypersensitivity toward monofunctional DNA alkylating agents (Sobol et al., 1996).

The enzymatic activities of Pol β have to be tightly coordinated in order to guarantee accurate repair of damaged DNA bases. The regulation of the polymerase activity of Pol β by posttranslational modification such as phosphorylation has already been described in vitro (Tokui et al., 1991). We provided earlier evidence that Pol β is acetylated by the transcriptional coactivator p300 (Hasan et al., 2002). Acetylation at K72 in vitro specifically reduces the dRP-lyase activity of Pol β, while its polymerase and AP-lyase activities were not affected (Hasan et al., 2002).

Protein arginine methylation is a posttranslational modification that results in symmetrical or asymmetrical dimethylarginines (Gary and Clarke, 1998). In humans, protein arginine methyltransferases (PRMTs) represent a family of eight known enzymes that utilize S-adenosyl methionine as a methyl donor (McBride and Silver, 2001). Despite the high degree of homology within the methyltransferase domain, there is only minor overlap in the protein substrate specificity of the mammalian PRMTs (Bedford and Richard, 2005). PRMTs were described to be involved in various signaling pathways (Aletta et al., 1998) including mitogen (Fabbrizio et al., 2002; Lin et al., 1996), steroid hormone (An et al., 2004; Metivier et al., 2003; Strahl et al., 1999), cytokine (Kwak et al., 2003; Covic et al., 2005), DNA damage (An et al., 2004), PMA (Ma et al., 2004), and interferon signaling (Mowen et al., 2001). The diversity of reported methylated substrates suggests that this typically eukaryotic modification may parallel other modifications in their level of complexity. Protein arginine methyltransferase 6 (PRMT6) was recently identified by sequence searches of the human genome for new PRMTs (Frankel et al., 2002; Miranda et al., 2004). PRMT6 displays automethylation activity and has distinct substrate specificity when

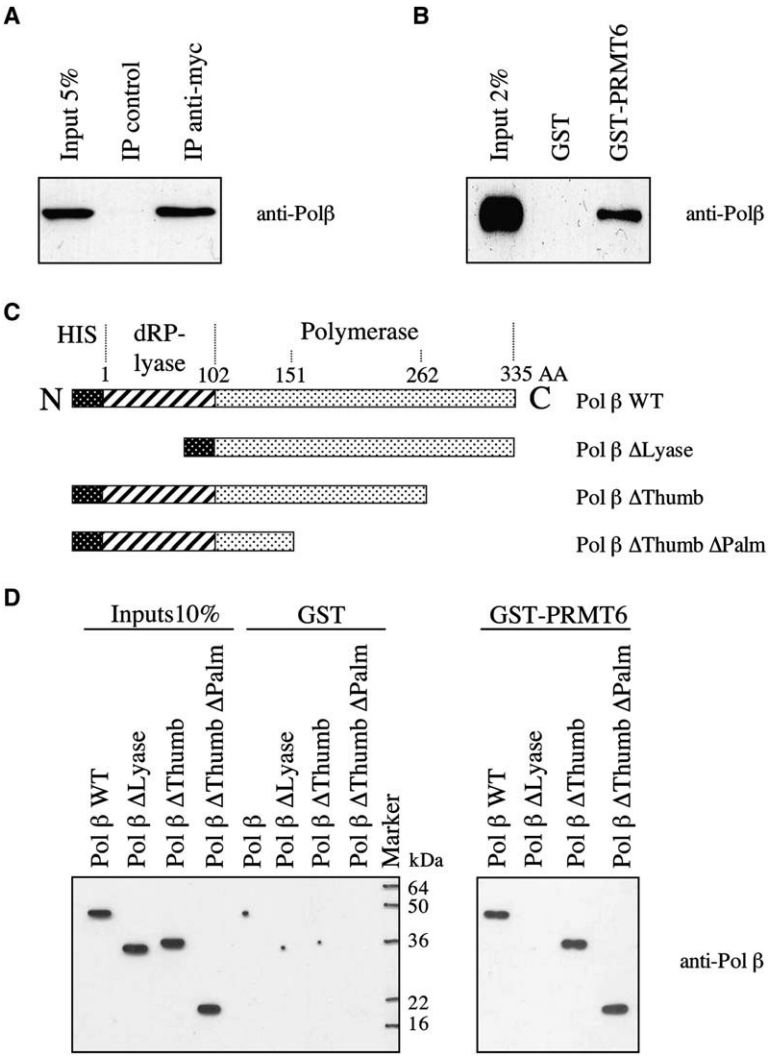

Figure 1. Pol β Directly Interacts with PRMT6 through Its dRP-Lyase Domain

(A) Myc-PRMT6 was immunoprecipitated from 293T extracts supplemented with recombinant 6His-Pol β using an anti-myc antibody (or a mouse antibody as a control). Coimmunoprecipitated proteins were analyzed by immunoblot using an anti-Pol β antibody.

(B) GST pull-down experiment using 6His-tagged Pol β and GST-PRMT6 (or GST as a control).

(C) Schematic representation of Pol β and deletion mutants.

(D) Full-length Pol β and deletion mutants of Pol β were analyzed in GST pull-down experiments using GST-PRMT6 (or GST as control).

compared to PRMT1 and PRMT4/CARM1 (Frankel et al., 2002).

To date, several proteins involved in BER have been shown to be regulated by different posttranslational modifications (Fan and Wilson, 2005). In this study, we show that Pol β forms a complex with and is methylated by PRMT6. Furthermore, we demonstrate that in vitro-methylated Pol β possesses significantly higher DNA polymerase activity when compared to that of unmodified enzyme. The increase in DNA polymerase activity upon methylation was due to the enhanced DNA binding and processivity of Pol β. Mutation of methylation sites identified in Pol β significantly reduced the ability of enzyme to protect complemented Pol $\beta^{-/-}$ cells against MMS-induced DNA damage. Together, our results suggest that PRMT6, a member of the methyltransferase family, might play a direct role in the regulation of DNA repair processes.

Results

Pol β Forms a Complex with PRMT6

To examine whether members of the PRMTs are able to interact with Pol β, we performed immunoprecipitations of PRMTs from total extracts of 293T cells transfected with different myc-tagged PRMTs and supplemented with recombinant Pol β. Pol β was specifically coimmunoprecipitated with PRMT6, suggesting that both proteins may form specific complexes (Figure 1A and data not shown).

To investigate whether PRMT6 directly interacts with Pol β, we performed in vitro GST pull-down experiments. Purified full-length His-tagged Pol β was incubated with affinity-purified GST-PRMT6 fusion protein or GST alone immobilized on glutathione-Sepharose beads. After extensive wash of the beads, bound proteins were separated by SDS-PAGE, and Pol β was detected by immunoblot analysis. We observed that purified GST-PRMT6, but not GST, efficiently pulled down Pol β (Figure 1B), suggesting that PRMT6 directly interacts with Pol β.

The Lyase Domain of Pol β Is Required for the Interaction with PRMT6

To further characterize the interaction of Pol β with PRMT6, different deletion mutants of Pol β were generated, expressed in *E. coli*, and purified as His-tagged proteins (Figure 1C). Two of these mutants lacked the C-terminal thumb or both thumb/palm subdomains,

respectively. A third mutant lacked the N-terminal lyase domain. GST pull-down experiments were performed with these deletion mutants of Pol β using GST-PRMT6 or GST alone as a negative control. This experiment revealed that Pol β lacking the lyase domain was no longer able to interact with PRMT6 (Figure 1D). In contrast, deletion of the thumb or thumb/palm regions in Pol β did not affect the interaction of Pol β with PRMT6. Together, these results indicate that the lyase domain of Pol β is strictly required for the interaction with PRMT6.

Pol β Is Methylated In Vitro by PRMT6

Since PRMT6 and Pol β interacted directly, we next investigated whether Pol β could serve as a substrate for PRMT6 in an in vitro methylation assay. GST-PRMT6 expressed and purified from bacteria was incubated with recombinant Pol β in the presence of radiolabeled S-adenosyl methionine (C^{14}-SAM) as a donor of the methyl group. Core histones and Fen-1 were used as positive and negative controls of methylation, respectively. Pol β was strongly methylated by GST-PRMT6 bound to glutathione beads (Figure 2A). Moreover, methylation of Pol β was observed with baculovirus expressed and purified full-length PRMT6 (data not shown), indicating that methylation of Pol β was indeed mediated by PRMT6. Quantitation of the methylation efficiency revealed that 20% of the Pol β molecules were methylated in standard reactions in the presence of a 10-fold molar excess of C^{14}-SAM (one site of modification was considered).

Identification of PRMT6 Methylation Sites in Pol β

To identify the methylated residues, in vitro-methylated Pol β was digested with trypsin or chymotrypsin, and the resulting peptides were analyzed by LC/MS/MS. Two monomethylated peptides, LPGVGTKIAEKIDEFLATG KL(metR83) and RIP(metR152)EEMLQMQDIVLNEVK, were found. The identified peptides harbored a triple positive charge and had a significant Xcorr factor higher than the threshold limit of 2.5. Furthermore, their theoretical masses corresponded to those measured by mass spectrometry. Together, these data indicate that arginine 83 and 152 were methylated by PRMT6.

To confirm these findings, the corresponding arginines were replaced with lysine residues by site-directed mutagenesis. Substitution of arginine to lysine maintains the positive charge at the position and causes only minimal changes in the local environment of the protein. Wild-type or mutated Pol β harboring R83K, R152K, or both R83/152K substitutions were expressed and purified from *E. coli*. Subsequently, all proteins were subjected to in vitro methylation by PRMT6. While methylation of Pol β mutated at single R83 or R152 was only slightly affected, mutation of both R83 and R152 significantly reduced methylation of Pol β (Figure 2B). These results clearly indicated that R83 and R152 were targets for modification by PRMT6 in vitro. Nevertheless, after prolonged exposure, some residual methylation of the R83/152K Pol β mutant was detected. The presence of an additional methylation site(s) in Pol β can therefore currently not be excluded. Together, these data provide strong evidence that R83 and R152 of Pol β were the principal targets for PRMT6-mediated methylation.

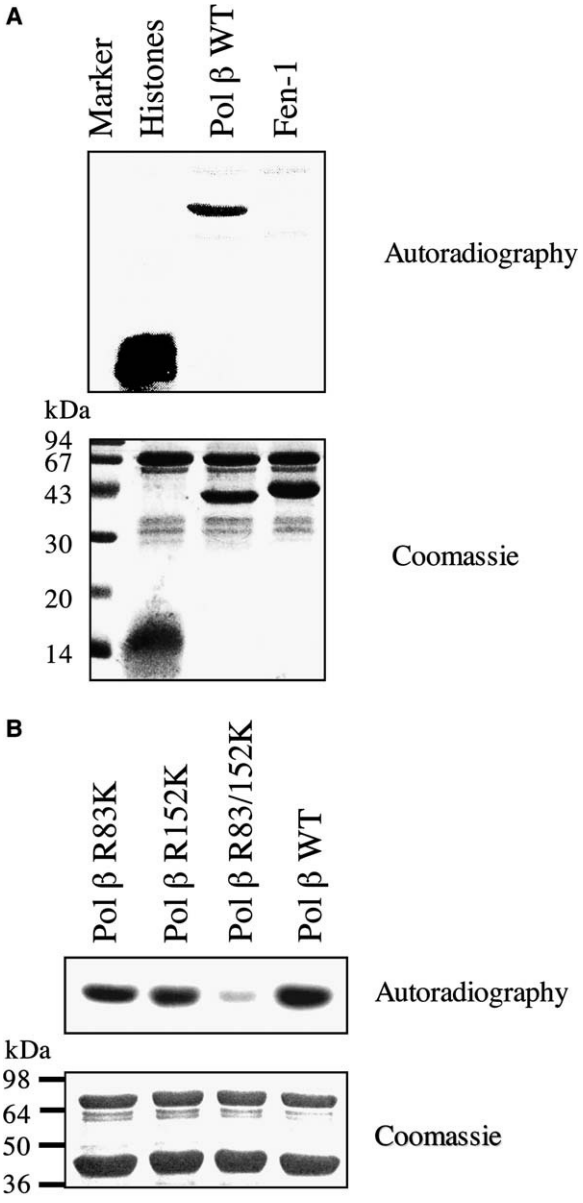

Figure 2. Pol β Is Methylated In Vitro by PRMT6 at R83 and R152

(A) GST-tagged PRMT6 was incubated with C^{14}-SAM and histones (10 μg), Pol β (5 μg), or Fen-1 (10 μg). The proteins were resolved using 15% acrylamide SDS-PAGE gels, stained with Coomassie blue (lower panel), and analyzed by autoradiography (upper panel).

(B) In vitro methylation of wild-type Pol β and Pol β mutants harboring mutations at methylation sites by GST-PRMT6. The proteins were resolved using 12% acrylamid SDS-PAGE gel, stained with Coomassie blue (lower panel), and analyzed by autoradiography (upper panel).

Pol β Is Methylated In Vivo by PRMT6

In order to investigate whether Pol β is methylated in vivo, 293T cells were transfected with either a vector expressing HA-tagged Pol β or an empty vector. The cells were treated with 0.5 mM MMS for 1 hr and then were metabolically labeled with L-[*methyl*-^{3}H]-methionine for 3.5 hr in the presence of translation inhibitors as described by Kzhyshkowska et al. (2001). Recombinant Pol β was immunoprecipitated with an anti-HA antibody,

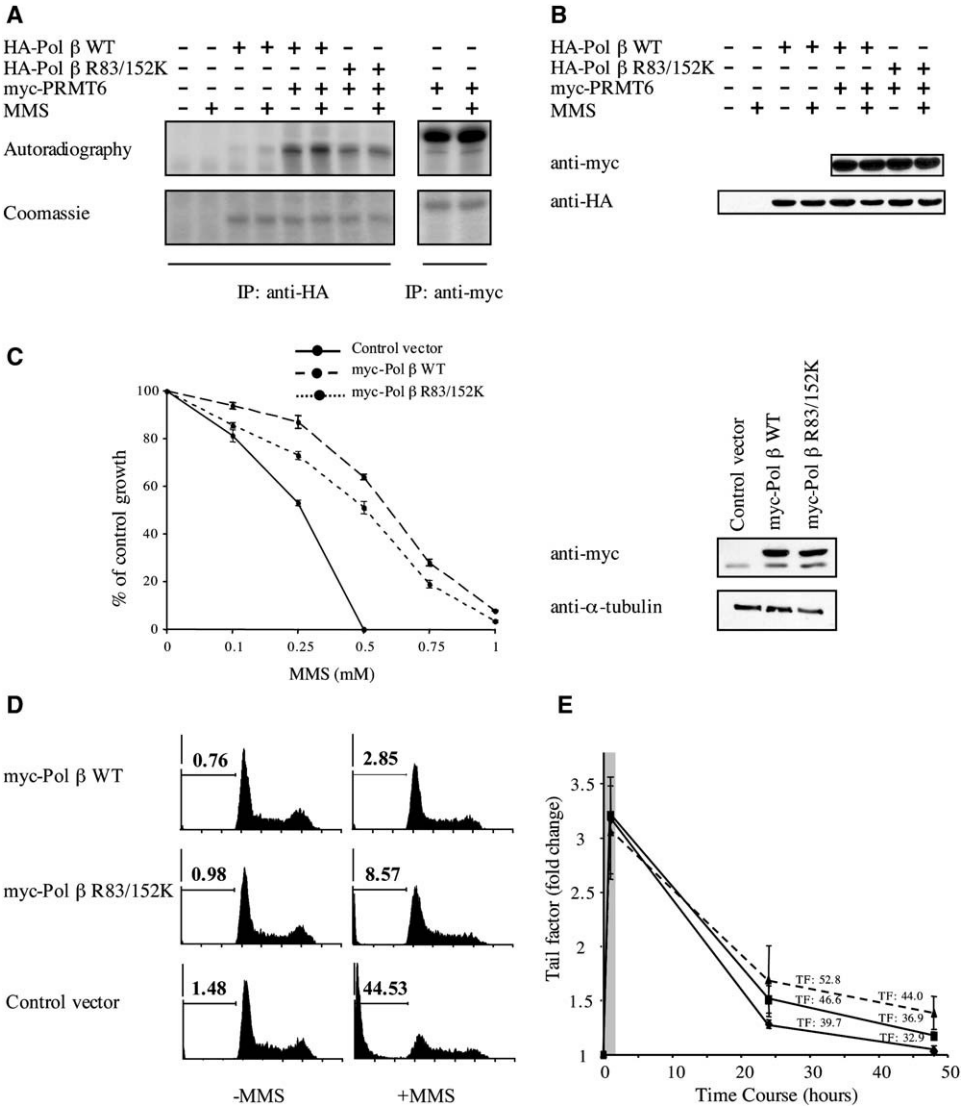

Figure 3. Functional Relevance of Pol β Methylation In Vivo

(A) Methylation of Pol β by PRMT6 in vivo. 293T cells were labeled 24 hr after transfection with L-[*methyl*-^{3}H]-methionine as described in Experimental Procedures. Recombinant HA-tagged Pol β and myc-tagged PRMT6 were immunoprecipitated from the cell lysates and analyzed by SDS-PAGE (lower panel) followed by autoradiography (upper panel).

(B) Expression of HA-Pol β and myc-PRMT6 was analyzed in total cell lysates by immunoblot with anti-HA and anti-myc antibodies, respectively.

(C) Growth inhibition curves of Pol $\beta^{-/-}$ cells (solid line) or Pol $\beta^{-/-}$ cells stably complemented with either wild-type Pol β (broken line) or the R83/152K Pol β mutant (dotted line) treated with different concentration of MMS (left panel). Error bars represent SEM of three independent experiments. Expression of recombinant myc-Pol β wt and myc-Pol β R83/152K mutant in the complemented cell lines (right panel).

(D) Effect of MMS on induction of apoptosis in complemented Pol $\beta^{-/-}$ MEFs. Pol $\beta^{-/-}$ MEFs complemented with control vector, wild-type, or the R83/152K mutant of Pol β were exposed to 0.5 mM MMS for 1 hr and then incubated in normal medium without the drug. Cells, both adherent and floating, were harvested after 24 hr and analyzed by flow cytometry. The percentage of the sub-G1 fraction is indicated.

(E) Occurrence and persistence of DNA strand breaks upon MMS exposure. Complemented Pol $\beta^{-/-}$ cell lines were exposed to 0.25 mM MMS for 1 hr and then examined by alkaline COMET assays. The graphs represent COMET TF changes relative to mock-treated controls at different time points before and after MMS treatment. Shaded and nonshaded areas indicate exposure and postexposure periods, respectively. The TFs indicated and the fold changes plotted were calculated from three independent experiments, each comprising more than 2500 scored COMET events (nuclei). Error bars represent SEM.

separated by SDS-PAGE, and analyzed by autoradiography. While Pol β methylation was detectable in untreated cells (Figure 3A), the levels increased after MMS treatment (Figure 3A). To investigate the involvement of PRMT6 in Pol β methylation in vivo, wild-type Pol β or R83/152K mutant was cotransfected with PRMT6. Expression of recombinant proteins was controlled by Western blotting with indicated antibodies (Figure 3B). In vivo activity of recombinant PRMT6 expressed in 293T cells was monitored as automethylation of the enzyme (Figure 3A). The level of Pol β methylation was substantially higher in cells overexpressing PRMT6 when compared to that in cells transfected with Pol β alone (Figure 3A). Importantly, the R83/152K mutant was methylated to a less extent than wild-type Pol β under comparable conditions. However, the residual

methylation of the R83/152K mutant suggested the presence of an additional methylation site(s) in Pol β that can be modified by PRMT6 in vivo. Together, these results indicate that Pol β is an in vivo substrate for arginine methylation by PRMT6.

R83 and R152 Are Important for Pol β-Mediated Repair of MMS-Induced DNA Damage

To investigate whether Pol β methylation of R83 and R152 is biologically relevant, we subjected Pol $\beta^{-/-}$ cells to genetic complementation by retroviral transduction with wild-type or the double mutant (R83/152K) cDNAs of Pol β. After selection of infected cells, the expression of recombinant Pol β was analyzed by Western blotting with an anti-myc antibody. This confirmed that the expression levels of the recombinant wild-type and mutant Pol β proteins were comparable in these cell lines (Figure 3C, right panel). Also, there was no difference in growth for cells complemented with wild-type Pol β or R83/152K mutant under the normal growth conditions (data not shown). Pol $\beta^{-/-}$ cells and the complemented cells were subsequently treated with different concentrations of MMS, and cell growth inhibition was analyzed as described by Sobol et al. (2000). Cells transduced with the control vector were hypersensitive to MMS and stopped growing at a concentration of 0.5 mM MMS (Figure 3C, right panel). In contrast, complementation of Pol $\beta^{-/-}$ cells with recombinant wild-type Pol β reduced the MMS hypersensitivity as previously described (Sobol et al., 2000; Figure 3C and data not shown). In the presence of 0.5 mM MMS, growth retardation of wild-type Pol β-expressing cells was only about 35%. Complementation with the double mutant variant (R83/152K), however, was much less efficient. These cells were significantly more sensitive to MMS than those complemented with the wild-type Pol β (Figure 3C, left panel). These results clearly demonstrated that both residues R83 and R152 are important for the function of Pol β in vivo after MMS treatment.

The effect of MMS on the cell cycle distribution and the induction of apoptosis in these cell lines were further analyzed by FACS analysis. MMS induced transient S phase delay followed by a late arrest in both G1 and G2/M phases (data not shown). After 24 hr of recovery, the majority of cells restored normal cell cycle progression similar to that of untreated cells. However, we observed a substantial increase of cells with a sub-G1 DNA content, which is an indicator of apoptosis (Figure 3D). The amount of cells with a sub-G1 DNA content was 44.5%, 2.9%, and 8.6% for the cells complemented with control vector, wild-type, or the R83/152K mutant of Pol β, respectively.

Next, we examined the role of R83/152K methylation in repair of MMS-induced DNA strand breaks. Using the same set of control and complemented Pol $\beta^{-/-}$ cell lines, we assessed steady-state levels of DNA fragmentation immediately before and at different time points after exposure of cells to MMS. To be able to detect all possible intermediates of BER, i.e., abasic sites and DNA single- and double-strand breaks, as quantitatively as possible, we performed COMET assays under alkaline conditions. We then evaluated both the COMET tail factors (TFs) and the overall distribution of COMET events into defined stages of DNA fragmentation (Figure 3E and see Figure S1 in the Supplemental Data available with this article online). These stages range from cells with no DNA fragmentation (stage A, <5% fragmentation) to cells with heavy DNA fragmentation (stage E, >95% fragmentation). To avoid a contribution of apoptotic cells to the outcome of the COMET assay, we adjusted the concentration of MMS to a level that was tolerable by all three cell lines and excluded rarely occurring apoptotic nuclei from the analysis. Figure 3E shows the COMET TFs as calculated from the distribution of individual cells/events into the five distinct COMET stages (Anderson et al., 1994). The TFs thus represent an average degree of DNA fragmentation in the cell populations. Untreated controls revealed that all three cell lines had relatively high levels of spontaneous DNA strand breaks, with TFs ranging between 31.4 and 32.3. Immediately after MMS exposure, all cell lines showed severe amounts of DNA damage, translating into TFs higher than 95. Twenty-four and 48 hr posttreatment, however, differences between the cell lines became apparent. The cells complemented with wild-type Pol β showed a stronger reduction of the TFs than those complemented with the R83/152K mutant ($p < 0.05$, Student's t test), i.e., they had significantly lower levels of persisting DNA strand breaks up to 48 hr after exposure. The more thorough examination of the COMET stage distributions confirmed a highly significant difference between wild-type and R83/152 complemented cells 24 and 48 hr posttreatment ($p < 0.001$, contingency tables, chi-square test, Figures S1A and S1B, and data not shown).

Methylation of R83 and R152 Does Not Affect the Functionality of Pol β in Short-Patch BER

We used an in vitro-reconstituted short-patch BER assay to investigate a possible role of R83 and R152 methylation in this repair process (Figure 4). A BER intermediate was first generated by digestion of a 60-mer G•U mismatched oligonucleotide with uracil DNA glycosylase (UDG). The resulting AP site containing DNA was then treated either sequentially or simultaneously with purified recombinant human AP-endonuclease, methylated or unmethylated human Pol β, and the XRCC1/LIG3 complex. These reactions were done in the presence of either dCTP or dNTPs and varying concentrations of Pol β, providing an excess or limiting amounts of the polymerase relative to the substrate. Testing a wide range of conditions, we were not able to see any qualitative or quantitative effect of Pol β methylation (Figure 4) on BER. The same was true when we applied variants of the BER assay to monitor nucleotide insertion, strand displacement synthesis, and dRP lyase activity separately (Hasan et al., 2002) (data not shown). We therefore concluded that, in the context of a short-patch repair process, neither single nucleotide insertion nor dRP-lyase activity nor strand displacement synthesis is affected by PRMT6-mediated methylation of Pol β.

Methylation of R83 and R152 Stimulates DNA Polymerase Activity of Pol β in a Primer Extension Assay

To gain further insight into the importance of PRMT6-mediated methylation of Pol β, we investigated whether methylation of R83 and R152 affects the DNA

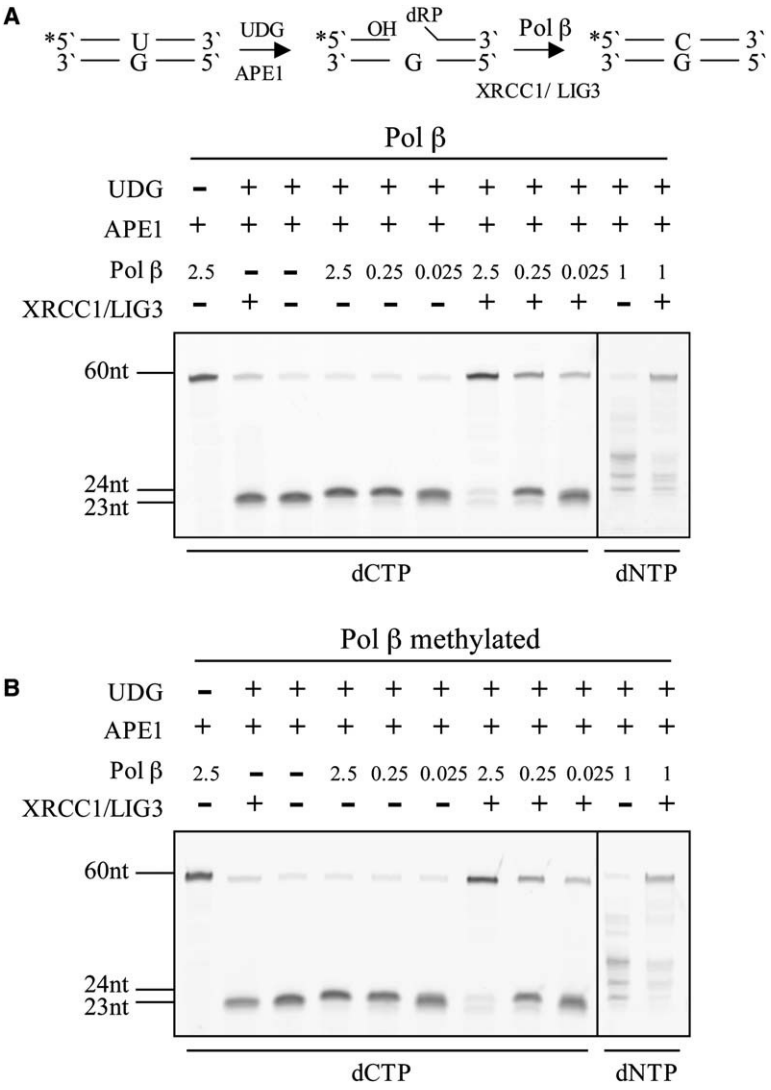

Figure 4. Methylation of Pol β Does Not Affect Its Functionality in Short-Patch BER

BER intermediate was generated by incubating 1 pmol of G•U mismatched oligonucleotide (60 nt) with 0.5 units UDG and 0.2 pmol APE1. The resulting incised AP site product was further incubated with varying concentrations of unmodified (A) or methylated (B) Pol β and 0.75 pmol of XRCC1/LIG3 complex in the presence of dCTP or dNTPs as indicated. BER intermediates were separated on a denaturing 14% polyacrylamide gel, visualized, and quantified on a fluorescent scanner. Fragments migrating at a length of 23 nt represent AP site incisions and those at 24 nt single nucleotide insertions; the ladder (panels on the right) documents the capacity of Pol β to incorporate multiple nucleotides by limited strand displacement.

polymerase activity of Pol β in a primer extension assay. To address this question, different amounts of the wild-type, single R83K and R152K or double R83/152K mutants of Pol β were methylated by PRMT6 in vitro and subsequently analyzed using a 17/73-mer primer/template. Methylated wild-type Pol β possessed significantly higher DNA polymerase activity when compared to that of the nonmethylated wild-type enzyme (Figure 5A). The observed effect was not due to the presence of PRMT6, since the nonmethylated samples were also incubated with the same amount of PRMT6 but without SAM. Moreover, the presence of SAM in the reaction mixture did not interfere with the DNA polymerase activity of Pol β (Figure 5A, left panel). Interestingly, both single mutants of Pol β (R83K and R152K) showed a substantially lower rate of DNA synthesis after PRMT6 methylation when compared to the wild-type Pol β. It is also important to notice that the DNA polymerase activities of the R83K and R152K mutants were comparable under the tested conditions. This may suggest an equal importance of these residues for PRMT6-mediated stimulation of Pol β DNA polymerase activity. Moreover, we have observed a complete abolishment of the methylation-dependent increase in DNA synthesis when the double R83/152K mutant of Pol β was tested. This indicated that the observed effect of PRMT6 on Pol β polymerase activity was directly mediated by methylation of R83 and R152 residues.

Methylation of Pol β Enhances Its DNA Binding and Processivity

To understand the mechanism of Pol β stimulation by PRMT6, we investigated the effect of methylation on the ability of Pol β to bind a DNA template. Purified Pol β was methylated by PRMT6 in vitro and subsequently tested in an electromobility shift assay (EMSA). The experiments demonstrated that methylation of Pol β by PRMT6 strongly stimulated binding of the polymerase to DNA (Figure 5B). Pol β mutation of either R83 or R152 to lysine decreased PRMT6-mediated stimulation of DNA binding. Furthermore, we found that methylation of R83 and R152 had an additive effect on the affinity of the polymerase to the DNA template. Indeed, simultaneous mutation of both R83 and R152 residues leads to a further decrease in DNA binding of Pol β under the tested conditions. These results correlated well with

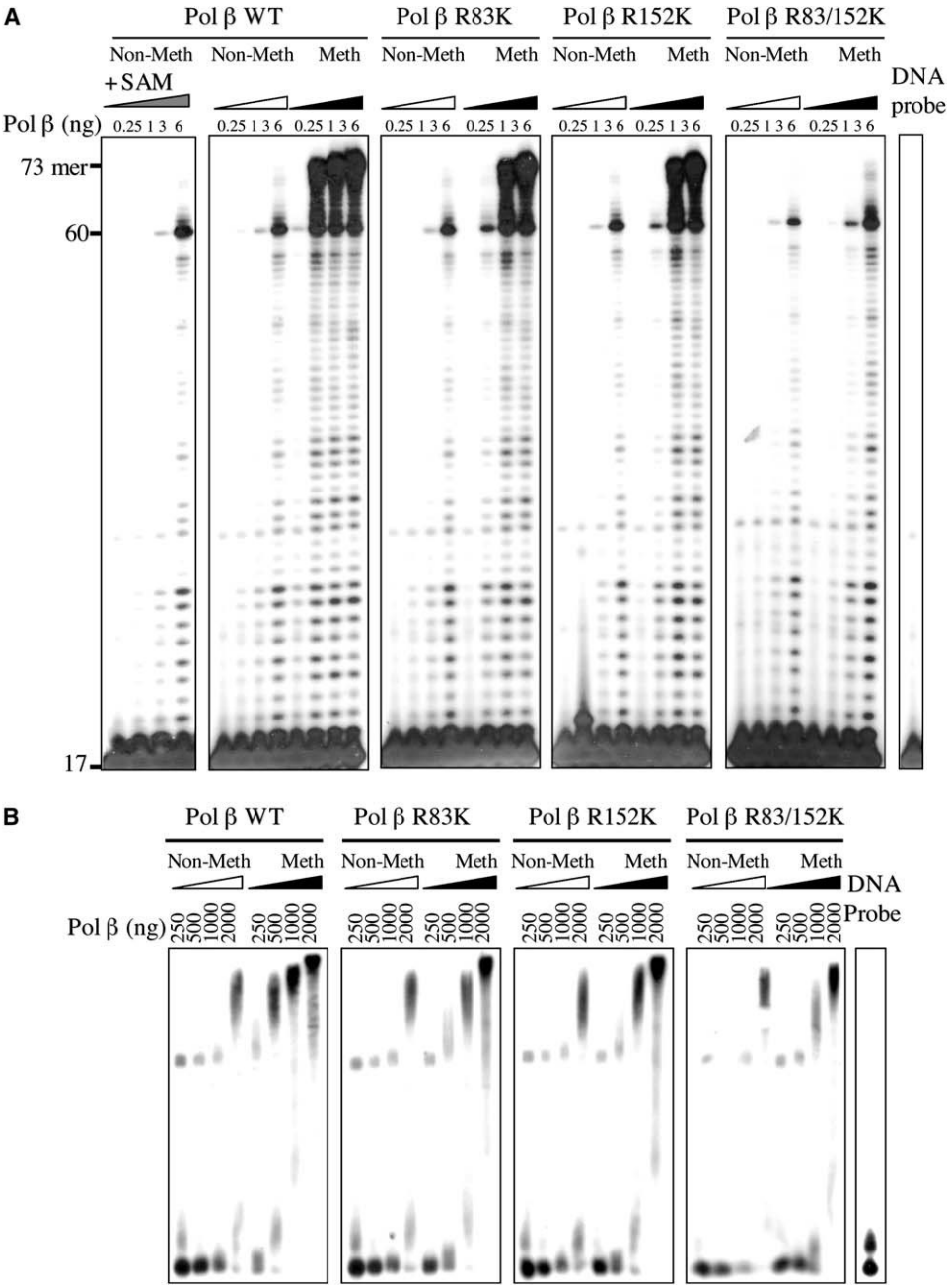

Figure 5. PRMT6 Methylation of Pol β Stimulates Its Polymerase Activity by Enhancing Its DNA Binding Activity

(A) DNA polymerase activities of wild-type Pol β or mutants R83K, R152K, and R83/152K were measured in a primer extension assay using a 17/73-mer DNA template. Recombinant proteins were methylated with GST-PRMT6 prior to the DNA polymerase reaction as described in Experimental Procedures.

(B) EMSA using wild-type Pol β or mutants R83K, R152K, and R83/152K. Recombinant proteins were methylated with GST-PRMT6 prior to the EMSA as described in (A).

the methylation-induced DNA polymerase activity of Pol β observed in Figure 5A.

Finally, the effect of methylation on the processivity of Pol β was tested. In the presence of a 100-fold molar excess of unlabeled DNA as a trap, methylation of Pol β increased the processivity by a factor of 20 (Figure 6), while the R83/152K mutant of Pol β did not possess a PRMT6-mediated increase in processivity. These data clearly demonstrated that methylation of Pol β at R83 and R152 substantially increased its binding to DNA.

Discussion

In this study, we have addressed the role of PRMT6 in the regulation of human Pol β. We found that Pol β forms a complex with PRMT6. Their direct physical interaction was confirmed with bacterially expressed

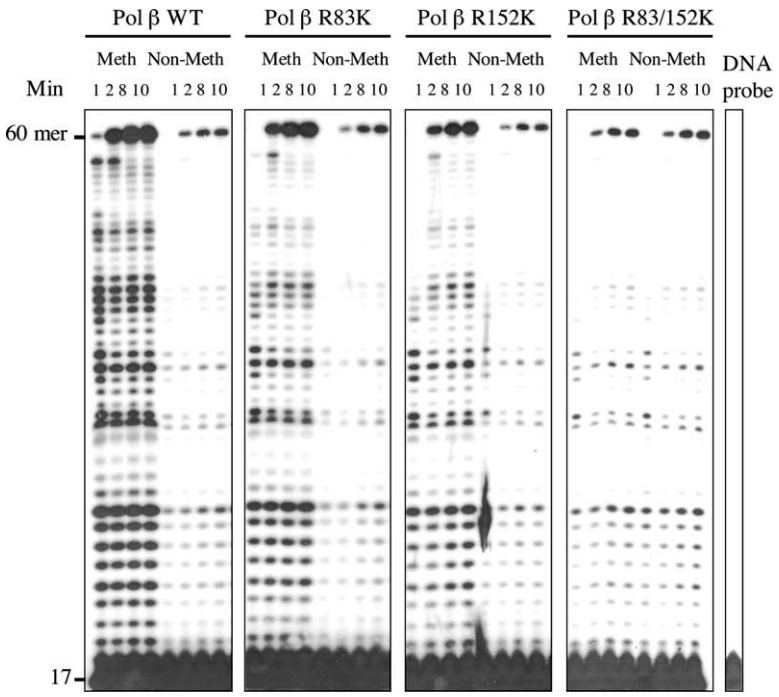

Figure 6. Methylation of Pol β Increases Its Processivity

Primer extension assay was performed using 2 ng (50 fmol) of wild-type (wt) polβ or mutants R83K, R152K, and R83/152K in the presence of 2 pmol of trap DNA template. Recombinant proteins were methylated with GST-PRMT6 prior to the DNA polymerase reaction as described in Experimental Procedures.

recombinant proteins. Mutation analysis of Pol β indicated that the lyase domain was strictly required for the interaction with PRMT6. Lyase domains have also been identified in pols γ (Longley et al., 1998), ι (Bebenek et al., 2001), and λ (Garcia-Diaz et al., 2001). Whether or not these also interact with PRMT6 remains to be elucidated.

Pol β was methylated in vitro by PRMT6 at R83 and R152. The X-ray structure of Pol β (Davies et al., 1994; Sawaya et al., 1994) shows that both arginines are exposed on the surface, allowing easy access for PRMT6. Surprisingly, no common motifs were found between the amino acid sequences surrounding R83 and R152. Moreover, both arginine residues do not reside within a glycine-rich (GAR) consensus sequence observed in other type I arginine-methylated proteins (Clarke, 1993; Gary and Clarke, 1998). Consistently, PRMT4/CARM1 was not able to methylate Pol β in vitro under the similar conditions (data not shown). These results confirmed the unique substrate specificity of PRMT6 and correlated with an earlier report demonstrating that PRMT6 did not recognize the same substrate motifs as PRMT4/CARM1 and displayed limited substrate overlap with PRMT1 (Frankel et al., 2002).

The relevance of these findings was confirmed by the ability of PRMT6 to methylate Pol β in vivo. Pol β methylation was stimulated in cells treated with the DNA alkylating agent MMS, suggesting that methylation of Pol β follows genotoxic stress. The inducible nature of Pol β methylation would require the presence of mechanisms that negatively control this modification. Recently, PADI4 was shown to deiminate unmodified arginine and monomethyl (but not dimethyl) arginine to citrulline in histone H3 antagonizing the transcriptional activation mediated by arginine methylation (Cuthbert et al., 2004). Whether deimination antagonizes arginine methylation of Pol β remains to be investigated.

Stable complementation of Pol $\beta^{-/-}$ cells with either a control vector, wild-type Pol β, or the R83/152K mutant has revealed that methylation at R83 and R152 is important for the ability of the enzyme to protect cells against MMS-induced DNA damage. Importantly, the introduction of the R83K and R152K mutations did not affect the specific intrinsic activities of Pol β, i.e., the DNA polymerase activity, the dRP-lyase activity, and the binding to DNA template (Figures 5A and 5B and data not shown). This minimizes the possibility that the R83/152K Pol β mutant harbors defects other than methylation.

Pol β was not required for the activation of cell cycle checkpoints, since similar profiles of cell cycle distribution were observed for the complemented Pol $\beta^{-/-}$ cells after MMS treatment. However, methylation of Pol β very strongly influenced the efficiency of the repair of MMS-induced DNA damage. Cells complemented with the R83/152K variant of Pol β were less efficient in DNA strand break repair following MMS exposure and, consequently, had a higher propensity to enter apoptosis.

It was previously reported that the dRP-lyase activity of Pol β is sufficient to reverse hypersensitivity of Pol $\beta^{-/-}$ cells to MMS, suggesting that removal of the dRP group is a pivotal step in BER in vivo (Sobol et al., 2000). However, BER can not be completely restored in Pol $\beta^{-/-}$ cell extracts by a Pol β mutant lacking DNA polymerase activity, strengthening the importance of the DNA synthesis mediated by Pol β (Podlutsky et al., 2001). To further understand the differences between cells complemented with wild-type Pol β or the R83/152K mutant in response to MMS, we investigated how methylation may influence specific enzymatic activities of Pol β. In the context of a short-patch BER process, single nucleotide incorporation, limited strand displacement synthesis, and dRP-lyase functions of Pol β were not notably affected by PRMT6-mediated

methylation. However, methylated Pol β induced an enhanced binding to a primer extension substrate and thus an increased DNA polymerase activity and processivity when compared to the nonmethylated enzyme. These results are in a good agreement with earlier studies, which suggest that R83 is one of the critical residues involved in DNA binding of Pol β (Beard and Wilson, 2000). Furthermore, our results provide first evidence that R152 might also be important for the binding of Pol β to DNA.

Together, our results suggest that methylation-induced changes in DNA synthesis activity of Pol β are responsible for the modulation of Pol β-dependent cell sensitivity to MMS. However, other methylation-dependent mechanisms may also play a role in determining efficiency of cellular BER. In fact, methylation-induced increase in DNA binding of Pol β may not only affect Pol β-specific activities but also be important for other functional properties of the polymerase. For example, a stronger affinity of methylated Pol β to DNA may have a direct implication in BER via stabilization of Pol β-specific protein complexes at the sites of DNA damage. Pol β was previously found to form a complex with the XRCC1-LIG3 heterodimer (Kubota et al., 1996). In vitro reconstitution experiments indicated that a mutant XRCC1-LIG3 heterodimer, in which XRCC1 has a point mutation (V86R) resulting in an inability to interact with Pol β, exhibits inefficient ligation activity compared to the wild-type XRCC1-LIG3 heterodimer (Dianova et al., 2004). Consistently, XRCC1-deficient CHO cells transfected with the V86R mutant of XRCC1 are more sensitive to DNA damage than wild-type complemented counterparts (Dianova et al., 2004). These observations imply a mechanism by which Pol β helps to recruit the XRCC1-LIG3 complex to the DNA substrate to facilitate BER. It will be of interest to investigate whether methylation of Pol β affects the recruitment of this and other BER factors to DNA. Alternatively, methylated Pol β could more efficiently protect DNA due to the higher affinity of the enzyme to DNA repair intermediates generated in BER. Further studies will be needed to clarify this issue.

Previous studies indicate that alkylating agents activate both the short-patch and the long-patch BERs (Miller and Chinault, 1982; Hammond et al., 1990). It is also well known that Pol β is involved in both of these BER processes as the primary polymerase. This raises the question for the role of Pol β methylation in the short-patch and the long-patch BERs. Here, we demonstrated that single nucleotide incorporation was not affected by methylation of Pol β as assessed in reconstituted short-patch BER with a nonchromatinized template. This suggests that methylation of Pol β has no functional consequences for short-patch BER. However, consistent with the effects seen in primer extension assays, methylation of Pol β is likely to improve its efficiency (and accuracy) in repair processes in which processive DNA synthesis provides an advantage, i.e., in long-patch BER.

To date, the role of protein arginine methylation in DNA damage checkpoint responses and DNA repair is largely unknown. In this view, our findings represent an interesting aspect that is additionally emphasized by the fact that the specific cellular role of PRMT6 is still unknown. When fused to GFP, PRMT6 resided solely in the nucleus (Frankel et al., 2002), suggesting that this methyltransferase may participate in nuclear processes. Interestingly, HIV-type I Tat protein has recently been found as an exogenous PRMT6 substrate (Boulanger et al., 2005). In contrast to its acetylation, methylation of Tat by PRMT6 negatively regulated its transactivation activity (Boulanger et al., 2005). Our study presents strong evidence that Pol β is a specific endogenous substrate for PRMT6, suggesting the involvement of PRMT6 in the regulation of BER. A similar scenario was recently discussed for PRMT1 (Boisvert et al., 2005). PRMT1 was shown to methylate MRE11, and the mutation of the methylation sites severely impaired the exonuclease activity of MRE11. Interestingly, the cells containing hypomethylated MRE11 displayed intra-S phase DNA damage checkpoint defects (Boisvert et al., 2005). It would also be important to investigate whether PRMT6 can functionally interact with other repair proteins involved in BER.

In conclusion, we propose that PRMT6 plays a regulatory role in BER via physical interaction with Pol β and stimulation of Pol β polymerase activity by methylation.

Experimental Procedures

Oligonucleotides and Plasmids

The full-length Pol β and the Pol β ΔLyase domain were cloned into pQE30 vector (Invitrogen) as previously described (Hasan et al., 2002). Pol βΔThumb and Pol βΔThumbΔPalm fragments were amplified by PCR from the pQE30-6HIS-Pol β plasmid and were then cloned into BamHI site of pQE30 vector.

R83K, R152K, and double R83/152K mutants of Pol β were generated by site-directed mutagenesis according to the standard procedure.

The pRRL lentiviral transfer vector used in this study has been previously described (Zufferey et al., 1998). Myc-Pol β wt and myc-Pol β R83/152K were cloned into pRLL vector by substituting GFP gene. IRES fused to the blasticidin resistance gene has been introduced into SalI site immediately downstream of Pol β gene. Control vector contains the IRES/blasticidin resistance gene insert instead of the GFP gene. The envelope plasmid pMD.G and the packaging plasmid pCMV ΔR8.91 have been previously described (Zufferey et al., 1997).

The 73-mer and the corresponding 17-mer primer substrates for DNA polymerase and EMSA were from Microsynth (Switzerland). The sequences are the following: 73-mer, 5′-GATCGGGAGGGTAG GAATATTGAGGATGAAAGGGTTGAGTTGAGTGGAGATAGTGGAG GGTAGTATGGTGGATA-3′; and 17-mer, 5′-TATCCACCATACTAC CC-3′.

Proteins

N-terminal 6His-tagged human Pol β full-length and amino acid point mutants were expressed in *E. coli* TG1 strain and purified by fast protein liquid chromatography (FPLC) on Ni-NTA HiTrap (Amersham Biosciences) and Mono-SP HiTrap columns (Amersham Biosciences). N-terminal 6His-tagged Fen1 was overexpressed in *E. coli* BL21(DE3) pLysS strain and purified as mentioned above. GST fusion proteins were expressed in *E.coli* TG1 strain. N-terminal 6His-tagged PRMT4 and -6 were expressed in SF9 insect cells and purified on Ni-NTA ProBond Resin (Invitrogen). Calf thymus histones (Type II-AS) were purchased from Sigma.

Antibodies

Pol β-specific antibody was purchased from Neo Markers. Mouse IgG (sc-2025), anti-myc (sc-9E10), and anti-tubulin (sc-8035) antibodies were obtained from Santa Cruz Biotechnology.

Cells

Pol $\beta^{-/-}$ mouse embryonic fibroblasts were described previously (Sobol et al., 1996). The cells were grown in Dulbecco's modified Eagle's medium supplemented with GlutaMAX, 10% fetal bovine serum, 100 units/ml penicillin, 100 μg/ml streptomycin, and 80 μg/ml hygromicin. 293T cells were cultivated in Dulbecco's modified Eagle's medium supplemented with GlutaMAX, 10% fetal bovine serum, 100 IU/ml penicillin, and 100 μg/ml streptomycin.

Lentivirus Production and Infection of Pol β Null Cells

Generation of viruses and transduction of cells were described previously (Zufferey et al., 1997). After several rounds of selection, expression of myc-tagged wild-type and mutant Pol β R83/152K was screened by immunoblot analysis.

Growth Inhibition Assay

Cytotoxicity was determined by growth inhibition assays as described previously (Sobol et al., 2000). Briefly, Pol β cells complemented with control vector, wild-type, or R83/152K mutant of Pol β were seeded at a density of 40,000 cells/well in 6-well dishes 36 hr prior to the treatment. Cells were exposed for 1 hr to a range of concentrations of MMS. After 1 hr treatment, cells were washed once with PBS, and then fresh medium was added. After 72 hr of recovery at 37ºC in a 5% CO2 atmosphere, cells were collected and stained with 0.4% trypan blue stain. Viable cells were counted in a Neubauer Hemocytometer according to the standard procedure. Growth inhibition was expressed as the number of cells in drug-treated wells relative to the number of cells in control wells (percent of control growth).

Cell Cycle Analysis

The cell cycle distribution of stably complemented cell lines was analyzed by FACS analysis. Harvested cells (2.5×10^5 cells) were fixed with ice-cold 70% ethanol, treated with 200 μg/ml RNase A (Qiagen), and subsequently stained with 20 μg/ml propidium iodide (Sigma) in the presence of 0.1% Triton X-100. Cells were analyzed by using Beckman Counter FC500/CXP.

COMET Assays

Pol β knockout cells complemented with control vector, wild-type, or the R83/152K mutant of Pol β were seeded 12 hr before treatment. Cells were exposed to 0.25 mM MMS for 1 hr, then washed with PBS and either analyzed directly or replated in normal medium and incubated for 24 hr or 48 hr. For the COMET assay, we applied the procedure described by Singh et al. (1988 and 1991). COMETs were visualized by ethidium bromide staining (20 μg/ml) and examined at 400× magnification with a fluorescence microscope (Axiovert 200 M, Zeiss, Germany). More than 2500 DNA spots from each sample were classified into five categories corresponding to the amount of DNA in the tail, in accordance with Anderson et al. (1994). Results were expressed as COMET TFs, calculated according to Ivancsits et al. (2002). Statistical evaluation was done on the COMET stage distributions (contingency tables and chi-square analyses) as well as on the COMET TFs (Student's t test; two tailed).

GST Pull-Down and Immunoprecipitation

GST-PRMT6 or GST alone bound to glutathione-Sepharose beads were incubated with indicated proteins in 50 mM HEPES (pH 8.0), 90 mM NaCl, 0.1% (v/v) NP-40, 1 mM DTT, 1 mM PMSF, protease inhibitors (2 μg/ml leupeptin, 1 μg/ml pepstatin, 1 μg/ml bestatin) for 2 hr at 4ºC. The beads were washed three times with the same buffer and heated at 95ºC for 5 min in SDS-PAGE sample buffer. Coprecipitated full-length Pol β or Pol β fragments were analyzed by immunoblot using anti-Pol β antibody.

For immunoprecipitation, cells were lysed in lysis buffer (50 mM Tris-HCl [pH 8.0], 90 mM NaCl, 1 mM DTT, 0.1% [v/v] NP-40, and protease inhibitors [2 μg/ml leupeptin, 1 μg/ml pepstatin, 1 μg/ml bestatin]) for 20 min at 4ºC. Lysates were centrifuged at 13,000 rpm for 30 min at 4ºC, and supernatants were incubated with indicated antibodies and protein G-Sepharose overnight at 4ºC. After extensive washing, samples were incubated at 95ºC for 5 min in SDS-PAGE sample buffer and used for further analysis.

Methylation Assays

Purified recombinant proteins were incubated with GST-PRMT6 in 30 μl methylation buffer (50 mM HEPES [pH 8.0], 0.01% [v/v] NP-40, 10 mM NaCl, 1 mM DTT, 1 mM PMSF) supplemented with 25 nCi of S-adenosyl-L-(methyl-^{14}C) methionine (^{14}C-SAM) (Amersham Biosciences) (radioactive methylation) or 20 nmol of S-adenosyl-L-methionine sulfate p-toluenesulfonate (SAMe-PTS) (Sigma) for 1 hr at 30ºC (cold methylation). Reactions were stopped either by adding 2× SDS-PAGE sample buffer followed by heating at 95ºC for 5 min, or by adding 100 mM of NaCl and incubating at 4ºC for 10 min.

The in vivo methylation assay was performed by metabolic labeling of the cells with L-[*methyl*-^{3}H]-methionine for 3.5 hr in the presence of cycloheximide and chloramphenicol as described by Kzhyshkowska et al. (2001). Recombinant HA-Pol β and myc-PRMT6 were immunoprecipitated from the cell lysates and analyzed by SDS-PAGE followed by autoradiography.

BER Assay

BER assays were performed essentially as described by Hasan et al. (2002) except that the human XRCC1/LIG3 heterodimer was used instead of the T4 DNA ligase. All BER proteins used were purified to near homogeneity from *E. coli* according to standard procedures. Purification included affinity chromatography facilitated by affinity tags and ion exchange FPLC as follows: APE1, N-terminal 6His-tag, purification over Ni^{2+}-nitrilotriacetic acid (Ni-NTA)-agarose (Qiagen) and FPLC-UNO-S1 (Amersham Biosciences); XRCC1 C-terminal 6His-tag, purification over Ni-NTA agarose and FPLC-HiTrap™Q HP (Amersham Biosciences); LIG3, N-terminal GST-tag, purification over glutathione-Sepharose HP Amersham Biosciences) and FPLC-HiTrap™SP HP (Amersham Biosciences). Equimolar amounts of purified XRCC1 and LIG3 were allowed to form a stable complex at 4ºC for 15 min prior to their use in the BER assay.

Mass Spectrometry

Pol β was methylated in vitro by GST-PRMT6 bound to glutathione-Sepharose beads and subsequently treated with trypsin and chymotrypsin proteases. The peptide mixtures were purified using a C18 reversed-phase column (Millipore) and subjected to LC-MS/MS analyses on LCQ Deca XP ion trap mass spectrometer (Thermo Electron, San Jose, California).

DNA Polymerase Assays

DNA polymerase reaction was performed in a final volume of 10 μl containing 50 mM Tris-HCl (pH 7.6), 0.25 mg/ml BSA, 1 mM DTT, 0.8 mM $MnCl_2$, and 100 μM each of unlabeled dNTPs, [^{32}P]-5′ end-labeled primer annealed to the template, and the indicated amount of purified Pol β. The reaction was incubated for 15 min at 37ºC unless otherwise stated. The processivity assay was performed in the presence of a 100-fold molar excess of 17/73-mer DNA template as a trap. Reaction was terminated by adding gel-loading buffer (95% [v/v] formamide, 20 mM EDTA [pH 8.0]) and heating for 5 min at 95ºC. Reaction products were resolved on 10% polyacrylamide and 7 M urea sequencing gel, dried, and exposed to an X-ray film.

EMSA

Purified Pol β or Pol β mutants were incubated with 10 fmol of labeled oligonucleotide template in buffer containing 50 mM Tris-HCl (pH 8.0), 10 mM NaCl, 5 mM EDTA, 4% (v/v) ficol, and 50 μg/ml BSA for 20 min at RT. Complexes were loaded on 5% polyacrylamide gels containing 0.5×TBE, run at 100 V for 3 hr, and analyzed by autoradiography.

Supplemental Data

Supplemental Data include one figure and can be found with this article online at http://www.molecule.org/cgi/content/full/22/1/51/DC1/.

Acknowledgments

We thank M.T. Bedford (University of Texas) and D. Trono (University of Geneva, Switzerland) for providing PRMT6 and lentiviral constructs, respectively. We are grateful to all the members of the Institute of Veterinary Biochemistry and Molecular Biology (University of Zurich, Switzerland) for helpful advice and discussions. This work

was supported in part by the FEBS and the Swiss National Science Foundation program 31-67771.02, 31-109312.05, 31-109315.05, and 3339C0-101584/1. P.O.H., U.H., and M.O.H. are supported by the Kanton of Zurich.

Received: May 17, 2005
Revised: December 7, 2005
Accepted: February 10, 2006
Published: April 6, 2006

References

Aletta, J.M., Cimato, T.R., and Ettinger, M.J. (1998). Protein methylation: a signal event in post-translational modification. Trends Biochem. Sci. *23*, 89–91.

An, W., Kim, J., and Roeder, R.G. (2004). Ordered cooperative functions of PRMT1, p300, and CARM1 in transcriptional activation by p53. Cell *117*, 735–748.

Anderson, D., Yu, T.W., Phillips, B.J., and Schmerzer, P. (1994). The effect of various antioxidants and other modifying agents on oxygen-radical-generated DNA damage in human lymphocytes in the comet assay. Mutat. Res. *307*, 261–271.

Beard, W.A., and Wilson, S.H. (2000). Structural design of a eukaryotic DNA repair polymerase: DNA polymerase beta. Mutat. Res. *460*, 231–244.

Bebenek, K., Tissier, A., Frank, E.G., McDonald, J.P., Prasad, R., Wilson, S.H., Woodgate, R., and Kunkel, T.A. (2001). 5′-deoxyribose phosphate lyase activity of human DNA polymerase iota in vitro. Science *291*, 2156–2159.

Bedford, M.T., and Richard, S. (2005). Arginine methylation: an emerging regulator of protein function. Mol. Cell *18*, 262–272.

Biade, S., Sobol, R.W., Wilson, S.H., and Matsumoto, Y. (1998). Impairment of proliferating cell nuclear antigen-dependent apurinic/apyrimidinic site repair on linear DNA. J. Biol. Chem. *273*, 898–902.

Boisvert, F.M., Dery, U., Masson, J.Y., and Richard, S. (2005). Arginine methylation of MRE11 by PRMT1 is required for DNA damage checkpoint control. Genes Dev. *19*, 671–676.

Boulanger, M.C., Liang, C., Russell, R.S., Lin, R., Bedford, M.T., Wainberg, M.A., and Richard, S. (2005). Methylation of Tat by PRMT6 regulates human immunodeficiency virus type 1 gene expression. J. Virol. *79*, 124–131.

Casas-Finet, J.R., Kumar, A., Morris, G., Wilson, S.H., and Karpel, R.L. (1991). Spectroscopic studies of the structural domains of mammalian DNA beta- polymerase. J. Biol. Chem. *266*, 19618–19625.

Clarke, S. (1993). Protein methylation. Curr. Opin. Cell Biol. *5*, 977–983.

Covic, M., Hassa, P.O., Saccani, S., Buerki, C., Meier, N.I., Lombardi, C., Imhof, R., Bedford, M.T., Natoli, G., and Hottiger, M.O. (2005). Arginine methyltransferase CARM1 is a promoter-specific regulator of NF-kappaB-dependent gene expression. EMBO J. *24*, 85–96.

Cuthbert, G., Daujat, S., Snowden, A., Erdjument-Bromage, H., Hagiwara, T., Yamada, M., Schneider, R., Gregory, P., Tempst, P., and Bannister, A. (2004). Histone deimination antagonizes arginine methylation. Cell *118*, 545–553.

Davies, J.F., Jr., Almassy, R.J., Hostomska, Z., Ferre, R.A., and Hostomsky, Z. (1994). 2.3 A crystal structure of the catalytic domain of DNA polymerase beta. Cell *76*, 1123–1133.

Dianova, I.I., Sleeth, K.M., Allinson, S.L., Parsons, J.L., Breslin, C., Caldecott, K.W., and Dianov, G.L. (2004). XRCC1-DNA polymerase beta interaction is required for efficient base excision repair. Nucleic Acids Res. *32*, 2550–2555.

Fabbrizio, E., El Messaoudi, S., Polanowska, J., Paul, C., Cook, J.R., Lee, J.H., Negre, V., Rousset, M., Pestka, S., Le Cam, A., and Sardet, C. (2002). Negative regulation of transcription by the type II arginine methyltransferase PRMT5. EMBO Rep. *3*, 641–645.

Fan, J., and Wilson, D.M., 3rd. (2005). Protein-protein interactions and posttranslational modifications in mammalian base excision repair. Free Radic. Biol. Med. *38*, 1121–1138.

Frankel, A., Yadav, N., Lee, J., Branscombe, T.L., Clarke, S., and Bedford, M.T. (2002). The novel human protein arginine N-methyltransferase PRMT6 is a nuclear enzyme displaying unique substrate specificity. J. Biol. Chem. *277*, 3537–3543.

Garcia-Diaz, M., Bebenek, K., Kunkel, T.A., and Blanco, L. (2001). Identification of an intrinsic 5′-deoxyribose-5-phosphate lyase activity in human DNA polymerase lambda: a possible role in base excision repair. J. Biol. Chem. *276*, 34659–34663.

Gary, J.D., and Clarke, S. (1998). RNA and protein interactions modulated by protein arginine methylation. Prog. Nucleic Acid Res. Mol. Biol. *61*, 65–131.

Hammond, R.A., McClung, J.K., and Miller, M.R. (1990). Effect of DNA polymerase inhibitors on DNA repair in intact and permeable human fibroblasts: evidence that DNA polymerases delta and beta are involved in DNA repair synthesis induced by N-methyl-N′-nitro-N-nitrosoguanidine. Biochemistry *29*, 286–291.

Hasan, S., El-Andaloussi, N., Hardeland, U., Hassa, P.O., Burki, C., Imhof, R., Schar, P., and Hottiger, M.O. (2002). Acetylation regulates the DNA end-trimming activity of DNA polymerase beta. Mol. Cell *10*, 1213–1222.

Hoeijmakers, J.H. (2001). Genome maintenance mechanisms for preventing cancer. Nature *411*, 366–374.

Hubscher, U., Maga, G., and Spadari, S. (2002). Eukaryotic DNA polymerases. Annu. Rev. Biochem. *71*, 133–163.

Idriss, H.T., Al-Assar, O., and Wilson, S.H. (2002). DNA polymerase beta. Int. J. Biochem. Cell Biol. *34*, 321–324.

Ivancsits, S., Diem, E., Pilger, A., Rüdiger, H.W., and Jahn, O. (2002). Induction of DNA strand breaks by exposure to extremely-low-frequency electromagnetic fields in human diploid fibroblasts. Mutat. Res. *519*, 1–13.

Klungland, A., and Lindahl, T. (1997). Second pathway for completion of human DNA base excision-repair: reconstitution with purified proteins and requirement for DNase IV (FEN1). EMBO J. *16*, 3341–3348.

Kubota, Y., Nash, R.A., Klungland, A., Schar, P., Barnes, D.E., and Lindahl, T. (1996). Reconstitution of DNA base excision-repair with purified human proteins: interaction between DNA polymerase beta and the XRCC1 protein. EMBO J. *15*, 6662–6670.

Kwak, Y.T., Guo, J., Prajapati, S., Park, K.J., Surabhi, R.M., Miller, B., Gehrig, P., and Gaynor, R.B. (2003). Methylation of SPT5 regulates its interaction with RNA polymerase II and transcriptional elongation properties. Mol. Cell *11*, 1055–1066.

Kzhyshkowska, J., Schutt, H., Liss, M., Kremmer, E., Stauber, R., Wolf, H., and Dobner, T. (2001). Heterogeneous nuclear ribonucleoprotein E1B–AP5 is methylated in its Arg-Gly-Gly (RGG) box and interacts with human arginine methyltransferase HRMT1L1. Biochem. J. *358*, 305–314.

Lin, W.J., Gary, J.D., Yang, M.C., Clarke, S., and Herschman, H.R. (1996). The mammalian immediate-early TIS21 protein and the leukemia-associated BTG1 protein interact with a protein-arginine N-methyltransferase. J. Biol. Chem. *271*, 15034–15044.

Longley, M.J., Prasad, R., Srivastava, D.K., Wilson, S.H., and Copeland, W.C. (1998). Identification of 5′-deoxyribose phosphate lyase activity in human DNA polymerase gamma and its role in mitochondrial base excision repair in vitro. Proc. Natl. Acad. Sci. USA *95*, 12244–12248.

Ma, Z., Shah, R.C., Chang, M.J., and Benveniste, E.N. (2004). Coordination of cell signaling, chromatin remodeling, histone modifications, and regulator recruitment in human matrix metalloproteinase 9 gene transcription. Mol. Cell. Biol. *24*, 5496–5509.

Matsumoto, Y., and Kim, K. (1995). Excision of deoxyribose phosphate residues by DNA polymerase beta during DNA repair. Science *269*, 699–702.

McBride, A.E., and Silver, P.A. (2001). State of the arg: protein methylation at arginine comes of age. Cell *106*, 5–8.

Metivier, R., Penot, G., Hubner, M.R., Reid, G., Brand, H., Kos, M., and Gannon, F. (2003). Estrogen receptor-alpha directs ordered, cyclical, and combinatorial recruitment of cofactors on a natural target promoter. Cell *115*, 751–763.

Miller, M.R., and Chinault, D.N. (1982). Evidence that DNA polymerases alpha and beta participate differentially in DNA repair synthesis induced by different agents. J. Biol. Chem. *257*, 46–49.

Miranda, T.B., Miranda, M., Frankel, A., and Clarke, S. (2004). PRMT7 is a member of the protein arginine methyltransferase family with a distinct substrate specificity. J. Biol. Chem. *279*, 22902–22907. Published online March 24, 2004. 10.1074/jbc.M312904200.

Mowen, K.A., Tang, J., Zhu, W., Schurter, B.T., Shuai, K., Herschman, H.R., and David, M. (2001). Arginine methylation of STAT1 modulates IFNalpha/beta-induced transcription. Cell *104*, 731–741.

Nilsen, H., and Krokan, H.E. (2001). Base excision repair in a network of defence and tolerance. Carcinogenesis *22*, 987–998.

Podlutsky, A.J., Dianova, I.I., Wilson, S.H., Bohr, V.A., and Dianov, G.L. (2001). DNA synthesis and dRPase activities of polymerase beta are both essential for single-nucleotide patch base excision repair in mammalian cell extracts. Biochemistry *40*, 809–813.

Prasad, R., Beard, W.A., Chyan, J.Y., Maciejewski, M.W., Mullen, G.P., and Wilson, S.H. (1998). Functional analysis of the amino-terminal 8-kDa domain of DNA polymerase beta as revealed by site-directed mutagenesis. DNA binding and 5′-deoxyribose phosphate lyase activities. J. Biol. Chem. *273*, 11121–11126.

Sawaya, M.R., Pelletier, H., Kumar, A., Wilson, S.H., and Kraut, J. (1994). Crystal structure of rat DNA polymerase beta: evidence for a common polymerase mechanism. Science *264*, 1930–1935.

Singh, N.P., McCoy, M.T., Tice, R.R., and Schneider, E.L. (1988). A simple technique for quantitation of low levels of DNA damage in individual cells. Exp. Cell Res. *175*, 184–191.

Singh, N.P., Tice, R.R., Stephens, R.E., and Schneider, E.L. (1991). A microgel electrophoresis technique for direct quantitation of DNA damage and repair in individual fibroblasts cultured on microscope slides. Mutat. Res. *252*, 289–296.

Singhal, R.K., and Wilson, S.H. (1993). Short gap-filling synthesis by DNA polymerase beta is processive. J. Biol. Chem. *268*, 15906–15911.

Sobol, R.W., Horton, J.K., Kuhn, R., Gu, H., Singhal, R.K., Prasad, R., Rajewsky, K., and Wilson, S.H. (1996). Requirement of mammalian DNA polymerase-beta in base-excision repair. Nature *379*, 183–186.

Sobol, R.W., Prasad, R., Evenski, A., Baker, A., Yang, X.P., Horton, J.K., and Wilson, S.H. (2000). The lyase activity of the DNA repair protein beta-polymerase protects from DNA-damage-induced cytotoxicity. Nature *405*, 807–810.

Steitz, T.A. (1999). DNA polymerases: structural diversity and common mechanisms. J. Biol. Chem. *274*, 17395–17398.

Strahl, B.D., Ohba, R., Cook, R.G., and Allis, C.D. (1999). Methylation of histone H3 at lysine 4 is highly conserved and correlates with transcriptionally active nuclei in Tetrahymena. Proc. Natl. Acad. Sci. USA *96*, 14967–14972.

Tokui, T., Inagaki, M., Nishizawa, K., Yatani, R., Kusagawa, M., Ajiro, K., Nishimoto, Y., Date, T., and Matsukage, A. (1991). Inactivation of DNA polymerase beta by in vitro phosphorylation with protein kinase C. J. Biol. Chem. *266*, 10820–10824.

Zufferey, R., Nagy, D., Mandel, R.J., Naldini, L., and Trono, D. (1997). Multiply attenuated lentiviral vector achieves efficient gene delivery in vivo. Nat. Biotechnol. *15*, 871–875.

Zufferey, R., Dull, T., Mandel, R.J., Bukovsky, A., Quiroz, D., Naldini, L., and Trono, D. (1998). Self-inactivating lentivirus vector for safe and efficient in vivo gene delivery. J. Virol. *72*, 9873–9880.